TECHNISCHE UNIVERSITÄT MÜNCHEN

Fakultät für Medizin

III. Medizinische Klinik und Poliklinik

Klinikum rechts der Isar

Dissecting aberrant proteolytic ubiquitin networks in cancer

Carmen Gloria Richter (M.Sc.)

Vollständiger Abdruck der von der Fakultät für Medizin der Technischen Universität München zur Erlangung des akademischen Grades eines

Doktors der Naturwissenschaften (Dr. rer. nat.)

genehmigten Dissertation.

Vorsitzender: Prof. Dr. Dr. Andreas Pichlmair

Prüfer der Dissertation:

1. Prof. Dr. Florian Bassermann
2. Prof. Dr. Bernhard Küster
3. Prof. Dr. Sebastian Theurich

Die Dissertation wurde am 01.08.2019 bei der Technischen Universität München eingereicht und durch die Fakultät für Medizin am 07.04.2020 angenommen.

Content

1 Summary 1

2 Introduction 3

2.1 Multiple myeloma 3

2.1.1 Pathophysiology 3

2.1.2 Clinical manifestation and diagnosis 5

2.1.3 Treatment 6

2.1.4 The role of MYC in multiple myeloma 7

2.2 The ubiquitin code 7

2.2.1 Ubiquitin 8

2.2.2 Ubiquitylation cascade 9

2.2.3 SCF family of ubiquitin E3 ligases 10

2.2.4 The human F-box protein FBXL13 12

2.2.5 Deubiquitinases 12

2.2.6 The OTU family DUB OTUD6B 14

2.2.7 The proteasome 15

2.3 LIN28 16

2.3.1 Physiological role of LIN28 16

2.3.2 The role of LIN28B in cancer 18

2.4 The cell cycle 20

2.4.1 Overview of the cell cycle 20

2.4.2 G1/S transition 22

2.5 Centrosomes 22

2.5.1 Centrosome functions and structure 22

2.5.2 The centrosome cycle 23

2.6 Aim of the study 25

3 Material 27

3.1 Devices and instruments 27

3.2 Consumables 28

3.3 Chemicals and reagents 29

3.4 Commercial kits 32

3.5 Enzymes 32

3.6 Oligonucleotides 33

3.6.1 Cloning oligonucleotides 33

3.6.2 Oligonucleotides for amplicon deep-sequencing 34
3.6.3 qPCR oligonucleotides 34
3.6.4 Sequencing oligonucleotides 35
3.7 Sequences of shRNAs and siRNAs 35
3.7.1 Sequences of shRNAs 35
3.7.2 Sequences of siRNAs 36
3.8 Plasmids 36
3.9 Bacteria 38
3.10 Standards for DNA and proteins electrophoresis 38
3.11 Antibodies 38
3.11.1 Primary antibodies 38
3.11.2 Custom made primary antibodies 39
3.11.3 Conjugated primary antibodies 39
3.11.4 Conjugated secondary antibodies 39
3.12 Cell lines 40
3.13 Cell culture media and supplements 40
3.14 Patient samples 41
3.15 Solutions and buffers 41
3.16 Software and databases 44
4 Methods 45
4.1 Molecular cloning 45
4.1.1 Polymerase chain reaction (PCR) 45
4.1.2 Agarose gel electrophoresis and gel purification 45
4.1.3 DNA restriction digest and ligation 45
4.1.4 DNA mutagenesis 46
4.1.5 Bacterial transformation 46
4.1.6 DNA extraction from bacteria 47
4.1.7 Annealing of shRNA oligonucleotides 47
4.2 Generation of CRISPR/Cas9 sgRNA libraries 47
4.2.1 Designing CRISPR/Cas9 libraries 47
4.2.2 Annealing and dilution of libraries 48
4.2.3 Vector digest and ligation of libraries 48
4.2.4 Bacterial transformation and harvesting of libraries 48
4.2.5 CRISPR/Cas9 screen 49
4.2.6 Sample preparation for Illumina next-generation sequencing 49

4.2.7 Illumina MiSeq sequencing 50

4.3 Gene expression analysis 51

4.3.1 RNA extraction from eukaryotic cells 51
4.3.2 Reverse transcription of RNA 51
4.3.3 Quantitative PCR (qPCR) 51

4.4 Culture of eukaryotic cells and cell-based experiments 52

4.4.1 Cell culture 52
4.4.2 Freezing and thawing of cells 52
4.4.3 Harvesting cells 53
4.4.4 DNA transfection of cells 53
4.4.5 siRNA transfection of cells 54
4.4.6 Production of lentiviral particles 54
4.4.7 Viral transduction of cells 54
4.4.8 Isolation of $CD138^+$ cells from human bone marrow 54
4.4.9 Cycloheximide treatment 55
4.4.10 Synchronization of cells 55
4.4.11 Flow cytometry 56
4.4.12 Immunofluorescence analysis 57
4.4.13 Wound healing assay 57
4.4.14 Microtubule regrowth assay 58

4.5 Protein biochemistry 58

4.5.1 Cell lysis 58
4.5.2 SDS polyacrylamide gel electrophoresis (SDS-PAGE) 58
4.5.3 Silver staining 59
4.5.4 Immunoblot analysis (Western blot) 59
4.5.5 Stripping of membranes 60
4.5.6 Immunoprecipitation 60
4.5.7 FLAG-purification for mass spectrometric analysis 60
4.5.8 Proximity-dependent biotin identification (BioID) 61
4.5.9 Mass spectrometric analysis 61
4.5.10 *In vivo* ubiquitylation 63
4.5.11 DUB activity assay 64
4.5.12 Dephosphorylation of lysates 64
4.5.13 *In vitro* translation 64
4.5.14 *In vitro* binding assay 64

4.6 Protein purification from insect cells 65

4.6.1 Insect cell culture 65
4.6.2 Transfection of insect cells and virus production 65
4.6.3 Protein production 65
4.6.4 GST-purification of proteins 65

4.7 Statistical analysis 66

5 Results I 67

5.1 CRISPR/Cas9 screen of DUBs and F-box proteins in MM1.S cells 67

5.1.1 Establishment of a MM1.S Cas9 cell line 67
5.1.2 Generation of DUB and F-box protein sgRNA libraries 70
5.1.3 Pooled CRISPR/Cas9 screen in MM1.S Cas9 cells 71
5.1.4 CRISPR screen of F-box proteins identifies FBXW10 as potential oncogene 72
5.1.5 CRISPR-mediated knockout of FBXW10 confirms screening result 74
5.1.6 CRISPR screen of DUBs identifies OTUD6B as potential oncogene 75
5.1.7 CRISPR-mediated knockout of OTUD6B confirms screening result 75

5.2 OTUD6B is essential for cancer cell proliferation 78

5.2.1 OTUD6B is essential for proliferation of MM cells 78
5.2.2 OTUD6B is essential for proliferation of various cancer types 80

5.3 OTUD6B is involved in G1/S transition 81

5.3.1 OTUD6B is important for cell cycle progression 81
5.3.2 OTUD6B is involved in G1/S transition 82
5.3.3 OTUD6B activity is regulated in a cell cycle-dependent manner and peaks at G1/S transition 83

5.4 OTUD6B stabilizes LIN28B by K48 deubiquitylation at G1/S transition 85

5.4.1 Mass spectrometry-based screening approaches identify LIN28B as potential substrate 85
5.4.2 OTUD6B binds to LIN28B 89
5.4.3 OTUD6B interacts with the cold shock domain of LIN28B 91
5.4.4 OTUD6B binding to LIN28B is regulated by phosphorylation 92
5.4.5 RIOK3 represents a potential kinase of OTUD6B 94
5.4.6 OTUD6B deubiquitylates LIN28B 96
5.4.7 OTUD6B stabilizes LIN28B at G1/S transition 98
5.4.8 Overexpression of LIN28B attenuates the proliferation defect caused by OTUD6B depletion 101
5.4.9 LIN28B depletion phenocopies knockdown of OTUD6B 103

5.5 OTUD6B positively regulates MYC expression via LIN28B stabilization 104

5.5.1 Depletion of OTUD6B decreases MYC expression by LIN28B destabilization 104
5.5.2 OTUD6B and MYC levels positively correlate in MM patients 107

6 Discussion I 109

6.1 CRISPR/Cas9 screening approaches identify oncogenes in MM 109

6.1.1 Identification of established cancer-related genes 109
6.1.2 Identification of OTUD6B as a new oncogene in MM 110
6.1.3 Identification of other potentially oncogenic candidates 111

6.2 OTUD6B represents an important regulator of cell proliferation 112
6.2.1 OTUD6B is essential for MM cell proliferation 112
6.2.2 OTUD6B regulates cell cycle progression 113
6.3 OTUD6B mediates stabilization of LIN28B 114
6.3.1 OTUD6B prevents proteolytic degradation of LIN28B 114
6.3.2 Stabilization of LIN28B promotes MM cell proliferation 116
6.4 The role of OTUD6B in cancer 118
6.4.1 OTUD6B as a new oncogene 118
6.4.2 OTUD6B as a potential anti-cancer target 119
7 Results II 121
7.1 FBXL13 interacts with CEP192 and CEP152 121
7.1.1 FBXL13 binds to CEP192 and CEP152 121
7.1.2 FBXL13 binding to CEP192 is direct 123
7.1.3 CEP192 interacts with the leucine-rich repeat domain of FBXL13 124
7.2 FBXL13 targets CEP192 for proteasomal degradation 125
7.2.1 FBXL13 destabilizes CEP192 125
7.2.2 FBXL13 ubiquitylates CEP192 127
7.3 FBXL13 negatively regulates microtubule arrays via CEP192 degradation 128
7.3.1 FBXL13 downregulates centrosomal CEP192 and γ-tubulin 128
7.3.2 FBXL13 is important for microtubule nucleation 130
7.4 FBXL13 regulates cell motility by controlling CEP192 protein level 131
7.4.1 FBXL13 is important for proper cell migration 131
7.4.2 FBXL13 positively regulates cell motility by CEP192 degradation 132
8 Discussion II 134
8.1 FBXL13 represents a novel centrosomal regulator 135
8.1.1 FBXL13 interacts with centrosomal proteins 135
8.1.2 FBXL13 localizes at centrosomes 136
8.2 FBXL13 targets CEP192 for proteasomal degradation 137
8.3 FBXL13 has a central role in cell motility 138
8.4 FBXL13 as a potential anti-cancer target 140
9 Literature 142
10 List of figures and tables 171
10.1 List of figures 171
10.2 List of tables 172

11 Appendix 173
11.1 Sequences of sgRNA libraries 173
11.1.1 Sequences of F-box protein sgRNAs 173
11.1.2 Sequences of DUB sgRNAs 175
11.1.3 Sequences of non-targeting and positive control sgRNAs 179
11.2 Results of CRISPR/Cas9 screens 180
11.2.1 CRISPR/Cas9 screen of F-box proteins 180
11.2.2 CRISPR/Cas9 screen of DUBs 183
12 Publication 188
13 Danksagung 189

Abbreviations

°C	degree Celsius
A	alanine
AA	amino acid
AMP	adenosin-5'-monophosphate
APS	ammonium persulfate
ASCT	autologous stem cell transplantation
ATP	adenosin-5'-triphosphate
BES	N,N-Bis(2-hydroxyethyl)-2-aminoethanesulfonic acid
BioID	proximity dependent biotin identification
Blast	blasticidin
BM	bone marrow
BMSC	bone marrow stromal cell
bp	base pair
BrdU	5-bromo-2′-deoxyuridine
BSA	bovine serum albumin
C	cysteine
C-terminal	carboxy terminal
CCNF	Cyclin F
CDK	Cyclin-dependent kinase
cDNA	complementary DNA
Chk2	Checkpoint kinase 2
CHX	cycloheximide
CIP	calf intestinal phosphatase
CKI	CDK inhibitor
CP	core particle
CRISPR	clustered regularly interspaced short palindromic repeats
CRL	cullin-RING ligase
CSD	cold shock domain
Ctrl	control
CUL1	Cullin 1
D	aspartate
DAPI	4′,6-diamidino-2-phenylindole
DLBCL	diffuse large B-cell lymphoma
DMEM	Dulbecco's Modified Eagle's Medium
DMSO	dimethylsulfoxid
DNA	deoxyribonucleic acid
dNTP	2'-desoxynukleosid-5'-triphosphat

DSMZ	Deutsche Sammlung von Mikroorganismen und Zellkulturen
DTT	dithiothreitol
DUB	deubiquitinase
E. coli	Escherichia coli
ECL	enhanced chemiluminescence
EDTA	ethylenediaminetetraacetic acid
EGTA	ethylene-bis(oxyethylenenitrilo)tetraacetic acid
ESC	embryonic stem cell
EV	empty vector
FACS	fluorescence activated cell sorting
FBS	fetal bovine serum
FBXL	F-box and Leu-rich repeat
FBXO	F-box only
FBXW	F-box and WD40 domain
FGFR3	fibroblast growth factor receptor 3
FITC	fluorescein isothiocyanate
FSC	forward scatter
fw	forward
G	glycine
G-2-P	beta-glycerolphosphate disodium salt hydrate
GFP	green fluorescent protein
GSEA	gene set enrichment analysis
GST	glutathione S-transferase
H	histidine
h, hrs	hour, hours
HA	hemagglutinin
HBSS	Hank's Balanced Salt Solution
HECT	homologous to E6AP C-terminus
HEPES	N-(2-hydroxyethyl)piperazine-N`-2-ethane sulfonic acid
HRP	horse radish peroxidase
IF	isoform
IF	immunofluorescence
Igf2	Insulin-like growth factor 2
IgG	Immunoglobulin G
IgH	immunoglobulin heavy chain
IL	interleukin
IMDM	Iscove's Modified Dulbecco's Media
IMWG	Internal Myeloma Working Group
IP	immunoprecipitation

ISS	International Staging System
JAMM	JAB1/MPN/MOV34 metalloprotease
K	lysine
kb	kilobase
kD	kilodalton
LB	Luria-Bertani
LDH	lactate dehydrogenase
LE	long exposure
LFQ	label-free quantification
LRR	leucine rich repeat
M	molar
MACS	magnetic activated cell sorting
MAF	musculoaponeurotic fibrosarcoma
MCL	mantle cell lymphoma
MGUS	monoclonal gammopathy of undetermined significance
min	minute
MINDY	motif interacting with ubiquitin (MIU)-containing novel DUB family
miRNA	microRNA
MM	multiple myeloma
mM	millimolar
mRNA	messenger RNA
MS	mass spectrometry
MT	microtubule
MTOC	microtubule organizing centre
MW	molecular weight
n	number
N-terminal	amino terminal
Nava	Sodium orthovanadate (Na_3VO_4)
NGS	next generation sequencing
NLS	nuclear localization sequence
nM	nanomolar
NoLS	nucleolar localization signal
NSCLC	non–small cell lung cancer
NT	non-targeting
oligo	oligonucleotide
OTU	ovarian tumour
P/S	penicillin-streptomycin
PAGE	polyacrylamide gel electrophoresis
PAM	protospacer adjacent motif

PBMC	peripheral blood mononuclear cell
PBS	phosphate buffered saline
PC	plasma cell
PCM	pericentriolar material
PCR	polymerase chain reaction
PFA	paraformaldehyde
PI	proteasome inhibitor
PI	propidium iodide
PMSF	phenylmethanesulfonylfluoride
PNK	Polynucleotide Kinase
PPase	phosphatase
pre	precursor
pri	primary
PTM	post-translational modification
PVDF	polyvinylidene fluoride
qPCR	quantitative PCR
RBR	RING-between-RING
RBX1	RING-box protein 1
RING	really interesting new gene
RISC	RNA-induced silencing complex
RNA	ribonucleic acid
RNAi	RNA interference
RP	regulatory particle
RPLP0	ribosomal protein large subunit P0
rpm	revolution per minute
RPMI	Roswell Park Memorial Institute
rv	reverse
s	serine
S.D.	standard deviation
SCF	SKP1-CUL1-F-box protein
SDS	sodium dodecyl sulfate
SE	short exposure
sec	second
sgRNA	single guide RNA
shRNA	short hairpin RNA
siRNA	small interfering RNA
SKP1	S phase kinase-associated protein 1
SKP2	S phase kinase-associated protein 2
SMM	smouldering multiple myeloma

SOC	Super optimal broth
SSC	sideward scatter
TBE	TRIS-Borat-EDTA
TCA	trichloroacetic acid
TEMED	N,N,N`,N``-tetramethyl-ethylenediamine
TLCK	Nα-tosyl-L-lysine chloromethyl ketone hydrochloride
TPCK	N-p-tosyl-L-phenylalanine chloromethyl ketone
Tris	tris(hydroxymethyl)aminomethane
TuRC	tubulin ring complex
Ub	ubiquitin
UCH	ubiquitin C-terminal hydrolase
ULP	ubiquitin-like protease
UPS	ubiquitin proteasome system
USP	ubiquitin-specific protease
UV	ultraviolet
V	volt
VS	vinyl sulfone
w/v	weight per volume
WCE	whole cell extract
WT	wildtype
Znf	zinc finger

1 Summary

Cancer represents one of the leading causes of death worldwide and despite recent therapeutic advances, many malignancies are incurable necessitating the identification of new druggable vulnerabilities. Among them, multiple myeloma (MM) represents the second most common haematological malignancy, accounting for approximately 10% of all tumours of the haematopoietic and lymphoid tissues and for 1% of all cancers (Rajkumar et al. 2014; Siegel, Miller, and Jemal 2016; Teras et al. 2016; Vincent Rajkumar 2014). High response rates to proteasomal inhibition in MM patients implicate that aberrant functions of the ubiquitin proteasome system (UPS) play a pivotal role in the pathophysiology of MM, thus indicating that components of the UPS represent attractive targets in anti-cancer therapies.

In search for UPS components, namely F-box proteins and deubiquitinases (DUBs), which contribute to myelomagenesis and hence represent potential new drug targets, pooled CRISPR/Cas9 negative selection screens were performed in a human MM cell line in this study. The largely uncharacterized DUB OTUD6B was identified to promote cell proliferation in MM and other malignancies by driving cell cycle progression. Moreover, two proteome-wide mass spectrometry-based screening approaches revealed LIN28B, an oncogenic RNA-binding protein associated with adverse prognosis in MM (Manier et al. 2017), as a new interactor of OTUD6B. By cleaving K48-linked polyubiquitin chains from LIN28B, OTUD6B prevents proteolytic degradation of LIN28B specifically at G1-S transition, at which OTUD6B activity was found to peak. Additionally, the interaction between OTUD6B and LIN28B depends on phosphorylation, which might be mediated by the kinase RIOK3. Overexpression of LIN28B partially rescued the proliferation defect of MM cells caused by OTUD6B loss, supporting the importance of OTUD6B-mediated stabilization of LIN28B for MM growth. Furthermore, shRNA-mediated depletion of OTUD6B and LIN28B in MM cells caused a cell cycle arrest at late G1 phase resulting from an accumulation of p27 and a strong decrease in MYC expression, in line with LIN28B-mediated inhibition of *let-7* miRNAs and hence stabilization of MYC mRNA. Finally, OTUD6B and MYC mRNA levels were found to significantly correlate in primary patient-derived MM samples at diagnosis, further underlining an OTUD6B-dependent regulation of MYC expression in MM patients. Taken together, this study uncovers a new ubiquitin-dependent mechanism controlling cell cycle progression and hence proliferation of MM cells and specifies OTUD6B as a proto-oncogene and potential therapeutic target in this disease.

Besides the unbiased screen for UPS components involved in the pathophysiology of a defined malignancy, the cellular role of an orphan F-box protein FBXL13 and its potential implication in cancer was investigated in this study. FBXL13 could be identified as a novel centrosomal protein, which specifically interacts with Centrin-2, Centrin-3 and CEP192 at the centrosomes. While FBXL13 binds to Centrin-2 and Centrin-3 via its N-terminus, CEP192 interacts with the leucine rich repeat (LRR) domain of FBXL13. Furthermore, CEP192, an important regulator of centriole duplication and centrosome maturation (Joukov, Walter, and De Nicolo 2014;

Sonnen et al. 2013), could be identified as a proteolytic substrate of FBXL13. As a consequence of CEP192 proteasomal degradation, ectopic expression of FBXL13 reduces γ-tubulin levels at the centrosomes, thereby decreasing the capacity of the cells to nucleate centrosomal microtubules. Additionally, FBXL13 promotes cell motility by targeting CEP192 for degradation and consequently reducing centrosomal levels of CEP192. Overall, this study describes a new function of the orphan F-box protein FBXL13 in centrosome homeostasis and cell migration, thereby providing a potential link between the UPS and cancer metastasis.

In summary, the present study gives new mechanistic insight into aberrant ubiquitin networks in cancer and identifies components of the UPS as novel vulnerabilities that can serve as new therapy targets in the future.

2 Introduction

2.1 Multiple myeloma

Multiple myeloma (MM) represents a malignancy of clonal plasma cells in the bone marrow and is the second most common haematological malignancy, accounting for approximately 10% of all tumours of the haematopoietic and lymphoid tissues and for 1% of all cancers (Rajkumar et al. 2014; Siegel, Miller, and Jemal 2016; Teras et al. 2016; Vincent Rajkumar 2014). MM occurs mainly in elderly people at a median age of 65-70 years at first diagnosis and despite recent improvements in the treatment, MM remains an incurable disease with a median survival of 5-7 years (Kyle and Rajkumar 2009; Rajkumar and Kumar 2016).

2.1.1 Pathophysiology

As a part of the adaptive immune system, plasma cells (PCs) represent terminally differentiated B cells, which generate and secrete specific antibodies in order to neutralize pathogenic antigens (Nutt et al. 2015). PCs originate from activated B cells, which undergo class switch recombination and somatic hypermutation in the germinal centres, thereby differentiating into PC precursor cells. Latter are highly proliferative and finally differentiate to quiescent PCs residing in the bone marrow (O'Connor et al. 2003).

MM cells are most likely derived from PC precursor cells and, in most cases, the initiation event of MM takes place at an early stage during plasma cell development, when a B cell undergoes immunoglobulin heavy chain (IgH) switch recombination in order to produce specific antibodies, which bind with high affinity to their antigens (Figure 1) (Bergsagel and Kuehl 2001; Fonseca et al. 2002; Kuehl and Bergsagel 2002; Kumar et al. 2017). The introduction of DNA double strand breaks, which is necessary for this process, can result in aberrant reciprocal translocations of oncogenes into the Ig locus resulting in enhanced expression of these genes and thus in increased proliferation. These primary translocations can give rise to a pre-MM stage called monoclonal gammopathy of undetermined significance (MGUS), which is characterized by an increased number of clonal plasma cells in the bone marrow and elevated serum levels of monoclonal (M) protein as a result of the secretion of dysfunctional immunoglobulins (Figure 1) (Kuehl and Bergsagel 2002; Kumar et al. 2017; Kyle and Rajkumar 1999). A subset of genes, which undergo IgH associated translocation on chromosome 14, are recurrently found in MGUS and MM patients and includes Cyclin D1 (t(11;14)), FGFR3 (fibroblast growth factor receptor 3) (t(4;14)) and the transcription factor MAF (t(14;16)) (Chesi et al. 1996; Chesi et al. 1997; Chesi et al. 1998). MGUS patients are asymptomatic, however, in 1% of the cases per year MGUS develops to MM with defined end-organ damages (see section 2.1.2) (Kyle and Rajkumar 1999). The progression of MGUS to MM is caused by the acquisition of additional genetic aberrations, like gain or loss of certain chromosomes, and mutations, which are also referred to as secondary genetic changes and which arise at different rates depending on the type of the primary translocations (Figure 1)

(Rajan and Rajkumar 2015). For instance, the progression from MGUS to MM occurs faster in patients with t(4;14) translocation than in patients with t(11;14) (Rajkumar et al. 2013; Kumar et al. 2017). Common secondary chromosomal alterations include gain of chromosome 1q and deletions of chromosomes 1p, 17p and 13 (Hanamura et al. 2006; Neben et al. 2013; Rajan and Rajkumar 2015; Tricot et al. 1995). Moreover, the oncogenes RAS and MYC are often found to be mutated or enhanced by secondary translocations, respectively, latter often driving progression to refractory MM and plasma cell leukaemia (Figure 1) (Glitza et al. 2015; Rajan and Rajkumar 2015; Kumar et al. 2017). Altogether, MM represents a highly heterogenetic disease and can be classified in different risk groups depending on the cytogenetic abnormalities (Rajan and Rajkumar 2015).

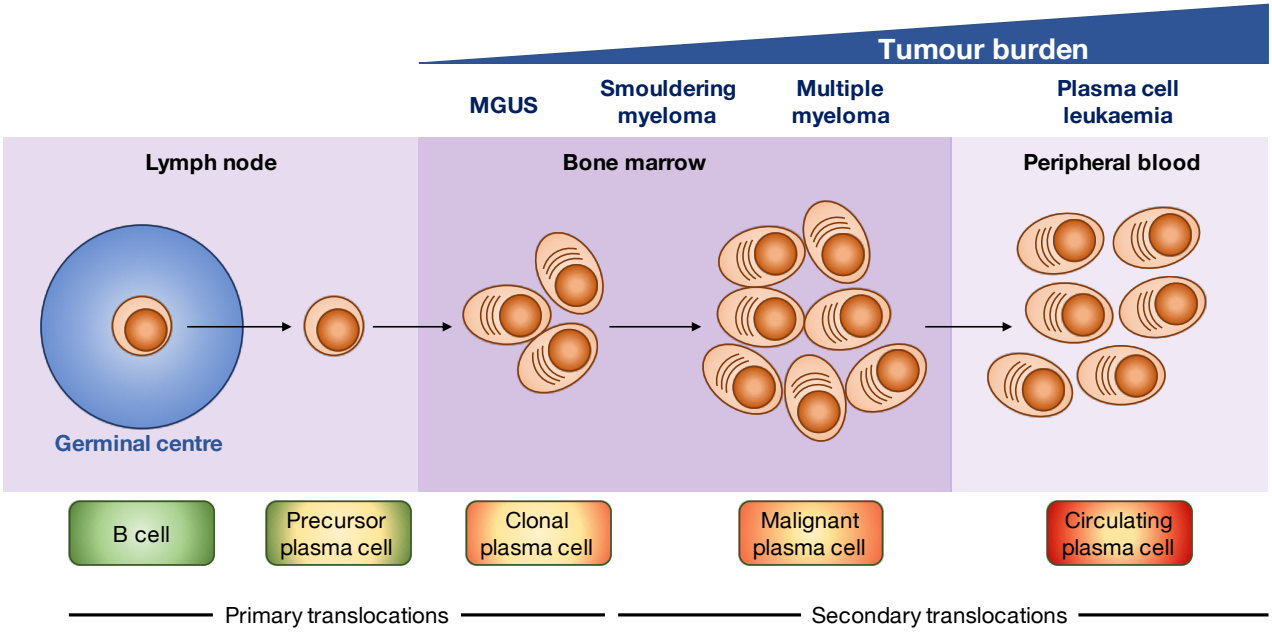

Figure 1: Development of multiple myeloma. Malignant plasma cells originate from a germinal centre B cell, which undergoes immunoglobulin heavy chain (IgH) switch recombination in order to produce specific antibodies. This can result in aberrant reciprocal translocations of oncogenes into the Ig locus leading to enhanced expression of these genes and thus in increased proliferation. These primary translocations can give rise to a pre-MM stage called monoclonal gammopathy of undetermined significance (MGUS), which is characterized by an increased number of clonal plasma cells in the bone marrow. The acquisition of secondary translocations and mutations can drive the progression to smouldering and multiple myeloma and, in the end, can lead to plasma cell leukaemia, which represents an extramedullary disease (Kuehl and Bergsagel 2002; Kumar et al. 2017).

Besides genetic alterations, the development and progression of MM is driven by and highly dependent on the microenvironment in the bone marrow involving different cell types like haematopoietic cells, osteoclasts, stromal cells, osteoblasts and endothelial cells (Kumar et al. 2017). The interplay between malignant plasma cells and surrounding cells is essential for MM cell survival and proliferation as this triggers the secretion of different cytokines like IL-6, IL-10, VEGF or TNFα by the bone marrow stromal cells (BMSCs) (Hideshima et al. 2007; Podar et al. 2001; Podar et al. 2002). Furthermore, the interaction between MM cells and BMSCs leads to

deformation of the bone as a consequence of imbalanced activation and number of bone absorbing (osteoclasts) and bone forming (osteoblasts) cells (Oranger et al. 2013; Roodman 2009).

2.1.2 Clinical manifestation and diagnosis

MM is preceded by MGUS, which is often detected only by chance due to its asymptomatic nature. It is characterized by the presence of less than 10% of clonal plasma cells in the bone marrow and a serum concentration of monoclonal protein smaller than 3 g/dL (Kyle and Rajkumar 1999). In contrast, smouldering multiple myeloma (SMM), which represents an intermediate stage, is defined by 10-60% plasma cell infiltration in the bone marrow and the risk for progression to MM is 10% per year within the first five years (Kyle et al. 2007).

MM is diagnosed when certain criteria, which are defined by International Myeloma Working Group (IMWG), are fulfilled (Rajkumar et al. 2014). These criteria include the presence of monoclonal protein (M-protein) in the serum and that the percentage of clonal plasma cells in the bone marrow is equal or greater than 10%. In addition, there must be an evidence for end-organ damages defined by the CRAB features (hyper**c**alcaemia, **r**enal insufficiency, **a**naemia and **b**one lesions) (Rajkumar et al. 2014). In this context, hypercalcaemia and bone lesions are consequences of the imbalance in activity and numbers between osteoclasts and osteoblasts (Giuliani, Rizzoli, and Roodman 2006; Mundy et al. 1974; Yaccoby et al. 2002). The latter is thereby assessed by low-dose computer tomography scans or bone radiographies and causes bone pain in the patient (Rajkumar and Kumar 2016; Regelink et al. 2013). High levels of M-protein are often the cause for renal impairment as they can form precipitates in the distal segment of the nephron, thereby damaging the tubules, and is diagnosed by measuring the serum creatinine level (Batuman 2012; Rajkumar and Kumar 2016). The high burden of plasma cells in the bone marrow causes anaemia, which is expressed in fatigue and tested by a complete blood count in the laboratory (Kumar et al. 2017; Mittelman 2003). Besides routine testing of serum and blood, bone marrow aspiration is conducted in order to determine the amount of malignant plasma cells in the bone marrow by morphological examination and flow cytometry (Kyle and Rajkumar 2009).

In order to determine the prognosis and the optimal treatment for the patient, the tumour burden (stage) is assessed according to the Durie-Salmon staging system, which takes the amount of bone lesions and the concentration of haemoglobin, serum calcium and M-protein levels into account, or by using the International Staging System (ISS) (Durie and Salmon 1975; Greipp et al. 2005). The latter also accounts for albumin and β_2-microglobulin levels and, since 2015, the revised ISS includes the level of lactate dehydrogenase (LDH) and the presence of cytogenetic abnormalities and defines three different risk groups accordingly (Greipp et al. 2005; Palumbo et al. 2015). For instance, some chromosomal aberrations are associated with high risk and poor prognosis, e.g. deletion of 17p and the translocation t(4;14) (Avet-Loiseau et al. 2007).

2.1.3 Treatment

The treatment of MM has been advanced within the last decades as a consequence of a better understanding of the underlying mechanisms as well as due to the invention of new combination therapies and drugs. However, despite recent advances in treatment, MM remains incurable and thus patients suffering from MM will invariably relapse in the end, which reflects the need of additional treatment options (Kumar et al. 2017).

Patients that have been diagnosed with MM by fulfilling the CRAB features (see 2.1.2) are classified according to the presence of comorbidities, age, risk stratification and performance status, which determines the course of the treatment and whether a patient is eligible for autologous stem cell transplantation (ASCT) (Kumar et al. 2017; Rajkumar and Kumar 2016). Several classes of drugs are currently used for the treatment of MM including alkylating agents (e.g. melphalan), corticosteroids (e.g. dexamethasone), immunomodulatory drugs (e.g. lenalidomide) and proteasome inhibitors (e.g. bortezomib) (Kumar et al. 2017). The standard first-line therapy for patients below 65-70 years of age, which are eligible for a multi-drug regimen, is currently a combination therapy including an immunomodulatory drug (lenalidomide), a proteasome inhibitor (bortezomib) and dexamethasone followed by high-dose treatment with melphalan and ASCT as consolidation approach (Attal et al. 1996; Child et al. 2003; Durie et al. 2017; Kumar et al. 2017). After ASCT, the maintenance therapy with lenalidomide, which has been shown to increase the overall survival, or bortezomib is considered as standard treatment (Kumar et al. 2017; McCarthy et al. 2017; Sonneveld et al. 2012). Patients older than 65-70 years and ineligible for ASCT are treated with combinations of one immunomodulatory drug (e.g. lenalidomide or thalidomide) and/or bortezomib with melphalan and/or prednisone in doublet or triplet regimens (Facon et al. 2007; Kumar et al. 2017; Palumbo et al. 2006; San Miguel et al. 2008).

The medical care of relapsed patients strongly depends on their treatment history and on many other factors like response to previous therapies or aggressiveness of the relapse (Rajkumar and Kumar 2016). However, combination therapies, such as doublet or triplet regimens, composed of classic and novel drugs, which have not been used for the previous treatment of the patient, are commonly used (Rajkumar and Kumar 2016). For instance, the application of novel monoclonal antibodies against CD38 (daratumumab) or SLAMF7 (elotuzumab) together with lenalidomide and dexamethasone or in case of daratumumab with bortezomib and dexamethasone results in significantly longer progression-free survival in patients with relapsed/refractory multiple myeloma (Dimopoulos et al. 2018; Dimopoulos et al. 2016; Naymagon and Abdul-Hay 2016; Palumbo et al. 2016). In patients with repeated relapsed disease, salvage therapies lose their efficacy as a consequence of additional acquired mutations and other genetic and epigenetic aberrations, reflecting the need for new drugs and druggable targets (Kumar et al. 2017).

2.1.4 The role of MYC in multiple myeloma

The proto-oncogene MYC represents a transcription factor, which is associated with 10-15% of genomic loci, thus being involved in controlling a large number of genes (Eilers and Eisenman 2008; Fernandez et al. 2003). As a consequence, many pathways concerning cell proliferation, protein synthesis, survival and metabolism are regulated by MYC and promote tumorigenesis when deregulated (Hoffman and Liebermann 2008; Prochownik 2008). Dysregulation or overexpression of MYC can be found in many cancer types as a result of changes in the genetic locus or upstream pathways (Jovanovic et al. 2018; Kuehl and Bergsagel 2012). In multiple myeloma, genetic aberrations involving the genetic locus of *MYC*, 8q24, are frequently observed at the transition from MGUS to MM or at later timepoints as secondary translocations (Chesi et al. 2008; Chiecchio, Dagrada, Protheroe, et al. 2009; Jovanovic et al. 2018; Kuehl and Bergsagel 2012). Moreover, abnormalities regarding the *MYC* locus are associated with more aggressive forms of MM, such as plasma cell leukaemia, and poor outcome (Chiecchio, Dagrada, White, et al. 2009; Glitza et al. 2015). Indeed, gene set enrichment analysis revealed a MYC activation signature in 67% of MM, but not in MGUS cells, supporting an involvement of MYC in disease progression (Chng et al. 2011; Jovanovic et al. 2018). Besides genetic alterations of the *MYC* locus, an activation can also be achieved by post-transcriptional events, which involve RAS-mediated stabilization of MYC protein or mRNA stabilization by the DIS3/LIN28B/*let-7*-axis (see 2.3.2) (Sears et al. 1999; Sears et al. 2000; Segalla et al. 2015). MYC has been reported to promote cancer progression by various pathways, including DNA repair, ribosome biogenesis, apoptosis and metabolism (Jovanovic et al. 2018). Furthermore, MYC is also involved in cell cycle regulation by promoting the transition from G1 to S phase by different mechanisms (Jovanovic et al. 2018). For instance, MYC induces the expression of various cell cycle regulators, such as CDKs and cyclins, which drive cell cycle progression, as well as of proteins, which target cell cycle inhibitors like p27 for degradation (see 2.4.2) (Bretones et al. 2011; Mateyak, Obaya, and Sedivy 1999; Vlach et al. 1996).

Because of its prominent role in the progression of MM, MYC represents a suitable target for cancer therapy. However, targeting MYC itself turned out to be challenging because of its structure and its broad function (Jovanovic et al. 2018). Consequently, current approaches focus on interfering with MYC expression and regulation, making the identification of druggable regulators of MYC very important (Jovanovic et al. 2018).

2.2 The ubiquitin code

Protein ubiquitylation represents a post-translational modification, which can have tremendous effects on the fate of a protein or its cellular function (Swatek and Komander 2016). The molecular basis for this process is the attachment of one or more ubiquitin molecules to a lysine residue or the N-terminus of a target protein, which, depending on the type of ubiquitylation, can lead to a change in its activity, binding partners or cellular localization or it marks the protein

for proteasomal degradation (Komander and Rape 2012). Ubiquitylation of proteins reflects a highly dynamic process, which is catalysed by a three-step ubiquitylation cascade involving different enzymes (see 2.2.2), but which can also be quickly reversed by so-called deubiquitinases (see 2.2.5) (Hershko and Ciechanover 1998; Komander and Rape 2012). Thousands of proteins have been described to be ubiquitylated, reflecting the significance of this modification (Kim et al. 2011). As a consequence, ubiquitylation plays an important role in a wide range of biological processes including cell cycle regulation, DNA damage response, apoptosis, immunity and transcription (Dhananjayan, Ismail, and Nawaz 2005; Hershko and Ciechanover 1998; Huang and D'Andrea 2006; Kim, Kim, et al. 2013; Rahighi et al. 2009). Moreover, because of its involvement in the regulation of numerous cellular mechanisms, deregulation of ubiquitylation has been reported to be associated with many diseases including cancer (Fang et al. 2003; Jiang and Beaudet 2004).

2.2.1 Ubiquitin

Ubiquitin represents a highly conserved 8 kDa protein, which is composed of 76 amino acids (Haglund and Dikic 2005; Swatek and Komander 2016). Ubiquitylation takes place, when the C-terminus of ubiquitin becomes covalently attached to the ε-amino group of a lysine (K) residue in a substrate, resulting in the formation of an isopeptide bond (Ciechanover and Ben-Saadon 2004). Ubiquitin itself possesses seven lysine residues (K6, K11, K27, K29, K33, K48 and K63), which in turn can be connected to other ubiquitin molecules, thereby forming polyubiquitin chains (Dammer et al. 2011; Xu et al. 2009). Apart from polyubiquitylation via one of the seven lysine residues, ubiquitin can also form linear chains when it is attached to the N-terminal methionine of another ubiquitin protein (Kirisako et al. 2006). Besides the formation of polyubiquitin chains, in which the ubiquitin molecules are connected by the same linkage type, ubiquitin has been also shown to be modified at more than one lysine residue, giving rise to branched chains and thereby increasing the complexity and number of potential signals (Swatek and Komander 2016). However, the mostly found linkage type in cells is K48 ubiquitylation, which results in degradation of the substrate by the 26S proteasome (Figure 2) (Dammer et al. 2011). Besides K48 linkages, atypical K11-linked polyubiquitin chains have also been shown to mark substrates for proteasomal degradation specifically during mitosis (Jin et al. 2008; Matsumoto et al. 2010). Of note, polyubiquitylation can also mediate non-proteolytic cell signalling. For instance, K63-linked and linear ubiquitin chains are important regulators of the NF-κB pathway by influencing protein activities and by forming signalling scaffolds (Figure 2) (Deng et al. 2000; Komander et al. 2009; Rahighi et al. 2009). Aside from polyubiquitylation, single ubiquitin molecules can become attached to one or more lysine residues of a receptor protein leading to monoubiquitylation or multi-monoubiquitylation, respectively (Komander and Rape 2012). For instance, membrane proteins are targeted for lysosomal degradation by monoubiquitylation (Figure 2) (Mukhopadhyay and Riezman 2007).

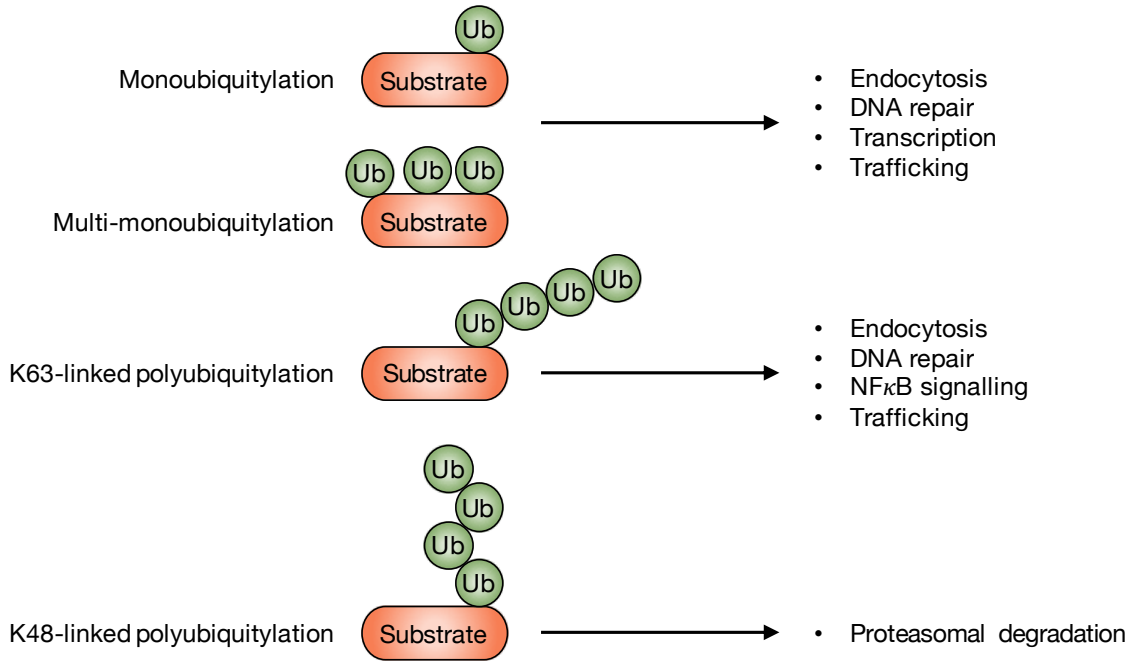

Figure 2: Overview of ubiquitin modifications and their cellular outcomes. A substrate can be modified by single ubiquitin (Ub) molecules at one or several lysine (K) residues resulting in monoubiquitylation or multi-monoubiquitylation, respectively. These modifications are involved in several non-proteolytic cell signalling cascades including endocytosis, DNA repair and transcription. In addition, proteins can be covalently linked to polyubiquitin chains, which are connected via K63 or K48 lysine residues, leading to different cellular outcomes. Whereas K63-linked chains are found to be involved in similar cellular functions to monoubiquitylation and additionally in NFκB signalling, K48 polyubiquitylation mainly results in the proteasomal degradation of the substrate. [Figure adapted from (Buetow and Huang 2016; Haglund and Dikic 2005)].

In summary, given the numerous possibilities of diverse ubiquitin chain topologies, the ubiquitin code is highly complex and far from being completely understood.

2.2.2 Ubiquitylation cascade

The attachment of ubiquitin to the receptor protein by the formation of an isopeptide bond is catalysed by a tree-step enzymatic cascade, in which ubiquitin is first activated by a ubiquitin-activating enzyme (E1), then it is transferred to the ubiquitin-conjugating enzyme (E2) and finally it becomes covalently bound to the substrate by the ubiquitin ligase (E3) (Figure 3). In the first step, the C-terminal glycine of ubiquitin is activated by hydrolysing ATP and forming ubiquitin-adenylate as an intermediate, which then becomes attached to the catalytic cysteine residue of the E1 enzyme by forming an energy-rich thioester bond upon AMP release. Subsequently, the activated ubiquitin is transferred to the cysteine of the E2 enzyme and finally, the C-terminal glycine of the ubiquitin molecule becomes attached to the ε-amino group of a lysine (K) residue of the substrate with help of the ubiquitin E3 ligase (Hershko and Ciechanover 1998; Scheffner, Nuber, and Huibregtse 1995).

Since only two E1 and approximately 40 different E2 enzymes exist in human cells, the substrate specificity is given by a large number of E3 ligases, which can be subdivided into three

different classes (Buetow and Huang 2016; Schulman and Harper 2009; Stewart et al. 2016). These classes are represented by the RING (really interesting new gene), HECT (homologous to E6AP C-terminus) and RBR (RING-between-RING) ubiquitin E3 families, all of which possess specific E2 binding domains. The difference between these classes lies in the distinct mode of the ubiquitin transfer and their structure (Buetow and Huang 2016; Metzger, Hristova, and Weissman 2012). For instance, HECT and RBR enzymes first receive the ubiquitin molecule by forming a thioester bond between their catalytic cysteine residue and the ubiquitin before transferring it to the substrate, whereas RING E3 ligases mediate ubiquitylation of the substrate by bringing it in close proximity to the E2 enzyme (Buetow and Huang 2016).

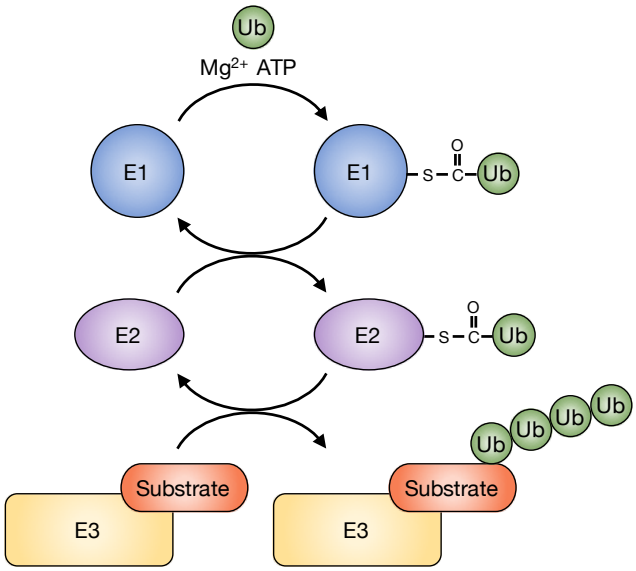

Figure 3: Enzymatic cascade of the ubiquitin system. Ubiquitylation of substrates requires the consecutive activities of three enzymes. First, ubiquitin (Ub) is activated in an ATP-dependent manner and gets covalently attached via an energy-rich thioester bond to the E1 enzyme. Subsequently, the ubiquitin molecule is transferred to the catalytic cysteine of the E2 enzyme and eventually covalently linked to a lysine residue of the substrate with help of the E3 ligase.

2.2.3 SCF family of ubiquitin E3 ligases

The cullin-RING ligase (CRL) family, which is subdivided into eight types depending on the complex formation, represents the largest family of ubiquitin E3 ligases (Petroski and Deshaies 2005). The best characterized member is the S phase kinase-associated protein 1 (SKP1)-cullin 1 (CUL1)-F-box protein (SCF) E3 ligase complex, which catalyses the ubiquitin transfer by binding specific substrates and a E2 enzyme (Figure 4) (Bai et al. 1996; Wang et al. 2014). The SCF complex is composed of the scaffold protein CUL1, which binds via its C-terminus to the RING domain protein RBX1 and with its N-terminus to the adaptor protein SKP1 (Bai et al. 1996; Frescas and Pagano 2008). RBX1 is necessary for the recruitment of the E2 enzyme to the complex and SKP1 in turn recruits one of 69 different F-box proteins, which confer the substrate specificity of the complex, as every F-box protein binds to a subset of substrates (Figure 4) (Petroski and Deshaies 2005; Wang et al. 2014). Three subtypes of F-box proteins exist, which are classified

according to the structure of their protein-protein interaction domain, responsible for the substrate recognition: The F-box and WD40 domain (FBXW) family, the F-box and Leu-rich repeat (FBXL) family and F-box only (FBXO) proteins, which in most of the cases possess other conserved homology domains (Cenciarelli et al. 1999; Jin et al. 2004; Winston et al. 1999). Besides these specific protein-protein interaction domains, F-box proteins, as the name suggests, also contain a conserved F-box domain, which mediates the binding to SKP1 (Bai et al. 1996). The binding and recruitment of substrates to the SCF complex is tightly regulated and requires the recognition of a so-called degron by the F-box protein, which is a conserved, short amino acid sequence within the substrate. Most often, these degrons need to be phosphorylated (phospho-degrons) in order to be recognized, thus allowing selective ubiquitylation of a substrate upon certain stimuli (Ravid and Hochstrasser 2008; Skaar, Pagan, and Pagano 2013). Although polyubiquitylation mediated by SCF complexes usually reflects K48-linked chain formation and therefore targets substrates for proteasomal degradation, some F-box proteins have been recently described to also regulate non-proteolytic K63-linked ubiquitylation (Chan et al. 2012; Yao et al. 2018; Zhang et al. 2016).

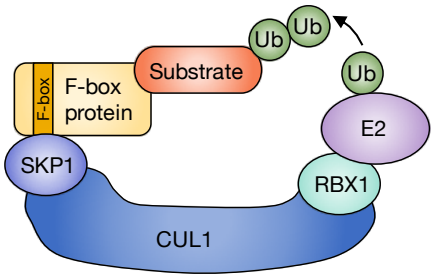

Figure 4: SCF complex-mediated ubiquitylation. The SCF complex is composed of the large scaffold protein CUL1, which binds via its C-terminal part to the RING domain protein RBX1. At its N-terminus, CUL1 associates with the adaptor protein SKP1, which in turn recruits one of roughly 70 F-box proteins by binding to the F-box domain. As substrate receptors of the complex, F-box proteins target a subset of proteins and ubiquitin (Ub) is eventually transferred from the RBX1-bound E2 enzymes onto the substrate.

SCF-mediated ubiquitylation is important for a wide range of biological processes and thus, dysregulations of certain F-box proteins have been linked to various diseases including cancer (Akhoondi et al. 2007; Bour et al. 2001; Di Fonzo et al. 2009; Skaar, Pagan, and Pagano 2013; Wang et al. 2014). For instance, different SCF complexes mediate ubiquitylation of important cell cycle regulators and thus are important for cell cycle control and progression (Nakayama and Nakayama 2006). Consequently, the deregulation of certain F-box proteins, like SKP2 and FBXW7, has been shown to drive cancer as a result of uncontrolled cell proliferation (Nakayama and Nakayama 2005). In this context, SKP2 degrades the CDK inhibitors p27 and p21 and was described as an oncogene, whereas another F-box protein, FBXW7, reflects a tumour suppressor by targeting oncogenes like MYC and Cyclin E for proteasomal degradation (Carrano et al. 1999; Frescas and Pagano 2008; Koepp et al. 2001; Wang et al. 2014; Yada et al. 2004; Yu, Gervais, and Zhang 1998).

2.2.4 The human F-box protein FBXL13

FBXL13 represents an orphan F-box protein with a predicted molecular weight of approximately 84 kDa, which is localized on chromosome 7q22.1. Four different isoforms of FBXL13 are described (UniProt: Q8NEE6-1, -2, -3 and -4), of which the first isoform represents the longest, comprising 735 amino acids (AA). Besides the N-terminal F-box domain (AA 152-198), FBXL13, as a member of the FBXL family, contains also 17 leucine rich repeats (AA 230-667) (Figure 5). So far, no cellular function of FBXL13 has been described, however, a study using a parallel adaptor capture proteomics approach linked FBXL13 to centrosome function as FBXL13 was found to be associated with Centrin-2 (Tan et al. 2013). Furthermore, RNAi screens in mice and human non-small cell lung cancer cell lines identified FBXL13 as a regulator of normal growth and cell proliferation (Beronja et al. 2013; Cron et al. 2013). Despite various reports, which suggest an implication of FBXL13 in cancer, it is not clear whether FBXL13 acts as a tumour suppressor or as an oncogene. For instance, FBXL13 has been found to be amplified or mutated in various solid tumours (cBioPortal) and cancer lines (Barretina et al. 2012) and was linked to genomic stability (Paulsen et al. 2009), suggesting a role in cancer development. In contrast, a gene segment of 7q22, which includes the gene of FBXL13, has been found to be commonly deleted in myeloid tumours (Curtiss et al. 2005), indicating rather a potential tumour suppressor role for FBXL13. Overall, the implication of FBXL13 in various malignancies might depend on the cellular context and on specific substrates, which have not been identified so far.

Figure 5: Schematic overview of FBXL13. FBXL13 isoform 1 (UniProt: Q8NEE6-1) represents a F-box protein belonging to the FBXL family and comprises 735 amino acids (AA). It contains two domains, an N-terminal F-box domain (AA 152-198, blue) and 17 leucine rich repeats (AA 230-667, yellow). LRR, leucine rich repeat.

2.2.5 Deubiquitinases

Ubiquitylation is an impactful post-translational modification (PTM) and, similarly to other protein PTMs, it is reversible, allowing a fast and tightly controlled protein regulation, which can rapidly react to cellular changes. The responsible enzymes, which erase or modify ubiquitylation on specific substrates, are called deubiquitinases (DUBs). Six different groups classify the approximately 100 human DUBs according to their catalytic domain and structure (Mevissen and Komander 2017). Among these, five families are cysteine proteases including 54 members of the ubiquitin-specific proteases (USPs), 16 members of the ovarian tumour proteases (OTUs), 4 members of the ubiquitin C-terminal hydrolases (UCHs), 4 members of the Josephin family and the very recently discovered motif interacting with ubiquitin (MIU)-containing novel DUB family (MINDYs) with also 4 members (Abdul Rehman et al. 2016; Clague et al. 2013; Mevissen and Komander 2017; Reyes-Turcu, Ventii, and Wilkinson 2009). The last family is represented by 16

members of the JAB1/MPN/MOV34 metalloprotease DUBs (JAMMs), which are zinc-dependent metalloenzymes (Cope et al. 2002; Mevissen and Komander 2017). Apart from theses DUBs, other cysteine proteases exist, which specifically cleave ubiquitin-like proteins such as SUMO or NEDD8 and thus are referred to as ubiquitin-like proteases (ULPs) (Bruderer et al. 2011; Cope et al. 2002; Hochstrasser 2009).

Many DUBs, especially USPs, are not restricted to cleave a specific linkage type, but rather are specific for a subset of substrates, from which they remove different types of ubiquitin and in most of the cases also the substrate bound ubiquitin (Faesen et al. 2011; Mevissen and Komander 2017; Ritorto et al. 2014). In this context, DUBs specifically regulate signalling pathways and biological processes. In contrast, some DUBs only bind to a specific ubiquitin signal, which they cleave, or act in large protein complexes and thus do not possess substrate specificity (Mevissen and Komander 2017). For instance, the metalloprotease PSMD14 represents a subunit of the 26S proteasomes and specifically cleaves K63-linked ubiquitin chains independently of the substrate (Hao et al. 2013; Yao and Cohen 2002). In contrast to USPs, members of the OTU family have been reported to possess preferences for one or several linkage types (Ritorto et al. 2014; Mevissen et al. 2013). Moreover, JAMM metalloproteases, like the above described PSMD14, mostly cleave K63 linkages whereas the recently discovered MINDYs are K48 linkage-specific (Abdul Rehman et al. 2016; Hao et al. 2013; Ritorto et al. 2014).

DUBs are tightly regulated in order to response to various stimuli or cellular changes (Sahtoe and Sixma 2015). For instance, the abundance of a DUB can be altered by either regulation of the transcription and translation or by changing its degradation rate (Mevissen and Komander 2017). Another way to change the activity of a DUB towards a certain substrate is given by the regulation of its cellular localization (Urbe et al. 2012). This can be achieved by protein-protein interactions at the specific cellular sites or by PTMs, which influence the localization to a certain compartment like the nucleus (Herhaus et al. 2015; Mevissen and Komander 2017; Urbe et al. 2012). Apart from that, PTMs can also directly change the catalytic activity of a DUB in a positive or negative way (Mevissen and Komander 2017). For instance, phosphorylation of DUBA (OTUD5) has been shown to be necessary for its activity and substrate binding. Here, a conserved serine residue immediately preceding the OTU domain was identified to be phosphorylated and to be critical for ubiquitin recognition (Huang, Ma, et al. 2012).

Because of the involvement of DUBs in numerous cellular processes, their deregulation can lead to the development of various diseases including cancer. Most notably, DUBs, which regulate cancer related pathways, like DNA repair or proliferation, are potential oncogenes or tumour suppressors (D'Arcy, Wang, and Linder 2015). For instance, USP28 is involved in the DNA damage response by stabilizing Chk2 and 53BP1 and therefore is important for p53-mediated apoptosis upon DNA double strand breaks (Zhang et al. 2006). Since DUBs possess a catalytic cysteine in their active site, they are “druggable” and thus, the identification of oncogenic DUBs is highly relevant for the development of new anti-cancer therapies.

2.2.6 The OTU family DUB OTUD6B

OTUD6B represents a largely uncharacterized DUB of the OTU family. The gene of OTUD6B is localized on chromosome 8q21.3 and ubiquitously expressed in all human tissues. Two isoforms of OTUD6B have been described, of which the longer first isoform (UniProt: Q8N6M0-1) composed of 293 amino acids reflects the canonical sequence of OTUD6B. The first isoform differs from the second, 192 amino acid long isoform (UniProt: Q8N6M0-2) in the first 105 amino acids (Figure 6). Like all DUBs of the OTU family, OTUD6B contains a conserved OTU domain with a catalytic triad composed of cysteine 158 (C158), aspartate 155 (D155) and histidine 277 (H277). In addition, there are three N-terminal coiled coil domains in OTUD6B isoform 1 and one in the second isoform (Figure 6). Recombinant human OTUD6B purified from *E. coli* has been shown to be reactive towards ubiquitin propargylamide but did not reveal any activity in linkage specific cleavage assays using all types of di-ubiquitin (Mevissen et al. 2013).

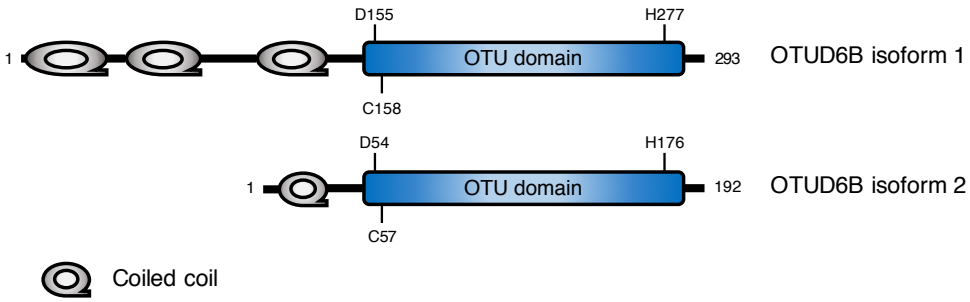

Figure 6: Schematic overview of OTUD6B isoforms. Two isoforms of OTUD6B exist, of which the first isoform comprises 293 amino acids (AA) and the second 192 AA. The isoforms differ in their N-terminus, which is 101 AA longer in the first isoform. The C-terminal OTU domain composed of 138 AA and depicted in blue contains the catalytic triad of cysteine (C), aspartate (D) and histidine (H), of which the respective position is indicated in the scheme. Besides the OTU domain, OTUD6B isoform 1 exhibits three N-terminal coiled coil domains while the second isoform only possesses a short single coiled coil structure.

Recent studies demonstrated that the two isoforms of OTUD6B have opposite functions, thereby either stimulating or inhibiting protein translation by modification of the 48S preinitiation complex (Sobol et al. 2017). In this context, OTUD6B isoform 1 has been reported to inhibit proliferation of non–small cell lung cancer (NSCLC) cells whereas OTUD6B isoform 2 promotes it by positively regulating cyclin D1 translation and c-MYC protein stability (Sobol et al. 2017). Another study showed that mouse Otud6b expression was induced upon cytokine stimulation in mouse Ba/F3 cells and primary B lymphocytes followed by a fast decrease and that forced expression of Otud6b had an antiproliferative effect by arresting cells in G1 phase (Xu et al. 2011). Both studies were using a longer OTUD6B isoform 1 composed of 324 AA, which correspond to the GeneBank entry NM_016023, however, this sequence has been updated and replaced by the above described OTUD6B transcript variant 1 (Figure 6).

Homozygous dysfunctional mutations in the *OTUD6B* gene give rise to severe developmental defects in humans. In this context, two studies reported that biallelic variants in *OTUD6B* causes

intellectual disability syndrome associated with seizures and dysmorphic features (Santiago-Sim et al. 2017; Straniero et al. 2018). In line with the global developmental delay, the microcephaly and the congenital heart disease observed in these patients, homozygous *Otud6b* knockout mice are subviable and also feature smaller sizes and congenital heart defects (Koscielny et al. 2014; Santiago-Sim et al. 2017). Further analysis of peripheral blood mononuclear cells from patients revealed defects in proteasome assembly and accumulation of ubiquitylated protein aggregates, suggesting a functional involvement of OTUD6B in the proteasome pathway (Santiago-Sim et al. 2017).

Last, analysis of autoantibodies in sera from transgenic mice prior to spontaneous development of mammary tumours identified antibodies against Otud6b and thus, the presence of such autoantibodies was suggested as a marker for the early detection of human breast cancer (Mao et al. 2014).

2.2.7 The proteasome

As a ~2.4 mDa-large multi-subunit protein complex, the 26S proteasome represents a huge cellular proteolytic machine, which catalyses the hydrolysis of ubiquitylated proteins (Bard et al. 2018; Dou and Zonder 2014). The selective degradation of proteins reflects an important regulatory instrument of cells to react on various intracellular changes, like cellular stress, and to regulate essential pathways, for instance, to drive cell cycle progression or to modulate signal transduction (Bard et al. 2018; Nakayama and Nakayama 2006). Thus, the 26S proteasome is involved in numerous cellular processes, requiring a tightly regulated activity and highly specific recognition of ubiquitylated proteins.

The proteasome is composed of a 19S regulatory particle (RP), which is important for the recognition and unfolding of ubiquitylated proteins, and a barrel-shaped 20S core particle (CP), which builds a channel and mediates the proteolytic cleavage of substrates into 2-10 amino acid long peptides (Coux, Tanaka, and Goldberg 1996; Deveraux et al. 1994; Kisselev et al. 1999). The RP can be further biochemically dissected into lid and base complexes, of which the first mainly comprises structural subunits but also the deubiquitinase PSMD14 (see 2.2.5) (Bard et al. 2018; Glickman et al. 1998; Saeki and Tanaka 2012). Unfolding of proteins requires energy and is catalysed by six AAA+-type ATPase subunits, which are located at the centre of the base subcomplex (Bard et al. 2018; Sauer et al. 2004). In addition, three ubiquitin and ubiquitin-like binding proteins are part of the base subcomplex and function as ubiquitin receptors (Bard et al. 2018; He et al. 2012; Husnjak et al. 2008; Shi et al. 2016). Here, only proteins, which have been modified with K11-, K48- or K29- linked ubiquitin, are recognized by these receptors and eventually become degraded (Chau et al. 1989; Jin et al. 2008; Xu et al. 2009). Besides PSMD14, two additional deubiquitinases, namely USP14 and UCHL5, can be found associated with the RP and are important for ubiquitin recycling (Borodovsky et al. 2001; Chernova et al. 2003; Collins and Goldberg 2017; Stone et al. 2004). Moreover, deubiquitylation of substrates impacts the dwell time of substrates on the proteasome and sometimes helps substrates to escape from

proteasomal degradation (Collins and Goldberg 2017; Crosas et al. 2006). However, once a protein has been unfolded and gated into the 20S CP, it becomes cleaved by the proteolytic subunits. The CP is composed of 28 subunits, which are arranged in four rings and which possess different proteolytic activities (Finley 2009; Groll et al. 1997). The rings consist of seven different subunits and are arranged at twofold symmetry (Finley 2009). In this context, seven α-type subunits form the outer rings whereas seven β-type subunits, of which β1, β2, and β5 are catalytically active, build the two inner rings. Depending on their cleavage preference, the subunits are referred to as caspase like (β1), trypsin like (β2) or chymotrypsin like (β5), but rather feature low specificity (Borissenko and Groll 2007; Finley 2009).

Since the proteasome is involved in almost every cellular process including cell proliferation, malignant cells highly depend on proteasomal degradation, making the ubiquitin proteasome system (UPS) an attractive target in cancer therapy (Dou and Zonder 2014). Indeed, cancer cells have been shown to be more sensitive to proteasome inhibitors (PIs) than normal healthy cells, providing a therapeutic window for the treatment of patients with PIs (Adams 2004; Drexler 1997; Drexler, Risau, and Konerding 2000; Masdehors et al. 1999). Bortezomib represents the first approved proteasome inhibitor and is especially used for the treatment of multiple myeloma (see 2.1.3) (Dou and Zonder 2014). As a reversible inhibitor, bortezomib inhibits the active site of the β5 subunit and with lower affinity also binds to the β1 subunit (Dou and Zonder 2014; Okazuka and Ishida 2018). Next generation PIs have been developed in order to improve the anti-cancer activities, to reduce toxicity and to overcome acquired resistance against bortezomib (Dick and Fleming 2010; Dou and Zonder 2014). In summary, the potency of PIs in the treatment of multiple myeloma reflects the potential of targeting the UPS in certain malignancies and, at the same time, suggests the presence of relevant aberrant ubiquitin-dependent oncogenic processes that may serve as important new future therapeutic vulnerabilities.

2.3 LIN28

2.3.1 Physiological role of LIN28

LIN-28 was initially identified as an important developmental regulator of the nematode *Caenorhabditis elegans* (Moss, Lee, and Ambros 1997). In mammalians, two members of the LIN28 family exist, LIN28A and LIN28B, which are highly similar in sequence and function (Figure 7a) (Balzeau et al. 2017; Guo et al. 2006; Moss and Tang 2003). Both represent RNA binding proteins and contain two RNA binding domains, an N-terminal cold shock domain (CSD) and a C-terminal zinc finger domain composed of two cysteine cysteine histidine cysteine (CCHC) zinc knuckles (Figure 7a) (Guo et al. 2006; Moss, Lee, and Ambros 1997; Moss and Tang 2003). Like in *C. elegans*, *Lin28* is an essential gene for mammalian development and thus, the *Lin28a*/*Lin28b* double knockout is embryonic lethal in mice (Yang, Yang, et al. 2015). While *Lin28b* knockout alone does not affect embryonic development, heterozygous deletion of *Lin28b* has been shown to increase the defect in brain development caused by *Lin28a* knockout in mice, suggesting that

both proteins display functional redundancy (Balzeau et al. 2017; Shinoda et al. 2013; Yang, Yang, et al. 2015). In line with its role in development, Lin28 is highly expressed in developing cells and tissues but its expression becomes restricted to the epithelial cells of the kidney, cardiac and skeletal muscle and erythrocytes in adult mammalians (de Vasconcellos et al. 2014; Tsialikas and Romer-Seibert 2015; Yang and Moss 2003). Since LIN28 is expressed in human embryonic stem cells (hESCs) and becomes downregulated upon differentiation (Figure 7b), it has been suggested to contribute to stemness and together with the expression of OCT4, SOX2 and NANOG, LIN28 has been shown to reprogram somatic cells into pluripotent stem cells (Hanna et al. 2009; Richards et al. 2004; Yu et al. 2007).

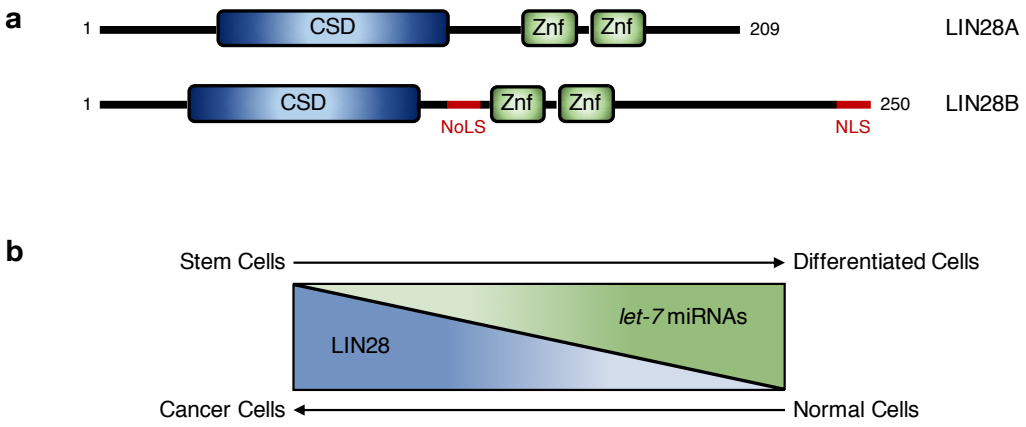

Figure 7: Overview of the LIN28 family. (a) Schematic of LIN28A and LIN28B. The closely related proteins harbour two RNA binding regions, a N-terminal cold shock domain (CSD) and two zinc fingers (Znf). Additionally, LIN28B exhibits a putative nucleolar localization signal (NoLS) and a C-terminal nuclear localization sequence (NLS). **(b)** Involvement of the LIN28/*let-7* axis in differentiation and cancer. LIN28 expression is high in stem cells, were it suppresses the maturation of the *let-7* miRNA family, but becomes lost upon differentiation, which leads to a stabilization of *let-7* miRNAs. *Let-7* miRNAs in turn target LIN28 mRNA, which further downregulates LIN28 expression. Transformation of cells can lead to reactivation of LIN28 and hence inhibition of *let-7* miRNAs, providing growth advantages for cancer cells. [Figure adapted from (Balzeau et al. 2017)].

The best described function of LIN28A and LIN28B is the suppression of *let-7* microRNAs (miRNAs) (Heo et al. 2008; Newman, Thomson, and Hammond 2008; Rybak et al. 2008; Viswanathan, Daley, and Gregory 2008). miRNAs target endogenous mRNAs leading to their inhibition or degradation. In brief, miRNAs are transcribed as long non-coding RNAs and processed in two steps to mature 19-22 nucleotide long double stranded RNAs (Kim, Han, and Siomi 2009). The first step involves microprocessor complex-mediated cleavage of the primary (pri-)miRNAs into precursor (pre-)miRNAs in the nucleus (Lee et al. 2003; Lee et al. 2002). Pre-miRNAs contain a characteristic stem loop and are exported into the cytoplasm, where they are further processed by the Dicer into mature miRNAs, which are finally incorporated into the RNA-induced silencing complex (RISC) (Bernstein et al. 2001; Hutvagner et al. 2001; Kim 2004; Martinez et al. 2002). On the one hand side, *lin-28* itself represents a target of *let-7* miRNA leading to suppression of *lin-28* upon development when *let-7* miRNAs become expressed (Figure 7b)

(Morita and Han 2006; Pasquinelli et al. 2000; Reinhart et al. 2000). However, in embryonic stem cells, Lin28 negatively regulates maturation of *let-7* miRNAs in order to preserve stemness and thus, differentiation requires a switch in this mutual regulation (Figure 7b) (Copley et al. 2013; Heo et al. 2008; Rybak et al. 2008; Shyh-Chang and Daley 2013). The *let-7* family comprises 12 members and has been reported to target a large number of mRNAs, which are involved in cellular proliferation and energetics, including numerous oncogenes like RAS, MYC, HMGA2 and Cyclin D1 (Balzeau et al. 2017; Johnson et al. 2007; Johnson et al. 2005; Mayr, Hemann, and Bartel 2007; Sampson et al. 2007). Although both LIN28 members repress maturation of *let-7* miRNAs, the mode of inhibition differs between LIN28A and LIN28B. In the cytoplasm, LIN28A recruits the TUTase Zcchc1 to the *let-7* pre-miRNA, which in turn polyuridylates pre-*let-7*, thereby preventing further processing by Dicer (Hagan, Piskounova, and Gregory 2009; Heo et al. 2009; Thornton et al. 2012). In contrast, different models have been suggested for how LIN28B suppresses *let-7* miRNA maturation (Balzeau et al. 2017). For instance, different studies reported that LIN28B binding to pri-*let-7* in the nucleus or to pre-*let-7* in the cytoplasm blocks its further cleavage by Drosha or Dicer, respectively (Newman, Thomson, and Hammond 2008; Piskounova et al. 2011; Rybak et al. 2008; Viswanathan, Daley, and Gregory 2008). Despite the reported differences in how LIN28A and LIN28B mediate suppression of *let-7* miRNA maturation, the mode of binding seems to be identical and is mediated by the two RNA-binding domains, the CSD and the zinc finger domain (Mayr et al. 2012; Piskounova et al. 2011). It has been proposed that the initial binding of the CSD to the terminal loop of pre-*let-7* leads to a remodelling of pre-*let-7*, thereby making the single stranded GGAG motif accessible for the binding to the zinc finger domain of LIN28 (Mayr et al. 2012).

Besides the suppression of *let-7* miRNAs, LIN28, as an RNA-binding protein, also directly regulates a large number of mRNAs (Shyh-Chang and Daley 2013; Tsialikas and Romer-Seibert 2015). For instance, Lin28a has been shown to promote Insulin-like growth factor 2 (Igf2) mRNA translation by binding to polysomes (Polesskaya et al. 2007). Moreover, direct binding of Lin28a to the mRNA of different cyclins and histone H2a in mouse ESC has been shown to promote their expression (Xu and Huang 2009; Xu, Zhang, and Huang 2009). Last, in HEK293T cells, LIN28B was found to be bound to a huge number of mRNAs, thereby stabilizing them and increasing the protein abundances (Hafner et al. 2013).

2.3.2 The role of LIN28B in cancer

As a regulator of development, LIN28 promotes stem cell proliferation and the capacity of self-renewal (Hanna et al. 2009; Richards et al. 2004; Yu et al. 2007). However, upon differentiation LIN28 expression is shut down in most tissues and consequently, *let-7* miRNAs become stabilized, thereby downregulating oncogenic proteins like RAS, MYC and HMGA2 (see 2.3.1 and Figure 8) (Balzeau et al. 2017; Johnson et al. 2005; Mayr, Hemann, and Bartel 2007; Sampson et al. 2007). In ~15% of human cancer cells, either LIN28A or LIN28B can be found reactivated leading to enhanced proliferation by preventing *let-7* miRNA maturation (Figure 7b) (Viswanathan

et al. 2009). In this case, the overexpression of LIN28 and downregulation of the tumour suppressor *let-7* miRNAs are often linked to poor prognosis and advanced malignancy (Viswanathan et al. 2009). The LIN28/*let-7* axis has been shown to regulate most of the hallmarks of cancer including cell proliferation, metabolism, immune evasion, metastasis, genomic instability and cell death (Figure 8) (Geng et al. 2011; King et al. 2011; Ma et al. 2014; Mayr, Hemann, and Bartel 2007; Tian, Han, et al. 2014; Wang et al. 2013; Wang, Wang, et al. 2015). In cancer cells, re-activation of LIN28B is often achieved by genetic and epigenetic events, such as hypomethylation of the *LIN28B* locus (Balzeau et al. 2017; Viswanathan et al. 2009). Moreover, it has been shown that MYC directly promotes LIN28B expression by associating with its promotor, thereby generating a positive feedback loop via *let-7* miRNAs (Figure 8) (Chang et al. 2009). Indeed, downregulation of MYC has been reported to increase *let-7a* levels whereas forced expression of *let-7a* in turn decreases MYC expression in Burkitt lymphoma cells (Sampson et al. 2007). Besides its transcriptional regulation, LIN28B has also been shown to be regulated on a post-transcriptional level. For instance, LIN28B is targeted for proteasomal degradation by the E3 ubiquitin ligase TRIM71, which can be found downregulated in various cancers (Yin et al. 2016). In addition, LIN28B mRNA has been shown to be degraded by the ribonuclease DIS3 in multiple myeloma cells, thereby regulating *let-7* miRNAs (Segalla et al. 2015). In line with this study, *DIS3* was found to be frequently mutated in multiple myeloma patients leading to a loss of function (Chapman et al. 2011). An oncogenic role of LIN28B in multiple myeloma was further supported by studies, which could show that knockdown and knockout of LIN28B led to a decrease in proliferation of myeloma cells by *let-7*-mediated downregulation of MYC expression (Manier et al. 2017). Furthermore, LIN28B expression correlates with MYC in multiple myeloma patients and is linked to adverse prognosis (Manier et al. 2017).

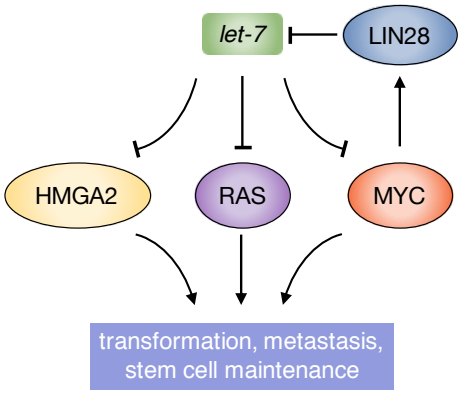

Figure 8: Oncogenic role of LIN28. The *let-7* miRNA family targets mRNAs of various oncogenes including HMGA2, RAS and MYC. Reactivation of LIN28 in cancer cells leads to an inhibition of *let-7* miRNAs and thus positively regulates the expression of oncogenes, thereby promoting transformation, metastasis and tumour stemness. Additionally, MYC directly promotes LIN28 expression, generating a positive feedback loop. [Figure adapted from (Hata and Lieberman 2015)].

2.4 The cell cycle

2.4.1 Overview of the cell cycle

The cell cycle is the basis for eukaryotic cell division and proliferation. Consequently, its correct progression and regulation are a precondition for the maintenance of genomic stability and thus for avoiding cancer initiation. To make sure that cell division only takes place after the DNA has been duplicated without any damage, that could interfere with chromosome segregation and would lead to the manifestation of mutations in the daughter cells, the cell cycle is subdivided into four phases, which are tightly controlled by different checkpoints (Figure 9a) (Kastan and Bartek 2004). In G1 phase, the cell decides whether it enters another cell cycle depending on extra- and intracellular signals. Extracellular signalling is triggered by mitogens, which bind to cell surface receptors and lead to a signal transduction cascade preparing the cell for entry into S phase (Besson and Yong 2001). However, when the DNA or other components of the cell are damaged, intracellular signals block entry into another round of the cell cycle by activating the G1/S checkpoint, which leads to a cell cycle arrest and gives the cell time to repair the damage or, if the damage is excessive, provokes cell apoptosis or senescence (Barnum and O'Connell 2014). In S phase the DNA is replicated and cells progress to G2 phase, which again allows the cell to control for correct chromosome duplication and to sense potential errors. Like the onset of S phase, entry into mitosis requires a switch-like signalling cascade to prevent uncontrolled and premature progression into division (Hochegger, Takeda, and Hunt 2008). In mitosis, chromosomes become condensed, attached to the mitotic spindle and eventually segregated. The latter only occurs when every chromosome is correctly attached and aligned in the metaphase

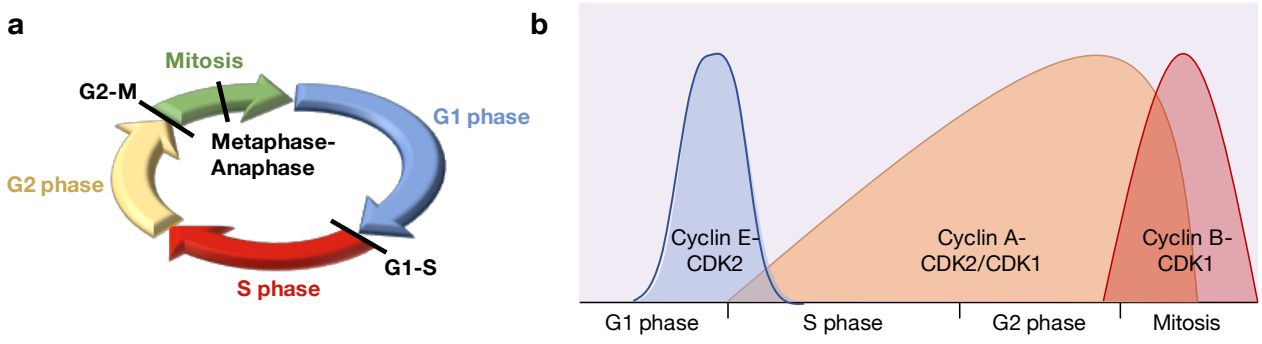

Figure 9: Overview of cell cycle regulation. (a) The human cell cycle is subdivided in four phases: G1, S, G2 and mitosis. In order to prevent, that cells divide despite the presence of DNA damages or failures in mitotic spindle formation, cycling cells have to go through three transitions, which are tightly controlled by so-called checkpoints. The transition from G1 to S and from G2 to mitosis requires the activation of Cyclin-dependent kinases (CDKs), whereas metaphase-to-anaphase transition is initiated by ubiquitin-dependent degradation of Cyclin B and other proteins by the APC complex. **(b)** Overview of cyclin-CDK activities at different cell cycle stages. Cyclin E-CDK2 becomes activated in late G1 phase and is crucial for initiation of S phase. Completion of S phase requires complex formation and activation of Cyclin A-CDK2/CDK1 and activity of Cyclin B-CDK1 regulates mitosis. [Figure adapted from (Hochegger, Takeda, and Hunt 2008)].

plate in order to prevent maldistribution of chromosomes. Once this is achieved, the spindle assembly checkpoint is satisfied and allows metaphase-to-anaphase transition and completion of cell division (Figure 9a) (Lara-Gonzalez, Westhorpe, and Taylor 2012).

The key players, which mediate a correct order of cell cycle events and phases, are Cyclin-dependent kinases (CDKs) in complex with different cyclins. Four different CDKs (CDK1, CDK2, CDK4 and CDK6) are involved in cell cycle progression and are only active upon binding of specific cyclins, the abundance of which is regulated in a cell cycle-dependent manner (Figure 9b) (Hochegger, Takeda, and Hunt 2008). In G1 phase, the activity of CDK4/6 in complex with Cyclin D is required for the activation of different transcription factors leading to expression of S phase genes (Ortega, Malumbres, and Barbacid 2002). Moreover, the entry into S phase necessitates Cyclin E-CDK2 activity, which phosphorylates different proteins involved in DNA replication and cell cycle progression (Honda et al. 2005). However, once the cell has initiated chromosome duplication, Cyclin E is rapidly degraded by SCF^{FBXW7}-mediated ubiquitylation and CDK2 and CDK1 become bound to Cyclin A to mediate progression through S phase and entry into mitosis (Figure 9b) (Katsuno et al. 2009; Koepp et al. 2001; Pagano et al. 1992; Vigneron et al. 2018). Last, many essential mitotic events require the activity of Cyclin B-CDK1, which is active until metaphase-to-anaphase transition, when Cyclin B becomes targeted for proteasomal degradation by the APC complex (Figure 9b) (Hershko 1999; Hochegger, Takeda, and Hunt 2008). Here, degradation of Cyclin B and therefore inactivation of CDK1 is necessary for mitotic exit and cell division. Besides the binding to specific, cell cycle-dependent cyclins, CDKs are regulated by CDK inhibitors, such as p21 and p27, but also by inhibitory or activating phosphorylation, which allows switch-like transitions into following cell cycle phases (Malumbres 2014). In addition, inhibitory phosphorylation as well as phosphorylation of mitotic proteins are reversed by phosphatases, which therefore allow cell cycle progression and mitotic exit (Novak et al. 2010).

Deregulation of the cell cycle can cause uncontrolled proliferation leading to cancer development. For instance, mutations or translocations in genes such as *KRAS* and *MYC*, which are involved in mitogen-driven signalling, can result in constitutive activation or uncontrolled expression, respectively, leading to cell cycle initiation independent of extracellular signals (Hobbs, Der, and Rossman 2016; Mateyak, Obaya, and Sedivy 1999; Otto and Sicinski 2017). Moreover, changes in the activity of CDKs and checkpoint proteins can cause uncontrolled progression through the cell cycle regardless of existing DNA damage and are often observed in cancer (Bartek, Lukas, and Lukas 2004; Kastan and Bartek 2004; Malumbres and Barbacid 2009). As a result, cells, which do not respond to the presence of DNA damage, transmit mutations to the daughter cells and, in case of unrepaired DNA double strand breaks, parts of chromosomes can be even lost during mitosis (Kops, Weaver, and Cleveland 2005). Overall, many rounds of cell cycle in the presence of unrepaired DNA damages causes genomic instability, a hallmark of cancer.

2.4.2 G1/S transition

The entry into the cell cycle and thus the transition from G1 to S phase requires the activation of the kinases CDK4/6 and CDK2 (Otto and Sicinski 2017). In order to avoid uncontrolled cell proliferation, this process is tightly regulated. First, binding of extracellular mitogens is necessary to initiate a signalling cascade resulting in the activation of the serine/threonine kinases CDK4 and CDK6 (referred to as CDK4/6), which have overlapping functions (Besson and Yong 2001). CDK4/6 activity is kept in check by binding to D-type cyclins (Cyclin D1-3) as well as by association to CDK inhibitors of the INK4 family (Anders et al. 2011; Malumbres and Barbacid 2001; Otto and Sicinski 2017). Once CDK4/6 are released from inhibitory proteins and activated by Cyclin D binding, they promote cell cycle entry by sequestering CDK inhibitors of the CIP/KIP family, such as p21 and p27, which bind and inhibit Cyclin E-CDK2 complex, and by phosphorylation of the retinoblastoma protein (RB1) (Ezhevsky et al. 2001; Harbour et al. 1999; Lundberg and Weinberg 1998; Sherr and Roberts 2004). Consequently, phosphorylated RB1 is released from E2F transcription factors, promoting their activity and resulting in expression of genes, which are necessary for G1/S transition, including Cyclin E (Morris and Dyson 2001). Subsequently, Cyclin E binds to CDK2 and Cyclin E-CDK2 complex further phosphorylates RB1 and other proteins, which drive initiation of S phase (Ezhevsky et al. 2001; Otto and Sicinski 2017). Furthermore, p27 and p21 are degraded by an SCF complex containing the F-box protein SKP2, thereby further promoting activation of Cyclin E-CDK2 complex (Bornstein et al. 2003; Carrano et al. 1999; Sutterluty et al. 1999). In early G1 phase, SKP2 is destabilized by the APC^{CDH1} ubiquitin E3 ligase and thus, SKP2 accumulation requires the inactivation of the APC, which is achieved by $SCF^{\beta\text{-}TrCP}$-mediated degradation of CDH1 (Fukushima et al. 2013; Wei et al. 2004). As a consequence of their involvement in cell cycle initiation, both F-box proteins, SKP2 and β-TrCP, are proto-oncogenes and linked to tumorigenesis (Wang et al. 2014).

2.5 Centrosomes

2.5.1 Centrosome functions and structure

Centrosomes are non-membranous organelles, which were first discovered in the late 1800s, and as primary microtubule organizing centres (MTOCs), they are involved in different cellular functions like cell division, motility, polarity and intracellular transport (Bettencourt-Dias and Glover 2007). Depending on the cell cycle stage, animal cells possess one or two centrosomes, which consist of two barrel-shaped centrioles embedded in the pericentriolar material (PCM). The proximal ends of the two centrioles, one mother and one daughter centriole, are arranged in close proximity at right angles to each other and are linked by interconnecting fibres (Conduit, Wainman, and Raff 2015). Both are composed of nine microtubule (MT) triplets, which form a cylindrical barrel-shaped structure with nine-fold symmetry. Here, the internal MT is called the A-tubule and it lies next to the middle B-tubule and the outer C-tubule, which is shorter and thus the distal end

of the centrioles only consists of MT doublets (Conduit, Wainman, and Raff 2015). Basis for the symmetry is thought to come from the central cartwheel structure, which is composed of SAS-6 oligomers and often lost in the older mother centriole (Kitagawa et al. 2011; van Breugel et al. 2011). In contrast to the younger daughter centriole, the older centriole reveals distal and sub-distal appendages, the latter contributing to anchorage of MTs (Paintrand et al. 1992; Piel et al. 2000). Besides the two centrioles, the PCM represents another important component of centrosomes and contains hundreds of proteins, which are important for structure, cellular signalling and cell cycle regulation (Andersen et al. 2003; Arquint, Gabryjonczyk, and Nigg 2014). In addition, the PCM also harbours the γ-tubulin ring complexes (γTuRCs), which contain γ-tubulin and five other proteins and serve as a template for MT protofilament nucleation (Moritz et al. 1995). Here, the growing MTs are polarized and are anchored with their minus ends at the centrosomes (Doxsey 2001). The PCM is organized as a concentrated ring around the mother centriole, in which the γTuRCs are localized in the middle layer. CEP152, CEP192 and NEDD1 are proteins found in the core of the PCM and play a critical role in centriole duplication (CEP152 and CEP192) and MT nucleation activity (CEP192 and NEDD1) (Lawo et al. 2012; Sonnen et al. 2012). In the outer layer, pericentrin forms fibrils, which point away from the mother centriole and together with CDK5RAP2 recruit γTuRCs to the PCM (Fong et al. 2008; Zimmerman et al. 2004).

The diverse functions of centrosomes are based on the ability to nucleate, anchor and release MTs (Bettencourt-Dias and Glover 2007). A central role of centrosomes is their function in the assembly of the mitotic spindle, which is important for proper chromosome segregation. In order to organize a bipolar spindle during mitosis, centrosomes must be duplicated once during S phase, resulting in two centrosomes forming the two opposite spindle poles, which are distributed respectively to the two daughter cells upon cell division (Doxsey 2001). In interphase cells, centrosomes are located in the centre of the cell in close proximity to the nucleus and are involved in the regulation of cell shape, polarity and motility (Bettencourt-Dias and Glover 2007; Tang and Marshall 2012). Moreover, in quiescent cells, centrosomes can move to the cell surface, where the mother centriole is converted into a basal body giving rise to a cilium (Vorobjev and Chentsov Yu 1982). Cilia play an important role in the detection and the movement of extracellular material and thus are indispensable for the function of specific cell types and during the development (Bettencourt-Dias and Glover 2007; Pazour and Witman 2003).

2.5.2 The centrosome cycle

In order to form a bipolar mitotic spindle and to transmit one centrosome to every daughter cell, centrosomes must be duplicated during the cell cycle. Like DNA replication, centrosome duplication is initiated at G1/S transition by Cyclin E-CDK2 and tightly regulated to ensure that the centrosome is duplicated only once during the cell cycle, thereby requiring a precise coordination with the cell cycle machinery (Doxsey 2001; Hinchcliffe and Sluder 2001). Failure in centrosome duplication can promote mis-segregation of chromosomes during mitosis, leading to genomic instability and cancer (Nigg 2002). Indeed, loss of centrosomes has been shown to lead

to p53-mediated cell cycle arrest at G1 or apoptosis (Bazzi and Anderson 2014; Lambrus et al. 2015; Wong et al. 2015).

The centrosome cycle involves three steps: centriole duplication, centrosome maturation and centriole disengagement (Bettencourt-Dias and Glover 2007). Centrosome duplication starts, when mother and daughter centrioles move apart at the transition from G1 to S phase. Subsequently, a new centriole (procentriole) is formed orthogonally to the proximal end of the two consisting centrioles during S phase (Doxsey 2001). The initiation of centriole duplication requires the two proteins CEP192 and CEP152, which recruit the kinase PLK4 to centrosomes, thereby promoting centrosome duplication (Sonnen et al. 2013). During G1 phase, CEP192 is localized to the walls of mother and daughter centrioles, whereas CEP152 can be only found at the proximal end of the mother centriole (Kim, Park, et al. 2013; Sonnen et al. 2013). At this time, PLK4 is associated with the mother centriole and forms a ring-like structure. However, at the transition to S phase, CEP152 and PLK4 become re-localized to the daughter centriole, which likely depends on CEP192 (Kim, Park, et al. 2013). Fully activated PLK4 in turn recruits SAS-6 and phosphorylates STIL, which form the cartwheel structure providing the nine-fold symmetry of the new centriole (Dzhindzhev et al. 2014; Kitagawa et al. 2011; Ohta et al. 2014; van Breugel et al. 2011). Last, CPAP and CEP135 associate with the outer structure of the cartwheel and mediate the assembly of the centriolar MTs. (Lin et al. 2013; Tang et al. 2009; Tang et al. 2011). Due to its central role in the initiation of centriole duplication, PLK4 needs to be tightly regulated in order to avoid centrosome loss or amplification. Indeed, overexpression of PLK4 has been shown to increase centriole numbers whereas depletion leads to centriole loss (Habedanck et al. 2005). In order to avoid centrosome reduplication, auto-phosphorylation of PLK4 generates a phospho-degron, which leads to ubiquitylation-mediated degradation of PLK4 by $SCF^{\beta\text{-}TrCP}$ (Cunha-Ferreira et al. 2009; Guderian et al. 2010; Holland et al. 2010).

Upon entry in mitosis, the PCM is dramatically expanded and its MT nucleation activity is strongly increased by the recruitment of γTuRCs (Palazzo et al. 2000; Woodruff, Wueseke, and Hyman 2014). This process is termed centrosome maturation and requires the activity of the mitotic kinases PLK1 and Aurora kinase A, which are recruited by CEP192 (Haren, Stearns, and Luders 2009; Joukov, Walter, and De Nicolo 2014; Kinoshita et al. 2005). For instance, PLK1-mediated phosphorylation of pericentrin and CEP192 is required for the recruitment of PCM proteins (Joukov, Walter, and De Nicolo 2014; Lee and Rhee 2011). Furthermore, phosphorylation of another protein kinase called NEK9 leads to phosphorylation of NEDD1, which together with CEP192 recruits γ-tubulin to the PCM (Gomez-Ferreria et al. 2012; Gomez-Ferreria et al. 2007; Sdelci et al. 2012). Besides the role in centrosome maturation, the CEP192-dependent Aurora A-PLK1 activity has been shown to be important for bipolar spindle formation and centriole disengagement (Joukov, Walter, and De Nicolo 2014). Like sister chromatids, centrioles are closely linked by cohesin protein complexes and centrosome engagement is important to prevent reduplication of centrioles, whereas their separation is required for centriole duplication in the next cell cycle (Tsou and Stearns 2006). Thus, a controlled coordination with the cell cycle is

indispensable and is achieved by the activation of a protein called separase, which becomes active at the metaphase-to-anaphase transition and cleaves cohesin of both, sister chromatids and centrioles (Schockel et al. 2011).

2.6 Aim of the study

The ubiquitin proteasome system (UPS) plays a pivotal role in cancer cells and many tumours depend on the ubiquitin-mediated degradation of tumour suppressors or the stabilization of oncogenes. Due to the crucial function of the UPS in cell proliferation and apoptosis, deregulation of its key components can be often found in cancer cells and thus, the UPS represents an attractive target in anti-cancer therapy (Shen et al. 2013). Indeed, the successful treatment of multiple myeloma (MM) patients with proteasome inhibitors such as bortezomib confirms that targeting the components of the UPS represents a valuable anticancer strategy. In order to identify and characterize the significance of unknown F-box proteins and deubiquitinases (DUBs) in the pathophysiology of cancer, the aim of this study was first to perform a multi-OMICs screening approach in MM cells (Results I and Discussion I) and second to evaluate a potential role of the orphan F-box protein FBXL13 in tumorigenesis (Results II and Discussion II).

Given the good responsiveness of MM patients to proteasomal inhibition, this study aimed to identify unknown oncogenic F-box proteins and DUBs in a human MM cell line and to unravel the responsible substrate and cellular mechanisms promoting the progression of MM. To this end, an unbiased multi-OMIC screening approach was performed starting with a CRISPR/Cas9 screen for all F-box proteins and DUBs in a human MM cell line. Two separate sgRNA libraries were generated allowing a pooled negative selection screen and the identification of targeted genes by next generation sequencing (NGS). Having identified a promising candidate, its biological relevance in various MM cell lines was elucidated and the respective substrate was determined by performing two mass spectrometry-based screening approaches comprising an affinity purification and a non-affinity-based proximity dependent biotin identification (BioID). Subsequently, a broad range of biochemistry-based analyses aimed to characterize the binding of the identified interaction partner and to confirm its role as a bona-fide substrate. Finally, the relevance of this interaction was analysed in various MM cell lines as well as in primary patient material.

The second part of this study aimed at the characterization of the orphan F-box protein FBXL13 in centrosome homeostasis and its potential involvement in tumorigenesis. Recent reports suggested an implication of FBXL13 in cancer, however, it is not clear whether FBXL13 acts as a tumour suppressor or as an oncogene (Barretina et al. 2012; Curtiss et al. 2005; Paulsen et al. 2009). So far, no cellular function of FBXL13 has been described, but previous studies found FBXL13 to be associated with several centrosomal proteins, linking FBXL13 to centrosome function (Fung 2017; Tan et al. 2013). Given the implication of aberrant centrosome assembly in cancer, the aim of this study was to investigate whether the centrosomal protein CEP192 represents a ubiquitylation substrate of FBXL13 and how FBXL13 is involved in centrosome

function. Furthermore, a potential contribution of dysfunctions in the FBXL13-substrate pathway to the pathophysiology of cancer was assessed.

Overall, the present study aimed to gain new insights into mechanisms leading to a deregulation of the UPS and contributing to cancer progression. Thus, the identification of novel targets within the UPS would provide new biomarkers and targets for molecular therapies in MM and other cancer types.

3 Material

3.1 Devices and instruments

Device	Manufacturer
Analytic balance ABJ 220	Kern & Son
Aqualine water bath	Lauda-Brinkmann
Axiovert 40 CFL with HBO50	Carl Zeiss
Centrifuge 5417R with rotor F453011	Eppendorf
Centrifuge 5424 with rotor FA452411	Eppendorf
Concentrator plus	Eppendorf
E-Box VX2 Imager	Vilber
Electroporater, GenePulser	Bio-Rad Laboratories
FACSAria III	BD Biosciences
FACSCalibur	BD Biosciences
FluoView FV 10i	Olympus
Fridges and lab freezers	Liebherr
HERAcell 150i CO_2 incubator	Thermo Fisher Scientific
HERAfreeze	Thermo Fisher Scientific
HERASafe KS safety cabinet	Thermo Fisher Scientific
Hypercassette™	Amersham Biosciences
Innova® 40 shaker for bacteria	New Brunswick Scientific
IX Inverted Fluorescence Microscope	Olympus
Invitrogen Chamber for Ready Gels	Invitrogen
LightCycler 480 System	Roche
LS4800 liquid nitrogen tank	Taylor-Wharton Lab Systems
LTQ Orbitrap Velos mass spectrometer	Thermo Fisher Scientific
MACS MultiStand	Miltenyi Biotec
Magnetic thermo stirrer RCT basic	IKA Laboratory Equipment
Mastercycler nexus	Eppendorf
MidiMACS Separator	Miltenyi Biotec
Mini-PROTEAN Tetra cell SDS electrophoresis system	Bio-Rad Laboratories
Mini-Sub® Cell GT system for agarose electrophoresis	Bio-Rad Laboratories
MiSeq system	Illumina
Multifuge 3SR+	Thermo Fisher Scientific
NanoPhotometer	Implen
Neubauer chamber	Marienfeld
Novex Mini cell system for precast NuPAGE gels	Thermo Fisher Scientific
peqSTAR Thermocycler	Peqlab Biotechnology

Pipetman neo (P2N, P10N, P20N, P100N, P200N and P1000N)	Gilson
Polymax 1040 platform shaker	Heidolph Instruments
PowerPac Basic power supply	Bio-Rad Laboratories
PowerPac HC power supply	Bio-Rad Laboratories
Precision balance 572-37	Kern & Son
Scanner V750 Pro	Epson
SevenCompact pH/Ion pH-meter	Mettler-Toledo
Sorvall® RC-5B with rotors SS-24 and GS-3	Du Pont Instruments
SRX-101A developer	Konica-Minolta
Thermo block MBT250	Kleinfeld Labortechnik
Thermomixer compact	Eppendorf
Tube rotator	Fröbel Labortechnik
Tumbling roller mixer RM5	Neolab

3.2 Consumables

Consumable	Manufacturer
3mm CHR paper (Whatman)	GE Healthcare
Cell culture flasks	Greiner Bio-One
Cell culture plates	Biochrom/Falcon
Cell scraper	Sarstedt
Clear qPCR sealers	Steinbrenner Laborsysteme
CL-XPosure™ Films	Thermo Fisher Scientific
Cryo tubes	Sarstedt
Eppendorf twin.tec PCR plates, semi-skirted, 96 well	Eppendorf
Graduated tubes	Greiner Bio-One
Hypodermic needles	Braun
Immobilon-P PVDF transfer membrane	Millipore
LightCycler 480 Multiwell Plate 96, white	Roche
LS columns	Miltenyi Biotec
Pipette tips	Sarstedt
SafeSeal tubes	Sarstedt
Serological pipettes	Greiner Bio-One
Syringe filters	TPP/Biochrom
Syringes	Braun
UVette routine pack	Eppendorf
x-well chamber slides on PCA detachable	Sarstedt

3.3 Chemicals and reagents

Chemical/reagent	Manufacturer
2-Mercaptoethanol	Sigma-Aldrich
2-Propanol	Carl Roth
3x FLAG Peptide	Sigma-Aldrich
5-Bromo-2′-deoxyuridine (BrdU)	Sigma-Aldrich
Acetic acid glacial	Carl Roth
Acetone	Carl Roth
Adefodur developer solution	Adefo Chemistry
Adefo-Fix fixer solution	Adefo Chemistry
Adenosine 5´-triphosphate (ATP)	Sigma-Aldrich
Agarose NEEO	Carl Roth
Albumin Fraction V (BSA)	Carl Roth
Ammonium persulfate (APS)	Sigma-Aldrich
Ampicillin sodium salt	Sigma-Aldrich
Anti-FLAG M2 Affinity Gel	Sigma-Aldrich
Anti-HA-Agarose	Sigma-Aldrich
Aprotinin from bovine lung	Sigma-Aldrich
Aqua ad injectabilia, sterile	B. Braun Melsungen
Bacfectin	Clontech
Bacto Agar	BD Diagnostics
Bacto Tryptone	BD Diagnostics
Bacto Yeast Extract	BD Diagnostics
BES buffered saline	Sigma-Aldrich
Beta-Glycerolphosphate disodium salt hydrate (G-2-P)	Sigma-Aldrich
Biotin	Sigma-Aldrich
Blasticidin S HCl	Thermo Fisher Scientific
Boric acid	Sigma-Aldrich
Bortezomib	Janssen-Cilag
Brilliant Blue R 250	Carl Roth
Bromphenol Blue	Sigma-Aldrich
Calcium chloride dihydrate	Sigma-Aldrich.
Cycloheximide (CHX)	Sigma-Aldrich
Deoxycholic acid sodium salt	Sigma-Aldrich
Dimethylsulfoxid (DMSO)	Carl Roth
Di-Sodium hydrogene phosphate dihydrate	Merck
DL-Dithiothreitol	Sigma-Aldrich
DNA Loading Dye (6x)	Thermo Fisher Scientific

dNTP Mix, 10 mM each	Thermo Fisher Scientific
Dodecylsulfate-Na-salt (in pellets, SDS))	SERVA
Ethanol	Merck
Ethylenediaminetetraacetic acid (EDTA)	Sigma-Aldrich
Ethylene-bis(oxyethylenenitrilo)tetraacetic acid (EGTA)	Sigma-Aldrich
FACS Flow	BD Biosciences
Fluoride ion solution (NaF)	Sigma-Aldrich
GelRed Nucleic Acid Gel Stain	Biotium
Glucose	Sigma-Aldrich
Glutathione Sepharose 4B	GE Healthcare
Glycerol	Sigma-Aldrich
Glycin	Carl Roth
HA-ubiquitin-vinyl sulfone (HA-Ub-VS)	BostonBiochem
Hexadimethrine bromide (polybrene)	Sigma-Aldrich
Hexanucleotide Mix, 10x conc.	Roche
Hydrochloric acid 32%	Carl Roth
Hydrochloric acid fuming 37%	Carl Roth
Imidazole	Sigma-Aldrich
Kanamycin sulfate	Sigma-Aldrich
Leupeptin	Sigma-Aldrich
L-Glutathione reduced	Sigma-Aldrich
Lipofectamine 2000 Reagent	Thermo Fischer Scientific
Lipofectamine RNAiMAX Reagent	Thermo Fischer Scientific
LightCycler 480 SYBR Green I Master	Roche
Magnesium chloride anhydrous	Sigma-Aldrich
Magnesium sulfate anhydrous	Sigma-Aldrich
Methanol	J. T. Baker
MG132	Tocris
N-(2-Hydroxyethyl)piperazine-N`-2-ethane sulfonic acid (HEPES)	SERVA
Nα-Tosyl-L-lysine chloromethyl ketone hydrochloride (TLCK)	Sigma-Aldrich
Ni-NTA Agarose	Qiagen
N,N,N`,N``-tetramethyl-ethylenediamine (TEMED)	Sigma-Aldrich
N-p-Tosyl-L-phenylalanine chloromethyl ketone (TPCK)	Sigma-Aldrich
Nocodazole	Sigma-Aldrich
Nonidet P-40 substitute (10%)	Roche
NuPAGE MES SDS Running buffer (20x)	Thermo Fisher Scientific
Okadaic Acid Prorocentrum sp.	Calbiochem
Palbociclib	Sigma-Aldrich
Paraformaldehyde, powder (PFA)	Sigma-Aldrich
PBS Dulbecco, powder	Biochrom

Phenylmethanesulfonylfluoride solution (PMSF)	Sigma-Aldrich
PI/RNase staining buffer	BD Pharmingen
Ponceau S solution	Sigma-Aldrich
Potassium chloride	Sigma-Aldrich
Propidium iodide (PI)	Sigma-Aldrich
Protein A Sepharose CL-4B	GE Healthcare
Protein G Agarose, Fast Flow	Sigma-Aldrich
Protein G Sepharose 4 Fast Flow	GE Healthcare
Puromycin	Thermo Fisher Scientific
RNaseOUT Recombinant Ribonuclease Inhibitor	Thermo Fisher Scientific
Rotiphorese NF-Acrylamide/Bis-solution 40% (29:1)	Carl Roth
SERVA DNA Stain Clear G	SERVA Electrophoresis
Silver nitrate	Sigma-Aldrich
Skim Milk Power	Sigma-Aldrich
SlowFade Gold antifade Reagent with DAPI	Thermo Fisher Scientific
SOC Medium	New England Biolabs
Sodium acetate	Merck
Sodium azide	Merck
Sodium carbonate	Merck
Sodium chloride	Carl Roth
Sodium dihydrogen phosphate monohydrate	Merck
Sodium fluoride	Sigma-Aldrich
Sodium hydroxide solution 45%	Carl Roth
Sodium orthovanadate	Sigma-Aldrich
Sodium phosphate dibasic	Sigma-Aldrich
Sodium tetraborate	Sigma-Aldrich
Sodium thiosulfate pentahydrate	Sigma-Aldrich
Strep-Tactin Superflow	IBA Lifesciences
SuperSignal West Pico Chemiluminescent Substrate	Thermo Fisher Scientific
SuperSignal West Femto Maximum Sensitivity Substrate	Thermo Fisher Scientific
Thymidine	Sigma-Aldrich
Trichloroacetic acid solution	Sigma-Aldrich
Tris	Carl Roth
Triton X-100	Sigma-Aldrich
Trypsin inhibitor from soybean	Sigma-Aldrich
Tween 20	Sigma-Aldrich
UltraPure TBE buffer (10x)	Thermo Fisher Scientific
Water	Sigma-Aldrich

3.4 Commercial kits

Kit	Manufacturer
DC Protein Assay	Bio-Rad
DNeasy Blood and Tissue Kit	Qiagen
GeneJET Gel Extraction Kit	Thermo Fisher Scientific
KAPA Library Quantification Kit	Kapa Biosystems
MiSeq Reagent Kit v2	Illumina
NucleoBond Xtra Midi	MACHEREY-NAGEL
peqGOLD Plasmid Miniprep Kit	Peqlab
PhiX Control v3	Illumina
QIAquick PCR Purification Kit	Qiagen
QIAshredder	Qiagen
Rapid DNA Dephos & Ligation Kit	Roche
RNeasy Mini Kit	Qiagen
SuperScript III First-Strand Synthesis System	Invitrogen
TNT T7 Coupled Reticulocyte Lysate System	Promega

3.5 Enzymes

Enzyme	Manufacturer
AgeI (BshTI)	Thermo Fisher Scientific
Alkaline Phosphatase, Calf Intestinal (CIP)	New England Biolabs
Antarctic Phosphatase	New England Biolabs
BamHI	Thermo Fisher. Scientific
BsmBI	New England Biolabs
EcoRI	Thermo Fisher Scientific
DNase I	New England Biolabs
DpnI	Thermo Fisher Scientific
HpaI	New England Biolabs
KpnI	Thermo Fisher Scientific
Lambda Protein Phosphatase	New England Biolabs
NcoI	Thermo Fisher Scientific
NheI	Thermo Fisher Scientific
NotI	Thermo Fisher Scientific
Pfu Ultra II DNA Polymerase	Agilent Technologies
SalI	Thermo Fisher Scientific
T4 DNA Ligase	Thermo Fisher Scientific
T4 Polynucleotide Kinase	New England Biolabs

XbaI	Thermo Fisher Scientific
XhoI	Thermo Fisher Scientific

3.6 Oligonucleotides

All oligonucleotides were purchased from Eurofins Genomics, Ebersberg, Germany.

3.6.1 Cloning oligonucleotides

Oligonucleotide	Sequence (5'-3')
FBXL13_AgeI_rv	GCCACCGGTTCACGCTGCTTGGTCTTCAC
FBXL13_HpaI_fw	GCCGTTAACATGACTCCGGAATTGATGATAAAAGCC
FBXL13_HpaI_rv	GCCGTTAACTCACGCTGCTTGGTCTTCACTG
FBXL13_KpnI_fw	GCCGGTACCGCCACCATGACTCCGGAATTGATGATAAAAG
FBXL13_NotI_fw	GCCGCGGCCGCGCCACCATGACTCCGGAATTGATG
FBXL13_SalI_fw	GCCGTCGACATGACTCCGGAATTGATGATAAAAG
FBXL13_XbaI_fw	GCCTCTAGAGCCACCATGACTCCGGAATTGATGATAAAAG
FBXL13_XbaI_rv	GCCTCTAGATCACGCTGCTTGGTCTTCACTG
FBXL16_BamHI_rv	GCCGGATCCCTACTCAATGACGAGGCAGCGGGGCAGG
FBXL16_EcoRI_fw	GCCGAATTCTCGAGCCCGGGCATCGACGGCGACCCCA
FBXL16_XbaI_rv	GCCTCTAGACTACTCAATGACGAGGCAGCGGGGCAG
LIN28B_BamHI_fw	GCCGGATCCATGGCCGAAGGCGGG
LIN28B_29_BamHI_fw	GCCGGATCCCGCGGAACTGGCC
LIN28B_103_BamHI_fw	GCCGGATCCGGTGGGAGCCCCTGTTTA
LIN28B_167_BamHI_fw	GCCGGATCCAAAAATGTTGCACAGCCACCC
LIN28B_BamHI_rv	CCGGGATCCTTATGTCTTTTTCCTTTTTTGAACTGAAGG
LIN28B_NotI_rv	GCCGCGGCCGCTTATGTCTTTTTCCTTTTTTGAAC
LIN28B_102_NotI_rv	GCCGCGGCCGCTTAAGGTCCTGTTACC
LIN28B_166_NotI_rv	GCCGCGGCCGCTTAATGTGGGCAGTTT
LIN28B_XbaI_fw	CCGTCTAGAGCCACCATGGCCGAAGGC
OTUB1_BamHI_fw	GCCGGATCCATGGCGGCGGAG
OTUB1_NotI_rv	GCCGCGGCCGCCTATTTGTAGAGGAT
OTUD2_BamHI_fw	GCCGGATCCATGTTTGGCCCCGCTAAAG
OTUD2_NotI_rv	GCCGCGGCCGCTCACACTTCTCCA
OTUD6A_BamHI_fw	GCCGGATCCATGGATGATCCGAAGAGTGAAC
OTUD6A_NotI_rv	GCCGCGGCCGCCTACAGGAGAC
OTUD6B_BamHI_fw (IF1)	CCGGGATCCATGGAGGCGGTATTG
OTUD6B_BamHI_fw (IF2)	CCGGGATCCATGATATCTAAGGAAAAGAAAGCTG
OTUD6B_BamHI_rv	CCGGGATCCGCTGCAATTTTCAGTAACTATG
OTUD6B_BamHI_pHIV_rv	CCGGGATCCTTAGCTGCAATTTTCAGTAACTATG

OTUD6B_C158A_fw	CCATCTGATGGCCACGCTATGTATAAAGCCATTGAAG
OTUD6B_C158A_rv	CTTCAATGGCTTTATACATAGCGTGGCCATCAGATGG
OTUD6B_EcoRI_Koz_fw (IF1)	CCGGAATTCGCCACCATGGAGGCGGTATTG
OTUD6B_EcoRI_Koz_fw (IF2)	CCGGAATTCGCCACCATGATATCTAAGGAAAAGAAAGCTG
OTUD6B_EcoRI_rv	CCGGAATTCTTAGCTGCAATTTTCAGTAACTATG
OTUD6B_S99A_fw	AATCAGCCACCTCGGATAGCAAAAGCACAAAAGAGACGG
OTUD6B_S99A_rv	TTTCCCGTCTCTTTTGTGCTTTTGCTATCCGAGGTGGCT
OTUD6B_XbaI_fw (IF1)	CCGTCTAGAGCCACCATGGAGGCGGTATTGACC
OTUD6B_XbaI_fw (IF2)	CCGTCTAGAGCCACCATGATATCTAAGGAAAAG
OTUD6B_XbaI_rv	CCGTCTAGATTAGCTGCAATTTTCAGTAACTATG
OTUD6B_XhoI_fw (IF1)	CCGCTCGAGATGGAGGCGGTATTG
OTUD6B_XhoI_fw (IF1)	CCGCTCGAGATGATATCTAAGGAAAAGAAAGCTG

3.6.2 Oligonucleotides for amplicon deep-sequencing

Oligonucleotides for amplicon generation were designed according to the Illumina's dual indexing strategy using a two-step protocol.

Oligonucleotide	Sequence (5'-3') (**Illumina 5' tails** and locus specific sequence)
Seq-adapt_Fw	TCGTCGGCAGCGTCAGATGTGTATAAGAGACAGCTTGAAAGTATTTCGATTTCTTGGC
Seq_adapt_Rv	GTCTCGTGGGCTCGGAGATGTGTATAAGAGACAGACTCGGTGCCACTTTTTCAAG

Oligonucleotide	Sequence (5'-3') (**Index sequence**)
NGS_i5_S505	AATGATACGGCGACCACCGAGATCTACAC**GTAAGGAG**TCGTCGGCAGCGTC
NGS_i5_S506	AATGATACGGCGACCACCGAGATCTACAC**ACTGCATA**TCGTCGGCAGCGTC
NGS_i7_N701	CAAGCAGAAGACGGCATACGAGAT**TCGCCTTA**GTCTCGTGGGCTCGG
NGS_i7_N702	CAAGCAGAAGACGGCATACGAGAT**CTAGTACG**GTCTCGTGGGCTCGG
NGS_i7_N704	CAAGCAGAAGACGGCATACGAGAT**GCTCAGGA**GTCTCGTGGGCTCGG
NGS_i7_N705	CAAGCAGAAGACGGCATACGAGAT**AGGAGTCC**GTCTCGTGGGCTCGG

3.6.3 qPCR oligonucleotides

Oligonucleotide	Sequence (5'-3')	
CEP192_fw	TCCCTCGACTCACACTCTTCT	(Primer-BLAST; NCBI)
CEP192_rv	TTTGGTGAGGACACTCTGCC	(Primer-BLAST; NCBI)
FBXL13_fw	GCACTGGCCATTTACTGCATTAACC	(Fung 2017)

FBXL13_rv	GCTGCCTTCTTGGAAATATTTGTGC	(Fung 2017)
HMGA1_fw	TCCAGGAAGGAAACCAAGG	(Akaboshi et al. 2009)
HMGA1_rv	AGGACTCCTGCGAGATGC	(Akaboshi et al. 2009)
LIN28A_fw	GAGTGAGAGGCGGCCAAAA	(Yang, Bennett, et al. 2015)
LIN28A_rv	TGATGATCTAGACCTCCACAGTTGTAG	(Yang, Bennett, et al. 2015)
LIN28B_fw	GCCCCTTGGATATTCCAGT	(Manier et al. 2017)
LIN28B_rv	TGACTCAAGGCCTTTGGAAG	(Manier et al. 2017)
MYC_fw	TCAAGAGGCGAACACACAAC	(Segalla et al. 2015)
MYC_rv	GGCCTTTTCATTGTTTTCCA	(Segalla et al. 2015)
OTUD6B_fw	ATTGACCGAAGAGCTTGATGAGG	(QuantPrime)
OTUD6B_rv	TTGGCTTGCAACTCCTTCTTCTC	(QuantPrime)
RPLP0_fw	GATTGGCTACCCAACTGTTG	(Fritah et al. 2005)
RPLP0_rv	CAGGGGCAGCAGCCACAAA	(Fritah et al. 2005)

3.6.4 Sequencing oligonucleotides

Standard sequencing primers were provided by Eurofins Genomics, Ebersberg, Germany. Sequences of additional primers used for sequencing in this study are listed below.

Oligonucleotide	Sequence (5'-3')
CEP192_seq1_fw	TGTTTTATGATGATCATTTG
CEP192_seq2_fw	GAACAACTGGCAATTCCAGGAATG
FBXL13_seq1_fw	CACTCTTATATGGAAGACCA
FBXL13_seq2_fw	CTGAGGGCTGCCCGGGGGTCCTG
FBXL13_seq3_fw	GTATCAATAGATCTCTCTGGAAC
FBXL16_fw	CACCTCGCTGAGCGTGAGTGACTGC
hU6_fw	ATTTCTTGGGTAGTTTGCAG
pHIV_fw	TGGAATTTGCCCTTTTTGAG
pHIV_rv	AGGAACTGCTTCCTTCACGA

3.7 Sequences of shRNAs and siRNAs

3.7.1 Sequences of shRNAs

Sequences of shRNAs were designed using the GPP Web Portal from the Broad Institute and ordered as following sequences in order to ligate the annealed shRNAs into the pLKO.1 TRC cloning vector:

Forward Oligo:

5'-CCGG-Target sequence-CTCGAG-Reverse complement target sequence-TTTTTG-3'

Reverse Oligo:

5'-AATTCAAAAA- Target sequence-CTCGAG-Reverse complement target sequence-3'

shRNA	Target sequence (5'-3')
shFBXL13	CTAAAGGAGCCTTAGAATTAA
shLIN28B	GCAGGCATAATAAGCAAGTTA
shOTUD6B-1	CAGCTAGACAGTTAGAAATTA
shOTUD6B-2	TGGCTTAGGAGAACATTATAA
shOTUD6B-3	GATTTGTCTTACCAGATATTT
shControl	CCTAAGGTTAAGTCGCCCTCG

3.7.2 Sequences of siRNAs

siRNA	Target sequence (5'-3')	Origin
siCEP152	GCGGATCCAACTGGAAATCTA	(Graser et al. 2007)
siCEP192	GCUUAAACUGCAAGUUUCAAUCAGA	(O'Rourke et al. 2014)
siFBXL13	UCAGAUAGGCUGCAAACAA	Dharmacon #J-016001-08
siGL	CGTACGCGGAATACTTCGA	(Elbashir et al. 2001)
siOTUD6B	GGAGCGAGAAGAACGGAUA	Dharmacon #J-008553-05
siRIOK3	GCUGAAGGACCAUUUAUUA	Dharmacon #J-005040-07
	GCAGGAAUGUCUCGCAGUU	Dharmacon #J-005040-08
	UUAAAGAUCGCUUCAGUAA	Dharmacon #J-005040-09
	GAAAGGAGUCUGUUGUCUU	Dharmacon #J-005040-10

3.8 Plasmids

Plasmid	Origin
pcDNA3.1(+) zeo	Thermo Fisher Scientific
pcDNA3.1-OTUD6B isoform1	C. Richter, this study
pcDNA3.1-OTUD6B C158A isoform1	C. Richter, this study
pcDNA3.1-N-myc-BioID2-MCS	Addgene (#74223), K. Roux
pcDNA3.1-N-myc-BioID2-OTUD6B isoform1	M. Walzik, this study
pcDNA3.1-N-myc-BioID2-OTUD6B isoform2	M. Walzik, this study
pcDNA3.1-N-FLAG	Prof. F. Bassermann
pcDNA3.1-N-FLAG-CEP192	C. Richter, this study
pcDNA3.1-N-FLAG-CEP192 AA 1-630	C. Richter, this study
pcDNA3.1-N-FLAG-FBXL13	E. Fung
pcDNA3.1-N-FLAG-FBXL13 AA 1-735	E. Fung
pcDNA3.1-N-FLAG-FBXL13 AA 1-151	E. Fung
pcDNA3.1-N-FLAG-FBXL13 AA 1-198	E. Fung
pcDNA3.1-N-FLAG-FBXL13 AA 199-735	E. Fung
pcDNA3.1-N-FLAG-LIN28B	C. Richter, this study
pcDNA3.1-N-FLAG-OTUB1	C. Richter, this study

pcDNA3.1-N-FLAG-OTUD2	C. Richter, this study
pcDNA3.1-N-FLAG-OTUD6A	C. Richter, this study
pcDNA3.1-N-FLAG-OTUD6B isoform1	M. Walzik, this study
pcDNA3.1-N-FLAG-OTUD6B isoform2	M. Walzik, this study
pcDNA3.1-N-FLAG-OTUD6B C158A isoform1	M. Walzik, this study
pcDNA3.1-N-FLAG-OTUD6B S99A isoform1	C. Richter, this study
pcDNA3.1-N-HA	Prof. F. Bassermann
pcDNA3.1-N-HA-LIN28B	C. Richter, this study
pcDNA3.1-N-HA-LIN28B AA 1-102	C. Richter, this study
pcDNA3.1-N-HA-LIN28B AA 1-166	C. Richter, this study
pcDNA3.1-N-HA-LIN28B AA 29-250	C. Richter, this study
pcDNA3.1-N-HA-LIN28B AA 103-250	C. Richter, this study
pcDNA3.1-N-HA-LIN28B AA 167-250	C. Richter, this study
pMD2.G	Addgene (#12259), D. Trono
psPAX2	Addgene (#12260), D. Trono
pHIV-EGFP-OTUD6B isoform1	M. Walzik, this study
pHIV-EGFP-OTUD6B isoform2	M. Walzik, this study
pHIV-EGFP-OTUD6B C158A isoform1	C. Richter, this study
lentiCas9-Blast	Addgene (#52962), F. Zhang
lentiGuide-GFP	O. Karpiuk, this study
lentiGuide-GFP FBXO3	O. Karpiuk, this study
lentiGuide-GFP-NT	O. Karpiuk, this study
lentiGuide-GFP-OTUD6B-1	C. Richter, this study
lentiGuide-GFP-OTUD6B-2	C. Richter, this study
lentiGuide-GFP-OTUD6B-3	C. Richter, this study
lentiGuide-GFP-POLR2I-1	C. Richter, this study
lentiGuide-GFP-POLR2I-2	C. Richter, this study
lentiGuide-GFP-RPL8-1	C. Richter, this study
lentiGuide-GFP-RPL8-2	C. Richter, this study
lentiGuide-GFP-USP24	O. Karpiuk, this study
lentiGuide-mCherry	O. Karpiuk, this study
pLKO.1 TRC cloning vector	Addgene (#10878), D. Root
pLKO.1-Puro-sh_scramble	Addgene (#1864), D. Sabatini
pLKO.1-Puro-shLIN28B	C. Richter, this study
pLKO.1-Puro-shOTUD6B-1	M. Walzik, this study
pLKO.1-Puro-shOTUD6B-2	M. Walzik, this study
pLKO.1-Puro-shOTUD6B-3	M. Walzik, this study
pLKO.1-GFP-sh_scramble	F. Loewecke
pLKO.1-GFP-shOTUD6B-1	M. Walzik, this study
pLKO.1-GFP-shOTUD6B-2	M. Walzik, this study

pLKO.1-GFP-shOTUD6B-3	M. Walzik, this study
VSV-G	Addgene (#14888), T. Reya
GAG/POL	Addgene (#14887), T. Reya
pBABE-Puro	Addgene (#1764), H. Land, J. Morgenstern, B. Weinberg
pBABE-Puro-FBXL13	E. Fung
pBABE-Puro-FBXL13 ΔF-box	E. Fung
pRK5-HA-Ubiquitin-K48	Addgene (#17605), T. Dawson
pRK5-HA-Ubiquitin-WT	Addgene (#17608), T. Dawson

3.9 Bacteria

Bacteria strain	Manufacturer
Endura ElectroCompetent Cells	Lucigen
NEB 5-alpha competent *E. coli*	New England Biolabs

3.10 Standards for DNA and proteins electrophoresis

Standard	Manufacturer
GeneRuler 1 kb DNA Ladder	Thermo Fisher Scientific
PageRuler Plus Prestained Protein Ladder	Thermo Fisher Scientific

3.11 Antibodies

3.11.1 Primary antibodies

Antibody (clone)	Species	Dilution	Manufacturer (Catalog#)
α-tubulin (DM1A)	Mouse	1:1000 (WB), 1:500 (IF)	Sigma-Aldrich (#T9026)
α/β-tubulin	Rabbit	1:1000 (WB)	Cell Signaling Technology (#2148)
Cas 9 (7A9-3A3)	Mouse	1:1000 (WB)	Active Motif (#61577)
Centrin-2	Rabbit	1:1000 (WB)	Santa Cruz Biotechnology (#sc-27793)
Centrin-3 (SS12)	Mouse	1:1000 (WB)	Santa Cruz Biotechnology (#sc-100933)
CEP152	Rabbit	1:500 (WB)	Kind gift of Prof. Erich A. Nigg
CEP192	Rabbit	1:1000 (WB)	Kind gift of Prof. Laurence Pelletier
β-actin (AC-15)	Mouse	1:5000 (WB)	Sigma-Aldrich (#A-1978)
c-MYC (9E10)	Mouse	1:500 (WB)	Santa Cruz Biotechnology (#sc-40)
CUL1 (2H4C9)	Mouse	1:500 (WB)	Sigma-Aldrich (#32-2400)
Cyclin A (H-432)	Mouse	1:1000 (WB)	Santa Cruz Biotechnology (#sc-751)
Cyclin B1	Rabbit	1:1000 (WB)	Cell Signaling Technology (#4138)
Cyclin D1 (G124-326)	Mouse	1:500 (WB)	BD Biosciences (#554180)

Cyclin E (HE12)	Mouse	1:1000 (WB)	Santa Cruz Biotechnology (#sc-247)
FBXL16	Rabbit	1:1000 (WB)	Thermo Fisher Scientific (#PA5-21094)
FLAG	Rabbit	1:1000 (WB)	Sigma-Aldrich (#F7425)
HA	Rabbit	1:1000 (WB)	Cell Signaling Technology (#3724)
LIN28A	Rabbit	1:1000 (WB)	Cell Signaling Technology (#3978)
LIN28B	Rabbit	1:1000-10000 (WB)	Cell Signaling Technology (#4196)
OTUD6B	Rabbit	1:1000 (WB)	Abcam (#ab127714)
p27 (G173-524)	Mouse	1:500 (WB)	BD Biosciences (#554069)
p53	Rabbit	1:1000 (WB)	Cell Signaling Technology (#9282)
p-p53 (S15)	Rabbit	1:1000 (WB)	Cell Signaling Technology (#9284)
p-Histone H3 (S10)	Rabbit	1:1000 (WB)	Cell Signaling Technology (#9701)
p-GSK-3β (S9)	Rabbit	1:1000 (WB)	Cell Signaling Technology (#9322)
PLK1 (PL6/PL2)	mouse	1:500 (WB)	Thermo Fisher Scientific (#33-1700)
RIOK3 (B-3)	mouse	1:1000 (WB)	Santa Cruz Biotechnology (#sc-398232)
SKP2	Rabbit	1:1000 (WB)	Zymed (#51-1900)
Ubiquitin K48 (Apu2)	Rabbit	1:1000 (WB)	Millipore (#05-1307)
USP24	Rabbit	1:1000 (WB)	Bethyl Laboratories (#A300-938)

3.11.2 Custom made primary antibodies

Polyclonal rabbit antibodies against human FBXL13 and FBXO3 were made by Innovagen, Sweden. The antibody against human FBXL13 was raised against amino acids 111-121 (LKHELQLKKWK) and 695-797 (VKKSTYSSEDQAA). The antibody against human FBXO3 was raised against amino acids 167-181 (NHYRSEDLLDVDTAA).

3.11.3 Conjugated primary antibodies

Antibody	Manufacturer
BrdU-FITC (clone B44)	BD Biosciences
CD138 microbeads	Miltenyi Biotec

3.11.4 Conjugated secondary antibodies

Antibody	Dilution	Manufacturer
anti-mouse IgG Alexa Fluor 488	1:2000 (IF)	Life Technologies
anti-mouse IgG Alexa Fluor 594	1:2000 (IF)	Life Technologies
anti-rabbit IgG Alexa Fluor 488	1:2000 (IF)	Life Technologies
anti-rabbit IgG Alexa Fluor 594	1:2000 (IF)	Life Technologies
ECL anti-mouse IgG, HRP-linked	1:5000 (WB)	GE Healthcare
ECL anti-protein-A, HRP-linked	1:5000 (WB)	GE Healthcare
ECL anti-rabbit IgG, HRP-linked	1:5000 (WB)	GE Healthcare

3.12 Cell lines

Cell line	Origin	Obtained from
A549	human lung carcinoma cells	ATCC (CCL-185)
AMO-1	human MM cell line	DSMZ (ACC-538)
ANBL-6	human MM cell line	kind gift of Dr. T. Dechow
Granta-519	human B cell lymphoma (MCL)	kind gift of Prof. M. Dreyling
H929	human MM cell line	DSMZ (ACC-163)
HEK293T	human embryonic kidney cell line	ATCC (CRL-3216)
High Five	Insect ovarian cells from *Trichopulsia ni*	Thermo Fisher Scientific
INA-6	human MM cell line	kind gift of Prof. U. Keller
JJN3	human MM cell line	DSMZ (ACC-541)
KMS12BM	human MM cell line	DSMZ (ACC-551)
L363	human MM cell line	DSMZ (ACC-49)
LP-1	human MM cell line	DSMZ (ACC-41)
MM1.S	human MM cell line	ATCC (CRL-2974)
OCI-LY7	human diffuse large B-cell lymphoma	DSMZ (ACC-688)
OCI-LY10	human diffuse large B-cell lymphoma	kind gift of Prof. M. Schmidt-Supprian
OPM2	human MM cell line	DSMZ (ACC-50)
RPMI8226	human MM cell line	DSMZ (ACC-402)
SF21	Insect ovarian cells from *Spodoptera frugip*	Thermo Fisher Scientific
U2OS	human osteosarcoma cells	ATCC (HTB-96)
U266	human MM cell line	DSMZ (ACC-9)

3.13 Cell culture media and supplements

Product	Manufacturer
Biocoll Separating Solution	Biochrom Merck
Dulbecco's Modified Eagle's Medium (DMEM)	Life Technologies
Express Five SFM	Life Technologies
FBS superior	Biochrom Merck
Gentamicin (50mg/ml)	Life Technologies
Grace's Insect Medium	Life Technologies
HBSS (Hank's Balanced Salt Solution) 10X	Life Technologies
HEPES Buffer Solution (1M)	Life Technologies
Interleukin 6 (IL-6), human	Thermo Fisher Scientific
Iscove's Modified Dulbecco's Media (IMDM)	Life Technologies
L-Glutamine 200mM (100X)	Biochrom Merck

McCoy's 5A Medium Modified	Life Technologies
Newborn Calf Serum	Biochrom Merck
Opti-MEM I, reduced serum media	Life Technologies
Phosphate buffered saline (PBS), 10X, sterile	Life Technologies
Penicillin/ Streptomycin (100X)	Life Technologies
RPMI 1640 GlutaMAX medium	Life Technologies
Trypan Blue Stain (0,4%)	Life Technologies
Trypsin-EDTA (10X) solution	Biochrom Merck

3.14 Patient samples

Dr. med. Jan Krönke from University of Ulm provided data from qPCR analysis of 89 MM patient samples at diagnosis on a collaborative basis. The samples were obtained with informed consent and in compliance with the institutional review board.

3.15 Solutions and buffers

All listed buffers were prepared in distilled water if not indicated otherwise.

Buffer or solution	Composition
DUB Activity Buffer	50 mM Tris pH 7.4 5 mM $MgCl_2$ 250 mM Sucrose 1 mM DTT 2 mM ATP
CIP Buffer	50 mM Tris (pH 7.8) 150 mM NaCl 0.1% NP40 10 mM $MgCl_2$ 5% Glycerol 1 mM DTT
FACS Buffer	PBS (1x) 3% FBS
Freezing medium	FBS 10% DMSO
GST Elution Buffer	35 mM glutathione 100 mM Tris (pH 8.0) 120 mM NaCl

HF2+ Buffer	HBSS (1×) 5% heat-inactivated FBS 1% Pen/Strep 1 mM HEPES
IF Blocking Buffer	PBS (1x) 0.1% Triton X-100 5% BSA
IF Washing Buffer	PBS (1x) 0.1% Triton X-100
Inhibitors	1 µg/mL aprotinin 1 mM DTT 10 mM G-2-P 1 µg/mL leupeptin 0.1 mM PMSF 0.1 mM Na_3VO_4 10 µg/mL soybean trypsin inhibitor 5 µg/mL TLCK 10 µg/mL TPCK
Laemmli Buffer (5x)	300 mM Tris (pH 6.8) 50% glycerol 10% SDS 5% β-mercaptoethanol 0.05% bromphenolblue
Luria-Bertani (LB) medium (1×)	1% Bacto Tryptone 0.5% Bacto Yeast Extract 170 mM NaCl
Luria-Bertani (LB)-agar plates	LB medium 1.5% Bacto Agar
Lysis Buffer (150 mM NaCl)	50 mM Tris (pH 7.5) 150 mM NaCl 0.1% NP40 5 mM EDTA 5 mM $MgCl_2$ 5% Glycerol

Lysis Buffer (250 mM NaCl)	50 mM Tris (pH 7.5) 250 mM NaCl 0.1% Triton X-100 1 mM EDTA 50 mM NaF
Modified RIPA Buffer	50 mM Tris (pH 7.5) 150 mM NaCl 1 mM EDTA 1 mM EGTA 1% Triton X-100 0.1% SDS 0.5% Sodium deoxycholate
SDS Running Buffer (10×)	250 mM Tris (pH 7.5) 1.92 M glycine 1% SDS
Silver Staining Solution A	50% methanol 12% acetic acid 0.0185% formaldehyde
Silver Staining Solution B	50% ethanol
Silver Staining Solution C	0.2% (w/v) sodium thiosulfate pentahydrate
Silver Staining Solution D	0.0278% formaldehyde 0.2% (w/v) silver nitrate
Silver Staining Solution E	6% (w/v) sodium carbonate 0.004% (w/v) sodium thiosulfate pentahydrate 0.0185% formaldehyde
Silver Staining Solution F	50% methanol 12% acetic acid
Stripping Buffer	62.5 mM Tris (pH 6.8) 0.867% β-mercaptoethanol 2% SDS
Transfer Buffer (10x)	48 mM Tris (pH 7.5) 39 mM glycine 20% methanol

Washing Buffer	PBS (1×) 0.1% Tween 20

3.16 Software and databases

Software or database	Manufacturer
BLAST Basic local alignment search tool	NCBI
cBioPortal	Memorial Sloan Kettering Cancer Center
CellQuest Pro	BD Biosciences
GPP Web Portal	Broad Institute
FlowJo Single Cell Analysis Software v10	Tree Star
ImageJ	Open source
MacVector	MacVector
Oncomine	Thermo Fisher Scientific
Prism	Graph Pad Software
QuantPrime	Max-Planck Institute for plant physiology
TillVision microscope imaging software	Till

4 Methods

4.1 Molecular cloning

Molecular cloning describes a method, which allows generation of recombinant gene expression vectors. The DNA of interest (insert) can be amplified by a PCR reaction from template DNA (see 4.1.1) and subsequently transferred into a vector (plasmid). Therefore, insert and vector are cut with bacterial restriction enzymes and are both fused by a ligation reaction (see 4.1.3). The resulting plasmid can then be amplified in bacteria (see 4.1.5) and finally extracted again (see 4.1.6). Furthermore, a given DNA sequence can also be modified by mutagenesis PCR (see 4.1.4).

4.1.1 Polymerase chain reaction (PCR)

Polymerase chain reaction (PCR) was used to amplify a DNA sequence of interest from template DNA. The following reaction mix with a total volume of 50 µL was pipetted on ice: 100 ng template DNA, 5 µL *PfuUltra* II reaction buffer (10x), 0.2 µM forward (fw) and reverse (rv) primer, 0.4 mM dNTPs (0.1 mM each dNTP) and 1 µL *PfuUltra* II fusion HS DNA polymerase in distilled water (dH_2O). The reaction mix was incubated in a thermo cycler to amplify the DNA. After an initial denaturation step of 2 min at 95°C, 25 cycles of consecutive DNA denaturation (20 sec, 95°C), primer annealing (20 sec, Primer Tm – 5°C) and DNA elongation (30 sec per kb DNA, 72°C) were performed. The reaction was ended with a final incubation step at 72°C for 10 min in order to finish uncompleted DNA elongation.

4.1.2 Agarose gel electrophoresis and gel purification

After PCR reaction (4.1.1) or DNA restriction digest (4.1.3), DNA was separated by size and analysed by agarose gel electrophoresis. Here, negatively charged DNA moves towards the positively charged electrode within an electric field. For this purpose, agarose was dissolved in TBE buffer to a final concentration of 0.8-2% (w/v) depending on the size of DNA, which was analysed, and boiled in a microwave. The fluid agarose was supplemented with SERVA DNA Stain Clear G and poured in a gel chamber. After it has cooled down to room temperature, DNA mixed with loading dye was loaded onto the gel in an electrophoresis chamber filled up with TBE buffer. To analyse the size of DNA, a DNA ladder was loaded next to the DNA sample. Gel electrophoresis was performed at 70-100 V and DNA was visualized under UV light. If the DNA was further used for cloning, the gel containing the DNA was cut out with a scalpel and DNA was purified using the GeneJet Gel Extraction Kit (Thermo Scientific) according to the manufacturer's protocol.

4.1.3 DNA restriction digest and ligation

DNA can be cut by bacterial restriction enzymes, which recognize and cleave specific sequences. This results into DNA fragments with defined 5'- and 3'- single stranded overhangs

(sticky ends) or blunt ends. DNA fragments cut with the same restriction enzymes reveal corresponding sticky or blunt ends, which can be fused again by a ligation reaction.

For restriction digest, 1-2 µg plasmid or PCR amplified DNA was mixed with 1 µL restriction enzyme in the respective buffer and incubated for 1.5 hrs at the manufacture's recommended temperature (in most cases at 37°C). For digest with two different enzymes at the same time, buffers were chosen according to the manufacturer's instructions. After digest, plasmids were gel purified (see 4.1.2), whereas in case of inserts, enzymes and buffer were directly removed using the the GeneJet Gel Extraction Kit (Thermo Scientific) according to the manufacturer's protocol. The Rapid DNA Dephos & Ligation Kit (Roche) was used to ligate insert and plasmid DNA according to manufacturer's protocol. For this purpose, a molar ratio of 3:1 insert to vector was chosen and 50-100 ng vector DNA was used.

4.1.4 DNA mutagenesis

Site-directed mutagenesis was performed to specifically change a codon within a cDNA sequence and therefore to exchange the amino acid. For this purpose, 35-50 bp long primer pairs, which carry the respective base pair change in the middle of the sequence, were designed. These primers were used to amplify the whole plasmid containing the cDNA by PCR. The protocol of the PCR corresponds to the protocol described in section 4.1.1 with a few changes. The cycle number was reduced to 16 cycles and the DNA elongation temperature to 68°C. In order to remove the DNA template, which does not carry the mutation, the reaction was incubated with 1 µL DpnI enzyme in the respective buffer for 60 min at 37°C. This enzyme cuts only methylated DNA, which was purified from bacteria, but not the unmethylated PCR product. The linear PCR product was then transformed into bacteria (see 4.1.5) and processed according to section 4.1.6.

4.1.5 Bacterial transformation

DNA can be delivered into bacteria by transformation. For this purpose, bacteria can be treated in different ways to allow the uptake of DNA. The bacteria used in this study are chemically competent, meaning that they were treated with $CaCl_2$ by the manufacturer.

In order to amplify plasmid DNA, for instance after a ligation reaction, NEB® 5-alpha Competent *E. coli* (High efficiency) from New England Biolabs were used for transformation. For this, 15-20 µL bacteria were incubated with 100 ng DNA for 20 min on ice followed by a heat shock at 42°C for 30 sec. Bacteria were then put back on ice for additional 2 min. In case of transformation with a plasmid containing a kanamycin resistance gene or with mutagenesis PCR products, bacteria were incubated in 500 µL SOC media at 300 rpm and 37°C for 60 min to allow expression of the resistance gene or ligation of the linear mutagenesis PCR product, respectively. Transformed bacteria were plated on LB agar plates containing antibiotics, either ampicillin or kanamycin depending on the resistance gene of the plasmid, and plates were incubated at 37°C overnight. The next day, single colonies were picked with a sterile pipette tip and inoculated in LB medium containing the respective antibiotic. Bacteria were grown at 37°C and 250 rpm overnight.

4.1.6 DNA extraction from bacteria

Plasmid DNA amplified in bacteria was isolated by commercially available plasmid purification kits. Depending on the volume of cultured bacteria, two different kits were used. The extraction from 4 mL culture was performed with the peqGOLD Plasmid Miniprep Kit (Peqlab Life Science) whereas the NucleoBond® Xtra Midi Kit (Macherey-Nagel) was used for the purification from 200 mL bacterial culture according to the manufacturer's protocol. For long time storage of plasmid transformed bacteria, 500 µL bacteria culture was mixed with 500 µL glycerol in cryo tubes and frozen at -80°C.

After molecular cloning of recombinant plasmid DNA, positive clones were identified by test digest using the respective restriction enzymes followed by agarose gel electrophoresis. Verification of the DNA sequence was performed by sequencing at Eurofins Genomics, Ebersberg, Germany, using promoter or gene specific primers.

4.1.7 Annealing of shRNA oligonucleotides

Oligonucleotides for shRNA cloning were annealed and ligated into the pLKO.1 TRC cloning vector. For annealing, 1 µL of each oligonucleotide (100 µM stock concentration) and Buffer G (Thermo Fisher Scientific) were diluted in water in a total volume of 50 µL. The mix was incubated at 95°C for 5 min and then cooled down to room temperature at 0.1°C per second. The vector was cut with the restriction enzymes AgeI and EcoRI in the recommended buffer and annealed shRNAs were ligated into the vector according to section 4.1.3.

4.2 Generation of CRISPR/Cas9 sgRNA libraries

4.2.1 Designing CRISPR/Cas9 libraries

In this study, two separate CRISPR/Cas9 libraries targeting 72 F-box proteins or 98 DUBs were designed and generated. Both libraries contained three different sgRNAs per gene as well as 12 non-targeting and 15 positive control sgRNAs. Positive controls target essential genes like ribosomal proteins and polymerases and thus, their expression in Cas9 positive cells leads to cell death. Sequences of libraries were taken from the human CRISPR knockout pooled library (GeCKO v2) from Feng Zhang (Sanjana, Shalem, and Zhang 2014). The chosen sequences were composed of 20 gene specific base pairs as well as overhang nucleotides at the 5'-end of forward (CACCG) and reverse oligos (AAAC). The reverse oligos contained additionally a 'C' at the 3'-end. All sequences from both libraries are listed in the appendix (see 11.1) and forward and reverse oligos were ordered pre-mixed in 96-well plates from Eurofins Genomics, Ebersberg, Germany. For the generation of libraries, mixed oligos were annealed and ligated into a lentiGuide-GFP vector, which contained the PAM sequence in its backbone (see 4.2.2 and 4.2.3). Finally, libraries were expanded in bacteria and subsequently isolated (see 4.2.4).

4.2.2 Annealing and dilution of libraries

Reverse and forward oligos were annealed in 96-well plates as described previously (Sanjana, Shalem, and Zhang 2014; Shalem et al. 2014). The master mix for one reaction contained 4 µL oligo mix (forward and reverse, 50 µM each), 2 µL T4 ligase buffer, 1 µL T4 Polynucleotide Kinase (PNK T4) and 13 µL water. The annealing reaction was performed on an Eppendorf Mastercycler nexus machine using the following program: 30 min 37°C, 5 min 95°C and cooling down to 25°C at 0.1°C per second. Finally, the annealed libraries were diluted 1:200 in a new 96-well plate.

4.2.3 Vector digest and ligation of libraries

Annealed oligos were ligated into a modified lentiGuide vector, generated by addition of an eGFP expression cassette, which allows sorting of infected (GFP positive) cells, into the lentiGuide-Puro vector (Sanjana, Shalem, and Zhang 2014). For this, an adequate amount of vector was digested by BsmBI (1 µL enzyme per 1 µg vector) in the respective buffer overnight at 55°C. The next day, the digest reaction was further supplemented with 1 µL BsmBI per 5 µg vector and incubated for 2-3 hours. After purifying the digested vector by gel purification (see 4.1.2), the vector was dephosphorylated by 2 µL Antarctic phosphatase per 5 µg vector at 37°C for 1 h and the enzyme subsequently inactivated at 70°C for 5 min. Finally, the digested vector was diluted to a final concentration of 50 ng/µL and stored at -20°C.

Ligation took place in 96-well plates using the following amounts of components for one reaction: 2 µL digested vector (lentiGuide-GFP), 2 µL T4 Ligase buffer, 2 µL T4 Ligase, 2 µL diluted and annealed oligos in 12 µL water. The ligation reaction was performed at 16°C overnight and ligated products were stored at -20°C.

4.2.4 Bacterial transformation and harvesting of libraries

Ligation products from every 96-well plate were pooled separately resulting in 7 pooled tubes. For this, 5 µL of ligation were mixed from every well into DNA low bind tubes, heat-inactivated at 70°C for 15 min and test-transformed in electro competent bacteria in order to determine library coverage. Bacteria were transformed with 1 µL mix containing 5 ng of library by electroporation using the following settings: 1500 V, 25 µF, 200 Ohm and 6.8 msec. After addition of 990 µL pre-warmed recovery medium and incubation at 37°C for 1 h, bacteria were further diluted 1:20 to a final concentration of 0.25 pg/µL. Finally, 20 µL of bacteria (5 pg of library) were seeded onto 10 cm agar plates containing ampicillin. Resulting number of colonies represented 1:10000 of total library DNA.

For the final pooling of DUB and F-box protein libraries, the respective tubes were mixed at a ratio which represented equal amounts of every oligo. After heat inactivation of the libraries at 70°C for 15 min, 60 ng DUB or 40 ng F-box protein library were transformed by electroporation as described above in 150 µL or 100 µL electrocompetent bacteria, respectively. Transformed bacteria were recovered in 1 mL recovery medium at 37°C for 1 h and subsequently seeded on 12 agar plates (15 cm, containing ampicillin) in case of DUB library and on 8 plates in case of F-

box protein library. Plates were incubated overnight at 34°C and bacteria were finally harvested. In order to estimate library coverage, recovered bacteria corresponding to 10 pg of library were plated on a 10 cm agar plate and also incubated overnight at 34°C. The next day, colonies were counted and library coverage was determined. For harvesting, bacteria were scraped in 7 mL LB medium per plate and pooled in centrifuge plastic bottles. Plates were washed with 5 mL LB medium to remove all bacteria from the plates and pooled bacteria were centrifuged at 5000 rpm and 4°C for 20 min. After spinning, supernatant was removed and bacteria pellets weighted to estimate number of columns needed to purify DNA. The NucleoBond® Xtra Midi Kit (Macherey-Nagel) was used to isolate the library DNA from bacteria according to manufacturer's protocol, thereby taking one column per 0.4 g of wet bacteria.

4.2.5 CRISPR/Cas9 screen

In order to screen for potential oncogenic DUBs and F-box proteins in multiple myeloma, a CRISPR/Cas9 screen was performed in stable Cas9 expressing MM1.S cells by using a two-vector system. First, MM1.S cells were lentivirally transduced with a Cas9 expression vector (lentiCas9-Blast) (Sanjana, Shalem, and Zhang 2014) and infected cells were selected by the addition of 3 µg/mL blasticidin for 2 weeks. For the screen, MM1.S Cas9 cells were infected with either the DUB or F-box protein sgRNA library and two days later, two million of infected GFP positive cells were sorted by FACS (see 4.4.11). One half of the sorted cells, which represented sgRNA composition on day 0 (T_0), were directly harvested and cell pellets were stored at -80°C. For the untreated condition, cells were grown in culture media supplemented with 3 µg/mL blasticidin for 14 days and subsequently, one million cells was harvested (T_{14}, untreated). In parallel, 5 days after sorting, cells were treated with 12 nM bortezomib for 8 days in total and harvested (Bortezomib).

4.2.6 Sample preparation for Illumina next-generation sequencing

To evaluate sgRNA representation within the cell samples, which were harvested during the screen (see 4.2.5), genomic DNA was isolated using the DNeasy Blood and Tissue Kit (Qiagen) according to manufacturer's protocol. In order to quantify sgRNA representation of the libraries before and after infection, a two-step PCR approach was performed to amplify the sgRNA specific locus and to add adaptors and barcodes, which allow deep sequencing and multiplexing of different samples, respectively. The primers used for the first PCR bind to the flanking region of the sgRNAs, therefore amplifying the respective sgRNA sequence, and contain a universal 5' tail for the Illumina sequencing platform (Seq-adapt_Fw and Seq_adapt_Rv) (3.6.2). A standard PCR reaction setup as described in section 4.1.1 using 200 ng plasmid DNA or 300 ng genomic DNA as template was pipetted on ice. Cycling conditions for both PCR reactions are listed in Table 1. After PCR reaction, products were purified using the QIAquick PCR Purification Kit (Qiagen) according to manufacturer's protocol and used as templates for the second PCR. Primers for the second PCR contained Illumina adaptors and indices and are listed in section 3.6.2. The following

combinations of forward and reverse primers were used for the different samples: DUB T_0 (NGS_i5_S505/NGS_i7_S701), DUB T_{14} (NGS_i5_S506/NGS_i7_S701), DUB Bortezomib (NGS_i5_S505/NGS_i7_S702), F-box T_0 (NGS_i5_S505/NGS_i7_S704), F-box T_{14} (NGS_i5_S506/NGS_i7_S704) and F-box Bortezomib (NGS_i5_S505/NGS_i7_S705). The second PCR was performed using the settings according to Table 1 and PCR products were purified as it was done for the first PCR.

Table 1: Two-step PCR program for NGS sample preparation.

	First PCR		Second PCR
Template	Plasmid DNA	Genomic DNA	1st PCR amplicons
Number of reactions	3*50 µL	4*50 µL	3*50 µL
Template amount	200 ng per reaction	300 ng per reaction	200 ng per reaction
Number of cycles	14	28	6
Initial denaturation	2 min at 95°C	3 min at 95°C	2 min at 95°C
Denaturing	20 sec at 95°C	20 sec at 95°C	20 sec at 95°C
Annealing	20 sec at 56°C	45 sec at 54°C	20 sec at 54°C
Extension	20 sec at 72°C	45 sec at 72°C	20 sec at 72°C
Final extension	2 min at 72°C	3 min at 72°C	1 min at 72°C

4.2.7 Illumina MiSeq sequencing

For deep sequencing of sgRNA libraries, the MiSeq system from Illumina was used. For this, the PCR amplified products (see 4.2.6) were quantified using the Illumina DNA standards from the KAPA Library Quantification Kit (Kapa Biosystems) by qPCR. First, samples were diluted 1:10000, 1:100000 and 1:1000000 and measured together with DNA standards. Latter was used to calculate a standard curve in order to determine the concentrations of the samples. The following reaction mix was pipetted in every well on ice: 7.5 µL LightCycler 480 SYBR Green I Master mix, 0.9 µL primer (forward and reverse, 10 mM each), 2 µL template and 4.6 µL water. The qPCR reaction was performed as described in 4.3.3 and samples were measured in triplicates. After calculating the concentration for every sample (8 samples in total), 5 nM of every sample was diluted in water to a final volume of 100 µL in order to obtain an end concentration of 40 nM library. Finally, library concentration was confirmed by repeating the qPCR together with DNA standard as described above.

Deep sequencing of samples was performed on a MiSeq Illumina machine (kindly provided by AG Rad, Klinikum rechts der Isar, München) using the MiSeq Reagent Kit v2 according to manufacturer's protocol. For this, the library sample was further diluted to 4 nM and 4 µL of library were mixed with 1 µL of Illumina PhiX Control. Finally, 6 pM of library was used for sequencing and resulting data were analysed and mapped by Thomas Engleitner from AG Rad, Klinikum rechts der Isar.

4.3 Gene expression analysis

Gene expression was analysed by quantitative PCR (qPCR). For this purpose, RNA was extracted from cells (see 4.3.1), transcribed into cDNA (see 4.3.2) and then measured by qPCR (see 4.3.3).

4.3.1 RNA extraction from eukaryotic cells

Before harvesting, cells were washed once with PBS and centrifuged at 1200 rpm for 4 min. Cell pellets were then frozen and stored at -80°C until RNA extraction. The RNeasy Mini Kit (Qiagen) containing silica-membrane RNeasy spin columns was used for RNA isolation according to manufacturer's protocol. Cells were homogenized by using QIAshredder (Qiagen) spin columns.

Since it was not always possible to design exon-exon spanning qPCR primer, a DNase digest was performed to ensure complete removal of genomic DNA. For this, RNA was supplemented with 0.5 µL DNase I (New England Biolabs) in the respective buffer and incubated at 37°C for 30 min. After addition of EDTA to a final concentration of 5 mM, the DNase was subsequently heat-inactivated at 75°C for 10 min. RNA concentration was measured by spectrophotometry and stored at -80°C.

4.3.2 Reverse transcription of RNA

RNA was transcribed into cDNA by an enzyme called reverse transcriptase, which is of viral origin. For this purpose, 1 µg RNA was mixed with 1 µL random hexamer (Roche) primers in a total volume of 17.5 µL dH_2O and incubated at 70°C for 5 min. After the mix cooled down to room temperature, 6 µL First-Strand Buffer (5x), 3 µL 0.1 M DTT, 1 µL 0.1 M dNTPs, 0.5 µL RNase Out and 1 µL SuperScript II reverse transcriptase (Thermo Fisher Scientific) were added and the mix was incubated at 42°C for 60 min to allow cDNA synthesis. Enzymes were then heat-inactivated at 95°C for 5 min and the cDNA was further used for qPCR or stored at -20°C.

4.3.3 Quantitative PCR (qPCR)

Expression of a gene of interest was analysed by quantitative PCR (qPCR). This method is based on a PCR performed on a cDNA sample with gene specific primers and the simultaneous use of a DNA intercalating fluorescent dye (SYBR green in this study), the intensity of which, measured by a LightCycler machine, proportionally increases to the amount of amplified DNA.

cDNA samples were diluted 1:10 before they were used for qPCR. A 25 µL mix containing 12.5 µL LightCycler 480 SYBR Green I Master mix, 1.5 µL primer (forward and reverse, 10 mM each), 5 µL diluted cDNA and 6 µL water was pipetted on ice in each well of a 96-well plate. Every measurement was performed in triplicates and a water control lacking the cDNA template was used for every primer pair to test for unspecific amplification. Before starting the qPCR reaction, the plate was sealed and briefly centrifuged. In this study, qPCRs (37 cycles) were run on a LightCycler® 480 instrument from Roche according to manufacturer's instructions. Gene specific

primers which were used in this study are listed in section 3.6.2. Samples were normalized to the house-keeping gene ribosomal protein large subunit P0 (RPLP0) and analysed by the ΔΔCt method (Livak and Schmittgen 2001).

4.4 Culture of eukaryotic cells and cell-based experiments

4.4.1 Cell culture

All cell lines were cultured in a humidified incubator at 37°C with 5% CO_2. The human embryonic kidney cell line HEK293T and the human lung carcinoma cell line A549 were cultured in Dulbecco's modified Eagle's medium (DMEM) with GlutaMAX supplemented with 1% penicillin-streptomycin (P/S) and 10% newborn calf serum or 10% fetal bovine serum (FBS superior), respectively. The human osteosarcoma cell line U2OS was cultured in McCoy's medium supplemented with 1% P/S and 10% FBS. The multiple myeloma cell lines MM1.S, RPMI8226, U266, KMS12BM, AMO-1, JJN3, OPM2, L363, H929, INA-6 and ANBL-6 were cultured in RPMI 1640 medium supplemented with 1% P/S and 10% FBS, heat-inactivated at 60°C for 30 min. For INA-6 and ANBL-6 cell lines, medium was additionally supplemented with 2 ng/mL of human IL-6. The human multiple myeloma cell line LP-1 was maintained in IMDM medium with 1% P/S and 10% heat-inactivated FBS. The DLBCL cell lines OCI-LY7 and OCI-LY10 were cultured in IMDM medium with 1% P/S and 20% heat-inactivated FBS.

Adherent cell lines were cultured on cell culture plates and split at a confluency of 80-100% every 1-3 days. For this, cells were washed once with PBS and then incubated in trypsin until they were detached from the plate. Trypsin digest was stopped by the addition of medium and removed by centrifugation of cells at 1200 rpm for 4 min. Next, the cell pellet was resuspended in fresh medium and 1/2-1/10 of cells were plated again on a cell culture dish. Suspension cells were grown in cell culture flasks at a density of 1-5 x10^5 cells/mL and split every 2-3 days at a ratio of 1:2-1:10 depending on the proliferation rate.

For some experiments, cells were counted to determine the total cell number or to seed a specific cell amount. For this purpose, cells were mixed at a ratio of 1:2 with trypan blue, which stains only damaged and dead cells and therefore allows the discrimination of viable cells. A Neubauer counting chamber was used for counting the cells.

4.4.2 Freezing and thawing of cells

For long-term storage of cell lines, cells were frozen in FBS supplemented with 10% DMSO (freezing medium). Therefore, cells were centrifuged at 1200 rpm for 4 min, resuspended in 1 mL freezing medium and transferred into a cryo tube. To allow slow freezing of cells, cryo tubes containing cells were put in an isopropanol-based freezing container and frozen at -80°C. After freezing, cells were transferred to a liquid nitrogen tank for long-term storage.

When thawing cells, it is important to quickly remove the DMSO containing medium from the cells, which will otherwise damage them. For this, cryo tubes containing the frozen cells were

thawed in a water bath at 37°C until only a small ice particle was left. Cells were then rapidly transferred into 10 mL culture medium and centrifuged at 1200 rpm for 4 min. Finally, cells were plated as described in section 4.4.1.

4.4.3 Harvesting cells

For analysis of cells by biochemical assays or qPCR experiments, cells were collected and transferred into Falcon tubes. In case of adherent cells, cells were removed from plates by scraping (A549 and U2OS cells) or rinsing (HEK293T cells). Cells were centrifuged at 1200 rpm for 3-4 min and then washed with 1 mL PBS followed by transferring the cells into a 1.5 mL tube. After centrifugation at maximum speed (13000 rpm) for 30 sec, PBS was removed and cell pellets were frozen at -80°C.

4.4.4 DNA transfection of cells

4.4.4.1 Calcium phosphate transfection

The calcium phosphate method is based on precipitation of DNA-calcium complexes by a BES-buffer system resulting in precipitates, which can be incorporated by adherent cells (Graham and van der Eb 1973; Kingston, Chen, and Rose 2003). In this study, this method was used to transfect HEK293T cells. For transfection of a 10 cm plate at a cell confluency of 50-70%, 10 µg DNA was dissolved in 450 µL dH_2O in a 15 mL Falcon and 50 µL $CaCl_2$ were added to a final concentration of 250 mM. The mix was vortexed and incubated for 5 min at room temperature. Next, 500 µL 2x BES solution was added dropwise while vortexing the mix. After 20 min, the transfection mix was dropped onto 10 mL medium and everything was carefully mixed by swirling the plate. The transfection medium was replaced by fresh medium after 4 hrs.

4.4.4.2 Transfection by Lipofectamine 2000

Lipofection is a transfection method based on the complex formation between DNA and liposomes containing cationic lipids. These complexes can fuse with the membrane of cells and thereby facilitate the delivery of DNA into the cell (Felgner et al. 1987). Lipofectamine 2000 reagent was used to transfect A549 and U2OS cells according to the manufacturer's protocol. Briefly, DNA and Lipofectamine 2000 reagent were separately mixed with serum-free Opti-MEM and incubated for 5 min at room temperature. The DNA solution was then added to the Lipofectamine mix and everything was mixed carefully by pipetting the solution up and down. After 20 min of incubation, the transfection mix was dropped onto cells in P/S-free medium. To reduce toxicity, the medium was replaced by fresh medium after 3 hrs. A DNA to Lipofectamine ratio of 1:3 was chosen and cells were transfected at a confluency of 80-90%.

4.4.5 siRNA transfection of cells

Knockdown of a protein of interest was achieved by transfection of adherent cells with siRNA to induce RNA interference. For this, Lipofectamine RNAiMAX transfection reagent was used according to the manufacturer's protocol. siRNA and Lipofectamine RNAiMAX reagent were separately mixed with serum-free Opti-MEM and incubated for 5 min at room temperature. The siRNA solution was then added to the Lipofectamine mix and everything was mixed carefully by pipetting the solution up and down. After 10-20 min of incubation, the transfection mix was dropped onto cells in P/S-free medium. Medium was changed after 5 hrs and the knockdown was analysed 2-3 days after transfection.

4.4.6 Production of lentiviral particles

The transfection methods described in 4.4.4 and 4.4.5 only leads to transient expression or knockdown of a protein, respectively. In order to achieve stable expression of a gene or an shRNA, cells were transduced with lentiviral particles, which allow genomic integration of DNA. Lentiviral particles were produced in HEK293T cells by transfecting a 10 cm plate with 15 µg packaging plasmid (psPAX2), 5 µg envelope plasmid (pMD2.G) and 20 µg transfer plasmid (pLKO.1 plasmid for shRNA and pHIV plasmid for cDNA) by the calcium phosphate method (see 4.4.4). After 24 hrs, the medium was replaced by 10 mL of the respective cell culture medium of the cell line, which was later transduced by the virus. The viral supernatant was harvested 48 hrs after transfection, passed through a 0.45 µm filter and directly used for infection or stored at -80°C.

4.4.7 Viral transduction of cells

For the infection of adherent cell lines, cells were plated one day before in a 6-well plate and infected at a confluency of 80-90% by replacing the medium with 2 mL viral supernatant supplemented with 8 µg/mL polybrene. To increase the transduction efficiency, U2OS cells were additionally centrifuged at 2000 rpm for 1.5 hrs. After 24 hrs, the virus was removed and cells were transferred to a 10 cm cell culture dish. For infection of suspension cell lines, 1 x10^6 cells were plated in 1 mL medium in one well of a 6-well plate and mixed with 2 mL viral supernatant. Polybrene was added to a final concentration of 8 µg/mL and cells were spun at 1000 rpm for 30 min. One day later, virus was removed by centrifugation and cells were transferred into cell culture flasks with fresh medium.

4.4.8 Isolation of CD138$^+$ cells from human bone marrow

Isolation of multiple myeloma (MM) (CD138$^+$) cells from human bone marrow samples was performed by PD Dr. med. J. Krönke and Denise Miller at University Hospital of Ulm.

Human MM cells were isolated from diagnostic bone marrow aspirations from MM patients at first diagnosis. Primary CD138$^+$ cells were purified using MACS magnetic CD138 MicroBeads (Miltenyi Biotec) according to manufacturer's protocol. To this end, bone marrow was diluted 1:2 with PBS and pipetted carefully on 10 mL Biocall medium in a 50 mL Falcon. After centrifugation

at 2100 rpm for 15 min with low acceleration and braking, the layer of peripheral blood mononuclear cells (PBMCs) between plasma and Biocoll medium was collected and washed with HF2+ buffer. Cells were centrifuged at 1400 rpm for 5 min and resuspended in 80 µL HF2+ buffer and supplemented with 20 µL magnetic beads against CD138 per 20 million cells. After incubation for 30 min at 4°C, cells were washed with 2 mL HF2+ buffer and loaded on prepared LS Columns assembled into a MACS. After washing cells three times with 3 mL HF2+ buffer, columns were removed from the separator and cells were flushed out in 5 mL HF2+ buffer by applying the plunger. Isolated cells were washed once with PBS, harvested and pellets were frozen at -80°C.

4.4.9 Cycloheximide treatment

Cycloheximide is an inhibitor of eukaryotic mRNA translation and can therefore be used to analyse protein turnover. Cycloheximide was dissolved in 100% ethanol to a concentration of 100 mg/mL and a stock solution was always freshly prepared before use. Cells were treated with 100-200 µg/mL cycloheximide and harvested at the indicated time points. In some experiments, 10 µM MG132 was simultaneously added for 5 hrs in order to inhibit the proteasome at the same time.

4.4.10 Synchronization of cells

In order to analyse cell cycle specific events, cells were synchronized at G1/S phase or mitosis and released to follow the transition through S and G2 or G1 phase, respectively.

4.4.10.1 Synchronization in G1/S phase

Synchronization of cells at the entry of S phase was achieved by a double thymidine block. An excess concentration of thymidine interferes with deoxynucleotide production and therefore inhibits DNA synthesis. As a consequence, DNA replication stops and cells arrest in S phase. Thymidine was dissolved in PBS to a concentration of 25 mg/mL and prepared freshly before every experiment. Cells were treated with 2 mM thymidine for 24 hrs and then released from S phase by thymidine washout. For this, cells were washed twice with PBS and once with medium for 10 min and then incubated for 12 hrs in normal growth medium to allow the exit from S phase. After this, thymidine was added a second time for 24 hrs, thereby arresting cells at the G1/S boarder. For analysis of cells in S and G2/M phase, thymidine was again removed and cells were harvested at indicated time points.

Alternatively, cells were treated for 24 hrs with 1 µM palbociclib, a cyclin-dependent kinase (CDK) 4/6 inhibitor, thereby inducing an arrest at late G1. In order to release cells into S phase, palbociclib was removed by washing cells two times with PBS and once with medium.

4.4.10.2 Synchronization in mitosis

Cells can be synchronized in prometaphase of mitosis by the addition of nocodazole, which depolymerases microtubules and therefore interferes with mitotic spindle formation. To this end, cells were first pre-synchronized in S phase by the addition of 2 mM thymidine for 24 hrs. Cells

were then released by removal of thymidine and stopped in prometaphase by the addition of 500 ng/mL nocodazole for 15-16 hrs. Mitotic cells are round and easy to detach from the cell culture plate by rocking the dish and therefore can be separated from non-mitotic adherent cells (mitotic shake-off). Cells were either harvested or released from mitosis by transferring the cells in tubes and washing them two times with PBS and once with medium. Cells were then re-plated and harvested at indicated time points.

4.4.11 Flow cytometry

Flow cytometry is a technique, which allows the detection of fluorescently labelled cells, either by antibodies conjugated to fluorophores, expression of a fluorescent protein or incorporation of a fluorescent dye. For this purpose, fluorescent cells are excited by laser light of a specific wave length at a single-cell resolution and the emitted light is consequently detected by the flow cytometer. At the same time, the physiological properties of a cell, e.g. size (forward scatter, FSC) and granularity (sideward scatter, SSC), can be measured, which allows the discrimination of dead and viable cells. Obtained data were analysed using the FlowJo v10 software.

4.4.11.1 Analysis of GFP and dsRed positive cells

The percentage of infected cells could be determined by flow cytometry since the fluorescent proteins eGFP or dsRed additionally were encoded on the viral transfer plasmid. For this purpose, cells were collected at indicated time points after infection, washed once with PBS and then analysed with a FACSCalibur machine. GFP positive cells were detected in the FL1-H and dsRed positive cells in the FL3-H channel.

4.4.11.2 Cell cycle analysis by flow cytometry

Flow cytometry can be used to analyse the cell cycle stage of cells. For instance, the cellular DNA content can be determined by staining DNA with the fluorescent dye propidium iodide (PI). Consequently, cells in G2/M phase can be distinguished from cells in G0/G1 as they exhibit the double amount of DNA and this can be measured by flow cytometry (max emission at 617 nm). Cells in S phase reveal an intermediate amount of DNA and therefore, the resulting intensity of PI lies between the intensity of cells in G1 and G2/M phase. In this study, PI/RNase staining buffer (BD Pharmingen) was used for cell cycle analysis according to the manufacturer's protocol.

To further analyse cells which are in S phase, cells were labelled with anti-BrdU and PI for flow cytometric analysis. Bromodeoxyuridine (BrdU) is a uridine derivative, which is incorporated into DNA during DNA replication when added to cells. After harvest and fixation of cells in ice cold 70% ethanol, the incorporated BrdU can be visualized by an anti-BrdU antibody conjugated to FITC and detected by flow cytometry. In this study, FITC Mouse Anti-BrdU (BD Biosciences) was used for BrdU/PI flow cytometry according to manufacturer's protocol.

4.4.11.3 Fluorescence-activated cell sorting (FACS)

FACS (Fluorescence-activated cell sorting) is a technique that allows sorting of a specific cell population from a sample. For this, cells, which correspond to user-defined physiological and fluorescent characteristics, are electrically charged by the FACS machine and sorted into separate tubes by electromagnets.

In case of insufficient infection rates (below 80%), infected cells which additionally expressed GFP or dsRed as a marker were sorted in order to separate infected from non-infected cells and thus to perform experiments with a homogenous cell population. For this, cells were harvested, washed twice with PBS and passed through a cell strainer. Next, cells were resuspended in FACS buffer at a concentration of 1-10 x10^6 cells/mL and viable GFP and/or dsRed positive cells were sorted and recovered in tubes containing FBS. FACS was performed on a FACSAria II by Markus Utzt at the cell analysis core facility of the Center for Translational Cancer Research (TranslaTUM), Klinikum rechts der Isar. After sorting, cells were either taken up in culture or directly harvested for further analysis by immunoblotting or qPCR.

4.4.12 Immunofluorescence analysis

Protein localization within a cell can be visualized using specific fluorescently labelled antibodies and a fluorescence microscope. To this end, cells were seeded in detachable multi-well cell culture chambers on PCA slides and transfected the next day with indicated vectors using Lipofectamine 2000 (see 4.4.4). For immunofluorescence analysis, cells were washed twice with PBS and fixed with ice-cold methanol at -20°C for 5 min. Methanol was washed away twice with PBS and cells were blocked with 5% BSA (w/v) in PBS/0.1% Triton X-100 (blocking solution) for 1 hour at room temperature. Primary antibodies were diluted in blocking solution as detailed in 3.11.1 and cells were incubated for 1 hour. Excess antibody was washed away three times with 0.1% Triton X-100 in PBS for 10 min. Subsequently, cells were incubated with fluorescently labelled secondary antibodies diluted in blocking solution for 1 hour. After three times washing with 0.1% Triton X-100 in PBS for 10 min, chambers were detached and cells were mounted in SlowFade Gold antifade Reagent with DAPI (Thermo Fisher Scientific). Finally, cells were covered with a coverslip, which was sealed with clear nail polish and images were acquired with an Inverted Fluorescence Microscope (Olympus) using TillVision imaging software.

4.4.13 Wound healing assay

In order to analyse the migration capability of cells, scratch assays were performed. Two days after siRNA transfection, 400 000 cells per well were seeded in 6-well plates and grown until they have reached confluency. A linear scratch was generated using a sterile 200 µL pipette tip and floating cell debris was washed away with PBS. Cells were covered again in growth media and images were acquired at indicated time points using an Inverted Fluorescence Microscope (Olympus) and the TillVision microscope imaging software. The ability of the cells to migrate was

determined by measuring the area of a wound over time using the ImageJ software and the MRI Wound Healing Tool as ImageJ macro.

4.4.14 Microtubule regrowth assay

Microtubule growth capacity was assessed by a microtubule regrowth assay as described previously (Abal et al. 2002). To this end, cells were seeded in detachable multi-well cell culture chambers on PCA slides. The next day, microtubules were completely depolymerized by treating the cells with 10 µM nocodazole for 2 hrs at 4 °C. To allow regrowth of microtubules, cells were rewarmed and nocodazole was washed away three times with PBS. After 1 min, cells were fixed with ice-cold methanol for 5 min at -20°C and microtubules were stained by immunofluorescence as described in section 4.4.12 using anti-α-tubulin primary antibody at 1:500 dilution.

4.5 Protein biochemistry

4.5.1 Cell lysis

To analyse protein content and interactions within cells, cellular membranes need to be disrupted by cell lysis with specific buffers containing salt and detergents. For this purpose, frozen cell pellets (see 4.4.3) were resuspended in an appropriate volume of 150 mM NaCl lysis buffer supplemented with DTT as well as protease and phosphatase inhibitors (PMSF, Nava, G-2-P, TLCK, TPCK, Pin). For complete cell lysis, cells were incubated on ice for 20 min and membranes and DNA were subsequently removed by centrifugation at 14000 rpm and 4°C for 20 min. After supernatants were transferred into fresh tubes on ice, protein concentration was determined based on the Lowry method (Lowry et al. 1951) using the Bio-Rad DC protein assay according to manufacturer's protocol. Protein samples were denatured by the addition of Laemmli buffer and subsequent cooking at 95°C for 5 min. Finally, proteins were analyzed by SDS gel electrophoresis (see 4.5.2) or stored at -20°C.

4.5.2 SDS polyacrylamide gel electrophoresis (SDS-PAGE)

SDS polyacrylamide gel electrophoresis (SDS-PAGE) is a technique that allows separation and analysis of proteins according to their molecular weight. Proteins are covered by SDS and thereby become negatively charged, allowing the separation only according to their mass. Consequently, when loaded on an SDS polyacrylamide gel, proteins migrate towards the anode when an electric field is applied and at the same time are separated by size as smaller proteins migrate faster through the mesh of the gel than bigger ones.

The percentage of acrylamide (between 6 and 15%) in a gel was chosen according to the molecular weight of proteins that were analysed. Gels composed of a separating gel (375 mM Tris pH 8.8, 10% SDS, 10% APS, acrylamide) and a stacking gel (125 mM Tris pH 6.8, 10% SDS, 10% APS, 4.4% acrylamide) were poured freshly before use. Polymerization of gels were initiated by the addition of 5 µL TEMED per 5 mL stacking and 4 µL TEMED per 10 mL separating gel. Protein

samples supplemented with Laemmli buffer and corresponding to 10-25 µg protein were loaded next to a protein molecular weight ladder on a polyacrylamide gel, which was assembled before in an electrophoresis chamber filled with 1x SDS running buffer, and electrophoresis was started at 90 V to allow accumulation of proteins in the stacking gel and then continued at 140 V. After SDS-PAGE was completed, proteins within the gel were either analysed by silver staining of the gel (see 4.5.3) or transferred onto a membrane for immunoblot analysis (see 4.5.4).

4.5.3 Silver staining

After SDS-PAGE, proteins in the gel can be analysed by silver staining. Silver ions interact with negatively charged proteins and are reduced to elemental silver which makes proteins visible. In this study, silver staining was used to analyse the amount of purified proteins. The composition of the solutions used are listed in section 3.15. Proteins were separated by SDS-PAGE using gradient NuPAGE Bis-Tris ready gels (4-12%) and NuPAGE MES SDS Running buffer. Subsequently, the gel was fixed in solution A for 1 hour and then washed three times in solution B for 20 min. After incubation in solution C for 1 min, the gel was washed three times with distilled water for 20 sec and then further incubated in solution D containing the silver ions for 20 min. Excess silver ions were washed away two times with distilled water for 20 sec and subsequently, the gel was incubated in solution E until proteins became visible. After washing the gel two times with distilled water for 2 min, the reaction was stopped by incubation with solution F for 10 min. Finally, the gel was washed in 50% methanol for 20 min and then stored in water.

4.5.4 Immunoblot analysis (Western blot)

Immunoblot analysis, also called western blot, was used to detect proteins by antibodies after they have been separated by SDS-PAGE and transferred onto a membrane. Therefore, polyvinylidene fluoride (PVDF) membranes were briefly activated in methanol and together with the gel containing the proteins assembled in a wet blot chamber filled with transfer buffer. Proteins were transferred onto the membrane by electroblotting for 3 hrs at 60 V or overnight at 30 V and equal protein loading was controlled by Ponceau S staining of the membrane. Membranes were cut in order to analyse several proteins of different molecular weight at the same time and destained in washing buffer. After the membranes were blocked with blocking solution (5% (w/v) milk in washing buffer) for 30 min at room temperature, they were incubated with the respective primary antibodies diluted in blocking solution on a roller mixer overnight at 4°C. The next day, membranes were washed three times with washing buffer for 10 min and then incubated at room temperature for 60 min with a secondary antibody conjugated to horse radish peroxidase (HRP) (1:5000 in blocking solution) and directed against the species of the primary antibody. After washing the membranes three times with washing buffer for 10 min, proteins were visualized by incubation of membranes in ECL solution. The ECL solution is converted into a chemiluminescent signal by the HRP and signals are detected by exposure of membranes to light-sensitive X-ray films. Quantification of protein bands was performed using the ImageJ software.

4.5.5 Stripping of membranes

In order to analyse proteins of similar sizes by western blot (see 4.5.4), primary and secondary antibodies can be removed again by incubating the membranes in a denaturing buffer containing β-mercaptoethanol and SDS. For this, membranes were incubated and shaken in stripping buffer for 40 min at room temperature and consequently washed four times with PBS for 15 min. Finally, membranes were blocked and the protein of interest was analysed as described under 4.5.4.

4.5.6 Immunoprecipitation

Immunoprecipitation (IP) describes a method, which uses specific antibodies bound to beads in order to precipitate the respective protein containing the antigen from a cell lysate. For IP experiments, cells were lysed with 500-1000 µL of 150 mM NaCl lysis buffer supplemented with inhibitors as described under 4.5.1 and 40 µL of lysate were taken as 'Input' sample to analyse protein levels in the whole cell extract (WCE). When performing an HA- or FLAG-IP from cells expressing FLAG- or HA-tagged proteins, monoclonal anti-HA-Agarose (clone Ha-7) or anti-FLAG M2 affinity agarose (both from Sigma-Aldrich) were used, respectively. Before use, beads were washed 3 times with 500-1000 µL lysis buffer by centrifugation at 1200 rpm and 4 °C for 2 min and then mixed 1:1 (v/v) with lysis buffer. FLAG M2 beads were additionally blocked with 1% (w/v) BSA in PBS for 1 h at 4°C in order to reduce unspecific binding of proteins to the beads. After blocking, beads were washed again three times with lysis buffer. A pre-clear of lysates was performed to further capture proteins, which tend to bind unspecifically to the beads. To this end, lysates were incubated with washed agarose beads for 30 min at 4°C on a rotating wheel and beads were removed again from lysates by centrifugation at 1200 rpm and 4°C for 10 min. For IP, 15 or 30 µL of bead slurry were added to lysates of cells from 10 or 15 cm plates, respectively, and incubated for 1.5-2 hrs at 4°C on a rotating wheel. Afterwards, beads were washed four times with lysis buffer as described above and then mixed with 40 µL 2x Laemmli buffer and cooked at 95°C for 5 min. For IP of endogenous proteins, cell lysates were incubated with 4 µg control IgG or specific antibody overnight at 4°C on a rotating wheel and then supplemented with protein A or G coupled to agarose or sepharose beads to capture rabbit or mouse antibodies, respectively. After further incubation for 1 h at 4°C, beads were washed and processed as described above. Finally, input and IP samples were analysed by SDS-PAGE and immunoblotting (see 4.5.2 and 4.5.4).

4.5.7 FLAG-purification for mass spectrometric analysis

In order to identify interaction partners and therefore potential substrates of OTUD6B, N-terminal FLAG-tagged OTUD6B was immunoprecipitated from HEK293T cells and co-purified proteins were analysed by mass spectrometry. To this end, thirty 15 cm plates of HEK293T cells were transfected with either FLAG empty vector or FLAG-OTUD6B by calcium phosphate transfection (see 4.4.4). Cells were harvested one day later and pellets were frozen at -80°C. Every condition was lysed in 20 mL 150 mM NaCl lysis buffer according to section 4.5.1 and lysates

were additionally passed three times through a 22 G and one time through a 26 G syringe needle to get proteins from less accessible compartments into solution. Pre-clear and FLAG immunoprecipitation was performed as described in section 4.5.6 using 600 µL beads slurry per condition without blocking the beads. After incubation with FLAG M2 beads, beads were washed four times with 30 mL lysis buffer and one time with 20 mL TBS. Subsequently, beads were transferred in 1 mL TBS in 1.5 mL tubes and FLAG-OTUD6B was eluted from the beads by incubating them with 1 mg/mL 3x FLAG peptide in TBS for 10 min at room temperature. Eluates from the same sample were pooled and 1% of eluate was mixed with Laemmli buffer for analysis of purified proteins by silver staining (see 4.5.3). Proteins were precipitated by the addition of 10% TCA overnight at 4°C. The next day, proteins were pelleted by centrifugation at 13000 rpm and 4°C for 10 min and washed three times with ice-cold acetone. Finally, proteins were dried by speed vac centrifugation at 45°C for 20 min and sent to collaborators at the Department of Proteomics and Bioanalytics at TUM for mass spectrometric analysis (see 4.5.9).

4.5.8 Proximity-dependent biotin identification (BioID)

Proximity-dependent biotin identification (BioID) is a non-affinity-based protein purification approach to identify protein-protein interactions (Roux et al. 2012). In brief, a biotin ligase from *Escherichia coli* is fused to a protein of interest and transfected into cells. Addition of biotin to the cells leads to biotinylation of proteins in direct proximity of the biotin ligase fusion protein, which can be subsequently purified by streptavidin beads after harsh lysis of cells and analysed by mass spectrometry. In this study, a smaller and modified biotin ligase from *Aquifex aeolicus* (BioID2) was used and fused to the N-terminus of OTUD6B isoform 1 and isoform 2 (Kim et al. 2016). To identify potential substrates of OTUD6B, ten 15 cm plates of HEK293T cells were transfected with either myc-BioID2-OTUD6B isoform 1 or 2 (5 µg per plate) or with the myc-BioID2 empty vector (3 µg per plate) as control by calcium phosphate transfection (see 4.4.4). Additionally, ten 15 cm plates were left untreated as another control. One day later, 50 µM biotin was added to the cells for 16 hrs and subsequently, cells were harvested and cell pellets frozen at -80°C. For the purification of biotinylated proteins, cells were lysed with 10 mL modified RIPA buffer supplemented with inhibitors and lysates were passed three times through a 22 G and one time through a 26 G syringe needle. After lysis of cells for one hour on ice, lysates were cleared by centrifugation at 13000 rpm and 4 °C for 30 min and subsequently, supernatants were incubated with 100 µL washed Strep-Tactin beads for 3 hrs at 4°C on a rotating wheel. Finally, beads were washed two times with lysis buffer and once with 50 mM ammonium bicarbonate buffer at pH 8.5 (storing buffer) and beads were sent in storing buffer to collaborators at the Department of Proteomics and Bioanalytics at TUM for mass spectrometric analysis (see 4.5.9).

4.5.9 Mass spectrometric analysis

Sample preparation and mass spectrometric analyses of OTUD6B BioID and FLAG purifications were performed by Susan Kläger and Jana Zecha, respectively, in the group of Prof.

Dr. Bernhard Küster at the Department of Proteomics and Bioanalytics at TUM. The following protocols of this section were composed by Jana Zecha.

4.5.9.1 Sample preparation of FLAG-OTUD6B purification

Dried proteins were reconstituted in 2x NuPAGE LDS Sample Buffer, reduced with 10 mM dithiothreitol for 10 min at 90°C and alkylated with 50 mM chloroacetamide for 30 min at room temperature in the dark. Half of the sample was run 1 cm into a 4-12% Bis-Tris NuPAGE gel and proteins were stained with 7.5% Roti-Blue (Carl Roth) in 20% methanol for 20 min. Excessive staining solution was washed away with several 25% ethanol washes and the gel was stored in 1% acetic acid. In-gel digestion of proteins was performed under keratin-free conditions. Protein bands were cut out and destained twice using 100 µL of 50% ethanol in 2.5 mM triethylammonium bicarbonate (TEAB, 1 and 2 hrs at 50°C). Following 3 cycles of dehydration in 100 µL absolute ethanol (10 min at room temperature) and washing using 100 µL of 5 mM TEAB (20 min at room temperature), trypsin (250 ng in 25 µL of 5 mM TEAB) was added. After incubation for 15 min at 4°C, remaining trypsin was removed and 20 µL of 5 mM TEAB were added. Digestion was carried out overnight at 37°C. Digestion solutions were acidified using 5 µL of 5% formic acid (FA) and peptides were extracted in three steps (each for 20 min at room temperature) adding twice 20 µL of 1% FA and once 20 µL of 60% acetonitrile (ACN) in 0.04% FA. Gel slices were dried twice for 15 min using 30 µL and 20 µL ACN. All extraction and drying fluids were collected and dried in a speedvac and stored at -20° C.

4.5.9.2 Sample preparation of OTUD6B BioID purification

Samples of the OTUD6B BioID purification were prepared as described previously (Comartin et al. 2013). Streptavidin beads with bound proteins were spun down and ammonium bicarbonate was removed. Beads were re-suspended in 200 µL of 50 mM TEAB and proteins were reduced adding 10 µL of 1 M DTT (1 h, 37°C, 600 rpm) and alkylated adding 20 µL of 550 mM CAA (30 min, at room temperature in the dark). Digestion was performed overnight at 37°C and 700 rpm using trypsin (3 µL of 1µg/µL trypsin solution in 1 mM HCl). The next morning, another 1.5 µg trypsin were added and incubated for 2 hrs at 37°C and 700 rpm. After centrifugation, supernatant containing peptides was transferred to a new reaction vessel and beads were washed twice using 150 µL TEAB. The washes were combined with the peptide solution, dried down in a speedvac and stored at -20°C.

4.5.9.3 LC-MS/MS measurements

Tryptic peptides were reconstituted in 0.1% FA and analysed by nanoLC-MS/MS on an Eksigent NanoLC-Ultra 1D+ system or a Dionex Ultimate 3000 UHPLC+ system coupled to a Q Exactive HF mass spectrometer (Thermo Fisher Scientific). For FLAG-IP and BioID samples 25% and 5%, respectively, were injected. After 10 min of washing (0.1% FA, 5 µL/min) on a trap column (75 µm x 2 cm, 5 µm C18 resin; Reprosil PUR AQ, Dr. Maisch), peptides were transferred to an

analytical column (75 µm x 45 cm, 3 µm C18 resin; Reprosil Gold, Dr. Maisch) and separated at 300 nL/min using a 100 min (FLAG-IP) or 50 min (BioID) linear gradient from 4% to 32% LC solvent B (0.1% FA, 5% dimethyl sulfoxide (DMSO) in ACN) in LC solvent A (0.1% FA in 5% DMSO). The Q Exactive HF was operated in data dependent and positive ionization mode. For FLAG-IP samples, MS1 spectra were recorded in the Orbitrap from 360 to 1300 m/z at a resolution of 60K (automatic gain control (AGC) target value of 3e6 charges, maximum injection time (maxIT) of 10 ms). After peptide fragmentation via higher energy collisional dissociation (normalized collision energy of 25%), MS2 spectra for peptide identification were recorded in the Orbitrap at 30K resolution via sequential isolation of up to 20 precursors (isolation window 1.7 m/z, AGC target value of 2e5, maxIT of 50 ms, dynamic exclusion of 35 s). BioID samples were measured as specified above with following modifications: MS1 maxIT was set to 50 ms. MS2 spectra were recorded at 15k resolution using an AGC target value of 1e5 and a dynamic exclusion of 20 s.

4.5.9.4 MS data base search and analysis

Peptide and protein identification and quantification for BioIDs were performed using MaxQuant 1.5.3.30 by searching the MS2 spectra against the human reference proteome supplemented with common contaminants. FLAG-IP raw data were searched using MaxQuant v1.5.6.5 and the SwissProt database. The match-between-runs and label-free quantification algorithms were enabled. All other search parameters were left as default. Protein intensities were computed as the sum of the area-under-the-curve of chromatographic elution profiles of peptides assigned to the proteins.

4.5.10 *In vivo* ubiquitylation

Whether knockdown or overexpression of a ubiquitin E3 ligase or a DUB have an effect on ubiquitylation of another protein (substrate) was analysed by *in vivo* ubiquitylation assays under denaturing conditions. For this, 10 cm plates of HEK293T cells were transfected by lipofection (see 4.4.4) with the following amounts of plasmid: 1-3 µg HA-ubiquitin, 5 µg FLAG-tagged substrate and 5 µg untagged E3 ligase or DUB, the latter only for overexpression studies. For knockdown experiments, cells were transfected one day before with the respective siRNA targeting the E3 ligase or DUB or control siRNA. One day after DNA transfection, cells were harvested and directly lysed with 100 µL of 250 mM NaCl lysis buffer supplemented with inhibitors for 10 min on ice without freezing cells. After centrifugation for 10 min at 13000 rpm and 4 °C, 10 µL were taken as input sample and diluted 1:3 with lysis buffer. The lysates were denatured by the addition of 10 µL 10% SDS and boiling at 95°C for 5 min. After the samples have cooled down to room temperature, they were diluted with 900 µL lysis buffer supplemented with 1% Triton X-100 and incubated on ice for 15 min. Finally, the FLAG-tagged substrate was immunoprecipitated using FLAG M2 beads as described in 4.5.6.

4.5.11 DUB activity assay

DUB activity assay was performed to analyse whether a specific DUB is catalytically active by using the HA-ubiquitin-vinyl sulfone (HA-Ub-VS) probe as substrate. Ubiquitin-vinyl sulfone is a specific inhibitor of most DUBs as it irreversibly modifies the catalytic centre if the DUB possesses catalytic activity (Borodovsky et al. 2001). The N-terminal HA-tag allows immunoprecipitation of active DUBs, which have been modified by ubiquitin-vinyl sulfone.

Cells were lysed with DUB activity buffer without any inhibitors as described under 4.5.1. After measuring protein concentrations, lysates corresponding to 62.5 µg protein were mixed with 5 µL 25 µM HA-Ub-VS (4-6 µM final concentration) and incubated at 37°C for 45 min. The reaction was stopped and lysates were denatured by the addition of 1% SDS and subsequent boiling at 95°C for 5 min. After the lysates have cooled down to room temperature for 5 min, they were diluted with DUB activity buffer to a final volume of 500 µL and put back on ice. Active DUBs modified by HA-Ub-VS were immunoprecipitated by 15-20 µL HA-Agarose as described under 4.5.6. Finally, the beads were washed four times with 250 mM lysis buffer and diluted with 30-40 µL 2x Laemmli buffer. Whole cell extracts and IP samples were analysed by SDS-PAGE and immunoblotting (see 4.5.2 and 4.5.4) using antibodies detecting the DUB of interest.

4.5.12 Dephosphorylation of lysates

In order to dephosphorylate proteins by Lambda Protein Phosphatase (λ-PPase), cell lysates were supplemented with 1x PMP Buffer (NEB), 1 mM $MnCl_2$ (NEB) and 40 units λ-PPase per 50 µL lysate and incubated at 30°C for 30 min.

For dephosphorylation of cell lysates by Calf Intestinal Alkaline Phosphatase (CIP), cells were lysed in CIP buffer and supplemented with 20 units CIP per 1 mL lysate. The reaction mix was incubated for 10 min at room temperature for IP experiments.

4.5.13 *In vitro* translation

In vitro translation describes a method which allows translation and transcription of a protein in a cell-free system. In this study, the TNT T7 Coupled Reticulocyte Lysate System (Promega) containing T7 RNA polymerase was used to produce FLAG-tagged CEP192 according to manufacturer's protocol. The reaction was performed at 23°C for 90 min.

4.5.14 *In vitro* binding assay

To investigate whether FBXL13 binding to CEP192 is direct, an *in vitro* binding assay was performed using *in vitro* translated and transcribed FLAG-CEP192 and FBXL13 purified from insect cells (see 4.5.13 and 4.6.4, respectively). To this end, two IVT reactions of FLAG-tagged proteins were pooled and filled up to 200 µL with 150 mM lysis buffer and incubated with 10 µL washed FLAG M2 bead slurry for 1.5 hrs at 4°C. Beads were washed three times with lysis buffer and then incubated together with purified FBXL13 or FBXL16 in 100 µL lysis buffer for 1 h at 4 °C

on a rotating wheel. Finally, beads were washed four times and mixed with 40 µL 2x Laemmli buffer for analysis by SDS-PAGE and immunoblotting (see 4.5.2 and 4.5.4).

4.6 Protein purification from insect cells

Insect cells are commonly used for large-scale purification of recombinant eukaryotic proteins as protein yields are higher than in mammalian expression systems and many post-translational modifications are conserved. In this study, the BacPAK Baculovirus Expression System (Clontech) was used to purify GST-SKP1 together with FBXL13 or FBXL16 according to manufacturer's protocol.

4.6.1 Insect cell culture

Sf21 cells derived from *Spodoptera frugiperda* were used for the production and amplification of the virus. Cells were cultured in Grace's insect medium supplemented with 10% heat-inactivated FBS and 10 µg/mL gentamycin at 27°C in cell culture flasks and split when they reached 80-90% confluency.

High Five cells derived from *Trichoplusia ni* were used for protein production. Cells were cultured in Express Five SFM medium supplemented with 10 mM L-Glutamine and 10 µg/mL gentamycin at 27°C in cell culture flasks.

4.6.2 Transfection of insect cells and virus production

For production of virus, 1x 10^6 Sf21 cells were seeded per 4 cm plate and transfected after 1.5 hrs with pBacPAK9 plasmid containing either GST-SKP1, FBXL13 or FBXL16 cDNA using Bacfectin (Clontech) according to manufacturer's protocol. After 6 days, virus was harvested and passed through a 0.45 µM filter. In order to amplify virus, a 75 cm^2 flask of Sf21 cells in 30 mL growth medium was infected with 100 µL virus and amplified virus was harvested and filtered after 6 days.

4.6.3 Protein production

For large-scale production of protein, 90 mL of High Five cells were infected with 5 mL GST-SKP1 virus together with 5 mL FBXL13 or FBXL16 virus. After 6 days, cells were washed once with PBS, harvested and cell pellets were frozen at -80°C.

4.6.4 GST-purification of proteins

GST-tagged SKP1 bound to FBXL13 or FBXL16 was purified from High Five cells. To this end, cells were lysed in 10 mL of 250 mM NaCl lysis buffer supplemented with inhibitors and lysates passed once through a 22 G syringe needle and incubated for 20 min on ice. After centrifugation at 13000 rpm and 4°C, supernatant was incubated with 200 µL Glutathione Sepharose 4B bead slurry for 1 hour at 4°C on a rotating wheel. Beads were washed three times with lysis buffer and

proteins were eluted from beads by incubation two times with 300 µL elution buffer (35 mM glutathione, 100 mM Tris-HCl pH 8.0, 120 mM NaCl) at 4°C for 15 min. Purified proteins were aliquoted and frozen at -80°C.

4.7 Statistical analysis

All quantified experiments were performed in indicated numbers of biological replicates. qPCR analysis was additionally conducted in three technical replicates per biological replicate. Statistical evaluations of data sets were performed using the GraphPad Prism software and significance was analysed by one sample t-test, Student's t-test, unpaired t-test, Mann-Whitney test non-parametric, Pearson's correlation or linear regression, according to the assumption of the test and depending on the data. One sample t-tests of relative ratios were calculated using a hypothetical value of 1.0. Standard errors depicted in graphs represent means ± standard deviation (S.D.). Calculated *P* values are denoted in the figure legends and indicated in graphs according to following distributions: *, $P < 0.05$; **, $P < 0.01$; ***, $P < 0.001$; ****, $P < 0.0001$.

5 Results I

This study was conducted in the research group of Prof. Dr. Florian Bassermann at Klinikum rechts der Isar (Technical University of Munich) with help of collaborators from other research groups and institutes and contains parts of the master thesis of Michaela Walzik (Walzik 2017). For comprehensive reasons, some contributions by these collaborators are included in this thesis and these respective parts are indicated in the text and figure legends.

5.1 CRISPR/Cas9 screen of DUBs and F-box proteins in MM1.S cells

5.1.1 Establishment of a MM1.S Cas9 cell line

Despite intense research, multiple myeloma (MM) remains an incurable malignancy, making new treatment options an urgent need. Given the fact, that MM patients response to proteasomal inhibition, e.g. by the drugs bortezomib or carfilzomib, suggests that the ubiquitin proteasome system (UPS) plays a pivotal role in the development and maintenance of this disease.

In order to identify new oncogenic components of the UPS, which might play a role in the pathophysiology of MM and bortezomib resistance, a CRISPR/Cas9 screen was conducted in the MM cell line MM1.S. CRISPR/Cas9 system allows genomic alterations, e.g. gene knockout, due to the ability of Cas9 enzyme to cut genomic DNA in a precise locus, marked by sgRNA. A two-vector system, which has been previously described (Sanjana, Shalem, and Zhang 2014; Shalem et al. 2014), was chosen over a one-vector system to increase infection rates by generating viruses composed of smaller vectors. In the two-vector system, first a stable Cas9 expressing cell line is generated, which in turn can be infected by a second vector containing the sgRNA. By lentiviral infection and subsequent selection with blasticidin, Cas9 enzyme was stably integrated in MM1.S cells. Expression of FLAG-tagged Cas9 was confirmed by immunoblot analysis of whole cell extracts from MM1.S wildtype and Cas9 cell lines (Figure 10a). Importantly, analysis of proliferation rates revealed no differences in growth rates between MM1.S wildtype and Cas9 expressing cells, ensuring that Cas9 was not integrated in an essential or tumour suppressor gene locus (Figure 10b).

Next, MM1.S Cas9 cells were infected with constructs containing specific sgRNAs to test whether and in which time frame a CRISPR/Cas9-mediated knockout is achieved in these cells. In order to allow monitoring and flow cytometric analysis of infected cells, the puromycin resistance cassette of the lentiGuide-Puro vector was exchanged by eGFP (done by Oleksandra Karpiuk). Expression of sgRNAs targeting either FBXO3 or USP24 and subsequent cell sorting of GFP positive cells by FACS at different time points revealed a strong decrease in the protein levels of FBXO3 and USP24 within five days compared to control sgRNA (sgNT) expressing cells (Figure 11a, b). Of note, the decrease in USP24 protein level took twice as long as the knockout of FBXO3, suggesting that the knockout efficiency varies between sgRNAs and genes.

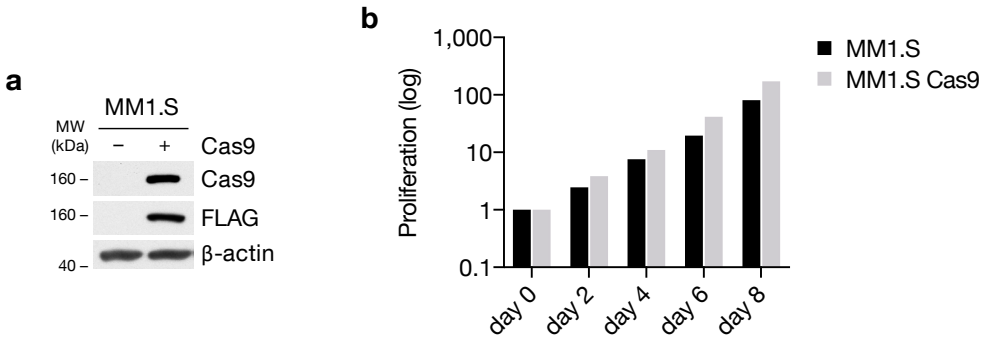

Figure 10: Generation of stable MM1.S Cas9 cells. (a) Immunoblot analysis of wildtype MM1.S cells and MM1.S cells, which were lentivirally transduced with Cas9 enzyme and selected with 3 µg/mL blasticidin for two weeks, using the indicated antibodies. β-actin served as a loading control. **(b)** Proliferation analysis of cell lines described in **a**. Equal numbers of cells were seeded on day 0 and viable cells were counted using the trypan blue exclusion method at indicated time points.

As the CRISPR/Cas9 screen conducted in this study represented a negative selection screen and thus cells expressing sgRNA targeting essential or oncogenic genes should exhibit a proliferation defect, MM1.S Cas9 cells were infected with sgRNAs targeting RNA polymerase II (sgPOLR2I) or ribosomal Protein L8 (sgRPLP8), both essential proteins, in order to test whether these cells die out compared to non-targeting sgRNA expressing cells. The percentage of infected, GFP positive cells expressing the respective sgRNAs compared to uninfected cells was determined over time by flow cytometric analysis. As expected, the portions of cells expressing sgPOLR2I or sgRPL8 were strongly reduced 12 days after infection (Figure 11c). Overall, the generated MM1.S Cas9 cell line revealed a fast knockout establishment, which could be confirmed by immunoblot and FACS analyses and therefore was concluded to be suitable for a CRISPR/Cas9 screen.

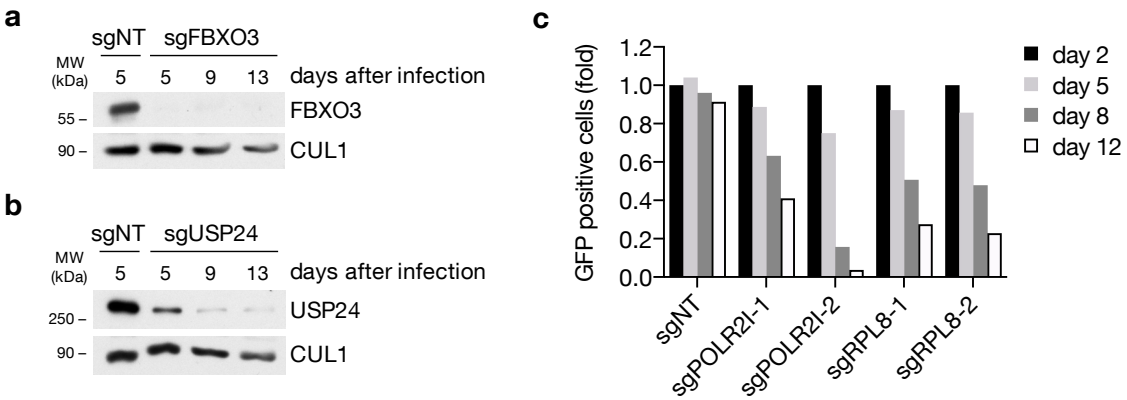

Figure 11: CRISPR/Cas9-mediated knockout in MM1.S Cas9 cells. (a, b) Immunoblot analysis of MM1.S Cas9 cells, which were lentivirally infected with constructs expressing a non-targeting sgRNA (sgNT) or sgRNAs targeting FBXO3 **(a)** or USP24 **(b)**. GFP expressing cells were sorted and harvested at indicated time points after infection and whole cell extracts were probed with the indicated antibodies. CUL1 served as a loading control. **(c)** Proliferation analysis of MM1.S Cas9 cells infected with either control sgRNA (sgNT) or sgRNAs targeting RNA polymerase II (sgPOLR2I-1 and -2) and ribosomal Protein L8 (sgRPL8-1 and-2). The ratio of sgRNA expressing, GFP positive cells to uninfected cells was measured by flow cytometric analysis at the indicated time points after infection. Results are presented in relation to day 2.

Besides the generation of a fast and efficient knockout, it was important to infect cells at a low multiplicity of infection (MOI) in order to ensure that every cell expresses only one sgRNA when using a pooled screening approach. In order to estimate how much virus should be used for the screen, MM1.S Cas9 cells were infected with different volumes of virus containing lentiGuide-GFP or lentiGuide-mCherry at a ratio of 1:1 and the percentage of GFP/mCherry double positive cells was determined by flow cytometric analysis (Figure 12a, b). Both, the overall as well as the double infection rate, declined with decreasing volume of virus. However, the portion of GFP/mCherry positive cells reached a plateau and thus did not further decrease by lowering the virus amount, suggesting that some cells are prone to multiple infection events (Figure 12b). Since a certain infection rate was necessary to infect enough cells, a volume of 200 µL virus per one million cells was later on used for the screen.

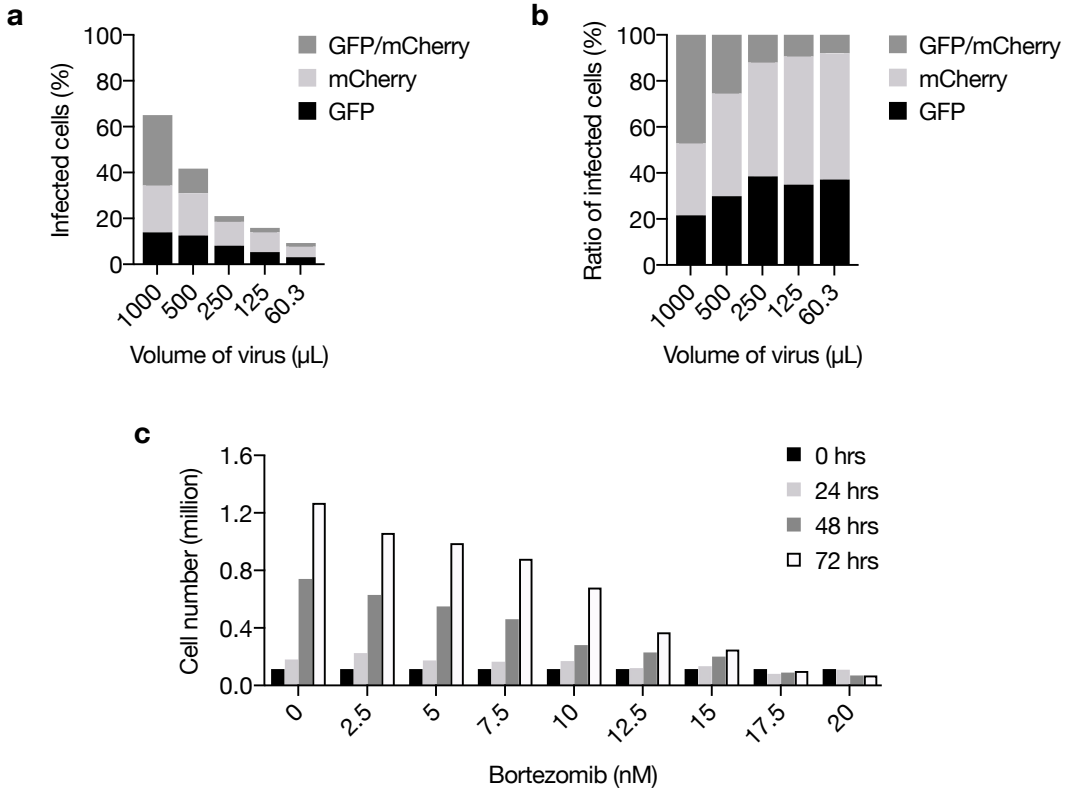

Figure 12: Analysis of infection rates and bortezomib response in MM1.S Cas9 cells. (a, b) Flow cytometric analysis of MM1.S Cas9 cells, which were lentivirally transduced with constructs expressing control sgRNA and either GFP or mCherry. Cells were infected with indicated volumes of total virus (1:1 mixture of GFP and mCherry virus) and the percentage of cells expressing GFP, mCherry or both (GFP/mCherry) was determined by flow cytometric analysis 4 days after infection. Results depict the percentage **(a)** and the ratio of infected cells **(b)**. **(c)** Proliferation analysis of MM1.S Cas9 cells, which were treated with the indicated concentrations of bortezomib for 72 hrs. Viable cells were counted using the trypan blue exclusion method after 24, 48 and 72 hrs.

Last, MM1.S Cas9 cells were treated with different concentration of bortezomib, a proteasomal inhibitor, which is used for the treatment of MM, to determine a concentration, at which cells still proliferate (Figure 12c). Proliferation of cells under bortezomib treatment was necessary to allow negative selection of cells expressing sgRNAs, which confer bortezomib

resistance, during the CRISPR/Cas9 screen. For this purpose, bortezomib concentrations between 0 and 20 nM were chosen and cell numbers were determined every day over 72 hrs. Dose-dependent cell proliferation rates could be observed, in which a concentration of 12.5 nM bortezomib allowed slow cell growth and therefore this concentration was suitable for screening (Figure 12c).

5.1.2 Generation of DUB and F-box protein sgRNA libraries

Two separate sgRNAs libraries targeting either 98 DUBs or 72 F-box proteins were designed and generated by Oleksandra Karpiuk (Figure 13). Sequences of sgRNAs were taken from the human CRISPR knockout pooled library (GeCKO v2) designed in the laboratory of Feng Zhang (Sanjana, Shalem, and Zhang 2014) and are listed in the appendix (see 11.1). Forward and reverse oligos were ordered premixed in 96-well plates and annealed and ligated into the lentiGuide-GFP vector. After pooling of ligated vectors, the libraries were amplified in bacteria. Both libraries contained 12 non-targeting sgRNAs and 5 positive controls targeting essential genes encoding for RNA polymerase II (POLR2I), ribosomal proteins (RPL8, RPL32, RPS19) and Replication protein A (RPA3). Three sgRNAs were chosen per gene ending up with 321 constructs for the DUB and 243 constructs for the F-box protein library.

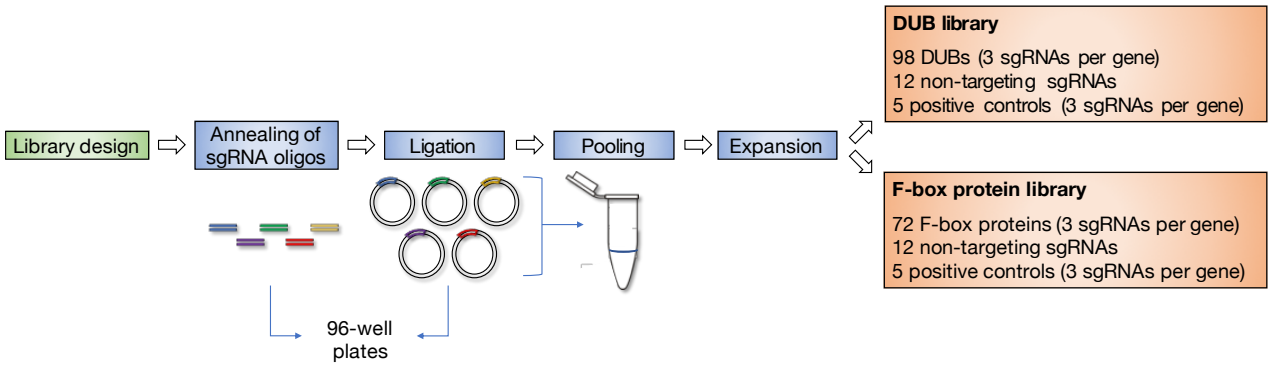

Figure 13: Workflow of CRISPR/Cas9 sgRNA library preparation. Sequences of sgRNAs for DUB and F-box protein libraries were taken from the human CRISPR knockout pooled library (GeCKO v2) from Feng Zhang (Sanjana, Shalem, and Zhang 2014). sgRNA oligos were ordered premixed, annealed in 96-well plates and ligated into the lentiGuide-GFP vector in 96-well plates. Ligated vectors were mixed and pooled libraries were expanded in bacteria. Both libraries contained three sgRNAs per gene as well as non-targeting control sgRNAs.

To ensure an equal sgRNA distribution within the libraries, sgRNAs were amplified by a two-step PCR approach and analysed by next generation sequencing (NGS). Data analysis and mapping was performed by Thomas Engleitner from the group of Roland Rad (Department of Medicine II at the Klinikum rechts der Isar). Importantly, most of the sgRNAs were detected by 3000-10000 reads representing an applicable distribution and abundance of sgRNAs (Figure 14a, b). Another important requirement for the screen was that the sgRNA distribution does not change after infection to ensure that all sgRNAs are represented. To test this, MM1.S Cas9 cells were infected with either of both libraries and GFP positive cells were sorted two days later. sgRNAs

were amplified from genomic DNA and analysed by NGS. Comparison of sgRNA reads before and after infection revealed that infection did not influence the composition of the libraries (Figure 14c, d).

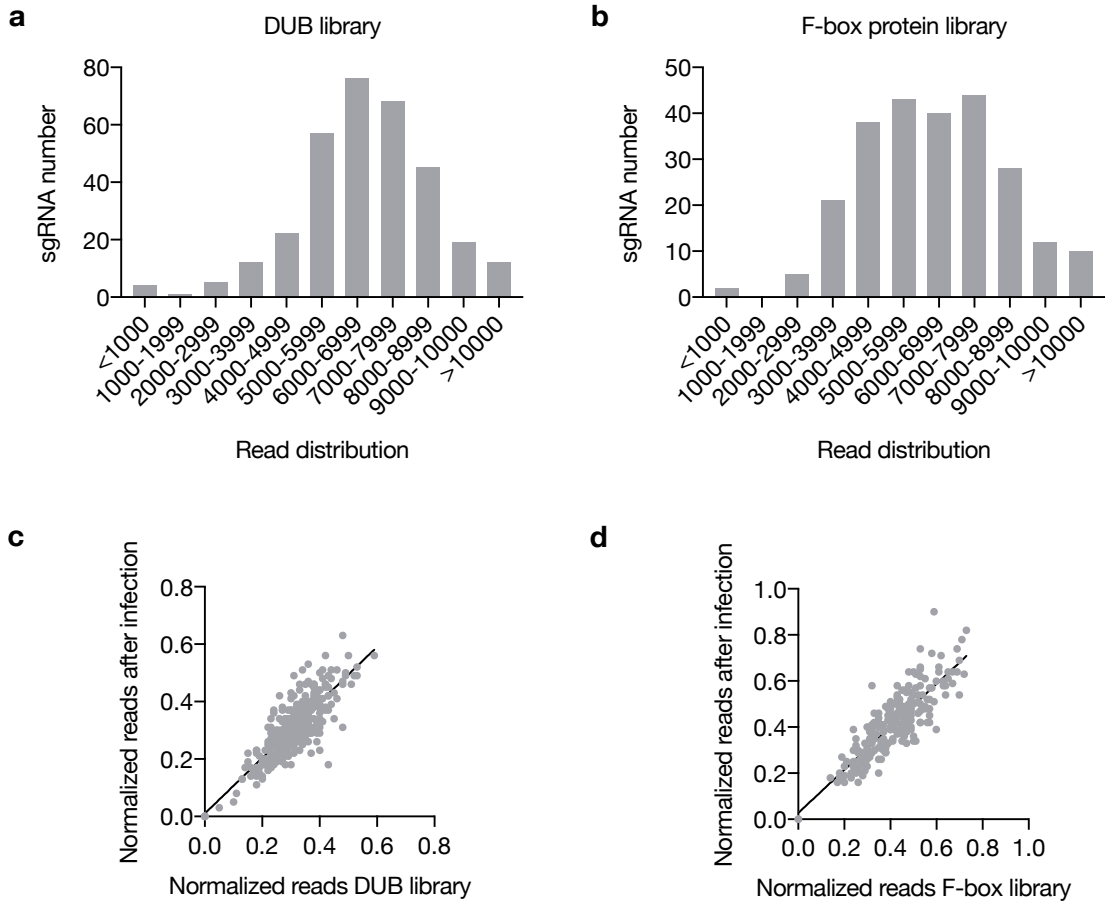

Figure 14: Quantification of sgRNA libraries. (a, b) Analysis of sgRNA abundance in the pooled DUB **(a)** and F-box protein libraries **(b)**. sgRNAs were amplified by a two-step PCR approach and analysed by next generation sequencing (NGS). **(c, d)** Comparison of sgRNA abundance before and after infection of MM1.S Cas9 cells. Cells were transduced with the pooled DUB **(c)** or F-box protein library **(d)** and two days later, GFP expressing cells were sorted by FACS and harvested. sgRNAs were amplified from genomic DNA or from library vectors and analysed by NGS.

5.1.3 Pooled CRISPR/Cas9 screen in MM1.S Cas9 cells

High response rates to proteasomal inhibition (e.g. by bortezomib) in MM patients implicate aberrant functions of UPS components in this pathology. In order to identify new oncogenes within the UPS, which are involved in the pathophysiology of MM and bortezomib resistance, a CRISPR/Cas9 screen of all DUBs and F-box proteins was conducted in the stably Cas9 expressing MM cell line MM1.S. For this purpose, MM1.S Cas9 cells were infected with low virus titres of either DUB or F-box protein library (200 µL virus per million cells) to ensure single infection events and GFP expressing cells were sorted two days later by FACS. Half of the cells were harvested and reflected the sgRNA composition on day 0. For the untreated condition, cells were cultured for 14 days. In parallel, cells were treated with a sub-lethal dose (12.5 nM) of bortezomib

for eight days in order to screen for genes, which mediate bortezomib resistance (Figure 15). Genomic DNA from day 0, the untreated condition and bortezomib treatment was isolated and sgRNAs were amplified by a two-step PCR approach and analysed by NGS. Data analysis and mapping was performed by Thomas Engleitner from the group of Roland Rad (Department of Medicine II at the Klinikum rechts der Isar). The conditions chosen for the screen corresponded to a negative selection screen and thus, cells expressing sgRNAs targeting essential or oncogenic genes were expected to drop out during the screen. Consequently, the ratio of reads between day 0 and day 14 was decreased in this case. The same is true for reads of sgRNAs targeting genes which confer bortezomib resistance under bortezomib treatment. Genes were presumed as hits and therefore were further investigated when the following criteria were fulfilled: (1) at least two sgRNAs are depleted, (2) the sgRNAs are depleted to at least 30% (< 0.7-fold change) and (3) the gene is mostly uncharacterized.

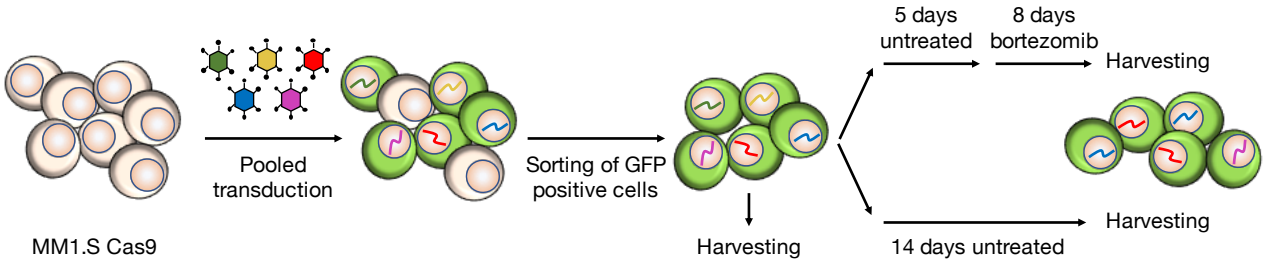

Figure 15: Workflow of CRISPR/Cas9 screen in MM1.S Cas9 cells. MM1.S Cas9 cells were infected with low virus titres of either DUB or F-box protein library and two days later, GFP expressing cells were sorted by FACS. Half of the cells were harvested and reflected sgRNA composition on day 0. For the untreated condition, cells were cultivated for 14 days and harvested. In parallel, cells were treated with a sub-lethal dose (12.5 nM) of bortezomib for eight days. Genomic DNA was isolated from samples and sgRNAs were amplified by a two-step PCR approach and analysed by next generation sequencing.

5.1.4 CRISPR screen of F-box proteins identifies FBXW10 as potential oncogene

For the F-box protein screen, sgRNAs targeting 72 F-box protein genes described in the human genome were chosen. A list of the screening data is attached in the appendix (see 11.2.1). Of note, all positive controls targeting essential genes were strongly reduced and represented the most depleted sgRNAs in both conditions, untreated and under bortezomib treatment (Figure 16a, b). Besides the positive controls, many F-box proteins that have been previously described to be important for cell survival or proliferation scored. For instance, FBXW11, also known as β-TrCP2, has been described to be involved in many cellular mechanisms including cell cycle regulation (Fuchs et al. 1999; Kitagawa et al. 1999; Shirane et al. 1999). Other known genes were Cyclin F (CCNF) and SKP2, two F-box proteins playing an important role in cell cycle progression (Bai, Richman, and Elledge 1994; Tsvetkov et al. 1999; Yu, Gervais, and Zhang 1998).

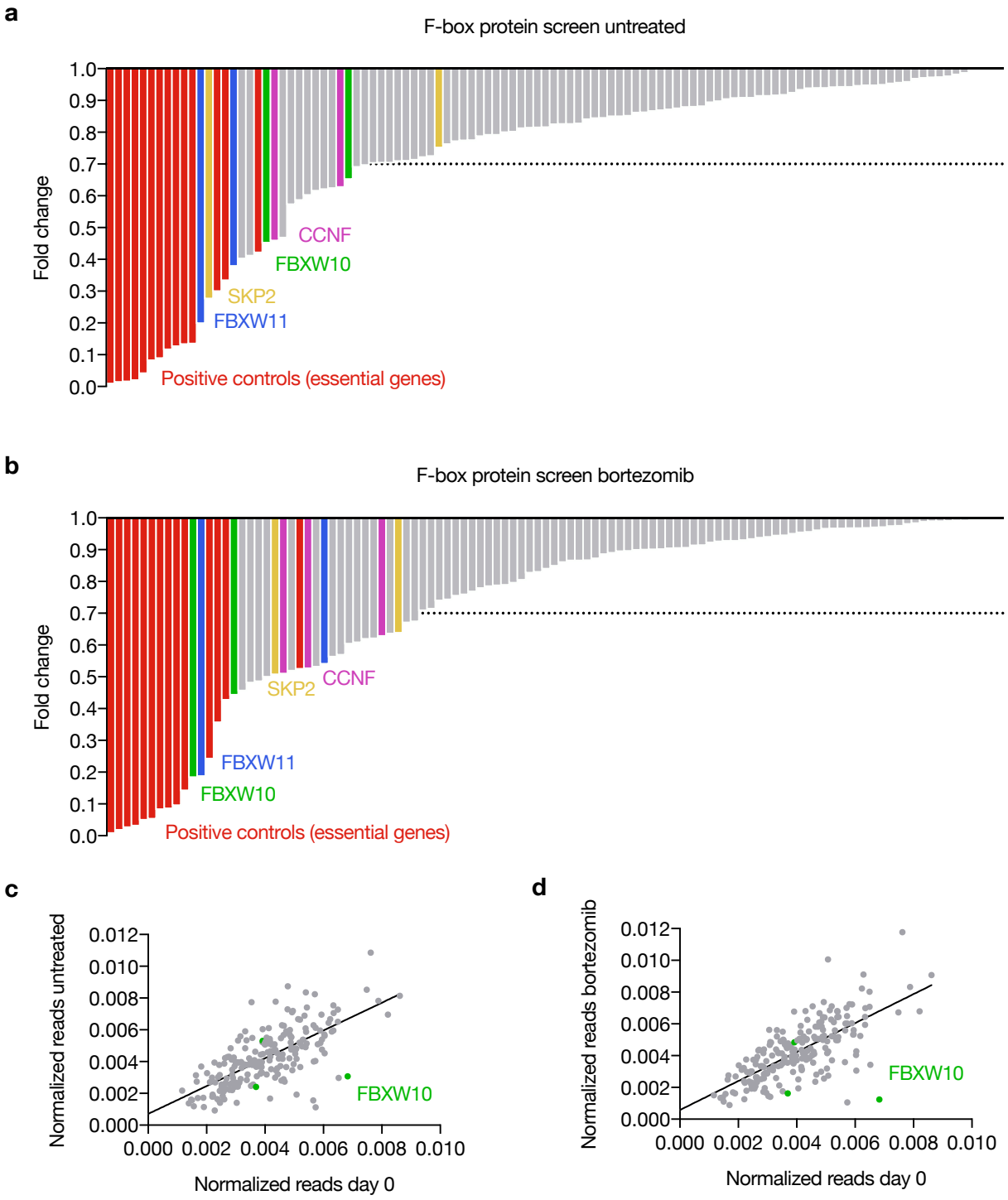

Figure 16: CRISPR/Cas9 screen of F-box proteins in MM1.S Cas9 cells. (a-d) MM1.S Cas9 cells were infected with virus of the pooled F-box protein library and two days later, GFP expressing cells were sorted by FACS. Half of the cells were harvested and reflected sgRNA composition on day 0. For the untreated condition **(a, c)**, cells were cultivated for 14 days. In parallel, cells were treated with a sub-lethal dose (12.5 nM) of bortezomib for eight days **(b, d)**. Genomic DNA was isolated from samples and sgRNAs were amplified by a two-step PCR approach and analysed by next generation sequencing. Reads of individual sgRNAs were normalized to the total number of reads and results of the untreated condition or bortezomib treatment are depicted in relation to **(a, b)** or blotted against **(c, d)** reads on day 0. Known F-box proteins are highlighted in blue, purple and yellow and positive controls are shown in red **(a, b)** whereas uncharacterized hits are marked in green **(a-d)**. Dashed line in **a** and **b** marks a change of 0.7-fold.

Given a strong depletion of sgRNAs of the positive controls and many known F-box proteins, the screen was successful and could be used to identify new potential oncogenes. Strikingly, two sgRNA of the uncharacterized F-box protein FBXW10 (sgFBXW10-1 and -2) were strongly decreased in the untreated condition (down to 0.45 and 0.65) and even more reduced upon bortezomib treatment (down to 0.18 and 0.44) (Figure 16a-d), thus corresponding to the hit criteria defined in 5.1.3.

5.1.5 CRISPR-mediated knockout of FBXW10 confirms screening result

Since the pooled CRISPR/Cas9 screen was based on a highly dynamic cell population, in which every cell carried a different gene knockout, it was important to verify the results. Therefore, MM1.S Cas9 cells were individually infected with the three sgRNAs targeting FBXW10 and the percentage of GFP positive cells was measured over time by flow cytometric analysis. Like in the screen, expression of sgFBXW10-1 and -2 strongly reduced the ratio of sgRNA expressing, GFP positive cells to uninfected cells (down to 0.45 and 0.65 in the screen versus 0.50 and 0.60 in the validation) (Figure 17a). Importantly, the simultaneous treatment of cells with bortezomib increased the growth disadvantage caused by FBW10 knockout, which was observed before in the untreated condition, in line with the results of the screen (Figure 17b). Interestingly, when infected individually, also the third sgRNAs against FBXW10 (sgFBXW10-3) showed a slight effect, which was not the case in the screen (Figure 16). Taken together, knockout of FBXW10 in MM1.S cells led to a decreased cell number within a mixed population composed of infected and uninfected cells. Whether this reduction is caused by a decrease in cell proliferation or an increase in cell death remains unclear.

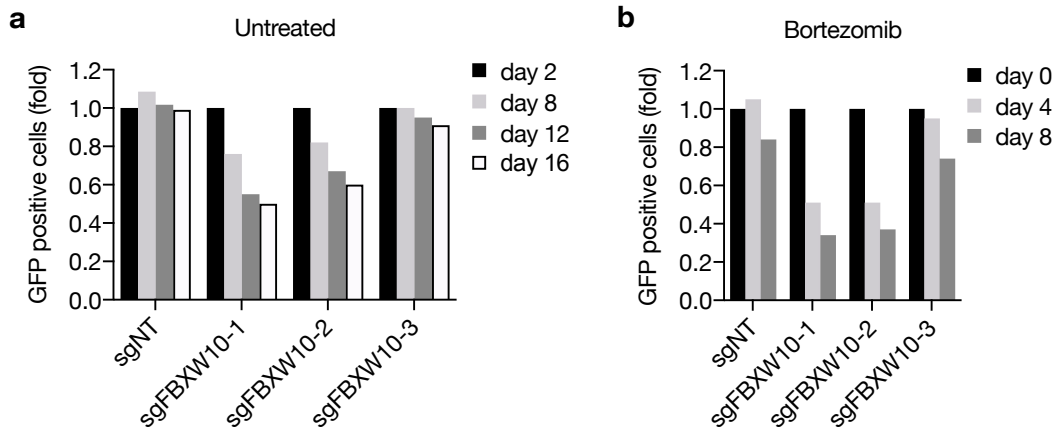

Figure 17: CRISPR-mediated knockout of FBXW10 leads to a growth disadvantage. Proliferation analysis of MM1.S Cas9 cells infected with either control sgRNA (sgNT) or 3 different sgRNAs targeting FBXW10 (sgFBXW10-1, -2 and -3). The ratio of sgRNA expressing, GFP positive cells to uninfected cells was measured by flow cytometric analysis at the indicated time points. Cells were let untreated **(a)** or treated with 12.5 nM bortezomib for 8 days starting at day 12 after infections (day 0) **(b)** and results are depicted in relation to day 2 after infection.

In order to confirm that the sgRNAs against FBXW10 indeed caused a specific knockout of FBXW10, different qPCR oligonucleotides were designed and tested. However, qPCR analysis of FBXW10 in various MM cell lines including MM1.S cells could hardly detect FBXW10 mRNA, suggesting that FBXW10 is very little or not expressed in these cells, thus questioning whether FBXW10 could represent a potential new oncogene. Since no functional antibody against FBXW10 was available, knockout of FBXW10 could also not be confirmed by immunoblotting. As the aim of this study was to identify new potential oncogenes within the UPS, a gene, that is hardly detectable in a cell, does not represent a promising candidate and therefore this hit was not further followed up.

5.1.6 CRISPR screen of DUBs identifies OTUD6B as potential oncogene

There is a growing list of DUBs, which are involved in cancer cell biology by regulating various pathways like proliferation, DNA repair and gene transcription (Henry et al. 2003; Li et al. 2002; Zhang et al. 2006). In order to screen for new oncogenic DUBs in MM, sgRNAs against 98 DUBs were used in a pooled CRISPR/Cas9 screen. In line with the previous results of the F-box protein screen, many positive controls were depleted to more than 80%, however this time also other sgRNAs scored in this range (Figure 18a, b). Of note, these sgRNAs were targeting essential proteins like PSMD14, a component of the 26S proteasome, or USPL1, which is a SUMO-specific isopeptidase and thus desumoylates other proteins (Schulz et al. 2012). A list of all screening results is attached in the appendix (see 11.2.2). Similarly to the F-box protein screen, many well described DUBs could be found depleted in both conditions. Some examples are BAP1, a histone H2A deubiquitinase (Scheuermann et al. 2010) and USP5, which was shown to stabilize c-Maf, a key transcription factor in MM (Wang, Juan, et al. 2017) (Figure 18a, b). Strikingly, two sgRNAs against USP14 were only depleted under bortezomib treatment (Figure 18b), in line with a previous publication, which showed that inhibition of USP14 in MM cells overcomes bortezomib resistance (Tian, D'Arcy, et al. 2014). Most importantly, two sgRNAs against OTUD6B (sgOTUD6B-2 and -3), a mostly uncharacterized DUB, were decreased to 0.56 and 0.65 in the untreated condition (Figure 18a, c) and to 0.19 and 0.47 under bortezomib treatment (Figure 18b, d), thus matching the hit criteria (see 5.1.3).

5.1.7 CRISPR-mediated knockout of OTUD6B confirms screening result

The strong depletion of cells expressing sgRNAs against OTUD6B during the screen suggests that OTUD6B has an impact on MM proliferation or viability. To confirm this hypothesis, MM1.S Cas9 cells were individually infected with the three sgRNAs used in the screen (sgOTUD6B-1, -2 and -3) or a non-targeting control (sgNT) and the percentage of GFP positive cells was monitored over time by flow cytometric analysis. In agreement with the results of the screen, the number of cells expressing sgOTUD6B-2 or -3 decreased significantly, while the number of control sgRNA infected cells did not change compared to uninfected cells (Figure 19a). When infected individually, sgOTUD6B-1 also caused a small but significant decrease in the percentage of GFP

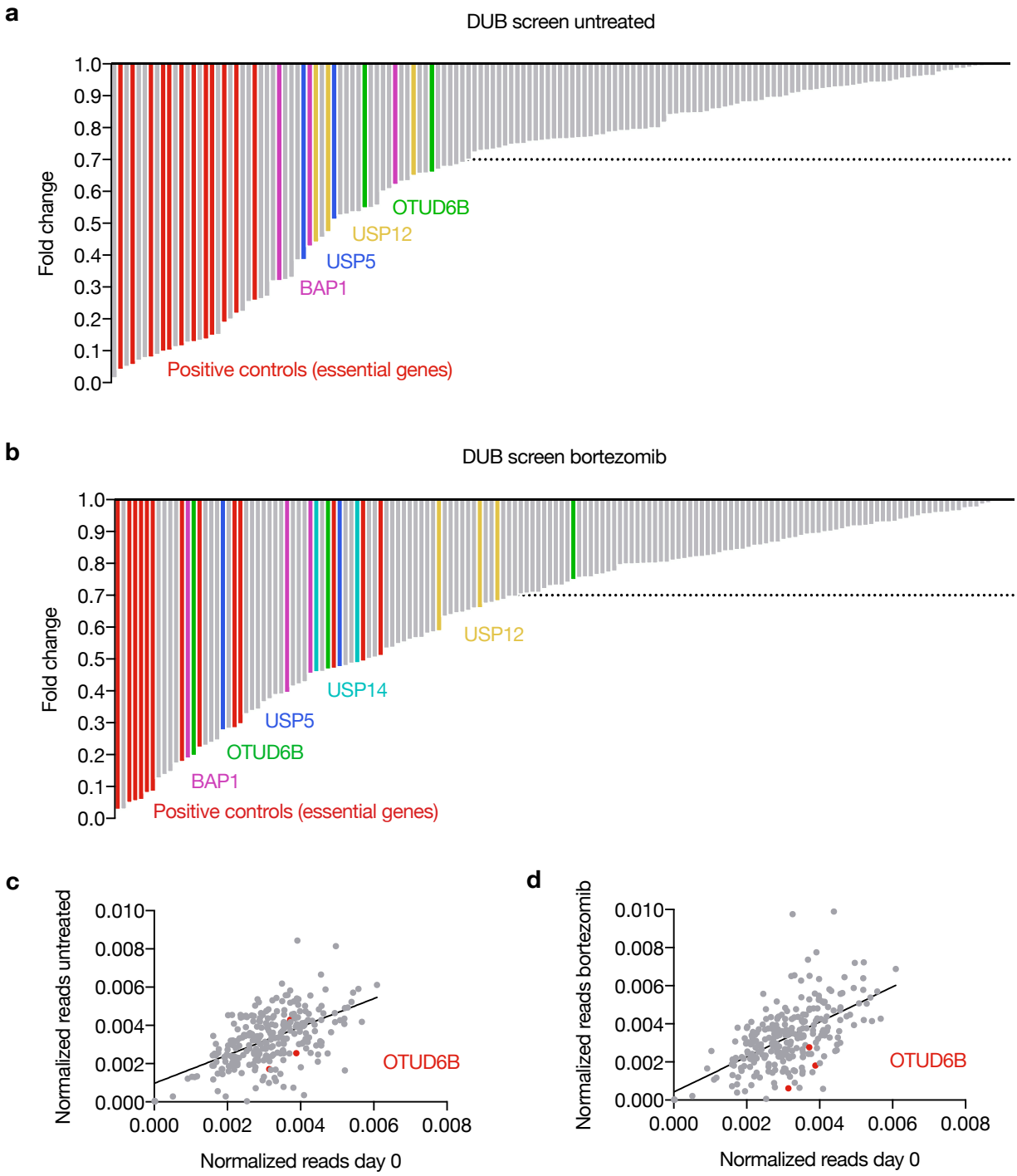

Figure 18: CRISPR/Cas9 screen of DUBs in MM1.S Cas9 cells. (a-d) MM1.S Cas9 cells were infected with virus of the pooled DUB library and two days later, GFP expressing cells were sorted by FACS. Half of the cells were harvested and reflected sgRNA composition on day 0. For the untreated condition **(a, c)**, cells were cultivated for 14 days. In parallel, cells were treated with a sub-lethal dose (12.5 nM) of bortezomib for eight days **(b, d)**. Genomic DNA was isolated from samples and sgRNAs were amplified by a two-step PCR approach and analysed by next generation sequencing. Reads of individual sgRNAs were normalized to the total number of reads and results of the untreated condition or bortezomib treatment are depicted in relation to **(a, b)** or blotted against **(c, d)** reads on day 0. Known DUBs are highlighted in light and dark blue, purple and yellow and positive controls are shown in red **(a, b)** whereas uncharacterized hits are marked in green **(a-d)**. Dashed line in **a** and **b** marks a change of 0.7-fold.

positive cells over time, in contrast to the screening results (Figure 16c). Furthermore, treatment of cells with sub-lethal doses of bortezomib enhanced this effect and led to a change by a factor of 0.61 for sgOTUD6B-1, 0.28 for sgOTUD6B-2 and 0.49 for sgOTUD6B-3 (Figure 19b), similarly to the results of the screen, in which the sgRNAs decreased to 0.75, 0.20 and 0.47, respectively (Figure 18b). An efficient knockout of OTUD6B by sgOTUD6B-2 and -3 could be confirmed by immunoblot analysis of cells, which were sorted five days after infection (Figure 19c). However, longer exposure times revealed an uncomplete knockout, reflecting the asynchronous induction of knockout in the cell population and thus explaining the rather slow decrease of GFP positive cells over time (Figure 19c). Overall, these results confirm the data of the screen and suggest that OTUD6B is essential for MM cell growth or viability, thereby indeed representing a potential new oncogene.

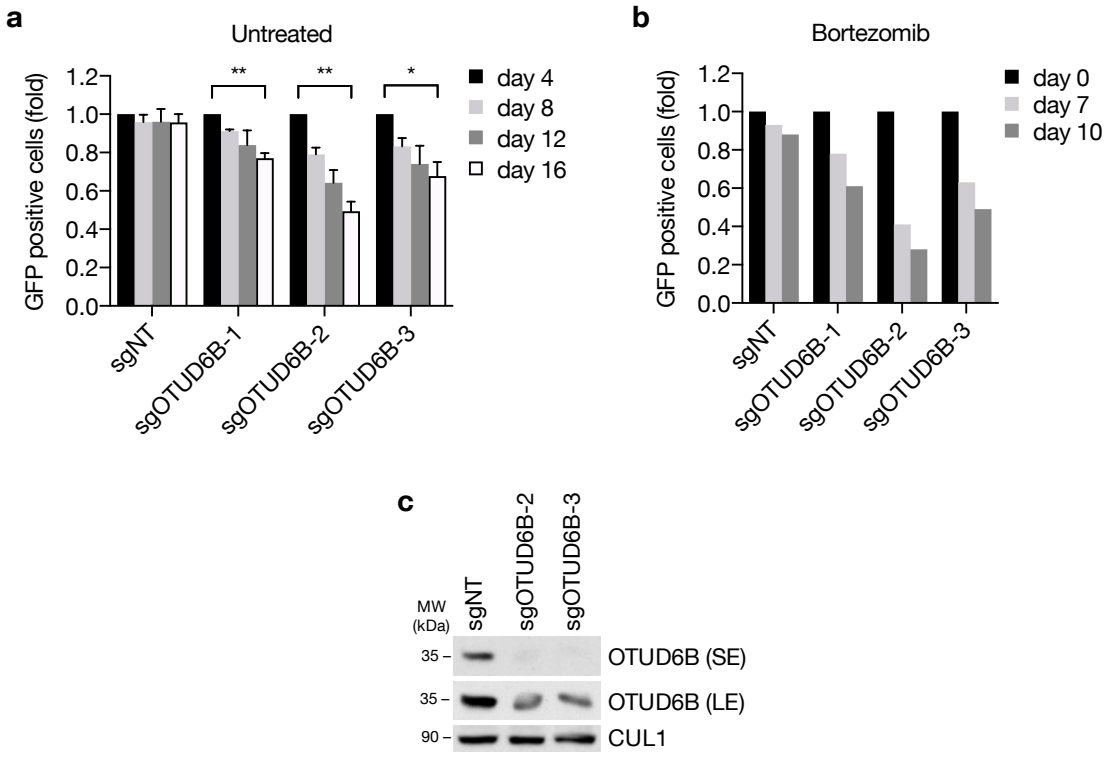

Figure 19: CRISPR/Cas9-mediated knockout of OTUD6B in MM1.S cells has an anti-proliferative effect. (a) Proliferation analysis of MM1.S Cas9 cells infected with either control sgRNA (sgNT) or 3 different sgRNAs targeting OTUD6B (sgOTUD6B-1, -2 and -3). The ratio of sgRNA expressing, GFP positive cells to uninfected cells was measured by flow cytometric analysis at the indicated time points after infection. Results are depicted in relation to day 4 (n = 3 independent experiments, mean ± S.D.). *, $P < 0.05$; **, $P < 0.01$; by one sample t-test. **(b)** Proliferation analysis of MM1.S Cas9 cells infected with either control sgRNA (sgNT) or two different sgRNAs targeting OTUD6B (sgOTUD6B-2, and -3) treated with 12.5 nM bortezomib for 10 days. The ratio of sgRNA expressing, GFP positive cells to uninfected cells was analysed by flow cytometric analysis at the indicated time points after addition of bortezomib (day 0; 5 days after infection) and data are shown in relation to day 0. **(c)** Immunoblot analysis of MM1.S Cas9 cells infected with either control sgRNA (sgNT) or two different sgRNAs targeting OTUD6B (sgOTUD6B-2, and -3). Infected, GFP expressing cells were sorted by flow cytometric analysis and harvested 5 days after infection. Whole cell extracts were probed with the indicated antibodies. CUL1 served as a loading control. SE, short exposure; LE, long exposure. [Data for **c** provided by M. Walzik (Walzik 2017)].

5.2 OTUD6B is essential for cancer cell proliferation

5.2.1 OTUD6B is essential for proliferation of MM cells

The results of the screen identified OTUD6B as a protein essential for cell viability of MM1.S cells and thus as a potential new oncogene in MM. To further test this hypothesis and to reproduce the growth disadvantage caused by CRISPR-mediated OTUD6B knockout in other MM cell lines, RPMI8226, U266 and KMS12BM cells were stably infected with constructs of Cas9 enzyme and selected with blasticidin for two weeks. Stable Cas9 expression could be verified on protein level in comparison to wildtype cells by immunoblot analysis (Figure 20a). To generate a knockout of OTUD6B, Cas9 cell lines were infected with either sgOTUD6B-2 or -3, which previously caused the strongest anti-proliferative effect in MM1.S cells, and a strong knockout of OTUD6B could be

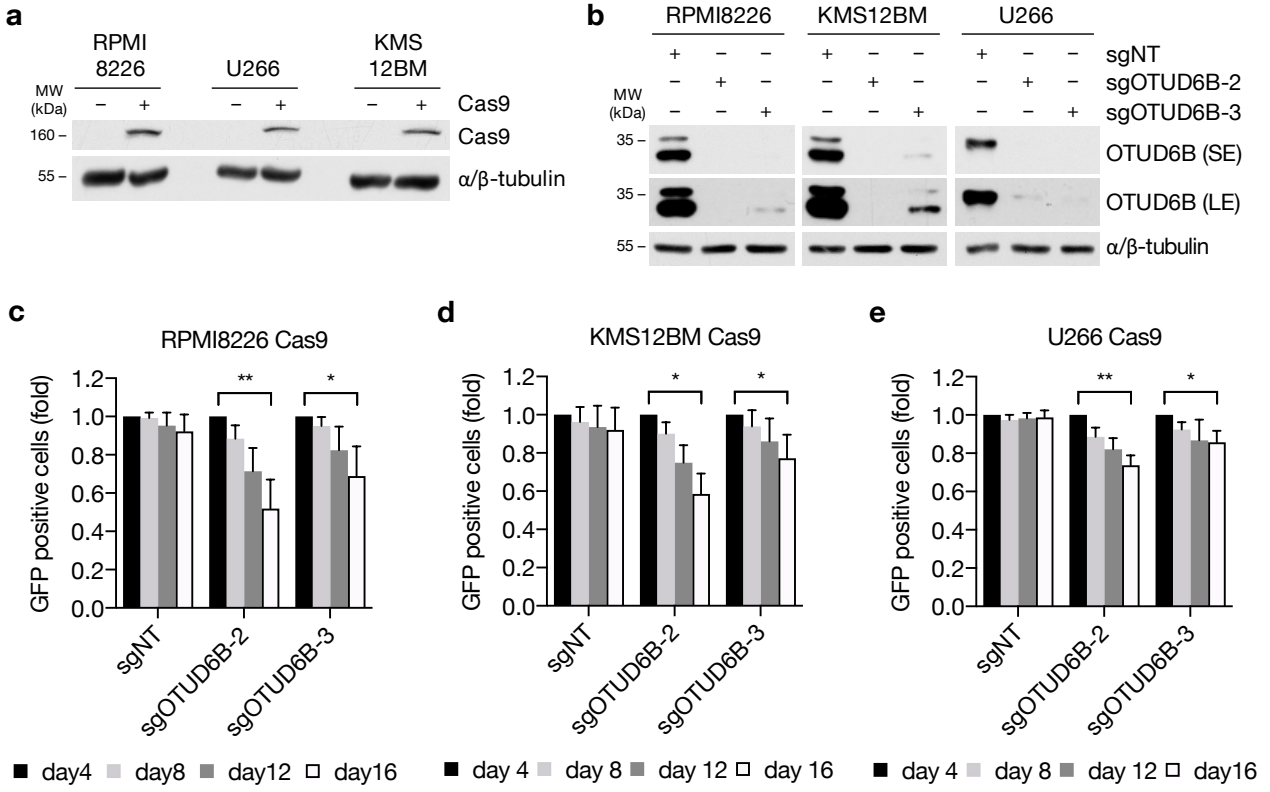

Figure 20: OTUD6B is essential for multiple myeloma proliferation. (a) Immunoblot analysis of wildtype and stable Cas9 MM cell lines, which were lentivirally transduced with Cas9 enzyme and selected with 5 µg/mL blasticidin for two weeks. Whole cell extracts were probed with the indicated antibodies. α/β-tubulin served as a loading control. **(b)** Immunoblot analysis of MM Cas9 cell lines, which were transduced with sgRNA targeting OTUD6B (sgOTUD6B-2 and -3) or control (sgNT). Infected, GFP expressing cells were sorted by FACS 11 days after infection and whole cell extracts were probed with indicated antibodies. α/β-tubulin served as a loading control. SE, short exposure; LE, long exposure. **(c-e)** Proliferation analysis of MM Cas9 cell lines infected as in **b**. The ratio of sgRNA expressing, GFP positive cells to uninfected cells was measured by flow cytometric analysis at the indicated time points after infection. Results are depicted in relation to day 4 (n = 3 independent experiments, mean ± S.D.). *, $P < 0.05$; **, $P < 0.01$; by one sample t-test.

confirmed by immunoblot analysis of cells, which were sorted by FACS 11 days after infection (Figure 20b). Proliferation analysis of these cells by flow cytometry-mediated monitoring of GFP positive cells over time revealed a significant decrease in the ratio of OTUD6B knockout to uninfected cells within 12 days, whereas control sgRNA (sgNT) expressing cells showed no difference in growth rates compared to the uninfected cell population (Figure 20c-e). Of note, a strong effect could be observed in RPMI8226 Cas9 and KMS12BM Cas9 cell lines, whereas U266 Cas9 cells showed only a weak, though significant, decrease in the percentage of GFP positive cells. Taken together, CRISPR/Cas9-mediated knockout of OTUD6B causes a strong proliferation defect in various MM cell lines.

One disadvantage of CRISPR/Cas9-mediated knockout is given by the fact that the knockout requires some time to be fully established and is achieved asynchronously within a cell population. Furthermore, depending on the capability of cells to repair CRISPR-mediated DNA double strand breaks, a certain fraction of cells did not reveal a knockout despite the expression of sgRNAs (Figure 20b). Moreover, infection rates of Cas9 cell lines were rather low (50-60%) and thus cells need to be sorted or selected when used for proliferation or immunoblot analysis. For this reason, the following experiments were performed using shRNA-mediated knockdown of OTUD6B to ensure an acute and efficient reduction of OTUD6B protein level. In line with previous observations, OTUD6B knockdown by two different shRNAs (shOTUD6B-2 and -3) also significantly impaired cell proliferation in different MM cell lines (RPMI8226, MM1.S, JJN3, H929) (Figure 21a). Furthermore, cell counts of OTUD6B knockdown cells dropped to 40-60% depending on the cell line within four days in relation to control shRNA expressing cells and thus the effects with regard to proliferation were even stronger than in case of CRISPR-mediated knockout. Immunoblot analysis of respective cell lines confirmed a strong reduction in OTUD6B protein level in shOTUD6B expressing cells (Figure 21b).

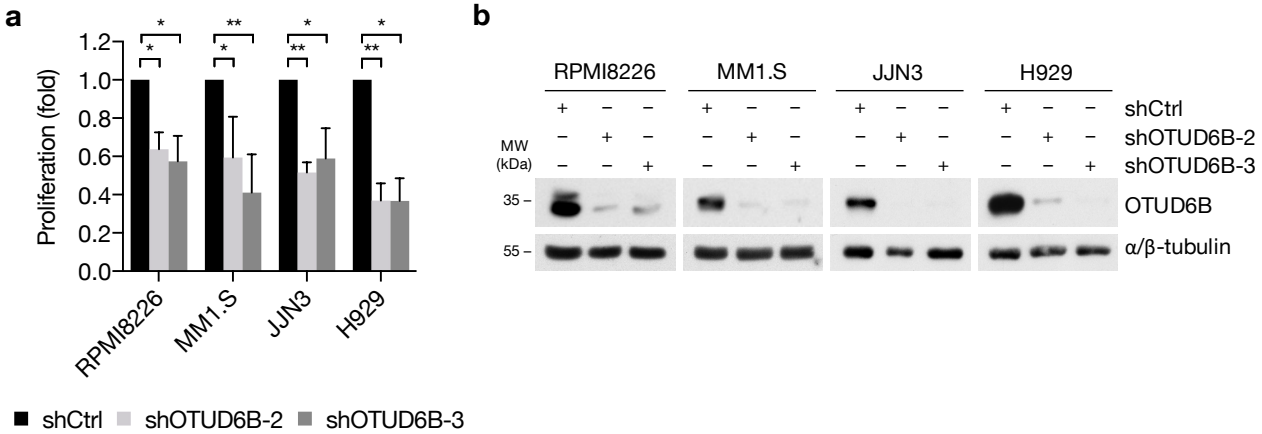

Figure 21: OTUD6B knockdown in MM cell lines has an anti-proliferative effect. (a) Proliferation analysis of MM cell lines, which were lentivirally transduced with shRNA constructs targeting OTUD6B (shOTUD6B-2 and -3) or control (shCtrl). Viable cells were counted using the trypan blue exclusion method 4 days after infection and results are presented in relation to control shRNA expressing cells (n = 3 independent experiments, mean ± S.D.). *, $P < 0.05$; **, $P < 0.01$; by one sample t-test. **(b)** Immunoblot analysis of cells described in **a** using the indicated antibodies. α/β-tubulin served as a loading control.

Taken together, both CRISPR/Cas9- as well as shRNA- mediated reduction of OTUD6B protein level leads to impaired cell proliferation in various MM cell lines.

5.2.2 OTUD6B is essential for proliferation of various cancer types

The previous experiments suggest that OTUD6B is involved in MM cell proliferation or viability, however, it is not clear whether this is only restricted to MM cells or if OTUD6B is also essential in other tumour entities. To test this, OTUD6B was silenced in Granta-519 cells, a mantle cell lymphoma derived cell line. Similar to MM cells, OTUD6B knockdown by infection with two different shRNA constructs led to a strong decrease in cell counts in relation to scrambled control expressing cells (Figure 22a). An efficient knockdown of OTUD6B on protein level could be confirmed by immunoblotting (Figure 22b). These data suggest that OTUD6B also plays a role in proliferation of other B cell derived cancer cells. In order to further investigate whether the anti-proliferative effect of OTUD6B loss is specific for B cell derived malignancies, stable Cas9 expressing A549 cells, which were previously generated by Oleksandra Karpiuk, were used to analyse the effect of OTUD6B knockout in a lung carcinoma derived cell line. In line with the previous results of CRISPR-mediated knockout in MM cells, OTUD6B loss led to a reduction of cell number compared to non-targeting sgRNA expressing cells measured by flow cytometric analysis of the ratio between GFP positive cells to uninfected cells over time (Figure 22c). Overall, these data provide evidence for OTUD6B involvement in cancer cell proliferation and strengthen the hypothesis that OTUD6B is a new oncogene in various cancer entities.

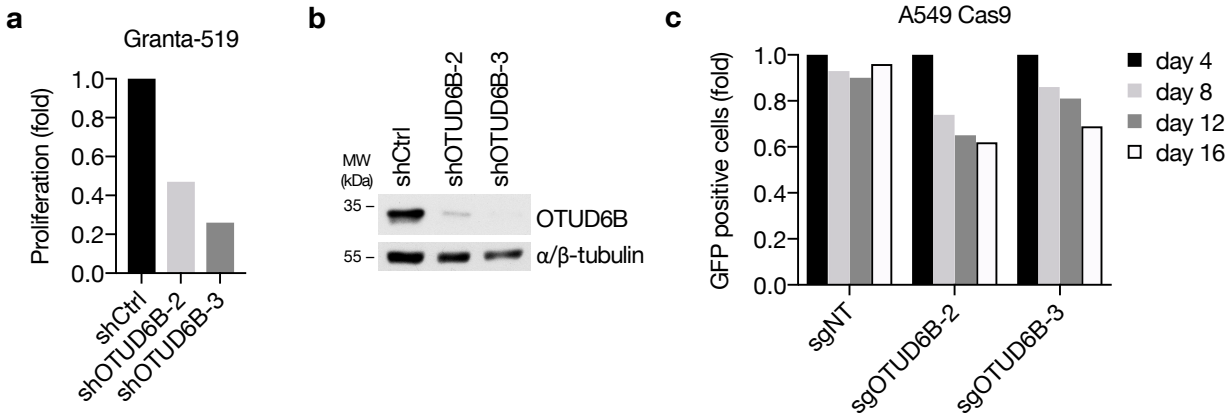

Figure 22: OTUD6B is essential for proliferation of various cancer types. (a) Proliferation analysis of Granta-519 cells, which were lentivirally transduced with shRNA constructs targeting OTUD6B (shOTUD6B-2 and -3) or control (shCtrl). Viable cells were counted using the trypan blue exclusion method 4 days after infection and results are presented in relation to control shRNA expressing cells. **(b)** Immunoblot analysis of cells described in **a** using the indicated antibodies. α/β-tubulin served as a loading control. **(c)** Proliferation analysis of A549 Cas9 cells infected with either control sgRNA (sgNT) or two different sgRNAs targeting OTUD6B (sgOTUD6B-2 and -3). The ratio of sgRNA expressing, GFP positive cells to uninfected cells was measured by flow cytometric analysis at the indicated time points after infection. Results are depicted in relation to day 4.

5.3 OTUD6B is involved in G1/S transition

5.3.1 OTUD6B is important for cell cycle progression

The impaired proliferation observed by CRISPR- and shRNA- mediated loss of OTUD6B can be a result of either a defect in cell cycle progression or an increase in cell death. To address this

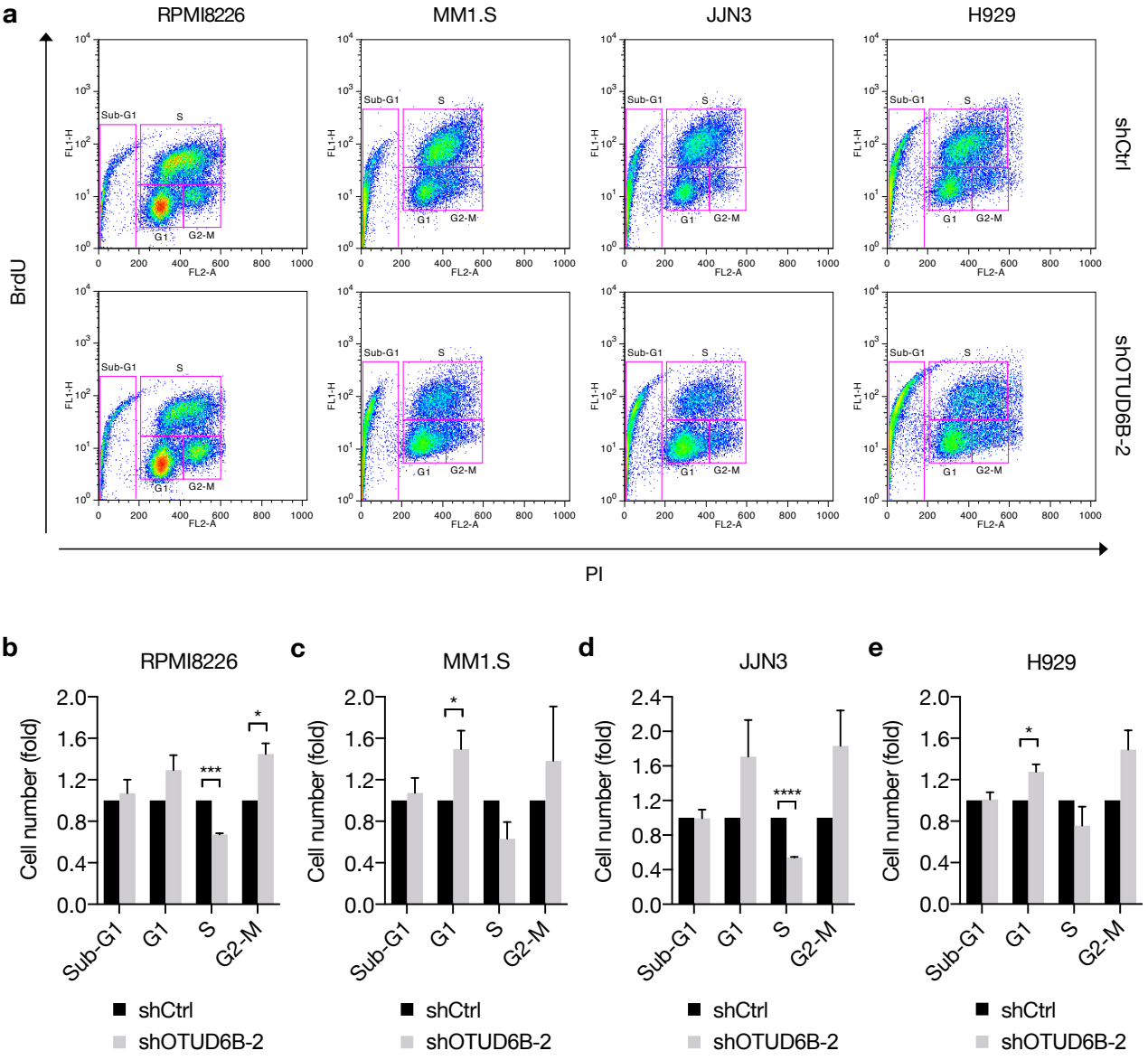

Figure 23: OTUD6B is essential for cell cycle progression. (a) BrdU/PI flow cytomretric analysis of indicated MM cell lines expressing shRNAs targeting OTUD6B (shOTUD6B-2) or control (shCtrl). Cells were incubated with BrdU for 40 min and fixed in ethanol at day 5 after infection. Cells in S phase that have incorporated BrdU were labelled with FITC-conjugated anti-BrdU antibody and DNA was stained with propidium iodide (PI). Data are depicted as graphs of BrdU positive cells (FL1-H, cells in S phase) versus PI staining (FL2-A, DNA content). **(b-e)** Quantification of cell cycle distribution (Sub-G1, G1, S and G2-M) of cells analysed in **a** presented in relation to control (n = 3 independent experiments, mean ± S.D.). *, $P < 0.05$; ***, $P < 0.001$, ****, $P < 0.001$; by one sample t-test.

question, the cell cycle distribution of various MM cell lines (RPMI8226, MM1.S, JJN3, H929) stably expressing shRNA against OTUD6B or a scrambled control, in which a significant decrease in the cell count could be observed upon OTUD6B knockdown (Figure 21a), was analysed by BrdU/PI flow cytometry five days after infection. Importantly, shRNA-mediated knockdown of OTUD6B led to a reduced number of cells in S phase and an increase in the G1 and G2-M populations (Figure 23a). By contrast, the Sub-G1 populations between OTUD6B knockdown and control shRNA expressing cells were comparable in all tested MM cell lines (Figure 23b-e), suggesting that the observed proliferation defect upon OTUD6B loss is caused by a failure in cell cycle progression rather than by an increase in the cell death rate.

5.3.2 OTUD6B is involved in G1/S transition

A change in the cell cycle distribution and the observed decrease in the S phase population could be a result of a check point activation at different cell cycle stages. MM1.S cells, for instance, displayed a significant increase in the G1 cell population upon OTUD6B loss (Figure 23c) and thus, it is conceivable that the cells arrested at the G1/S transition. To verify this assumption, MM1.S cells were lentivirally transduced with shRNA constructs targeting OTUD6B (shOTUD6B-1 or -2) or scrambled control (shCtrl) and synchronized at G1/S phase by a double thymidine block. Cells were released for eight hours into G2/M phase by thymidine wash-out and subjected to cell cycle analysis by flow cytometry of propidium iodide (PI) stained cells. Most of the control cells could be found in S and G2/M phase after release whereas a large portion of OTUD6B knockdown cells failed to enter S phase and arrested at G1/S transition (Figure 24a).

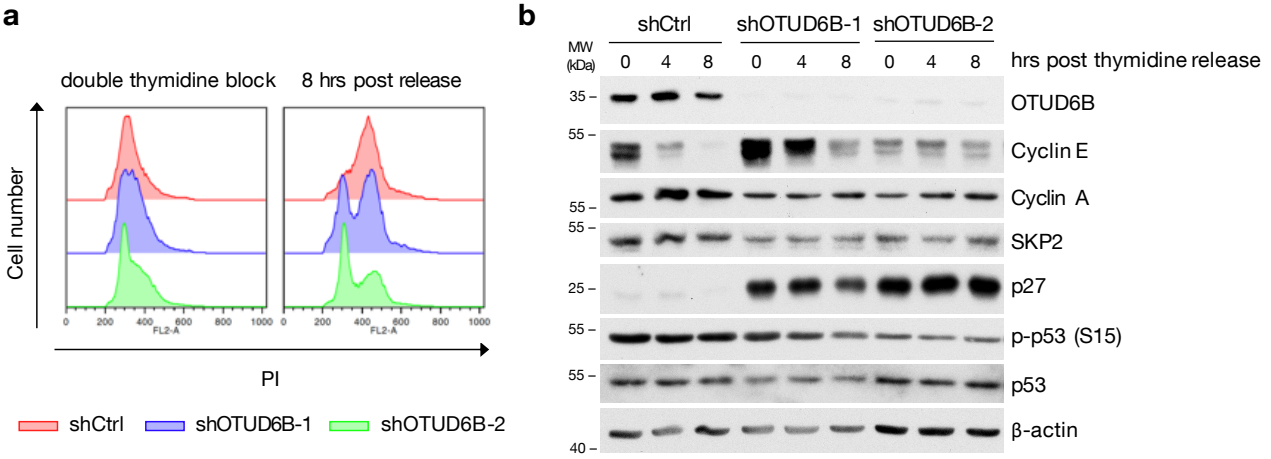

Figure 24: OTUD6B is important for G1/S transition. (a) Flow cytometric analysis of MM1.S cells transduced with shRNA constructs targeting OTUD6B (shOTUD6B-1 and -2) or scrambled control, which were synchronized at G1/S phase by a double thymidine block (left graph) and released for 8 hrs (right graph). DNA was stained with propidium iodide (PI) and results are depicted as histogram analysis of FL2-A (PI) signal intensity. **(b)** Immunoblot analysis of cells described in **a**, which were harvested at 0, 4 and 8 hrs after release from a double thymidine block using the indicated antibodies. β-actin served as a loading control.

Of note, not all knockdown cells were affected and thus a large number of cells could be also detected in G2/M phase. One explanation could be that silencing of OTUD6B per se impedes a

proper synchronization by double thymidine treatment, because cells pass more slowly through the cell cycle than control cells indicated by a broader peak at the double thymidine block (Figure 24a). An efficient knockdown of OTUD6B could be confirmed by immunoblot analysis (Figure 24b). Importantly, Cyclin E, a cell cycle regulated protein required for G1/S transition (DeGregori, Kowalik, and Nevins 1995; Hinds et al. 1992), was still detectable in OTUD6B knockdown cells eight hours after release, further providing evidence that these cells failed to progress towards G2 phase. Moreover, a strong induction of p27 could be observed in cells expressing either of the two shRNAs against OTUD6B, while the levels of p53 and phosphorylated p53 were comparable to control cells (Figure 24b). Of note, p27, as a member of the Kip/Cip family of CKIs, inhibits CDK2/Cyclin E complex and thus arrests cells at G1 phase (Polyak et al. 1994). Overall, these results confirm that silencing of OTUD6B impairs cell cycle progression by arresting cells at G1/S transition, which might be a consequence of high levels of p27.

5.3.3 OTUD6B activity is regulated in a cell cycle-dependent manner and peaks at G1/S transition

OTUD6B represents a scarcely described protein and there are conflicting data published with regard to its activity as a DUB (Mevissen et al. 2013; Xu et al. 2011). On the one hand, the two longest isoforms of OTUD6B described by NCBI (NM_016023) and UniProt (Q8N6M0) have recently been shown to be active towards different ubiquitin suicide probes (ubiquitin-β-galactosidase and ubiquitin propargylamide, respectively) that covalently bind to the catalytic site of the DUB, whereas OTUD6B purified from bacteria has been described to reveal no activity in linkage specific di-ubiquitin cleavage assays (Mevissen et al. 2013; Xu et al. 2011). To verify these data, the cysteine protease activity of OTUD6B isoform 1 (UniProt; Q8N6M0) was analysed by a DUB activity assay by M. Walzik using the suicide probe HA-ubiquitin vinyl sulfone (HA-Ub-VS) (Walzik 2017). Therefore, HEK293T cells transfected with constructs coding for FLAG-OTUD6B or

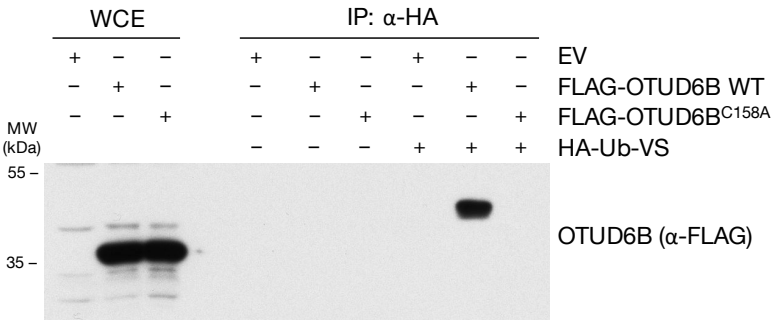

Figure 25: OTUD6B is an active cysteine protease DUB. DUB activity assay of FLAG-OTUD6B wildtype (WT) and FLAG-OTUD6B^{C158A} mutant, in which the catalytic cysteine was mutated. Whole cell extracts (WCE) of HEK293T cells transfected with FLAG-OTUD6B, FLAG-OTUD6B^{C158A} or empty vector (EV) were incubated with (+) or without (–) HA-ubiquitin-vinyl sulfone (HA-Ub-VS) and active DUBs were immunoprecipitated using HA-beads. WCE and immunoprecipitates (IP) were subjected to immunoblot analysis using α-FLAG antibody. [Data provided by M. Walzik (Walzik 2017)].

empty vector (EV) control were lysed with DUB activity buffer and incubated with or without the HA-Ub-VS probe to covalently capture active DUBs. Subsequently, latter could be precipitated by HA-IP and visualized by immunoblot analysis. As expected, the modified FLAG-OTUD6B wildtype (WT) could be detected by a strong signal providing further evidence that OTUD6B represents an active cysteine protease (Figure 25). Importantly, FLAG-OTUD6B mutant harbouring a C158A mutation, which is located in the active site (Xu et al. 2011), completely lost its activity (Figure 25).

Given the involvement of OTUD6B in cell cycle regulation (Figure 23) and G1/S transition (Figure 24), it is likely that OTUD6B itself is regulated in a cell cycle-dependent manner. To investigate this hypothesis, OTUD6B activity was analysed at different cell cycle stages by the DUB activity assay described before. Therefore, U2OS or A549 cells were chosen for their robust synchronization ability and synchronized at G1/S by a double thymidine block followed by a release for 6 hrs to allow progression to G2 phase, or at mitosis by a single thymidine block for 24 hrs followed by a release for 12 hrs in nocodazole. Mitotic cells were collected by mitotic shake-off and released for 4 hrs to let the cells enter G1 phase. Of note, immunoblot analysis of whole cell extracts at the different cell cycle stages revealed that OTUD6B protein level were constant throughout the cell cycle, suggesting that OTUD6B protein abundance is not regulated in a cell cycle-dependent fashion (Figure 26a, b). In contrast, OTUD6B activity was changed at different cell cycle stages in both cell lines, peaking at G1/S and being decreased in mitosis.

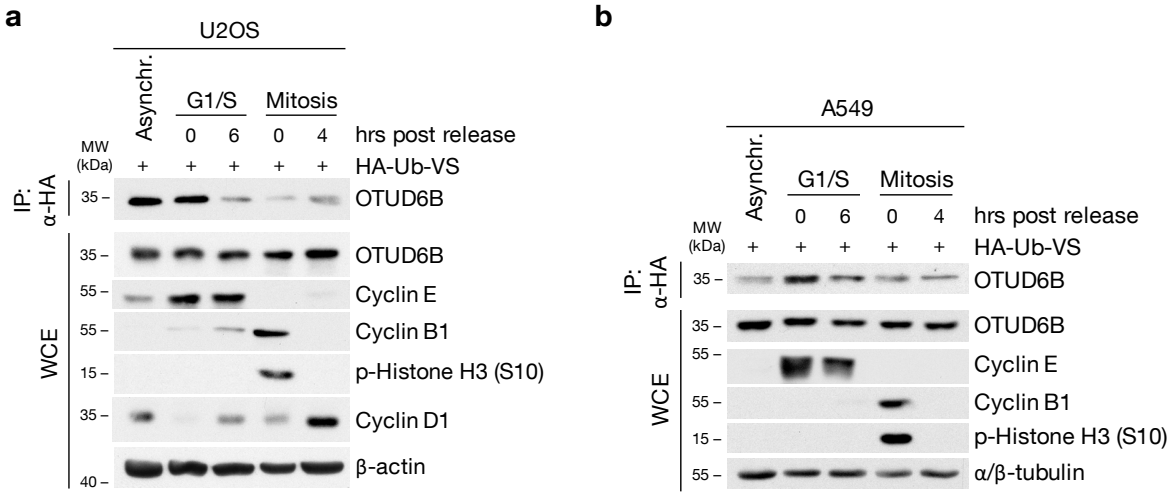

Figure 26: OTUD6B activity peaks at G1/S transition. DUB activity assay of endogenous OTUD6B in U2OS **(a)** and A549 **(b)** cells, which were synchronized either at G1/S by a double thymidine block and released for 6 hrs or at mitosis by a single thymidine block for 24 hrs followed by a release for 12 hrs in nocodazole. Mitotic cells were collected by a mitotic shake-off and released for 4 hrs. Whole cell extracts (WCE) from asynchronous or synchronized cells collected at the indicated time points were incubated with HA-ubiquitin-vinyl sulfone (HA-Ub-VS) and active DUBs were immunoprecipitated using HA-beads. WCEs and immunoprecipitates (IP) were subjected to immunoblot analysis using the indicated antibodies. β-actin **(a)** and α/β-tubulin **(b)** served as loading controls.

Taken together, OTUD6B represents an active cysteine protease possessing the highest activity at G1/S transition, which is in accordance with the previous results showing that OTUD6B

is essential for the entry into S phase (Figure 24). Thus, it is likely that OTUD6B is regulated on the post-translational level in a cell cycle-dependent manner, which impacts its activity.

5.4 OTUD6B stabilizes LIN28B by K48 deubiquitylation at G1/S transition

5.4.1 Mass spectrometry-based screening approaches identify LIN28B as potential substrate

Given that OTUD6B is an active cysteine protease and that OTUD6B activity is regulated in a cell cycle-dependent manner (Figure 26), it is likely that OTUD6B deubiquitylates one or several substrates in this context. To identify interaction partners and thus potential substrates of OTUD6B, two mass spectrometry-based proteome wide screening approaches were performed in collaboration with Prof. B. Küster, J. Zecha and S. Kläger at the Department for Proteomics and Bioanalytics (TUM). First, an affinity-based assay was used in order to identify proteins, which directly or indirectly interact with OTUD6B and thus are co-immunoprecipitated in a single FLAG purification. Therefore, 2 x10^9 HEK293T cells were transfected with either FLAG-OTUD6B or empty vector (EV) control and harvested 24 hrs after transfections. Cell pellets were lysed, subjected to FLAG-immunoprecipitation (IP) and FLAG-tagged and interacting proteins were eluted using 3x FLAG peptide. An acceptable amount of FLAG-OTUD6B could be enriched as shown by gel silver staining of eluates corresponding to 1% of total purifications (Figure 27a). Subsequently, the samples were analysed by mass spectrometry (MS) and data were processed by Jana Zecha. The resulting MS list comprised 973 proteins quantified in at least one of the two samples (Figure 27b). This large list of hits was probably due to contaminants and non-interacting proteins; however, this was expected from a single FLAG-IP, which was chosen to avoid loss of very transient interactions. In order to limit the number of potential interactors, the data were further processed and an arbitrary cut-off of all protein groups with LFQ intensity ratios FLAG-OTUD6B to EV > 2 (log2 ratio > 1) was applied (Figure 27b, samples are marked in blue). Values for proteins that could be only detected in one sample were replaced by 1000 in the respective other sample in order to be able to calculate ratios (imputed intensities, samples are marked in green). The resulting list comprised 212 proteins, which was further reduced to 29 potential substrates by subtracting agarose-binding proteins using Contaminant Repository for Affinity Purification v1.1 as a resource (Mellacheruvu et al. 2013) (Figure 27c).

The interaction of DUBs with their substrates have been described to be sometimes very transient, as DUBs need to release their substrates once they have cleaved off the ubiquitin (Reyes-Turcu, Ventii, and Wilkinson 2009). Consequently, an affinity-based purification approach is prone to lose the binding of substrates to the DUB and thus purified proteins might represent rather scaffold interactions than substrates. In addition, the list of potential interactors obtained from the FLAG-purification was long, making it difficult to identify a substrate. Hence, another non-affinity-based mass spectrometry approach was chosen in order to capture unstable interactors and to narrow down the list of substrate candidates by comparison the results of both

a

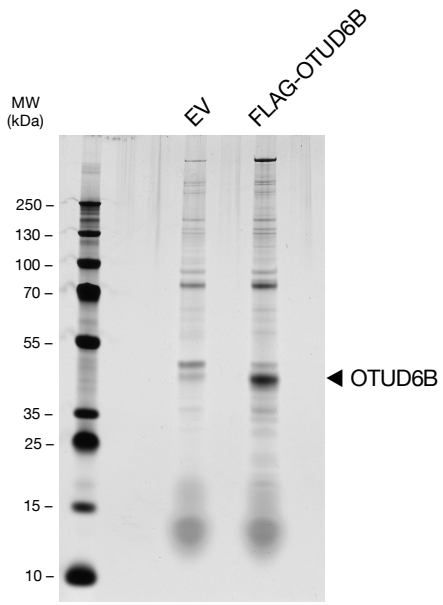

b

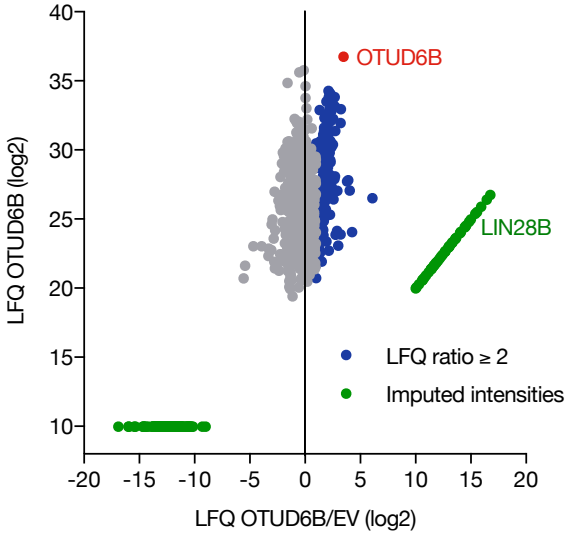

c

Protein	EV	OTUD6B IF1	Ratio OTUD6B/EV
OTUD6B	1.02E+10	1.15E+11	11.2
ASCC3	2.36E+08	1.24E+09	5.2
ASCC1	5.49E+07	2.67E+08	4.9
TRIP4	3.94E+07	2.48E+08	6.3
RRP7A	4.92E+07	1.93E+08	3.9
DHX57	3.56E+07	1.66E+08	4.6
ASCC2	3.74E+07	1.49E+08	4.0
RBM4	2.79E+07	1.26E+08	4.5
RIOK3	1.00E+04	8.92E+07	8916.5
PURA	2.34E+07	8.25E+07	3.5
SPAG1	1.00E+04	4.35E+07	4353.8
LIN28B	1.00E+04	3.30E+07	3296.0
ZCCHC3	9.39E+06	3.02E+07	3.2
XRRA1	1.00E+04	2.42E+07	2422.5
PNO1	1.00E+04	2.21E+07	2209.6
PLLP	1.00E+04	1.74E+07	1735.9
SLAIN1	1.00E+04	1.73E+07	1731.0
CASC3	4.68E+06	1.49E+07	3.2
MTDH	1.00E+04	1.28E+07	1284.7
WNT3A	1.00E+04	1.02E+07	1019.2
ARMC8	1.09E+06	8.83E+06	8.1
L1RE1	1.00E+04	8.35E+06	834.6
LLPH	1.00E+04	6.73E+06	673.5
NMNAT1	2.71E+06	6.04E+06	2.2
OIP5	1.00E+04	4.60E+06	459.6
WDR60	1.00E+04	3.73E+06	373.4
CBX4	1.00E+04	2.73E+06	272.7
APOBEC3B	1.00E+04	1.98E+06	198.1
GRN	8.60E+05	1.72E+06	2.0
FN3KRP	1.00E+04	1.57E+06	156.9

Figure 27: Mass spectrometric analysis of FLAG-purified OTUD6B. (a) Silver stained gel of FLAG-purified OTUD6B. N-terminal tagged OTUD6B isoform 1 (IF1) or empty vector (EV) control were transfected into HEK293T cells, which were harvested 24 hrs later. FLAG-OTUD6B was immunoprecipitated from whole cell extracts using FLAG M2 beads and subsequently eluted from beads by 3x FLAG peptide. The EV sample served as a control for unspecific binding of proteins to the beads. 1% of purification was separated by SDS-PAGE and proteins were visualized by silver staining of the gel. The arrowhead points to the prominent band at the expected size of OTUD6B. MW, molecular weight. **(b)** Mass spectrometric analysis of samples from **a**. Co-immunoprecipitated proteins were identified by mass spectrometry and log2 ratios of OTUD6B/EV LFQ values were blotted against log2 intensities (LFQs) of the OTUD6B sample. Potential interactors revealing LFQ ratios >2 were marked in blue. Missing values of proteins, which were only detected in one sample, were replaced by 1000 in the respective other sample (Imputed intensities) and are marked in green. **(c)** List of potential interactors obtained by subtracting typical contaminants and agarose-binding proteins from the blue samples and proteins with imputed values on the right site in **b**. Values represent LFQ intensities computed by MaxQuant and ratios between intensities of proteins from the FLAG-OTUD6B sample and EV control. [MS data for **b** provided by J. Zecha and Prof. B. Küster].

purifications. Therefore, a previously described method called proximity-dependent biotin identification (BioID) was performed (Kim et al. 2016; Roux et al. 2012). Here, a biotin ligase from *Aquifex aeolicus* (BioID2) was fused to OTUD6B isoform 1 and isoform 2 and transfected into HEK293T cells (Figure 28a). Addition of biotin to the cells led to biotinylation of proteins in direct proximity of the biotin ligase fusion proteins, which were subsequently purified using streptavidin beads after harsh lysis of cells. Untransfected cells and expression of BioID2 alone served as controls to identify proteins which interact with the beads and for unspecific biotinylation of proteins, respectively. Subsequently, purified proteins were identified by mass spectrometric analysis in collaboration with Prof. B. Küster and S. Kläger at the Department for Proteomics and Bioanalytics (TUM). Immunoblot analysis of whole cell extracts revealed expression of transfected proteins and successful biotinylation of proteins (Figure 28b). Furthermore, sufficient purification of biotinylated proteins including OTUD6B and BioID2 could be proven by silver staining of 5% of purification after separation by SDS-PAGE (Figure 28c) (Data for Figure 28b, c were obtained from M. Walzik, (Walzik 2017))

The MS analysis identified a total number of 4474 proteins, which were present in at least one sample. The list was further processed by subtracting proteins for which the log2 ratio of OTUD6B IF1 to EV was smaller than 1 ending up with a total number of 486 proteins. By comparison of these results with the list of the FLAG-OTUD6B IF1 purification (Figure 27c), 8 specific interactors and thus potential substrates of OTUD6B could be identified (Figure 28d). Besides the previously described interactor MTDH (Sowa et al. 2009), the list included many proteins, which are involved in RNA regulation such as LIN28B, LLPH, DHX57 and CASC3 (Castello et al. 2012; Heo et al. 2008; Noble and Song 2007). Given that LIN28B has been previously described to stabilize MYC mRNA by the degradation of *let-7* microRNAs in the context of MM, thereby promoting MM proliferation (Manier et al. 2017), LIN28B represented the most promising candidate for being a substrate of OTUD6B. In the MS analysis of the FLAG purification, LIN28B was only detected in the FLAG-OTUD6B sample but not in the EV control (Figure 27b. c), reflecting a very specific binding of LIN28B to OTUD6B. Furthermore, the intensity of LIN28B was 12.9-fold higher in the BioID2 sample of OTUD6B IF1 compared to the EV control, whereas LIN28B was only enriched by a factor of 2.8 in the sample of OTUD6B IF2 (Figure 28d). Overall, by performing two complementary MS approaches, the list of potential substrates of OTUD6B could be reduced to a small number of proteins, among which LIN28B was considered as a potential candidate.

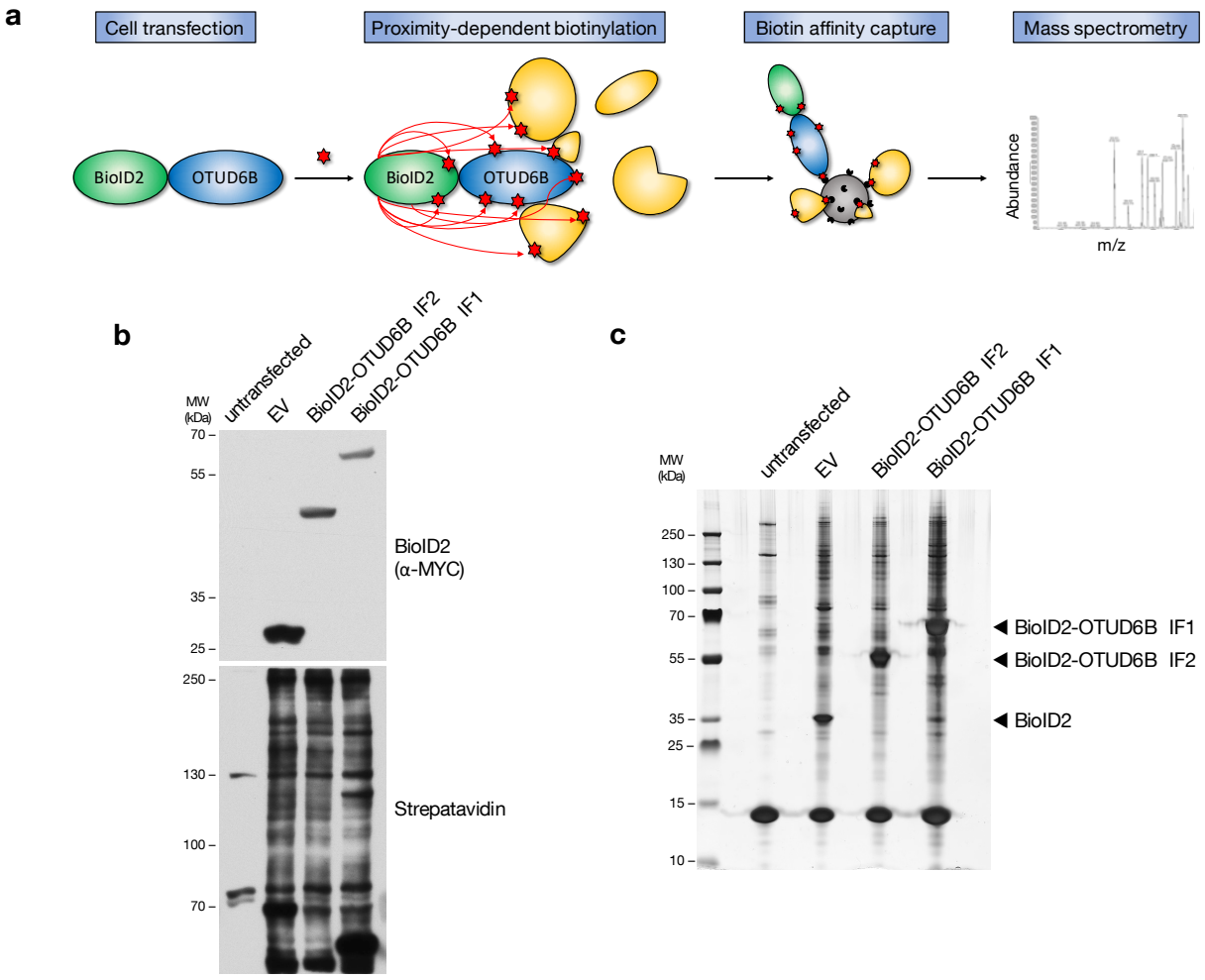

d

Protein	untransfected	EV	OTUD6B IF1	OTUD6B IF2	Ratio IF1/EV (log2)	Ratio IF2/EV (log2)
OTUD6B	3.76E+08	8.98E+08	8.15E+11	3.81E+11	9.83	8.73
LLPH	1.00E+03	1.00E+03	6.53E+07	7.37E+07	16.00	16.17
PURA	9.52E+06	1.00E+03	1.97E+07	1.25E+07	14.27	13.61
LIN28B	4.32E+06	1.40E+07	1.81E+08	3.90E+07	3.69	1.70
MTDH	2.77E+07	3.36E+08	1.54E+09	1.39E+08	2.12	-1.28
DHX57	1.00E+03	3.72E+07	1.28E+08	9.95E+06	1.79	-1.90
WDR60	1.00E+03	3.37E+07	1.07E+08	7.03E+06	1.67	-2.27
CASC3	1.00E+03	1.77E+07	3.96E+07	1.11E+07	1.17	-0.67
RIOK3	1.00E+03	8.82E+07	1.76E+08	1.21E+08	1.00	0.46

Figure 28: Mass spectrometric analysis of OTUD6B BioID2 purification. (a) Scheme of OTUD6B BioID2 purification. HEK293T cells were transfected with MYC-tagged BioID2 alone or BioID2-OTUD6B isoform1 (IF1) or 2 (IF2) fusion proteins. Untransfected cells served as a control. One day later, cells were incubated with 50 µM biotin for 16 hrs to allow for biotinylation of proteins in direct proximity to OTUD6B fused to the biotin ligase (BioID2). After harsh lysis of cells, biotinylated proteins were purified using Strep-Tactin beads and analysed by mass spectrometry (MS). **(b)** Immunoblot analysis of whole cell extracts from samples described in **a** using α-MYC antibody and HRP-conjugated streptavidin to detect biotinylated proteins. **(c)** Silver stained gel of BioID2 purified proteins from **a**. 5% of the BioID2 purification described in **a** were separated by SDS-PAGE and proteins were visualized by silver staining of the gel. The arrowheads point to the prominent bands at the expected sizes of BioID2 alone, BioID2-OTUD6B IF1 and IF2. **(d)** Intensities of proteins, which were identified in BioID2 and FLAG purifications with calculated log2 ratios of OTUD6B IF1 to EV >1. [Data for **b** and **c** provided by M. Walzik (Walzik 2017); MS data for **d** provided by S. Kläger and Prof. B. Küster].

5.4.2 OTUD6B binds to LIN28B

After the identification of LIN28B as a potential substrate by two mass spectrometric approaches, specific binding of OTUD6B to LIN28B was validated by performing bi-directional immunoprecipitation (IP) assays. First, HEK293T cells were transfected with either FLAG-OTUD6B IF1 or an empty vector (EV) control and FLAG-IP was conducted using FLAG M2 beads from whole cell extracts (WCE). Immunoblot analysis revealed a strong and specific interaction between FLAG-tagged OTUD6B and endogenous LIN28B, while no signal for LIN28B could be detected in the EV control (Figure 29a). Importantly, binding of endogenous LIN28B to other FLAG-tagged DUBs belonging to the OTU family, namely OTUD6A, OTUD2 and OTUB1, could not be detected by FLAG-IP from HEK293T cells (Figure 29b). Of note, despite its very low expression in HEK293T cells, LIN28A, which is closely related to LIN28B, also co-immunoprecipitated with FLAG-OTUD6B but not with the other FLAG-tagged DUBs (Figure 29b). Last, specific interaction between OTUD6B and LIN28B was further confirmed by reciprocal immunoprecipitation of FLAG-tagged LIN28B from HEK293T cells and co-IP of endogenous OTUD6B (Figure 29c).

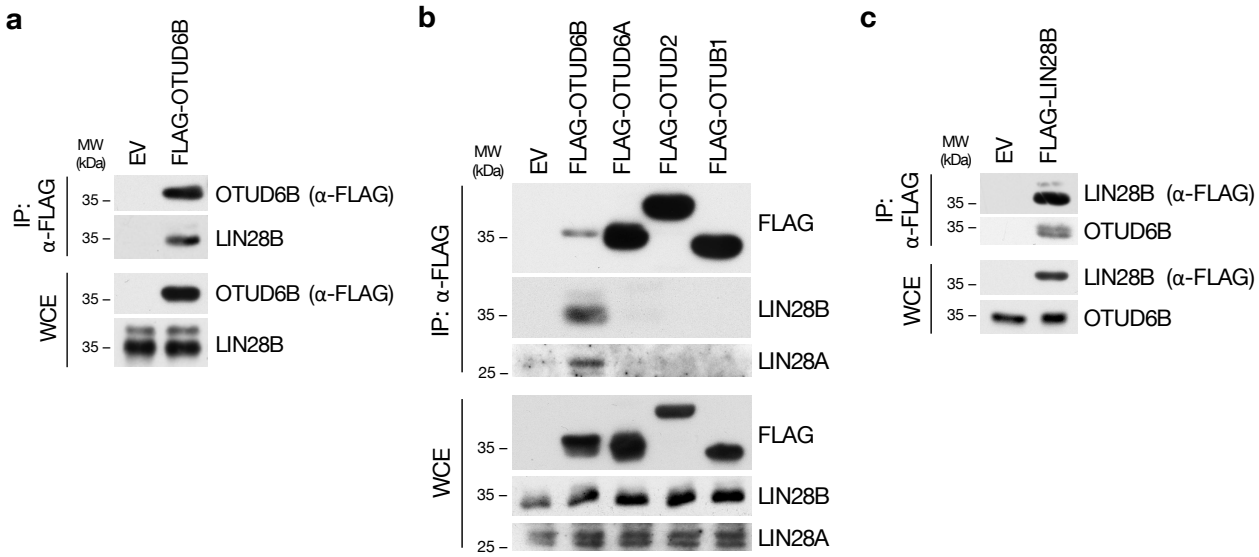

Figure 29: OTUD6B binds to LIN28B. (a-c) Immunoprecipitation (IP) of FLAG-OTUD6B **(a)**, FLAG-tagged OTUD6B, OTUD6A, OTUD2, OTUB1 **(b)** and FLAG-LIN28B **(c)**. HEK293T cells were transfected with constructs coding for indicated FLAG-tagged proteins or empty vector (EV) control and lysates were subjected to FLAG-IP. Whole cell extracts (WCE) and IPs were analysed by immunoblotting using the indicated antibodies.

The results from the BioID2 purification suggest that LIN28B predominantly interacts with OTUD6B isoform 1 (IF1) as the enrichment of LIN28B was much stronger for IF1 than for OTUD6B IF2 (Figure 28d). To test this hypothesis, HEK293T cells were transfected with FLAG-tagged OTUD6B IF1, IF2 or empty vector (EV) control and FLAG-IP was performed from whole cell lysates. Importantly, endogenous LIN28B only co-immunoprecipitated with OTUD6B IF1 whereas no signal could be detected in the FLAG-OTUD6B IF2 sample or in the EV control (Figure 30a),

confirming the results of the BioID2 purification that LIN28B only interacts with the longer isoform of OTUD6B.

Alignment of the protein sequences of OTUD6B IF1 and IF2 as depicted on UniProt (Q8N6M0-1 and -2, respectively) revealed that amino acids 1-105 of IF1 are missing in the second isoform and replaced by the amino acid sequence 'MISK' in IF2 (Figure 30b). Consequently, LIN28B might bind within the first 105 amino acids of OTUD6B IF1, which contain three predicted coiled-coil domains.

To further characterize the binding of LIN28B to OTUD6B, the dependency of LIN28B interaction on the catalytic activity of OTUD6B was analysed. Therefore, FLAG-IP was performed from HEK293T cells expressing either FLAG-tagged OTUD6B wildtype (WT) or the previously described catalytically inactive mutant OTUD6B^{C158A} (Figure 25). Immunoblot analysis detected equal signals of LIN28B in both samples, suggesting that LIN28B binding is independent of OTUD6B activity (Figure 30c).

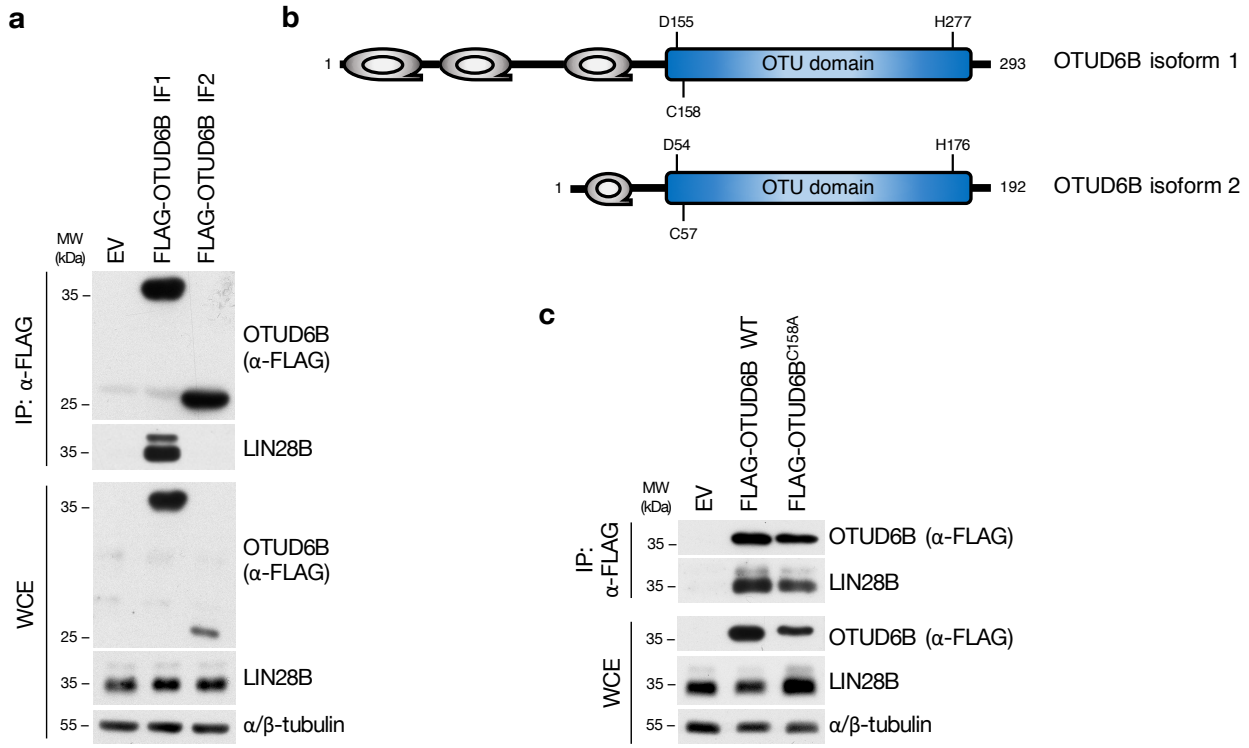

Figure 30: OTUD6B isoform 1 binding to LIN28B is independent of its catalytic activity. (a) Immunoprecipitation (IP) of FLAG-OTUD6B isoform 1 and 2. FLAG-OTUD6B isoform 1 (IF1), isoform 2 (IF2) or empty vector (EV) control were expressed in HEK293T cells and lysates were subjected to FLAG-IP. Whole cell extracts (WCE) and IPs were analysed by immunoblotting using the indicated antibodies. α/β-tubulin served as a loading control. **(b)** Schematic overview of OTUD6B isoform 1 and 2. Amino acids 1-105 of OTUD6B IF1 (UniProt: Q8N6M0-1) are missing in OTUD6B IF2 (UniProt: Q8N6M0-2). Positions of the catalytic triad composted of cysteine (C), histidine (H) and aspartate (D) are indicated within the OTU domain and the N-terminal coiled-coil domains are illustrated. **(c)** Immunoprecipitation (IP) of FLAG-OTUD6B wildtype (WT) and FLAG-OTUD6B^{C158A} mutant. HEK293T cells were transfected with constructs coding for FLAG-OTUD6B WT, FLAG-OTUD6B^{C158A} or empty vector (EV) control and lysates were subjected to FLAG-IP. Whole cell extracts (WCE) and IPs were analysed by immunoblotting using the indicated antibodies. α/β-tubulin served as a loading control.

5.4.3 OTUD6B interacts with the cold shock domain of LIN28B

The previous results revealed that LIN28B interacts with the N-terminal part of OTUD6B isoform 1 (Figure 30a). In order to further analyse which part of LIN28B is responsible for OTUD6B binding, mapping experiments were performed. LIN28B contains two domains, an N-terminal cold

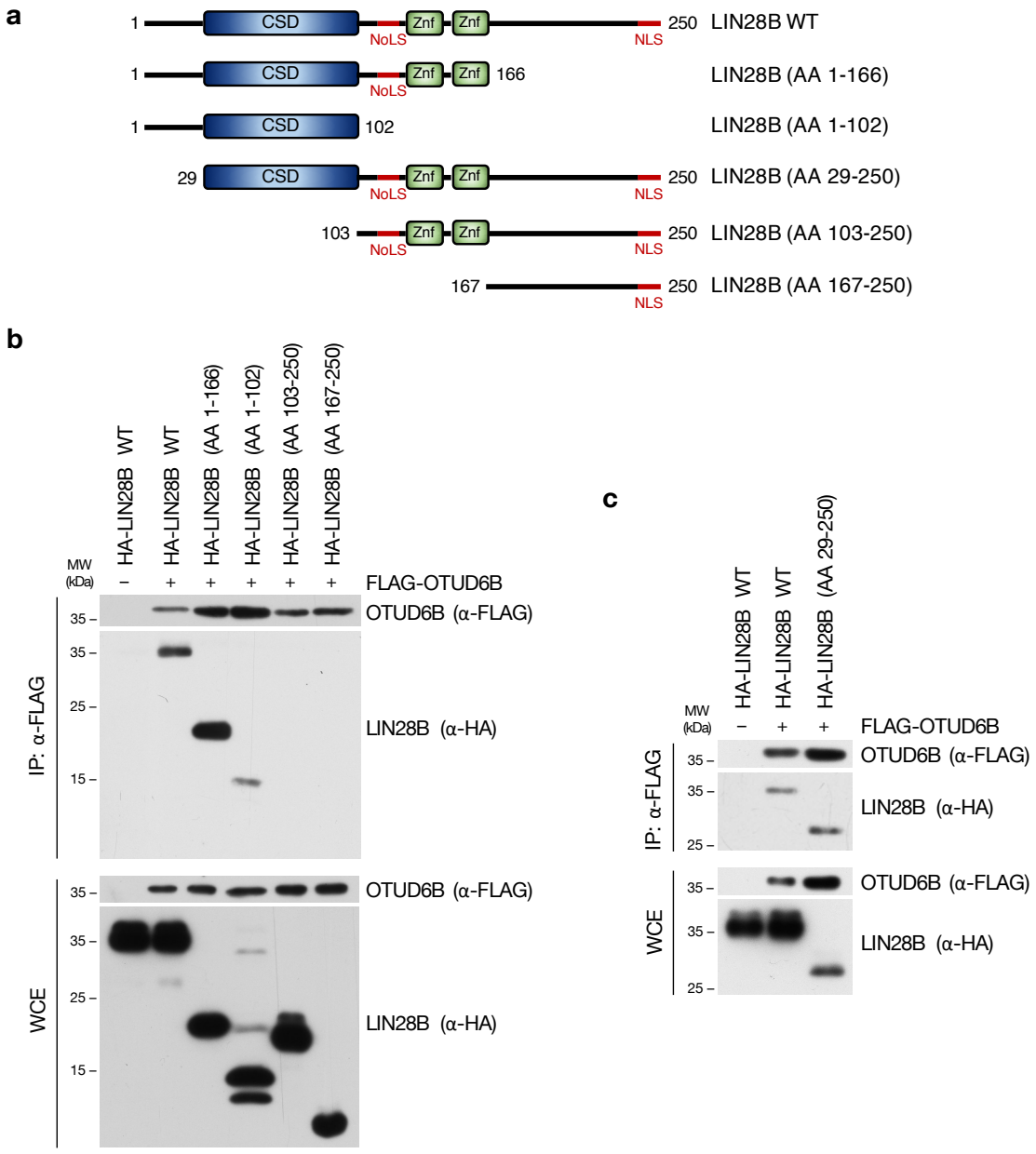

Figure 31: OTUD6B binds to the cold shock domain of LIN28B. (a) Schematic overview of LIN28B wildtype (WT) and fragments. AA, amino acid; CSD, cold shock domain; NLS, nuclear localization sequence; NoLS, nucleolar localization sequence; ZnF, zinc finger. **(b, c)** Interaction analysis of FLAG-OTUD6B with HA-LIN28B fragments. FLAG-OTUD6B and different HA-tagged fragments of LIN28B described in **a** were co-expressed in HEK293T cells and lysates were subjected to FLAG-IP. Whole cell extracts (WCE) and IPs were analysed by immunoblotting using the indicated antibodies.

shock domain (CSD) followed by two CCHC-type zinc finger (ZnF) domains (zinc knuckle domain (ZKD)), which have been reported to specifically interact with *let-7* microRNAs (Loughlin et al. 2011; Mayr et al. 2012; Nam et al. 2011). To identify the OTUD6B interaction site, different HA-tagged fragments of LIN28B containing either both, only one or none of the domains were cloned and expressed in HEK293T cells together with FLAG-OTUD6B (Figure 31a). By performing FLAG-IPs from whole cell extracts (WCE), interaction between FLAG-OTUD6B and a fragment containing both domains, but lacking the C-terminal part (AA 1-166), as well as a fragment only composed of the CSD and the very N-terminal part (AA 1-102) could be found (Figure 31b). In contrast, no binding could be detected between FLAG-OTUD6B and C-terminal fragments lacking the CSD (AA 103-250 and AA 167-250), suggesting that OTUD6B binds within the first 102 amino acids of LIN28B (Figure 31b). To further clarify, whether OTUD6B binds to the unstructured N-terminus comprising AA 1-28 or to the CSD (AA 29-102), HEK293T cells were transfected with FLAG-OTUD6B and HA-tagged LIN28B fragment lacking the first 28 amino acids, as the CSD alone was not expressed. Immunoblot analysis of the FLAG-IP revealed a similar binding of OTUD6B to the fragment as to full length LIN28B (Figure 31c), suggesting that the very N-terminal part of LIN28B is dispensable for OTUD6B binding. Taken together, these data provide evidence that OTUD6B interacts with the cold shock domain of LIN28B.

5.4.4 OTUD6B binding to LIN28B is regulated by phosphorylation

Given that OTUD6B is essential for cell proliferation (Figure 20, Figure 22) and that its activity is regulated in a cell cycle-dependent manner (Figure 26), it is conceivable that the binding to LIN28B is regulated on post-translational level in proliferating cells. To test whether the interaction depends on phosphorylation, HEK293T cells were transfected with a FLAG-OTUD6B expressing construct or empty vector (EV) control and whole cell extracts (WCE) were treated with calf intestinal alkaline phosphatase (CIP) for 10 min at room temperature before subjecting to FLAG-immunoprecipitation (IP). Incubation at higher temperatures was not possible as the binding of OTUD6B to LIN28B without the addition of CIP was completely abrogated at 37°C. However, CIP was active under the chosen conditions as phosphorylation of GSK-3β (p-GSK-3β) was abolished upon CIP treatment (Figure 32a). Strikingly, the interaction of OTUD6B with LIN28B was completely lost upon dephosphorylation (Figure 32a), suggesting that the binding indeed might be regulated by phosphorylation. Of note, it is not clear whether the phosphorylation of OTUD6B or LIN28B or both is necessary for interaction.

Interestingly, recently published data reported that DUBA (OTUD5), another DUB belonging to the OTU family, needs to be phosphorylated in order to be active and for substrate binding (Huang, Ma, et al. 2012). Here, a conserved serine residue immediately preceding the OTU domain was identified to be phosphorylated and to be responsible for activity and substrate binding. In search of an analogue serine residue within the OTUD6B amino acid sequence, a highly conserved serine at position 99 (S99) could be identified by aligning the OTUD6B sequences of various species (Figure 32b). Like for DUBA, in which the phosphorylated serine lies in front of the OTU

domain, OTUD6B S99 residue resides 48 amino acids before the OTU domain. In order to validate whether this residue is essential for OTUD6B activity, HEK293T cells were transfected with either FLAG-OTUD6B wildtype (WT), FLAG-OTUD6B^{S99A} mutant or empty vector (EV) control and cell lysates were subjected to DUB activity assay using the suicide probe HA-ubiquitin vinyl sulfone (HA-Ub-VS) as described before. Strikingly, FLAG-OTUD6B^{S99A} mutant was less active than wildtype OTUD6B (Figure 32c). Moreover, when performing FLAG-IP of either FLAG-OTUD6B wildtype (WT) or FLAG-OTUD6B^{S99A} mutant, the binding of LIN28B to FLAG-OTUD6B^{S99A} mutant was completely abolished (Figure 32d) and thus the serine residue S99 represents a promising candidate for phosphorylation.

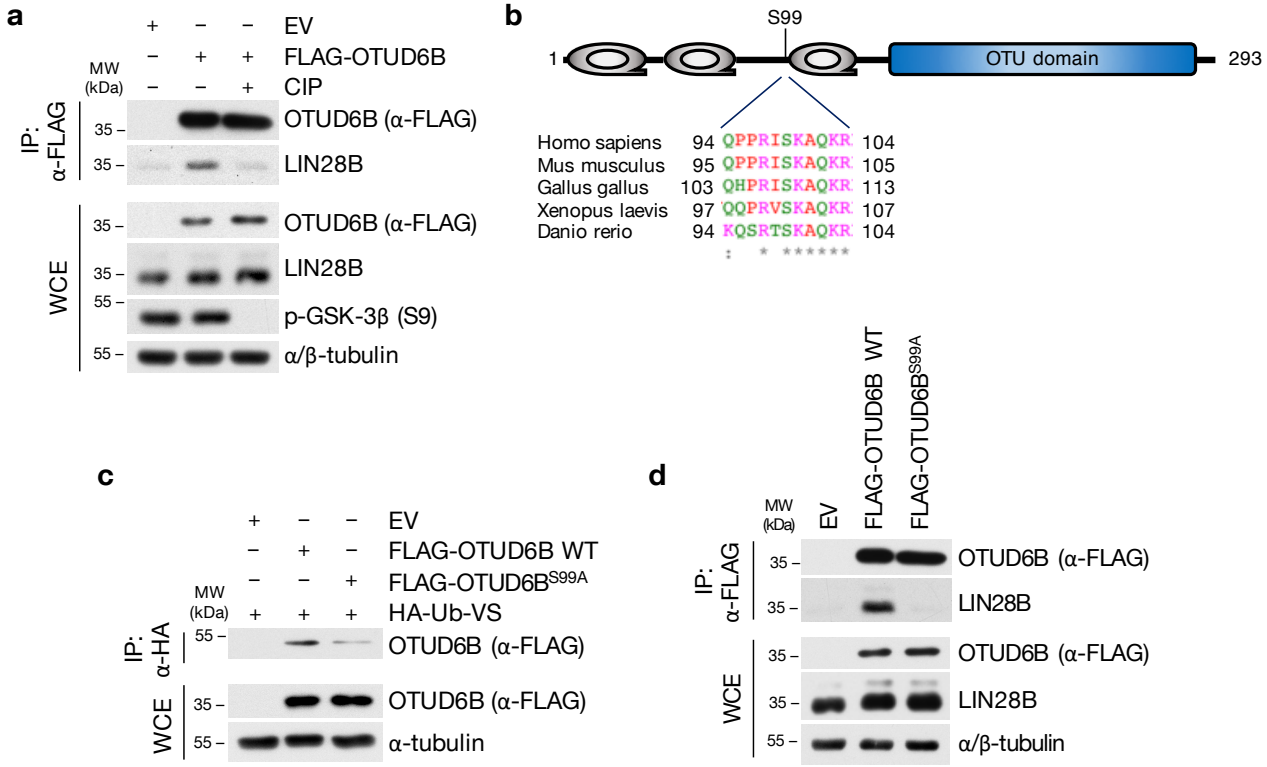

Figure 32: OTUD6B binding to LIN28B is phosphorylation-dependent. (a) Immunoprecipitation (IP) of FLAG-OTUD6B from whole cell extracts (WCE) of HEK293T cells transfected with FLAG-OTUD6B or empty vector (EV). WCE were treated with calf intestinal alkaline phosphatase (CIP) or vehicle for 10 min at room temperature as indicated and subjected to FLAG-IP. WCE and IP were analysed by immunoblotting using the indicated antibodies. α/β-tubulin served as a loading control. **(b)** Schematic overview of human OTUD6B structure and the position and adjacent amino acid sequence of the conserved serine 99 (S99) in comparison to the indicated species. **(c)** DUB activity assay of FLAG-OTUD6B wildtype (WT) and FLAG-OTUD6B^{S99A} mutant, in which the S99 depicted in **b** was mutated to alanine. Whole cell extracts (WCE) of HEK293T cells transfected with FLAG-OTUD6B, FLAG-OTUD6B^{S99A} or empty vector (EV) were incubated with HA-ubiquitin-vinyl sulfone (HA-Ub-VS) and active DUBs were immunoprecipitated using HA-beads. WCE and immunoprecipitates (IP) were subjected to immunoblot analysis using α-FLAG antibody. α-tubulin served as a loading control. **(d)** Immunoprecipitation (IP) of FLAG-OTUD6B wildtype and FLAG-OTUD6B^{S99A} mutant from whole cell extracts (WCE) of HEK293T cells transfected with respective expression constructs or empty vector (EV). WCE and FLAG-IP were subjected to immunoblot analysis using the indicated antibodies. α/β-tubulin served as a loading control.

5.4.5 RIOK3 represents a potential kinase of OTUD6B

The previous findings suggested that the interaction between OTUD6B and LIN28B depends on phosphorylation (Figure 32). Additionally, mutation of the conserved serine residue 99 to alanine in OTUD6B completely abrogated the binding of LIN28B to OTUD6B and decreased the catalytic activity of OTUD6B, indicating that the phosphorylation, which mediates the interaction, is located on OTUD6B (Figure 32). In search for the responsible kinase, RIOK3 was the only kinase, which could be identified as an interactor of OTUD6B by both mass spectrometric approaches performed in this study (Figure 27, Figure 28). In order to investigate whether RIOK3 could be a potential kinase of OTUD6B, the specific binding of RIOK3 to OTUD6B was analysed by IP experiments. To this end, HEK293T cells were transfected with constructs expressing FLAG-tagged OTUD6B or other DUBs of the OTU family or empty vector (EV) control and cell lysates were subjected to FLAG-IP. Importantly, this revealed a strong co-immunoprecipitation of endogenous RIOK3 from the FLAG-OTUD6B but not the EV sample (Figure 33a). Moreover, RIOK3 specifically interacted with OTUD6B while no binding could be observed to the closely related OTU DUB OTUD6A or OTUD2 and OTUB1 (Figure 33b). Like for LIN28B, only the longest isoform of OTUD6B (isoform 1) interacted with RIOK3, whereas there was no binding to isoform 2 (Figure 33c). Hence, RIOK3 represents a valid candidate as a mediator for LIN28B binding, as both proteins specifically interacted with the N-terminal part or OTUD6B isoform 1 (Figure 30, Figure 33).

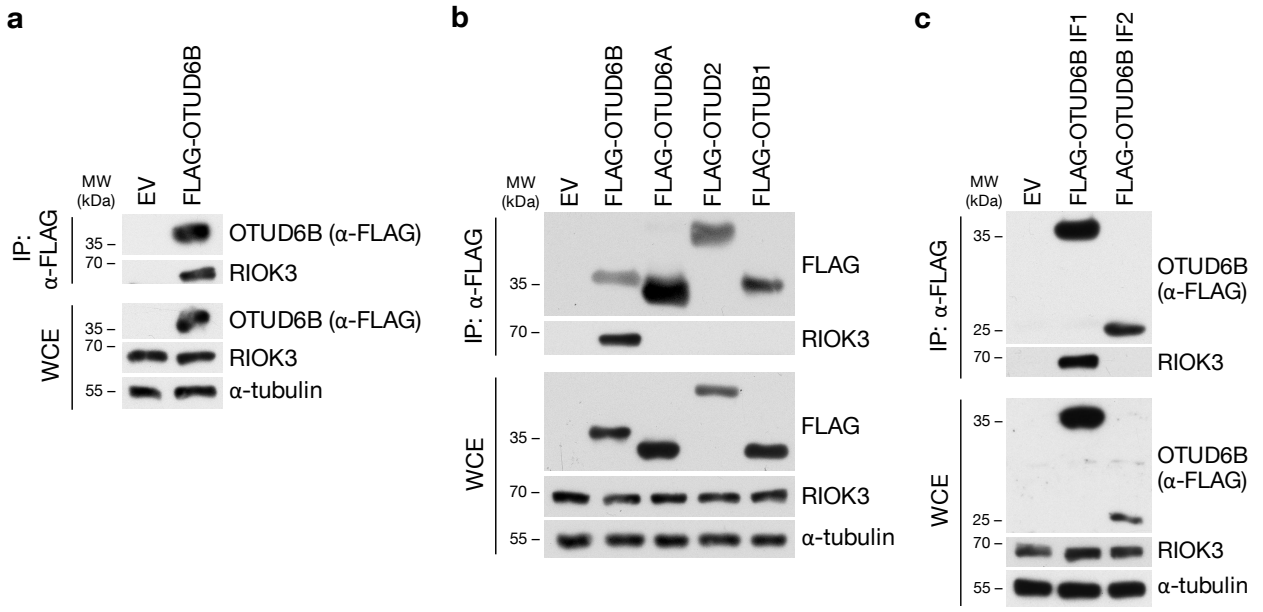

Figure 33: OTUD6B binds to RIOK3. (a-c) Immunoprecipitation (IP) of FLAG-OTUD6B **(a)**, FLAG-tagged OTUD6B, OTUD6A, OTUD2, OTUB1 **(b)** and FLAG-OTUD6B isoform 1 (IF1) and 2 (IF2) **(c)**. HEK293T cells were transfected with constructs coding for indicated FLAG-tagged proteins or empty vector (EV) control and lysates were subjected to FLAG-IP. Whole cell extracts (WCE) and IPs were analysed by immunoblotting using the indicated antibodies. α-tubulin served as a loading control.

As a serine/threonine-specific kinase, RIOK3 represents a potential kinase, which might phosphorylate the serine residue 99 of OTUD6B. In order to address this question, the binding of RIOK3 to FLAG-OTUD6B^{S99A} mutant was investigated by FLAG-immunoprecipitation experiments from HEK293T cells. Strikingly, binding of RIOK3 to the FLAG-OTUD6B^{S99A} mutant was completely abrogated (Figure 34a), as observed previously for LIN28B (Figure 32), supporting the assumption that RIOK3 phosphorylates OTUD6B at S99 to mediate activity and substrate binding of OTUD6B. Since the binding of LIN28B and RIOK3 to OTUD6B both depends on S99, it is conceivable that RIOK3 interacts indirectly with OTUD6B via LIN28B. Hence, to exclude the possibility of indirect binding, a potential interaction of LIN28B and RIOK3 was tested in the presence or absence of OTUD6B. To this end, HEK293T cells were transfected with siRNA targeting OTUD6B (siOTUD6B) or a control siRNA targeting luciferase (siGL) one day prior to transfection with FLAG-LIN28B or empty vector (EV). The interaction of FLAG-LIN28B with endogenous RIOK3 was analysed in the OTUD6B depleted or control cells by FLAG-IP. Importantly, the interaction between LIN28B and RIOK3 strongly depended on OTUD6B, as the co-immunoprecipitation of RIOK3 decreased to the same extent as the binding of LIN28B to OTUD6B in the OTUD6B knockdown setting (Figure 34b). In contrast, FLAG-IP of OTUD6B from HEK293T cells depleted of RIOK3 weakened the interaction between OTUD6B and LIN28B (Figure 34c), thus supporting that RIOK3 promotes substrate binding of OTUD6B. In summary, the strong and specific binding between OTUD6B and RIOK3 together with the observed dependency of OTUD6B binding to LIN28B on RIOK3 underline a potential role for RIOK3 as an activating kinase of OTUD6B.

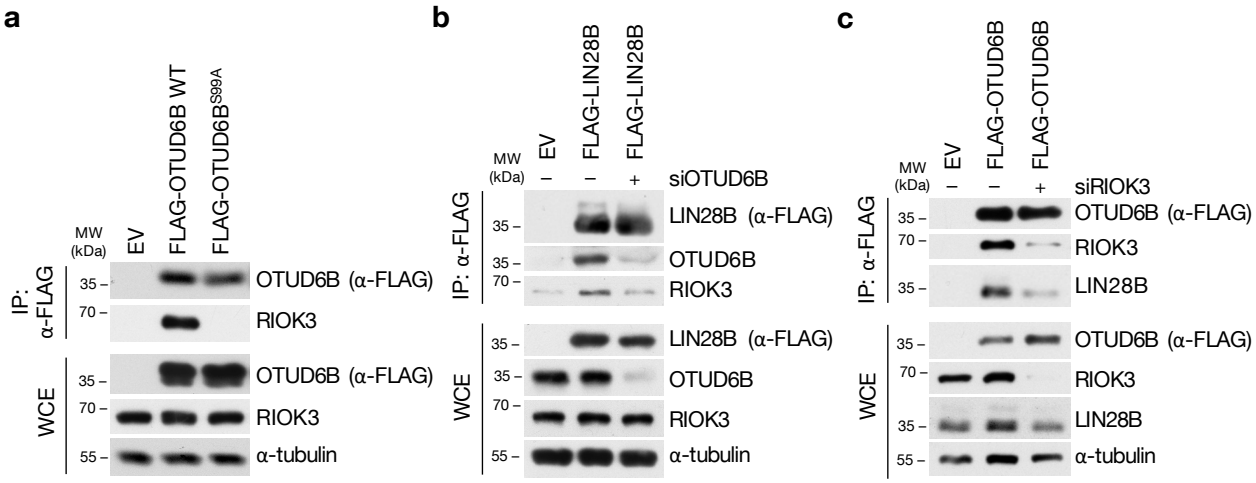

Figure 34: RIOK3 promotes binding of OTUD6B to LIN28B. (a) Immunoprecipitation (IP) of FLAG-OTUD6B wildtype and FLAG-OTUD6B^{S99A} mutant from whole cell extracts (WCE) of HEK293T cells transfected with respective expression constructs or empty vector (EV). WCE and FLAG-IP were subjected to immunoblot analysis using the indicated antibodies. α-tubulin served as a loading control. **(b, c)** Immunoprecipitation of FLAG-LIN28B **(b)** or FLAG-OTUD6B **(c)** from WCE of control or OTUD6B **(b)** or RIOK3 **(c)** depleted HEK293T cells. Cells were transfected with siRNA targeting OTUD6B (siOTUD6B) **(b)** or RIOK3 (siRIOK3) **(c)** or control siRNA (–) and one day later cells were further transfected with constructs coding for FLAG-LIN28B **(b)** or FLAG-OTUD6B **(c)** or empty vector (EV) control. Whole cell extracts (WCE) were subjected to FLAG immunoprecipitation (IP) and WCE and IP were analysed by immunoblotting using the indicated antibodies. α-tubulin served as a loading control.

5.4.6 OTUD6B deubiquitylates LIN28B

Given that OTUD6B represents an active cysteine protease (Figure 25) and specifically interacts with LIN28B (Figure 29), it is conceivable that LIN28B is a substrate and thus it is deubiquitylated by OTUD6B. To address this question, different *in vivo* ubiquitylation studies were performed in HEK293T cells. First, cells were transfected with siRNA against OTUD6B or control siRNA (siGL) to investigate the effect of OTUD6B loss on LIN28B ubiquitylation. Cells were additionally transfected with constructs coding for HA-Ubiquitin and FLAG-LIN28B and treated with the proteasome inhibitor MG132 to allow accumulation of ubiquitylated proteins. After lysis, whole cell extracts (WCE) were denatured by addition of SDS and boiling in order to disrupt protein

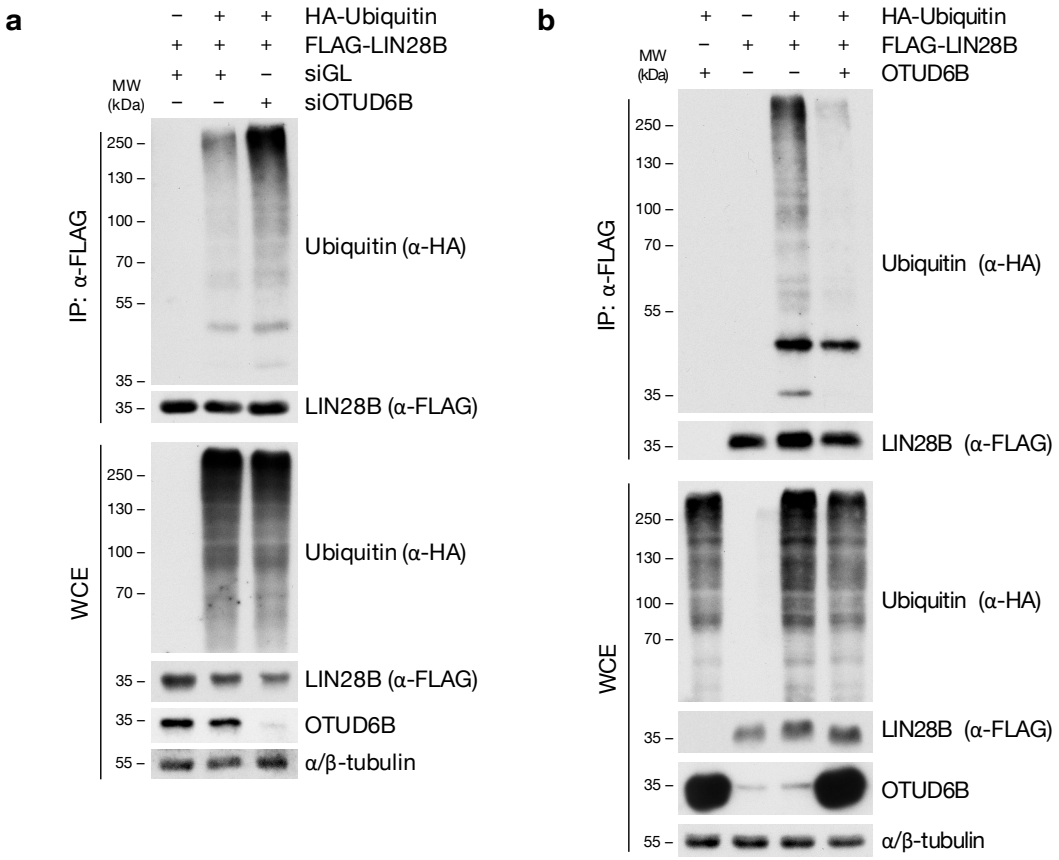

Figure 35: OTUD6B deubiquitylates LIN28B *in vivo*. (a) *In vivo* ubiquitylation assay of LIN28B in OTUD6B knockdown cells. HEK293T cells were transfected with siRNA targeting OTUD6B (siOTUD6B) or control siRNA (siGL) and one day later, cells were further transfected with constructs coding for FLAG-LIN28B together with HA-Ubiquitin or empty vector. The next day, cells were treated with 10 µM MG132 for 3 hrs and denatured whole cell extracts (WCE) of transfected cells were subjected to FLAG immunoprecipitation (IP). WCE and IP were analysed by immunoblotting using the indicated antibodies. α/β-tubulin served as a loading control. **(b)** *In vivo* ubiquitylation assay of LIN28B in OTUD6B overexpressing cells. HEK293T cells were transfected with indicated combinations of FLAG-LIN28B, HA-Ubiquitin, OTUD6B and empty vector control and FLAG immunoprecipitation (IP) was performed from denatured whole cell extracts (WCE). WCE and IP were analysed by immunoblotting using the indicated antibodies. α/β-tubulin served as a loading control.

interactions with FLAG-LIN28B, thus ensuring to only analyse ubiquitylation of LIN28B. WCE were subjected to FLAG-IP and ubiquitylation of LIN28B could be detected by immunoblot analysis using an anti-HA antibody. Strikingly, ubiquitylation of LIN28B was strongly increased in the OTUD6B knockdown sample, providing first evidence that OTUD6B deubiquitylates LIN28B (Figure 35a). To further investigate this hypothesis, LIN28B ubiquitylation was analysed in an OTUD6B overexpressing setting. Therefore, HEK293T cells were additionally transfected with a construct coding for OTUD6B and *in vivo* ubiquitylation was performed as before, but without treatment with MG132. Notably, this time the polyubiquitylation signal was significantly decreased upon forced OTUD6B expression, further supporting the hypothesis that LIN28B represents a substrate of OTUD6B (Figure 35b).

Despite recently published data addressing the question whether OTUD6B possesses ubiquitin chain linkage specificity, it remains unknown which type of ubiquitin chains is cleaved by OTUD6B, as recombinant OTUD6B was not active towards different di-ubiquitin chains in this context (Mevissen et al. 2013). However, it is still imaginable that OTUD6B needs binding to its substrate in order to cleave certain types of ubiquitin chains. To investigate whether OTUD6B regulates K48-linked ubiquitylation of LIN28B, *in vivo* ubiquitylation was performed in OTUD6B siRNA transfected cells as before, however this time using a construct, which encoded for HA-Ubiquitin that only can form K48-linkages as all other lysine residues were mutated (HA-Ubiquitin-K48). Indeed, the same strong increase in polyubiquitylation of FLAG-LIN28B could be observed upon OTUD6B knockdown as in the experiment before using wildtype HA-Ubiquitin, suggesting that OTUD6B might regulate protein stability of LIN28B by cleaving off K48-linked polyubiquitin (Figure 36a). Since it is possible that the ectopic HA-Ubiquitin-K48 protein formed polyubiquitin chains with endogenous wildtype ubiquitin, OTUD6B could still exhibit other linkage specificities. To further shed light on this question, a specific antibody was used which only recognized K48-linked ubiquitin. In accordance with the increase in polyubiquitylation detected by the anti-HA antibody, also the K48-linkage specific antibody gave rise to a significantly stronger signal in the OTUD6B knockdown sample compared to the non-targeting control (Figure 36a). Furthermore, by repeating the *in vivo* ubiquitylation experiment in the context of forced OTUD6B expression, in which HEK293T cells were transfected with wildtype HA-Ubiquitin, a strong reduction in polyubiquitylation signal could be observed by immunoblotting using both anti-HA or K48-linkage specific antibodies, further proving that OTUD6B removes K48-linked ubiquitin from LIN28B (Figure 36b). Importantly, the decrease in ubiquitylation caused by overexpression of OTUD6B wildtype (WT) could not be observed by forced expression of the catalytically inactive OTUD6B^{C158A} mutant, thus providing clear evidence that the effects on LIN28B polyubiquitylation were dependent on OTUD6B activity and thus were direct (Figure 36b). Altogether, these data showed that OTUD6B negatively regulates K48-linked polyubiquitylation of LIN28B, thus indicating that OTUD6B might prevent proteasomal degradation of LIN28B.

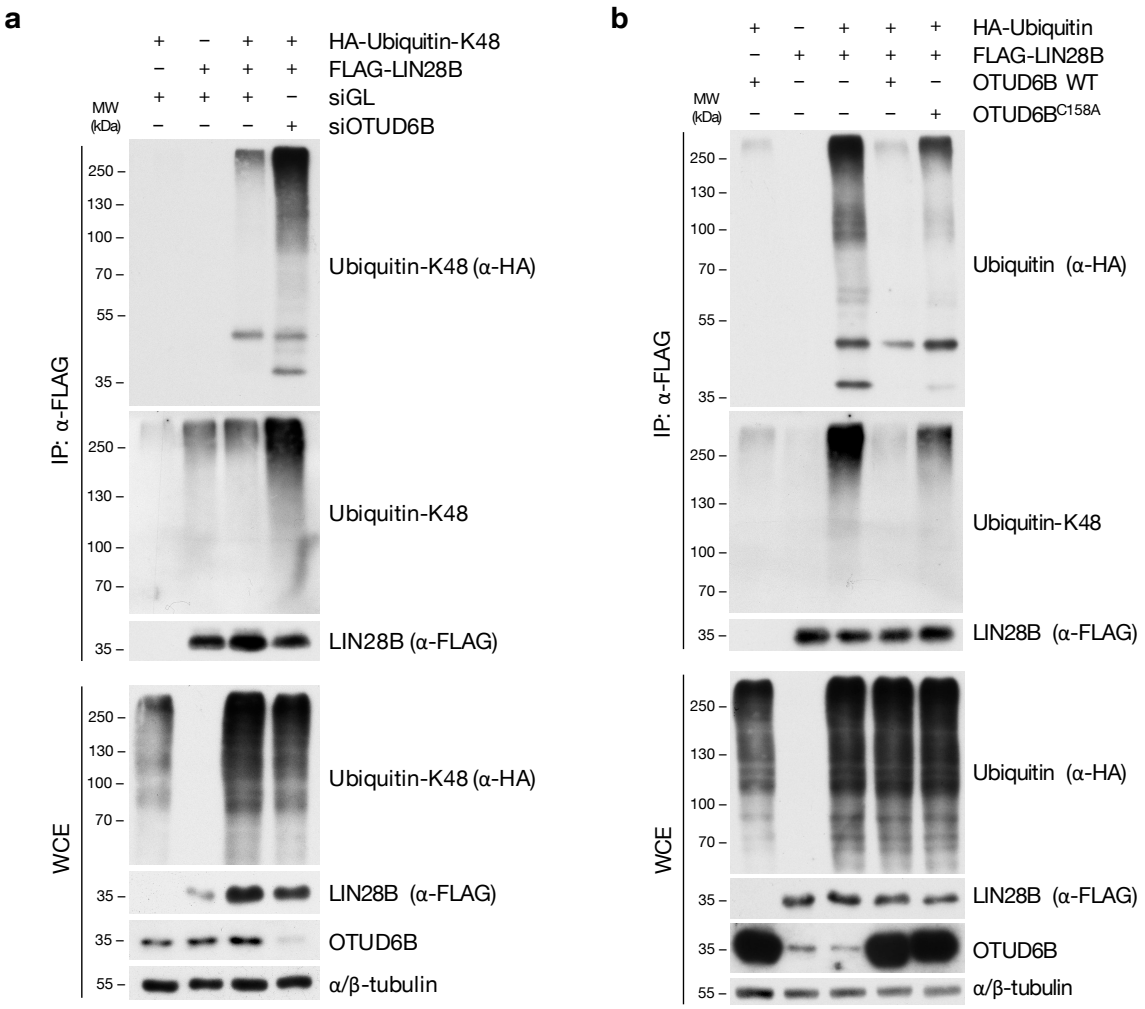

Figure 36: OTUD6B removes K48 ubiquitylation from LIN28B. (a) *In vivo* ubiquitylation assay of LIN28B in OTUD6B knockdown cells. HEK293T cells were transfected with siRNA targeting OTUD6B (siOTUD6B) or control siRNA (siGL) and one day later, cells were further transfected with constructs coding for FLAG-LIN28B together with HA-Ubiquitin-K48 or empty vector. The next day, cells were treated with 10 µM MG132 for 3 hrs and denatured whole cell extracts (WCE) of transfected cells were subjected to FLAG immunoprecipitation (IP) and WCE and IP were analysed by immunoblotting using the indicated antibodies. α/β-tubulin served as a loading control. **(b)** *In vivo* ubiquitylation assay of LIN28B in OTUD6B overexpressing cells. HEK293T cells were transfected with indicated combinations of FLAG-LIN28B, HA-Ubiquitin, OTUD6B wildtype (WT), catalytically inactive OTUD6B^{C158A} mutant and empty vector control (–) and FLAG immunoprecipitation (IP) was performed from denatured whole cell extracts (WCE). WCE and IP were analysed by immunoblotting using the indicated antibodies. α/β-tubulin served as a loading control.

5.4.7 OTUD6B stabilizes LIN28B at G1/S transition

The previously performed experiments suggest a cell cycle-dependent stabilization of LIN28B by OTUD6B, as, first, OTUD6B is necessary for S phase entry (Figure 24), second, OTUD6B activity was found to peak at G1/S transition (Figure 26) and third, OTUD6B removes K48-linked ubiquitin from LIN28B (Figure 36). To investigate this hypothesis, LIN28B protein levels were analysed in the course of the cell cycle. To this end, A549 cells were synchronized at either G1/S phase by a double thymidine block or at mitosis by a single thymidine block for 24 hrs followed by a release for 12 hrs in nocodazole. Mitotic cells were collected by mitotic shake-off and

synchronized cells were released and harvested at different time points in order to cover the entire cell cycle. Immunoblot analysis revealed that LIN28B protein level differed at different cell cycle phases, peaking in late G1 and S phase and thus correlating with OTUD6B activity (Figure 37a). Notably, the LIN28B band detected by immunoblot analysis shifted up in mitosis explaining the double band which could often be seen when blotting for LIN28B in asynchronous cells (Figure 30). To investigate whether the mobility shift of LIN28B in mitosis is caused by phosphorylation, A549 cells were synchronized in mitosis and cell lysates were treated with lambda phosphatase (λ-PPase) in order to dephosphorylate proteins. This showed that the mobility shift is a clear consequence of LIN28B phosphorylation as λ-PPase treatment led to downshifting of the LIN28B band detected by immunoblot analysis (Figure 37b). Of note, FLAG-OTUD6B immunoprecipitation experiments revealed binding to both forms of LIN28B (Figure 30), suggesting that OTUD6B binding to LIN28B is not restricted to G1/S phase but also occurs in mitosis. However, as OTUD6B activity significantly drops in mitosis (Figure 26), deubiquitylation might not take place at this cell cycle stage.

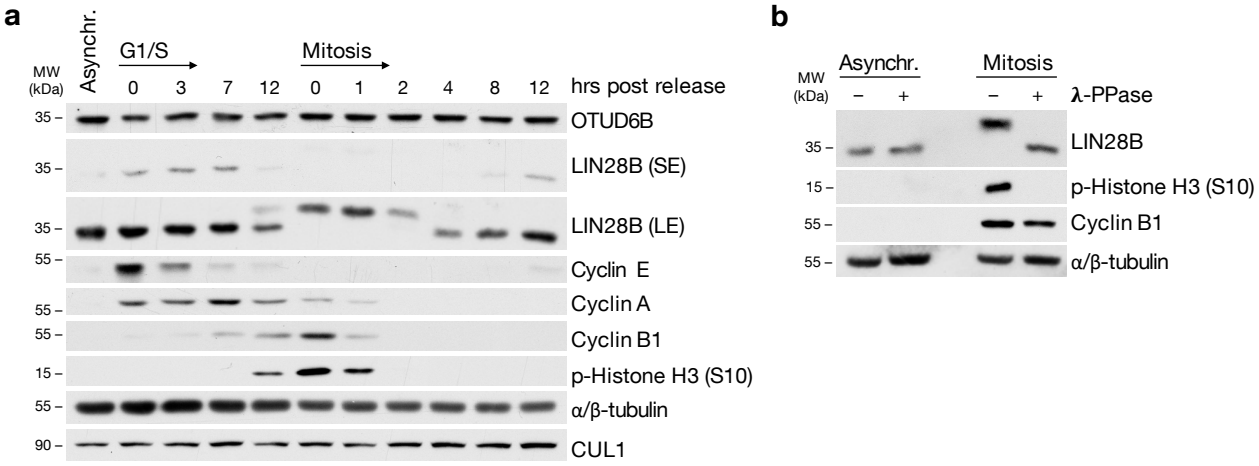

Figure 37: LIN28B protein levels are cell cycle regulated. (a) Cell cycle analysis of LIN28B and OTUD6B. A549 cells were synchronized at G1/S phase by a double thymidine block or at mitosis by a single thymidine block for 24 hrs followed by a release for 12 hrs in nocodazole. Mitotic cells were collected by mitotic shake-off and synchronized cells were released and harvested at the indicated time points. Whole cell lysates of asynchronous cells and collected samples were subjected to immunoblot analysis using the indicated antibodies. α/β-tubulin and CUL1 served as loading controls. **(b)** Asynchronous or mitotic A549 cells, which were synchronized like in **a**, were lysed and lysates were incubated with or without lambda phosphatase (λ-PPase) for 30 min at 30°C. Samples were subjected to immunoblot analysis using the indicated antibodies. α/β-tubulin served as a loading control.

Since both OTUD6B activity and LIN28B protein level are high at G1/S transition, it is likely that OTUD6B is necessary to stabilize LIN28B at this cell cycle stage. To validate this hypothesis, asynchronous A549 cells and cells synchronized at G1/S by a double thymidine block were transfected with siRNA targeting OTUD6B (siOTUD6B) or control siRNA (siGL) and treated with cycloheximide (CHX), which inhibits protein translation. Immunoblot analysis of cell lysates revealed that LIN28B protein levels were stable in asynchronous cells and no obvious difference

could be observed upon OTUD6B loss (Figure 38a). In contrast, OTUD6B knockdown in cells, which were synchronized at G1/S phase, clearly destabilized LIN28B upon CHX addition as LIN28B protein levels were decreasing with increasing time of CHX treatment (Figure 38b).

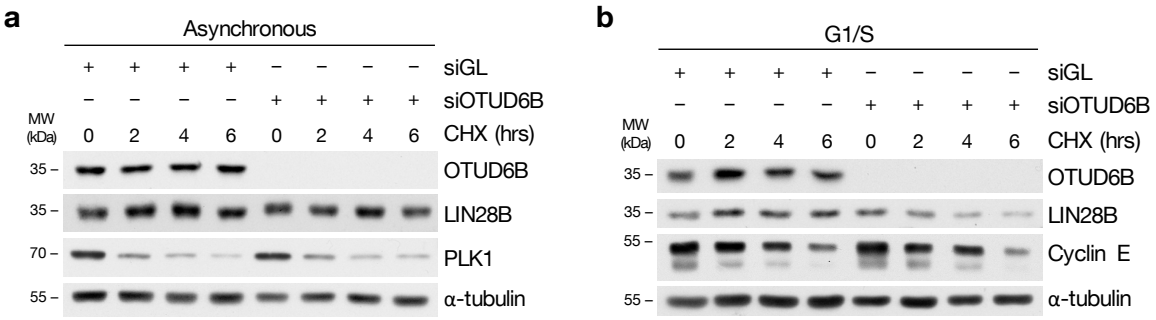

Figure 38: OTUD6B stabilizes LIN28B at G1/S transition. Immunoblot analysis of asynchronous **(a)** or G1/S phase arrested **(b)** A549 cells transfected with siRNA targeting OTUD6B (siOTUD6B) or control siRNA (siGL). Cells in **b** were synchronized at G1/S phase by a double thymidine block. 72 hrs after transfection, cells were treated with 200 µg/mL cycloheximide (CHX) for the indicated hrs and whole cell lysates were subjected to immunoblot analysis using the indicated antibodies. α-tubulin served as a loading control.

The previous *in vivo* ubiquitylation data suggest that OTUD6B removes K48-linked ubiquitin chains from LIN28B (Figure 36). To further prove that the observed destabilization of LIN28B caused by OTUD6B loss is mediated by an increase in proteasomal degradation, the CHX experiment in G1/S-synchronized A549 cells was repeated, but this time one sample was additionally treated with the proteasome inhibitor MG132 for 5 hrs. Strikingly, the simultaneous inhibition of the proteasome rescued the destabilization of LIN28B mediated by OTUD6B knockdown (Figure 39).

Overall, these data provide evidence that OTUD6B prevents proteasomal degradation of LIN28B at G1/S by K48-linkage specific deubiquitylation of LIN28B.

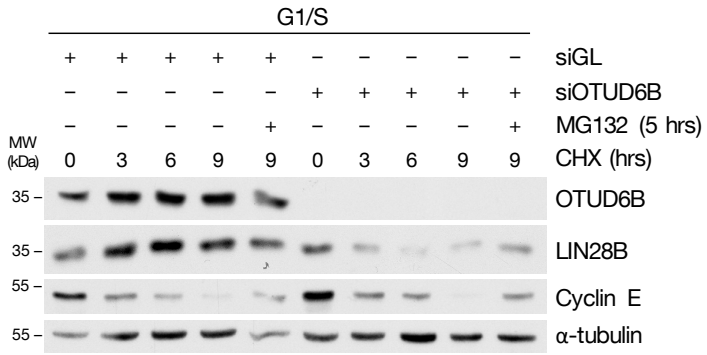

Figure 39: OTUD6B prevents proteasomal degradation of LIN28B at G1/S transition. Immunoblot analysis of A549 cells, which were transfected with siRNA targeting OTUD6B (siOTUD6B) or control siRNA (siGL) and which were synchronized at G1/S phase by a double thymidine block. Cells were treated with 100 µg/mL cycloheximide (CHX) for the indicated hrs and one sample of siOTUD6B and siGL transfected cells was additionally incubated with 10 µM MG132 for the last 5 hrs of CHX treatment. Whole cell lysates were subjected to immunoblot analysis using the indicated antibodies. α-tubulin served as a loading control.

5.4.8 Overexpression of LIN28B attenuates the proliferation defect caused by OTUD6B depletion

The previous experiments demonstrated that OTUD6B deubiquitylates LIN28B, thereby stabilizing it at G1/S transition. Given that LIN28B is essential for MM cell proliferation (Manier et al. 2017), it is conceivable that the growth defect observed upon OTUD6B depletion is caused by LIN28B destabilization. Since LIN28B is expressed in human embryonic stem cells (hESCs) and becomes downregulated upon differentiation (Tsialikas and Romer-Seibert 2015; Yang and Moss 2003), various MM cell lines were tested for LIN28B re-activation by qPCR analysis (Figure 40a). Notably, most of the cell lines expressed LIN28B while LIN28B mRNA was not detected in the two cell lines OPM2 and ANBL-6 (Figure 40a). Among the cells expressing LIN28B, four cell lines, JJN3, MM1.S, H929 and U266, revealed remarkably high levels of LIN28B whereas the other cell lines showed only modest amounts of LIN28B (Figure 40a). To further analyse whether LIN28B levels correlate with OTUD6B expression, OTUD6B mRNA levels were quantified in the same MM cell lines (Figure 40b). In this regard, no clear correlation between OTUD6B and LIN28B expression could be observed (Figure 40a, b). However, OPM2 and ANBL-6 cells, which did not express LIN28B, revealed the lowest mRNA levels of OTUD6B among the analysed cell lines (Figure 40a, b).

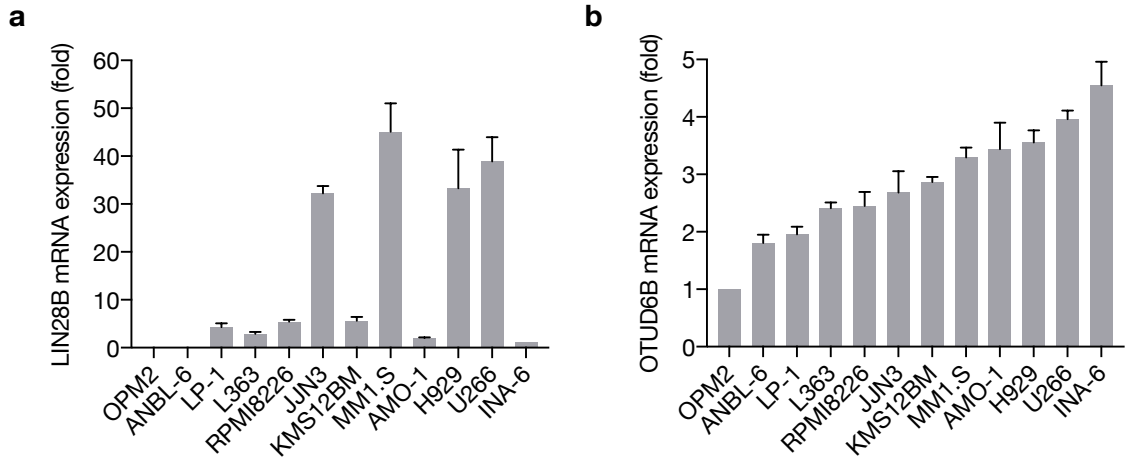

Figure 40: OTUD6B and LIN28B expression in various MM cell lines. (a, b) Quantification of mRNA levels from indicated MM cell lines by qPCR analysis using specific primers for LIN28B **(a)** and OTUD6B **(b)**. The mRNA levels were normalized to RPLP0 and INA-6 **(a)** or OPM2 **(b)** samples were set as 1 (n = 3 technical replicates, mean ± S.D.).

In order to further investigate the functional role of LIN28B destabilization for the defect of MM cell proliferation induced by OTUD6B loss, forced expression of LIN28B was analysed in view of its ability to rescue the proliferation phenotype of OTUD6B knockdown. To this end, proliferation assays were conducted in MM1.S cells, which revealed high expression of both, OTUD6B and LIN28B (Figure 40). Like seen before, shRNA-mediated knockdown of OTUD6B strongly reduced the proliferation capacity of MM1.S cells as measured by the drop in the dsRed positive cell population (Figure 38a). Strikingly, additional expression of LIN28B (GFP/dsRed positive cells) restored 20% of proliferation within 4 days, suggesting that the effect of OTUD6B

knockdown is partially caused by a reduction of LIN28B levels (Figure 38a). However, despite re-expression of LIN28B, cell proliferation was still reduced by 40% in OTUD6B knockdown cells compared to the control (Figure 38a), which could be either explained by an unphysiologically expression of ectopic LIN28B or the fact that other substrates of OTUD6B are responsible for the residual defect in cell proliferation. In order to test the latter possibility, the effect of CRISPR/Cas9-mediated knockout of OTUD6B was analysed in a cell line, which did not express LIN28B as measured by qPCR (Figure 40a). Like observed for other MM Cas9 cell lines (Figure 20), knockout of OTUD6B induced by two different sgRNAs significantly reduced the portion of GFP positive OPM2 Cas9 cells over time, reflecting an impaired ability of these cells to proliferate (Figure 38b). These data suggest that OTUD6B possesses additional substrates like it is known also for other DUBs.

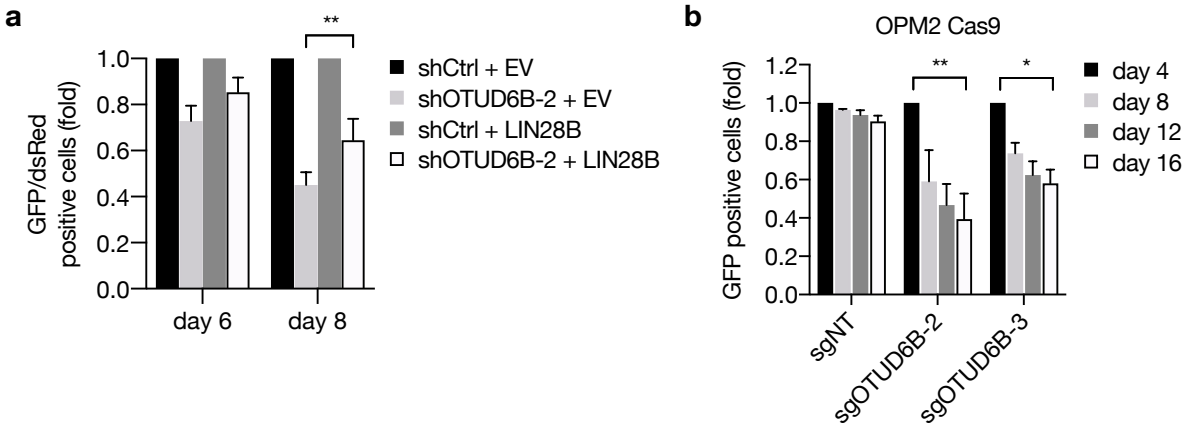

Figure 41: Overexpression of LIN28B partially counteracts the proliferation defect caused by OTUD6B depletion. **(a)** Proliferation analysis of MM1.S cells lentivirally transduced with constructs expressing empty vector (EV) or LIN28B and GFP together with indicated combinations of control shRNA (shCtrl) or shRNA targeting OTUD6B (shOTUD6B-2) and dsRed. The proportion of GFP/dsRed double positive cells were determined by flow cytometric analysis at the indicated days after infection and values were normalized to day 4. Results are depicted in relation to shCtrl in combination with EV or LIN28B expressing cells (n = 3 independent experiments, mean ± S.D.). **, $P < 0.01$; by Student's t-tests. **(b)** Proliferation analysis of LIN28B negative OPM2 Cas9 cells infected with either control sgRNA (sgNT) or two different sgRNAs targeting OTUD6B (sgOTUD6B-2 and -3). The ratio of sgRNA expressing, GFP positive cells to uninfected cells was measured by flow cytometric analysis at the indicated time points after infection. Results are depicted in relation to day 4 (n = 3 independent experiments, mean ± S.D.). *, $P < 0.05$; **, $P < 0.01$; by one sample t-test.

To further evaluate whether the importance of OTUD6B for cell proliferation depends on LIN28B, two diffuse large B-cell lymphoma (DLBCL) cell lines stably expressing Cas9 enzyme (generated by R. Spallek) were analysed with regard to OTUD6B knockout-induced proliferation defects. Of these two cell lines, only OCI-LY10 cells expressed LIN28B whereas no signal could be detected in OCI-LY7 cell lysates by immunoblot analysis (Figure 42a). CRISPR/Cas9-mediated knockout of OTUD6B led to a strong reduction in OCI-LY10 cells whereas non-targeting sgRNA expressing cells revealed the same proliferation capacity like non-infected cells (Figure 42c). Notably, this effect was not observed in OCI-LY7 cells, which did not express LIN28B (Figure 42b). Overall, these results suggest that the importance of OTUD6B for cell proliferation partially

depends on LIN28B and that the contribution of other substrates might depend on the cellular context.

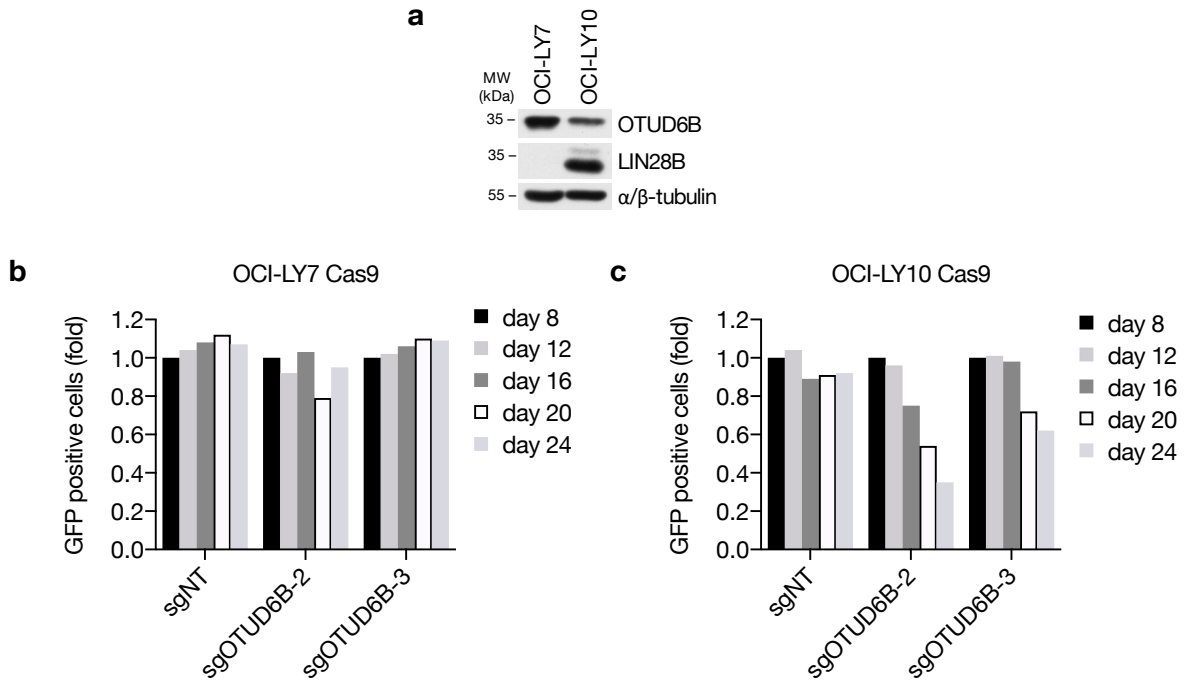

Figure 42: OTUD6B is essential for proliferation of LIN28B expressing DLBCL cells. (a) Immunoblot analysis of LIN28B negative (OCI-LY7) and positive (OCI-LY10) DLBCL cell lines. Whole cell extracts were probed with the indicated antibodies. α/β-tubulin served as a loading control. **(b, c)** Proliferation analysis of the stably expressing Cas9 cell lines OCI-LY7 **(b)** and OCI-LY10 **(c)** infected with either control sgRNA (sgNT) or two different sgRNAs targeting OTUD6B (sgOTUD6B-2 and -3). The ratio of sgRNA expressing, GFP positive cells to uninfected cells was measured by flow cytometric analysis at the indicated time points after infection and results are depicted in relation to day 8.

5.4.9 LIN28B depletion phenocopies knockdown of OTUD6B

LIN28B depletion has been previously described to arrest pancreatic ductal adenocarcinoma cells at G1 phase and, consequently, lead to a decrease in the S phase population (Wang, Li, et al. 2017). The same phenotype was observed upon OTUD6B knockdown in the present study (Figure 23), which is in line with a positive regulation of LIN28B by OTUD6B. To investigate the functional role of LIN28B in the G1/S transition of MM cells, MM1.S cells were lentivirally infected with shRNA constructs targeting LIN28B, OTUD6B or non-targeting control and synchronized at G1 phase by the addition of palbociclib for 24 hrs. Palbociclib represents a reversible CDK4/6 inhibitor and has been previously used for the synchronization of MM1.S cells (Huang, Di Liberto, et al. 2012). Cell cycle distribution was analysed by flow cytometry of propidium iodide (PI) stained cells, which confirmed that most of the cells were arrested in G1 phase after palbociclib treatment (Figure 43a). As expected, control cells progressed into S phase 12 hrs after palbociclib removal whereas OTUD6B depleted cells stayed in G1 phase (Figure 43a), similarly to the previously performed experiment using a double thymidine block for synchronization (Figure 24). Strikingly, LIN28B depleted cells phenocopied the knockdown of OTUD6B and stayed arrested in G1 cells

(Figure 43a), providing further evidence that OTUD6B is important for G1/S transition by positively regulating LIN28B.

To further characterize and compare the G1/S arrest caused by OTUD6B and LIN28B depletion, whole cell lysates of MM1.S cells infected with lentiviral particles encoding shRNAs against OTUD6B, LIN28B or non-targeting control were subjected to immunoblot analysis. In line with a G1/S arrest, silencing of either OTUD6B or LIN28B induced a strong increase of Cyclin E and p27 (Figure 43b). Together, OTUD6B and LIN28B depletion provoked the same phenotype by inducing a cell cycle arrest at G1/S as a consequence of an increase of p27 level and hence Cyclin E-CDK2 inhibition.

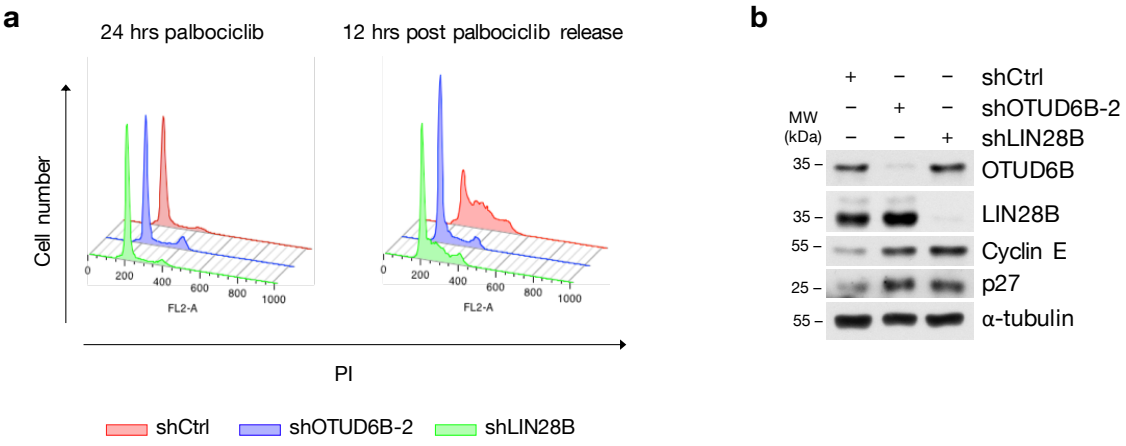

Figure 43: OTUD6B and LIN28B are essential for G1/S transition in MM cells. (a) Flow cytometric analysis of MM1.S cells transduced with shRNA constructs targeting OTUD6B (shOTUD6B-2), LIN28B (shLIN28B) or scrambled control (shCtrl), which were synchronized at G1/S phase by treating cells with 1 µM palbociclib for 24 hrs (left graph). Cells were released for 12 hrs (right graph) and fixed. DNA was stained with propidium iodide (PI) and results are depicted as histogram analysis of FL2-A (PI) signal intensity. **(b)** Immunoblot analysis of asynchronous MM1.S cells infected like in **a**. Whole cell extracts were probed with the indicated antibodies. α-tubulin served as a loading control.

5.5 OTUD6B positively regulates MYC expression via LIN28B stabilization

5.5.1 Depletion of OTUD6B decreases MYC expression by LIN28B destabilization

The oncogenic role of LIN28B relies on its positive regulation of the expression of various other oncogenes. Among these, MYC expression has been shown to be downregulated upon LIN28B depletion in MM cells (Manier et al. 2017) and hence could possibly be enhanced by OTUD6B-mediated stabilization of LIN28B.

In order to test this hypothesis, the influence of OTUD6B loss on MYC protein levels was investigated in various MM cell lines by shRNA-mediated depletion of OTUD6B. Cells were infected with respective shRNA constructs targeting OTUD6B or control and subjected to immunoblot analysis after four days. Indeed, this revealed a strong decrease of MYC protein levels in all three cell lines upon OTUD6B depletion using two different shRNAs (Figure 44), supporting the hypothesis that OTUD6B positively regulates MYC expression via LIN28B.

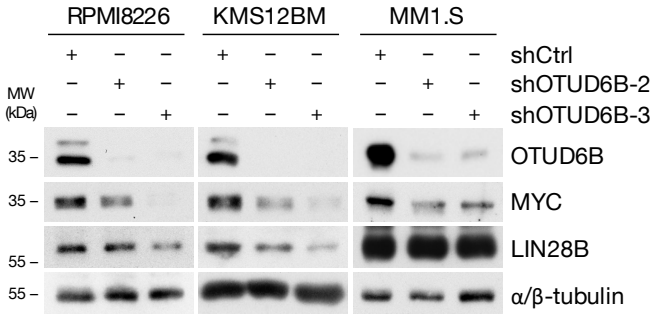

Figure 44: OTUD6B promotes MYC expression in MM cells. Immunoblot analysis of whole cell extracts of indicated MM cell lines, which were lentivirally infected with shRNA constructs targeting OTUD6B (shOTUD6B-2 and -3) or scrambled control (shCtrl), using the indicated antibodies. α/β-tubulin served as a loading control.

LIN28B-mediated upregulation of MYC depends on the inhibition of *let-7* miRNAs, which in turn degrade MYC mRNA (Balzeau et al. 2017; Sampson et al. 2007). Consequently, OTUD6B loss-induced downregulation of MYC protein could be caused by a decrease in MYC mRNA as a consequence of LIN28B deregulation. In order to test this assumption, mRNA levels of MYC were quantified in OTUD6B depleted RPMI8226 cells. As seen before, OTUD6B knockdown induced by lentiviral transduction of two different shRNAs caused a strong decrease of MYC protein levels compared to control cells (Figure 45a). Importantly, qPCR analyses of the same cells confirmed that the observed downregulation of MYC protein caused by OTUD6B loss was a consequence of a strong reduction of MYC mRNA levels, which correlated with the decrease of protein amounts (Figure 45b). As a transcription factor, MYC regulates the expression of a wide range of genes, thereby promoting tumorigenesis (Fernandez et al. 2003; Prochownik 2008). Among these, HMGA1 has been reported to drive proliferation in a MYC-dependent manner (Akaboshi et al. 2009), thus reflecting a potential target, which might also be indirectly influenced by changes in OTUD6B levels. Indeed, knockdown of OTUD6B significantly reduced the expression of HMGA1, which correlated with MYC mRNA levels (Figure 45b), suggesting that OTUD6B has an influence on the expression of many genes, which might promote cell proliferation. In addition, analysis of LIN28B mRNA levels in the same experiment revealed a strong downregulation upon OTUD6B knockdown mediated by shOTUD6B-3 (Figure 45b). However, since LIN28B expression itself is under the control of MYC (Chang et al. 2009), the observed decrease in LIN28B could be a consequence of the reduction of MYC expression, reflecting the positive feedback loop between LIN28B and MYC (Figure 8). To investigate this hypothesis, RPMI8226 cells were infected with shRNA constructs targeting OTUD6B or non-targeting control and mRNA levels of OTUD6B, MYC and LIN28B were monitored at different time points after infections. In fact, qPCR analyses after 24 hrs revealed a decrease in OTUD6B mRNA levels to 40% and a slight reduction of MYC mRNA level by 10%, whereas LIN28B levels were not decreased compared to control cells (Figure 45c). This effect was even more pronounced at 48 hrs post-infection, at which MYC level dropped to 60% whereas LIN28B levels were the same as the control (Figure 45c). Only after 72 hrs, the mRNA levels of LIN28B were reduced by a similar extent to the levels of MYC (Figure 45c),

supporting the hypothesis that the drop of LIN28B mRNA levels was a consequence of the decrease in MYC expression.

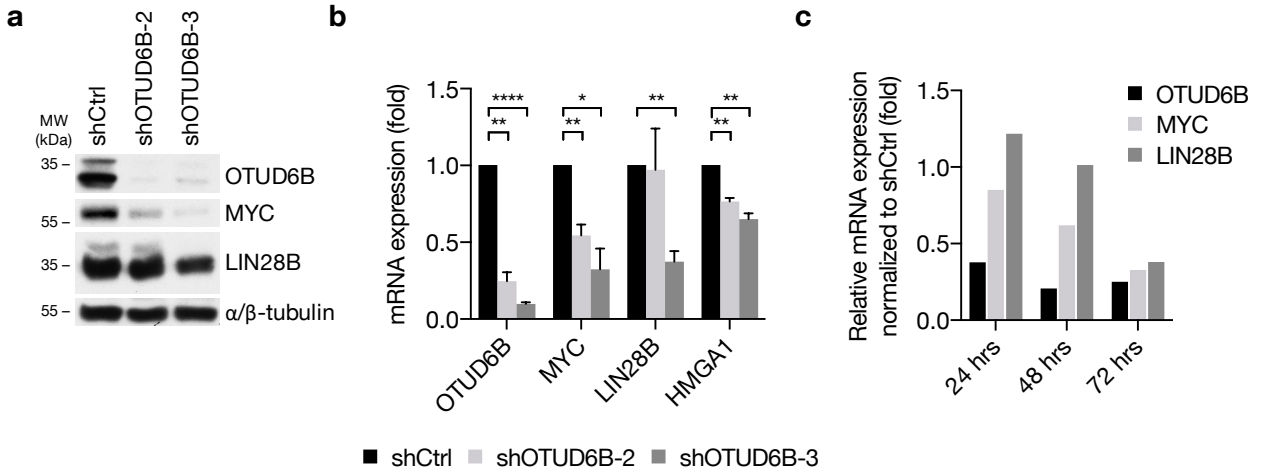

Figure 45: OTUD6B regulates MYC targets. (a) Immunoblot analysis of whole cell extracts of RPMI8226 cells, which were lentivirally infected with shRNA constructs targeting OTUD6B (shOTUD6B-2 and -3) or scrambled control (shCtrl), using the indicated antibodies. α/β-tubulin served as a loading control. **(b)** Quantification of mRNA levels from experiment depicted in **a** by qPCR analysis using specific primers for indicated genes. The mRNA levels were normalized to RPLP0 and the control shRNA infected samples were set as 1 (n = 3 independent experiments, mean ± S.D.). *, $P < 0.05$; **, $P < 0.01$; ****, $P < 0.0001$; by one sample t-test. **(c)** Quantification of mRNA levels from RPMI8226 cells lentivirally transduced with a shRNA construct targeting OTUD6B (shOTUD6B-2) or scrambled control (shCtrl) at the indicated time points after infection by qPCR analysis using specific primers for indicated genes. The mRNA levels were normalized to RPLP0 and data represent ratios of OTUD6B shRNA expressing cells to controls.

The previous experiments showed that OTUD6B is essential for MM cell proliferation (Figure 20, Figure 21) and that OTUD6B depletion negatively affects MYC expression (Figure 44, Figure 45). If these effects depend on OTUD6B-mediated regulation of LIN28B, knockdown of both proteins should have comparable effects to the depletion of the single proteins. In order to investigate whether OTUD6B and LIN28B act in the same pathway, RPMI8226 cells were lentivirally transduced with different combinations of shRNA constructs targeting OTUD6B, LIN28B or control. As expected, expression of shRNAs against either OTUD6B or LIN28B strongly suppressed cell counts to 40-60% in relation to control (Figure 46a). Strikingly, simultaneous depletion of both proteins affected cell proliferation by 50% and hence did not further impaired the cell counts when compared to the single knockdown of either proteins (Figure 46a). Moreover, qPCR analyses of the same cells revealed the same results for MYC mRNA levels, which were decreased to a comparable extent in cells depleted of either OTUD6B or LIN28B alone as in cells harbouring a knockdown of both proteins (Figure 46b). Efficient knockdown under different conditions was verified by immunoblot analysis, which also revealed a strong increase in p27 and Cyclin E protein levels and thus confirmed a cell cycle arrest at G1/S caused by OTUD6B or LIN28B depletion (Figure 46c). Importantly, the accumulation of p27 and Cyclin E was not further enhanced by the simultaneous depletion of OTUD6B and LIN28B (Figure 46), providing further evidence that both proteins regulate the same pathway.

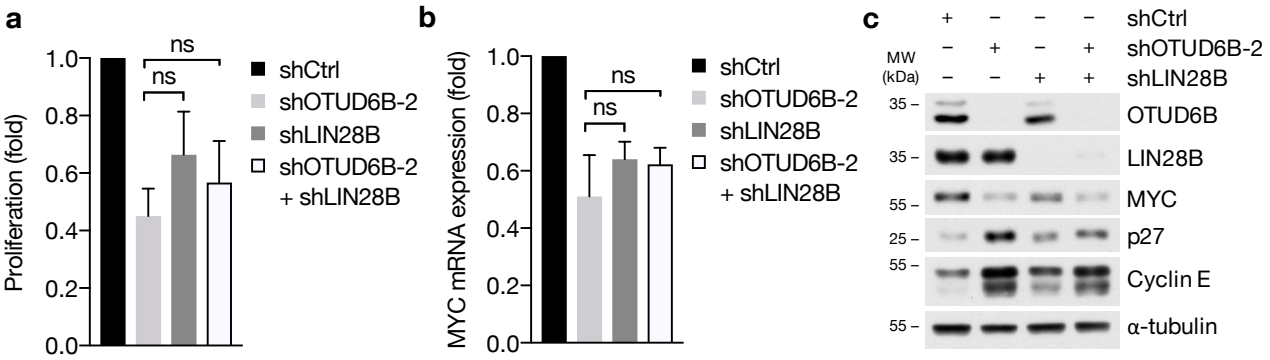

Figure 46: LIN28B and OTUD6B are part of the same signalling pathway. (a) Proliferation analysis of RPMI8226 cells, which were lentivirally transduced with indicated combinations of shRNA constructs targeting OTUD6B (shOTUD6B-2), LIN28B (shLIN28B) and control shRNA (shCtrl). Viable cells were counted using the trypan blue exclusion method 4 days after infection and results are presented in relation to control shRNA expressing cells (n = 3 independent experiments, mean ± S.D.). ns, not significant; by unpaired t-test. **(b)** Quantification of MYC mRNA levels from experiment depicted in **a** by qPCR analysis using specific primers for MYC and RPLP0. The mRNA levels were normalized to RPLP0 and the control shRNA infected sample was set as 1 (n = 3 independent experiments, mean ± S.D.). ns, not significant; by unpaired t-test. **(c)** Immunoblot analysis of whole cell extracts from experiment depicted in **a** using the indicated antibodies. α-tubulin served as a loading control.

Together, these results indicate that OTUD6B promotes MM cell proliferation by positively regulating the expression of MYC and other oncogenic proteins via stabilization of LIN28B.

5.5.2 OTUD6B and MYC levels positively correlate in MM patients

The previously performed experiments suggest a pivotal role for OTUD6B in MM cell proliferation and MYC expression. In order to further confirm the clinical relevance of OTUD6B-dependent regulation of MYC, expression levels of both proteins were analysed in primary patient samples. Respective experiments were conducted by PD Dr. med. J. Krönke and Denise Miller at

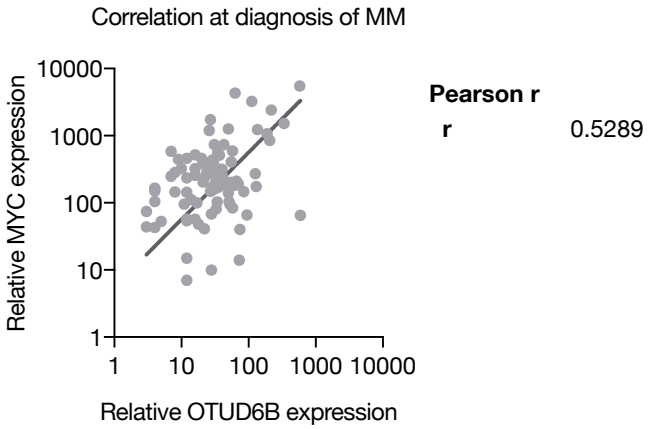

Figure 47: MYC and OTUD6B mRNA levels correlate in primary MM patient cells. Quantification of mRNA levels of MYC and OTUD6B from primary CD138+ cells derived from patients at diagnosis of MM by qPCR analysis. mRNA levels were normalized to GAPDH (n = 89 patient samples). ****, $P < 0.0001$; by Pearson's correlation and linear regression. The value of the Person's correlation coefficient (Pearson r) is indicated. [Data provided by PD Dr. med. J. Krönke].

University Hospital of Ulm. To this end, primary CD138$^+$ MM cells were isolated from bone marrow aspirations of 89 patients at first diagnosis using CD138 microbeads. Strikingly, qPCR analysis of patient-derived mRNA revealed a significant positive correlation between OTUD6B and MYC expression levels (Figure 47). These data provide further evidence that OTUD6B regulates MYC expression in MM patients, thereby supporting the previous results and strengthening the oncogenic relevance of OTUD6B in MM.

6 Discussion I

Despite recent therapeutic advances, MM represents an incurable malignancy necessitating the identification of new druggable vulnerabilities. Due to good responses to proteasomal inhibition reflecting the relevance of the UPS for the pathophysiology of MM, components of the UPS might serve as suitable drug targets. Starting form a CRISPR/Cas9-based screening approach in a human MM cell line, this study identified F-box proteins and DUBs, which influence the survival or proliferative capacity of MM cells and which might hence serve as therapeutic targets, providing new treatment options in the future. The efficiency of the screens was reflected by the strong depletion of cells expressing sgRNAs against known essential genes as well as well described oncogenes, highlighting the power of the screen to identify at the time unknown oncogenic proteins involved in MM. By meeting all selection criteria for being a potential new oncogene in MM, OTUD6B was identified and confirmed as a candidate for targeted therapy. First, OTUD6B promoted cell proliferation of MM cells by regulating cell cycle entry into S phase and depletion of OTUD6B consequently activated cell cycle arrest at late G1 phase, reflecting the clinical potential of chemical inhibition of OTUD6B. Second, by combining and cross validating two mass spectrometry-based screens, LIN28B, which has been previously described to play an oncogenic role in MM itself (Manier et al. 2017), was identified as a substrate of OTUD6B. By preventing proteolytic degradation of LIN28B, OTUD6B positively influenced the expression of downstream targets of LIN28B such as MYC, explaining the strong impact of OTUD6B on cell proliferation. Last, the clinical relevance of OTUD6B-mediated stabilization of LIN28B was reflected by a significant positive correlation of OTUD6B and MYC mRNA levels in patient-derived MM samples.

Overall, this study systematically uncovered the oncogenic potential of an uncharacterized DUB by combining multi-OMIC screening approaches. Starting from a CRISPR/Cas9 screen, a potential oncogene was identified on the genetic level, of which the relevant substrate could be found by different proteomic-based screens. Moreover, the underlying cellular mechanisms could be clarified on the cellular level and first data provided evidence for its relevance in MM patients.

The following chapters will discuss the above described aspects in detail, thereby responding to the identified hits of the CRISPR/Cas9 screens (6.1), to the role of OTUD6B in cell proliferation (6.2), to OTUD6B-mediated stabilization of LIN28B (6.3) and to the clinical relevance of OTUD6B (6.4).

6.1 CRISPR/Cas9 screening approaches identify oncogenes in MM

6.1.1 Identification of established cancer-related genes

Despite intense research on DUBs and F-box proteins over the last decades, many components of these protein families remained unexplored. However, due to the pivotal role of the UPS in many cancer-related cell pathways, such as cell proliferation, apoptosis and DNA

repair, components of the UPS have been suggested as attractive anti-cancer targets (Shen et al. 2013), underlining the importance for the identification and characterization of unstudied DUBs and F-box proteins. The urgent need for new treatment options for MM and the high response rates to proteasomal inhibition of MM patients provide a rationale for the identification of UPS components, which contribute to the pathophysiology of MM.

By performing CRISPR/Cas9 negative selection screens in a human MM cell line, the current study provided new insights into the potential involvement of DUBs and F-box proteins in this malignancy. The efficiency of the screen was reflected by the identification of genes, which are clearly linked to cancer and MM. For instance, SKP2 has been described to be an oncogene due to its role in p27 and p21 degradation (Bornstein et al. 2003; Carrano et al. 1999; Frescas and Pagano 2008). Moreover, chemical inhibition of SKP2 has been shown to overcome bortezomib resistance in MM cells (Malek et al. 2017). In line with these publications, cells expressing sgRNAs against SKP2 died out during the screen and this effect was enhanced under bortezomib treatment (Figure 16), thereby confirming the potential role of SKP2 in bortezomib resistance. Of note, only one sgRNA in the untreated condition and two sgRNAs under bortezomib treatment were depleted to more than 30%, which represented the selected threshold, and thus SKP2 did not fulfil the hit criteria demanding the depletion of at least two sgRNAs. This hence suggests that a higher number of sgRNAs per gene might be necessary for future screens to exclude false-negative results.

Another hit of the screen, which has been previously linked to MM, is represented by USP5. By deubiquitylating the transcription factor c-MAF, which is frequently overexpressed in MM cells, USP5 stabilizes c-MAF and prevents apoptosis of MM cells (Hurt et al. 2004; Wang, Juan, et al. 2017). Two sgRNAs targeting USP5 were depleted in the screen (Figure 18), in line with the previously published data (Wang, Juan, et al. 2017).

Besides the identification of new oncogenes involved in the development of MM, the present study aimed to find genes, which mediate bortezomib resistance. The potential of the screen to fulfil this aim was supported by the depletion of cells expressing sgRNAs against USP14, which could be only observed under bortezomib treatment (Figure 18). USP14 is a proteasome-associated DUB and its inhibition overcomes bortezomib resistance of MM cells (Borodovsky et al. 2001; Tian, D'Arcy, et al. 2014).

With regard to the degree of depletion, cells expressing sgRNAs against known oncogenic DUBs or F-box proteins were not as much affected as cells expressing positive control sgRNAs targeting essential genes like ribosomal proteins (Figure 16, Figure 18). Hence, there might be a therapeutic window for the development of DUB or F-box protein-based targeted cancer therapy in the future without affecting other cells of the body.

6.1.2 Identification of OTUD6B as a new oncogene in MM

As negative selection screens, the here performed CRISPR/Cas9 screens could confirm the involvement of many well described DUBs and F-box proteins in cell proliferation or survival.

Importantly, the screens also identified genes, which have been hardly described before, neither in respect of their oncogenic potential nor of their responsible substrates. In this regard, the ovarian tumour (OTU) family DUB OTUD6B met all the criteria for the selection of genes, which were further investigated (5.1.3). Two sgRNAs targeting OTUD6B were depleted by more than 30% in both conditions, thereby being under the defined threshold (Figure 18). The third sgRNA was also reduced upon bortezomib treatment, but not in the range of the chosen criteria. Strikingly, the same results could be achieved, when cells were individually infected with sgRNAs against OTUD6B (Figure 19), supporting the decision for defined sgRNA libraries and the efficiency of the chosen screening settings. Notably, CRISPR/Cas9-mediated knockout of OTUD6B, which could be confirmed on the protein level, had a stronger effect under bortezomib treatment with regard to the capacity of the cells to proliferate (Figure 18, Figure 19). So far, it is unclear whether OTUD6B knockout cells are specifically more sensitive to proteasomal inhibition or generally more susceptible to cellular stress and thus further analyses are required to investigate a potential role of OTUD6B in bortezomib resistance. However, previous studies suggested an involvement of OTUD6B in proteasome function, since peripheral blood mononuclear cells from patients expressing loss-of-functions variants of OTUD6B revealed a reduction in proteasome assembly and an increase in ubiquitylated proteins (Santiago-Sim et al. 2017). A role of OTUD6B in proteasome function could hence explain a potential involvement of OTDU6B in bortezomib resistance, as previously seen for USP14 (6.1.1) (Borodovsky et al. 2001; Tian, D'Arcy, et al. 2014).

6.1.3 Identification of other potentially oncogenic candidates

USP12 represents another DUB, for which all sgRNAs were depleted during the screen (Figure 18). Although certain functions of USP12 have been suggested in the literature (Aron et al. 2018; Jahan et al. 2016; Tang et al. 2016), the potential role of USP12 in MM or other malignancies remains largely unclear. However, there is evidence that USP12 is important for cell cycle progression, since depletion of USP12 induces cell cycle arrest in HeLa cells (Tang et al. 2016), in accordance with the result of the present study. A potential oncogenic role of USP12 in MM has to be elucidated in future studies in order to address the question whether USP12 might serve as potential drug target in this disease.

The F-box protein screen identified FBXW10 as potential oncogene, as two sgRNAs targeting FBXW10 were strongly depleted (Figure 16). By infecting cells with the individual sgRNAs the result of the screen could be confirmed (Figure 17). However, FBXW10 mRNA could hardly be detected in MM1.S cells and other MM cell lines, arguing against an oncogenic role. Moreover, database analysis confirmed that FBXW10 expression is extremely low in most of the cancer cell lines tested (Human Protein Atlas) and the gene locus of FBXW10 was found to be hypermethylated in cell renal cell carcinoma (Wang, Li, et al. 2015), supporting rather a tumour suppressor function of FBXW10. CRISPR/Cas9-based screens have been shown to have lower false-negative rates compared to RNAi-based screening approaches, but can produce false-positive effects when targeting amplified genomic regions (Munoz et al. 2016). In this regard, the

higher number of double strand breaks as a consequence of a higher copy number targeted by the Cas9 enzyme induces a cell cycle arrest and thus decreases the proliferation rate (Aguirre et al. 2016; Munoz et al. 2016). It is unclear, whether the genomic region of FBXW10 is amplified in the MM1.S cell line used for the screen. However, the genomic locus of FBXW10 has been duplicated during evolution resulting in a second gene, namely CDRT1, which is almost identical to FBXW10 and thus was also targeted by the sgRNAs against FBXW10 used in the present screen, thereby potentially inducing a gene-independent cell cycle arrest. In order to avoid such gene-independent effects, hit validations could be additionally performed in a haploid cell line in future studies, thereby excluding potentially false-positive results, although such a cell line would lack the specific disease background.

6.2 OTUD6B represents an important regulator of cell proliferation

6.2.1 OTUD6B is essential for MM cell proliferation

The CRISPR/Cas9 screen performed in the present study represented a drop-out screen with the aim to identify components of the UPS, which are involved in MM survival or cell proliferation. Since the read-out of the screen was depletion of sgRNAs, one could not distinguish whether the decrease of a certain sgRNA was a result of impaired cell proliferation or an increase in the cell death rate. Neither CRISPR-mediated knockout nor shRNA-mediated knockdown of OTUD6B led to a visible increase in the number of dead cells judged by trypan blue exclusion tests. Moreover, depletion of OTUD6B did not enhance the sub-G1 population of various MM cell lines (Figure 23), further suggesting that loss of OTUD6B inhibited cell proliferation and did not influence the survival of MM cells.

A false-positive screening result as a consequence of CRISPR-mediated targeting of an amplified genomic region, like discussed in the previous section (6.1.3), could be excluded, since shRNA-mediated knockdown showed the same anti-proliferative effect than CRISPR-mediated knockout. Moreover, the reduced ability of OTUD6B knockout cells to proliferate correlated with the knockout efficiency (Figure 20), further supporting that OTUD6B represented a true hit. Importantly, the antiproliferative effect of OTUD6B depletion was not restricted to the screening cell line but could be observed for many other MM cell lines (Figure 20, Figure 21). Hence, the successful inhibition of MM growth might not depend on specific genetic alterations in this case, making the potential treatment of MM patients with an OTUD6B-specific inhibitor attractive for future therapies.

In order to deplete OTUD6B, most experiments conducted in this study were using shRNAs and the observed antiproliferative effect was much stronger than effects caused by CRISPR-mediated knockout of OTUD6B (Figure 20, Figure 21). A possible explanation for this observation might be the faster and more synchronous depletion achieved by infections with shRNAs. Moreover, a complete knockout might cause compensatory effects by the upregulation of closely

related or redundant genes, which might also provide an explanation why not all cells infected with sgRNAs against OTUD6B were depleted (Figure 19, Figure 20).

OTUD6B has been previously described to regulate proliferation of non–small cell lung cancer (NSCLC) cells by modifying components of the 48S preinitiation complex (Sobol et al. 2017). In this context, OTUD6B isoform 1 inhibited cell proliferation whereas isoform 2 promoted it (Sobol et al. 2017). As the three sgRNAs used in the screen targeted all described splice variants of OTUD6B, no discrimination could be made with regard to the contribution of the different isoforms to the observed effect on cell proliferation. However, since the shorter isoform 2 could not be detected by immunoblot analyses in the screening cell line MM1.S, the observed effect is likely caused by the first isoform of OTUD6B. The discrepancy between the two studies might be a result of the different cellular systems used in the previous and in the present work. Moreover, the OTUD6B splice variant used in the previous publication was 30 AA longer than isoform 1 described on UniProt (Q8N6M0-1) (Sobol et al. 2017), providing another explanation for the different biological effects, as it is unclear whether longer splice variants of OTUD6B exist and if so whether they fulfil different functions. In line with this suggestion, two MM cell lines (RPMI8226 and KMSBM12) expressed two variants of the longer OTUD6B isoform, of which one was few kilodaltons smaller than the other, latter being the only variant expressed in all the other MM cell lines (Figure 20, Figure 21). So far, it is unclear how these two variants differ in their sequence and whether they have different cellular functions. However, the OTUD6B isoform 1 (UniProt entry Q8N6M0-1), which was used in the present study, corresponded to the longer variant expressed in all the MM cell lines tested (data not shown), suggesting that another slightly smaller variant of OTUD6B exists, which has not been described yet. Furthermore, it cannot be excluded that the two variants detected by immunoblot analysis are results of a post-translational modification other than phosphorylation, which could be excluded by performing dephosphorylation experiments (data not shown).

6.2.2 OTUD6B regulates cell cycle progression

A decrease in the cell proliferation rate can be caused either by interference with mitogenic pathways or by induction of cell cycle arrests at different stages of the cell cycle (2.4.1). Loss of OTUD6B had a clear influence on the cell cycle distribution of different MM cell lines (Figure 23), suggesting that OTUD6B regulates cell cycle progression. Although OTUD6B depletion increased both, the G1 and the G2/M cell population (Figure 23), the strong accumulation of Cyclin E and p27 supports a cell cycle arrest at late G1 phase (Figure 24, Figure 43, Figure 46). The observed cell cycle arrests could be a consequence of the decrease in MYC expression, which was evoked by knockdown of OTUD6B (Figure 44, Figure 45). MYC has been shown to be necessary for G2/M progression by regulating CDK1 (Song et al. 2013; Yang et al. 2018), in line with the observed increase of OTUD6B-depleted cells in G2/M phase (Figure 23). Moreover, the strong accumulation of p27 leading to the observed G1 arrest might also be caused by the reduction of MYC, since MYC has been reported to repress the transcription of p27 and to induce the expression of CKS1,

a component of the SCF^{SKP2} complex, which targets p27 for proteasomal degradation at late G1 phase (Carrano et al. 1999; Keller et al. 2007; Sutterluty et al. 1999; Yang et al. 2001). Although SKP2 protein levels were slightly decreased upon loss of OTUD6B, it is unlikely that this alone caused the strong increase of p27, as the changes were rather small (Figure 24). C-terminal phosphorylation of p27 at threonine 198 (T198) influences the stability of p27 (Kossatz et al. 2006; Liang et al. 2007), hence it would be interesting to see whether OTUD6B regulates one of the kinases AKT, RSK or LKB1-AMPK, which have been shown to phosphorylate p27 at T198 (Fujita et al. 2002; Fujita, Sato, and Tsuruo 2003; Liang et al. 2007). Of note, the increase of Cyclin E was likely a result of the arrest at late G1, at which Cyclin E expression is high, and not due to a direct regulation by OTUD6B. However, the precise mechanism leading to accumulation of p27 and Cyclin E needs to be investigated in future studies. Together with a defect in entering S phase after an induced G1/S arrest as a result of OTUD6B depletion (Figure 24), these data suggest an involvement of OTUD6B in the G1-S transition.

Further evidence for an OTUD6B-mediated regulation of S phase entry was provided by the observation, that the catalytic activity of OTUD6B was regulated in a cell cycle-dependent manner. OTUD6B activity clearly peaked at G1/S transition and declined during progression towards mitosis in two different cell lines (Figure 26), further supporting that OTUD6B positively regulates cell cycle progression from G1 to S phase. In contrast to the activity, OTUD6B protein level did not change throughout the cell cycle, indicating that OTUD6B might be regulated on post-translational level like many other proteins involved in cell cycle control (Novak et al. 2010).

6.3 OTUD6B mediates stabilization of LIN28B

6.3.1 OTUD6B prevents proteolytic degradation of LIN28B

By combining and cross-validating affinity and non-affinity mass spectrometry-based screening approaches, eight interactors and hence potential substrates of OTUD6B could be identified (Figure 27, Figure 28). Besides the known interactors MTDH and ASCC3 (Sowa et al. 2009), many of the identified proteins represented RNA-binding proteins, like LLPH, PURA, LIN28B, DHX57 and CASC3 (Castello et al. 2012; Moss and Tang 2003), suggesting a role of OTUD6B in RNA regulation. Among these proteins, LIN28B appeared as a likely candidate for being a substrate of OTUD6B due to its well described oncogenic role and its previously reported involvement in MM (Balzeau et al. 2017; Manier et al. 2017; Viswanathan et al. 2009).

The strong and very specific binding of LIN28B to OTUD6B, but not to other DUBs of the OTU family, confirmed the mass spectrometry results and suggested a functional role of this interaction (Figure 29). In accordance with the data of the BioID purification, LIN28B interacted only with OTUD6B isoform 1 but not with isoform 2 and hence the binding site resides in the N-terminal part of OTUD6B (Figure 28, Figure 30). Notably, OTUD6B interacted with the cold shock domain of LIN28B (Figure 31), which is very conserved between LIN28B and LIN28A (Figure 7). Moreover, OTUD6B also revealed binding to LIN28A in HEK293T cells (Figure 29), suggesting that OTUD6B

regulates both family members. However, since LIN28A was not expressed in the MM cell lines used in this study, the observed biological effects caused by OTUD6B deregulation did not depend on LIN28A. Nevertheless, since LIN28B and LIN28A are closely related and redundant in many functions, it is conceivable that OTUD6B regulates both proteins.

So far, it has been controversial in literature, whether OTUD6B represents an active DUB (Mevissen et al. 2013; Sobol et al. 2017; Xu et al. 2011). In accordance with the current study, OTUD6B has been shown to cleave ubiquitin suicide probes and thus to possess an active catalytic cysteine (Figure 25, Figure 26) (Mevissen et al. 2013; Xu et al. 2011). However, OTUD6B did not reveal any activity against ubiquitin chains in linkage specificity assays and hence it was thought to be an inactive DUB (Mevissen et al. 2013). Nonetheless, the present study clearly provided evidence that OTUD6B deubiquitylates LIN28B *in vivo*, thereby preventing proteolytic degradation of LIN28B. First, the amount of polyubiquitylated LIN28B strongly correlated with OTUD6B protein levels present in the cell (Figure 35, Figure 36). Importantly, the strong reduction in polyubiquitylation of LIN28B observed upon ectopic expression of OTUD6B WT could not be seen by overexpression of an inactive version of OTUD6B, in which the catalytic cysteine was mutated to an alanine (Figure 36), supporting that OTUD6B directly deubiquitylated LIN28B. The remaining question of the linkage specificity of OTUD6B was further addressed by two different means, namely by using a ubiquitin construct, which only could form K48 linkages, and by probing with a K48-specific antibody (Figure 36). Both approaches clearly showed that OTUD6B removed K48-linked polyubiquitin chains from LIN28B, thus suggesting that OTUD6B prevents its proteolytic degradation. In accordance with these findings, OTUD6B stabilized LIN28B by protecting it from degradation by the proteasome specifically in G1/S synchronized cells (Figure 38, Figure 39), the cell cycle stage, at which OTUD6B activity and LIN28B protein levels were found to be the highest (Figure 26, Figure 37). This clear correlation between OTUD6B activity and LIN28B stability further indicated that OTUD6B represents an active DUB *in vivo*.

The lack of OTUD6B activity against di-ubiquitin chains in the previous study might be explained by different reasons. On the one hand, the previous publication used recombinant OTUD6B protein purified from bacteria (Mevissen et al. 2013), which hence lacked potential post-translational modifications, potentially required for OTUD6B activity. In this regard, another DUB of the OTU family called DUBA (OTUD5) has been shown to require phosphorylation on a conserved serine residue immediately preceding the OTU domain in order to be active and to bind substrates (Huang, Ma, et al. 2012). Hence, it is conceivable that OTUD6B similarly requires a post-translational modification to be fully active in line with the present finding that OTUD6B activity changed during the cell cycle (Figure 26). In this context, OTUD6B could be in a closed conformation, which allows the binding of a small ubiquitin suicide probe but not cleavage of ubiquitin chains in accordance with the previous study (Mevissen et al. 2013). Consequently, a post-translational modification such as phosphorylation could lead to structural rearrangements and subsequently to an open conformation, which uncovers the substrate binding site and allows cleavage of polyubiquitin chains. It will be interesting to see in future experiments whether OTUD6B purified from insect or HEK293T cells is active in linkage specific cleavage assays. In

accordance with the suggested model, LIN28B binding to OTUD6B strongly depended on phosphorylation and mutation of an evolutionary conserved serine residue (S99) of OTUD6B in the binding region of LIN28B completely abolished the interaction (Figure 32), indicating that phosphorylation of OTUD6B is indeed essential for substrate binding. Notably, phosphorylation-dependent substrate binding of a DUB would reflect a new mode of action, which allows fast responses to cellular changes and cell cycle-dependent control of activity. However, whether OTUD6B is indeed phosphorylated on S99 and whether this is a prerequisite for LIN28B binding needs to be further addressed in future studies. Notably, the serine/threonine kinase RIOK3 identified in both mass spectrometric screens, which were performed in this study (Figure 27, Figure 28), represents a potential kinase of OTUD6B as it interacted very specifically with OTUD6B (Figure 33). Moreover, LIN28B binding to OTUD6B depended on RIOK3 (Figure 34), thus suggesting that RIOK3 promotes substrate binding by phosphorylating OTUD6B. Since the mutation of OTUD6B S99 abolished the binding to LIN28B and RIOK3 (Figure 34), this residue represents a potential phosphor-acceptor site. Nevertheless, since only one substrate of RIOK3 has been described so far (Takashima et al. 2015), a potential consensus sequence of RIOK3 is unknown. Consequently, kinase assays will be part of future studies, which will hopefully clarify whether RIOK3 phosphorylates OTUD6B.

Dysfunctional variants of the *OTUD6B* gene have been associated with an intellectual disability syndrome characterized by global developmental delay, microcephaly and structural brain abnormalities (Santiago-Sim et al. 2017; Straniero et al. 2018). Moreover, *Otud6b* knockout mice are subviable and also feature smaller sizes and congenital heart defects, in line with the defects observed in patients (Koscielny et al. 2014; Santiago-Sim et al. 2017). Strikingly, LIN28 is essential for mammalian development and *Lin28a* knockout mice lacking one *Lin28b* allele display smaller brains and reduced proliferation rates of neural progenitor cells (Yang, Yang, et al. 2015). Hence, it is conceivable that the strong developmental defects observed in individuals with predicted loss-of-function *OTUD6B* alleles is caused by a destabilization of LIN28.

6.3.2 Stabilization of LIN28B promotes MM cell proliferation

LIN28A and LIN28B were found to be re-expressed in ~15% of human cancer cells and are linked to poor prognosis (Viswanathan et al. 2009). Besides its transcriptional reactivation, LIN28B was reported to be stabilized in cancer by suppression and mutations of its negative regulators. For instance, LIN28B mRNA has been shown to be degraded in MM cells by the ribonuclease DIS3, which is frequently mutated and thereby inactivated in MM patients (Chapman et al. 2011; Segalla et al. 2015). Furthermore, LIN28B is targeted for proteasomal degradation by TRIM71 and hence TRIM71 can be found downregulated in various malignancies (Yin et al. 2016).

Strikingly, this study uncovered another mechanism of how cancer cells stabilize LIN28B protein and therefore acquire a growth advantage. By deubiquitylating LIN28B and preventing its proteasomal degradation, OTUD6B promoted MM cell proliferation (Figure 41, Figure 46). In this regard, OTUD6B might downregulate *let-7* miRNAs by stabilizing LIN28B protein levels, thereby

causing an increase in MYC expression, in line with previous studies, which showed that LIN28B positively regulates MYC in MM cells (Manier et al. 2017; Segalla et al. 2015). As a transcription factor, MYC regulates a huge number of genes and consequently controls many signalling pathways in the cell (Eilers and Eisenman 2008; Fernandez et al. 2003). Alteration of the genetic locus of *MYC* can be frequently observed in MM patients and is associated with more aggressive forms of MM (Chiecchio, Dagrada, White, et al. 2009; Glitza et al. 2015; Jovanovic et al. 2018; Kuehl and Bergsagel 2012), underlining the oncogenic contribution of MYC to this malignancy. The clear impact of OTUD6B on MYC expression might hence represent one mean how OTUD6B promotes MM cell proliferation. Importantly, OTUD6B also had an impact on the positive feedback loop described between LIN28B and MYC (Figure 8) (Chang et al. 2009; Manier et al. 2017) and consequently, OTUD6B depletion led first to the downregulation of MYC as a consequence of LIN28B degradation and caused subsequently a long-term decrease in LIN28B expression resulting from the lack of its transcriptional activation by MYC. Thus, loss of OTUD6B induced a robust depletion of LIN28B on protein and transcriptional level (Figure 45). Strikingly, further evidence that OTUD6B regulates MYC in the patient was given by the significant correlation of OTUD6B and MYC expression in primary patient-derived MM samples (Figure 47).

In line with OTUD6B-mediated stabilization of LIN28B at G1/S transition (Figure 38), both proteins were essential for entry into S phase in MM cells (Figure 43). Notably, LIN28B depletion also caused an accumulation of Cyclin E and p27 as seen before for OTUD6B loss (Figure 24, Figure 43; discussed in 6.2.2), hinting that the observed cell cycle arrest at late G1 indeed resulted from an OTUD6B-dependent regulation of LIN28B. As discussed in the previous section (6.2.2), p27 has been reported to be negatively regulated by AKT-mediated phosphorylation (Fujita et al. 2002). Importantly, LIN28B positively regulates AKT signalling pathway by different means (Wang, Wang, et al. 2015), providing a possible explanation for how LIN28B and OTUD6B depletion induced p27 accumulation and consequently a cell cycle arrest. Strikingly, loss of LIN28B has been previously reported to induce a reduction in S phase population and cell cycle arrest at G1 phase (Qin et al. 2014; Wang, Li, et al. 2017), thereby phenocopying the data of OTUD6B depletion of this study (Figure 23). Overall, these findings support that OTUD6B positively regulates LIN28B levels in MM cells, thereby promoting cell proliferation. Since LIN28B drives MM cell proliferation mainly by inhibiting *let*-7 miRNA maturation (Manier et al. 2017), it would be interesting to see whether OTUD6B has an influence on *let-7* levels in future experiments. Moreover, as an RNA-binding protein, LIN28B impacts the expression of many proteins involved in oncogenic pathways (Balzeau et al. 2017; Hafner et al. 2013; Johnson et al. 2005; Mayr, Hemann, and Bartel 2007; Sampson et al. 2007). Thus, RNA-seq analyses of OTUD6B and LIN28B depleted cells will be subject of future studies, which hopefully will clarify which common genes are regulated by the OTUD6B/LIN28B axis.

Taken together, by stabilizing LIN28B, OTUD6B positively regulates MYC expression likely via inhibition of *let-7* miRNAs, thereby initiating entry into the cell cycle (Figure 48). The binding of OTUD6B to LIN28B might be positively regulated by RIOK3-mediated phosphorylation. At late G1, MYC indirectly decreases p27 levels by inducing the expression of CKS1, a component of the

SCF^{SKP2} complex, which targets p27 for proteasomal degradation (Figure 48). In addition, LIN28B might also indirectly reduce p27 level by positively regulating AKT signalling, thereby activating Cyclin E-CDK2 and thus promoting entry into S phase (Figure 48).

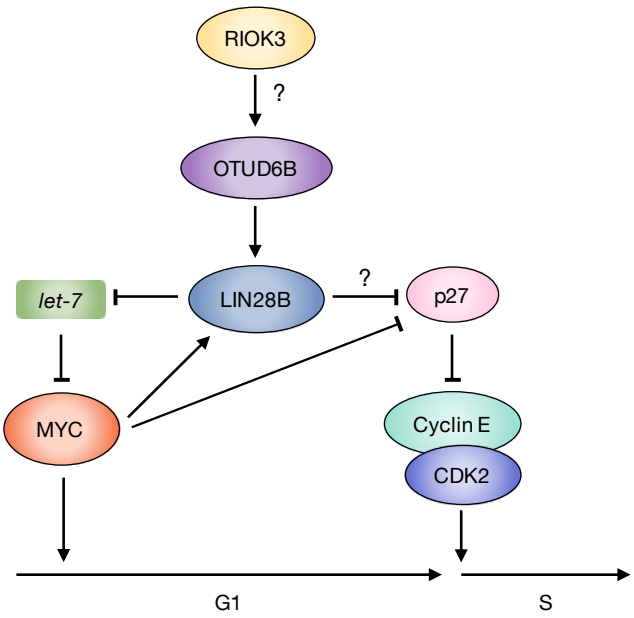

Figure 48: Model of OTUD6B-mediated entry into S phase. In a RIOK3-dependent manner, OTUD6B binds and stabilizes LIN28B at G1-S phase, thereby promoting MYC expression likely via inhibition of *let-7* miRNAs. MYC in turn induces gene expression of cell cycle proteins involved in progression to S phase and indirectly promotes p27 degradation. LIN28B might further destabilize p27 by positively regulating AKT signalling, thus activating Cyclin E-CDK2 complex, which mediates entry into S phase.

Although forced expression of LIN28B partially rescued the proliferation defect caused by OTUD6B depletion, cell growth could not be completely restored (Figure 41). Moreover, OTUD6B knockout also impaired cell proliferation of cells, which did neither express LIN28B nor LIN28A, indicating that OTUD6B promoted cell proliferation not solely by stabilization of LIN28B (Figure 41). It is conceivable that OTUD6B has several substrates as described for many other DUBs and also suggested by the additional interactors of OTUD6B, which could be identified by two mass spectrometry-based approaches performed in this study (Figure 27, Figure 28). Additional functional screening approaches, like quantitative ubiquitin proteomics in OTUD6B depleted versus control cells, could help to further narrow down the number of potential substrates in the future.

6.4 The role of OTUD6B in cancer

6.4.1 OTUD6B as a new oncogene

This study aimed to identify new potential oncogenes involved in the development and pathophysiology of MM. Starting from a CRISPR/Cas9 screen, OTUD6B was found to promote MM cell proliferation and hence represented a good candidate (Figure 18-Figure 21). By stabilizing

LIN28B and promoting MYC expression (Figure 44-Figure 46), OTUD6B positively regulated two well established oncogenes, which have been clearly linked to myelomagenesis (Chiecchio, Dagrada, Protheroe, et al. 2009; Chiecchio, Dagrada, White, et al. 2009; Glitza et al. 2015; Manier et al. 2017; Segalla et al. 2015), further providing evidence for an oncogenic role of OTUD6B in MM. Importantly, OTUD6B expression positively correlated with MYC mRNA levels in 89 patient-derived MM samples (Figure 47), bringing additional evidence that OTUD6B-mediated upregulation of MYC takes place in MM patients. In this regard, gene set enrichment analyses (GSEA) will further clarify in future studies whether OTUD6B is deregulated and whether OTUD6B expression correlates with *let-7* and MYC targets in gene expression profiling data sets containing healthy plasma cells and newly diagnosed MM patient samples, similarly to the correlations performed before for LIN28B (Manier et al. 2017). In addition, murine xenograft models with human MM cell lines depleted for OTUD6B are subject of future studies, which will further elucidate whether targeting OTUD6B inhibits tumour growth *in vivo* and whether the simultaneous overexpression of LIN28B counteracts the anti-tumour activity of OTUD6B loss.

Additional evidence for OTUD6B as an oncogenic driver of MM comes from gene expression profiling of different MM stages, in which expression of OTUD6B significantly increased with disease stage from healthy subjects over MGUS to smouldering myeloma patients (Zhan et al. 2007). Notably, RIOK3 was similarly overexpressed in the same study, underlining a potential functional connection between OTUD6B and RIOK3 in MM. Taken together, the present study identified the DUB OTUD6B as new potential oncogene and hence provide a new candidate for targeted MM therapy in the future.

Besides these strong indications for the involvement of OTUD6B in MM, there is evidence that OTUD6B might also play an oncogenic role in other malignancies. For instance, knockout and knockdown experiments performed in the current study revealed that OTUD6B is also essential for cell proliferation of other B cell-derived malignancies like MCL or DLBCL (Figure 22, Figure 42). Moreover, OTUD6B also promoted cell growth of a lung cancer-derived cell line (Figure 22), further indicating that OTUD6B might represent an oncogene in various cancer types. Strikingly, OTUD6B mRNA levels could be found overexpressed in breast, colorectal, gastric, liver and ovarian cancer (D'Errico et al. 2009; Kaiser et al. 2007; Richardson et al. 2006; Wurmbach et al. 2007; Yoshihara et al. 2009). In addition, OTUD6B has been found to be amplified on either genetic or mRNA levels in 9% of cancer cell lines (Barretina et al. 2012) and many solid tumours (TCGA Pan-Cancer Atlas Studies). Finally, a general role of OTUD6B in tumorigenesis is in line with the re-activation of its substrate LIN28 in ~15% of human cancer cells (Viswanathan et al. 2009).

6.4.2 OTUD6B as a potential anti-cancer target

This study provided evidence that OTUD6B represents an active DUB and thus it is suitable for targeted cancer therapy using specific inhibitors, which target the catalytic centre of OTUD6B. Since it is unclear how essential OTUD6B is for cell proliferation and viability of healthy cells, it remains an open question whether there will be a therapeutic window of an OTUD6B inhibitor as

an anti-cancer drug. However, since most of the cells in the human body do not divide, the toxicity of OTUD6B inhibition might be limited to proliferating cells. Strikingly, the present study suggests that substrate binding of OTUD6B depends on phosphorylation and provides hints that RIOK3 might represent the responsible kinase. Consequently, chemically targeting the kinase, which regulates OTUD6B activity, would represent another option to interfere with OTUD6B signalling in cancer patients. Of note, it has been challenging so far to directly target MYC, mainly due to difficulties with the identification of potent ligands, which would inhibit MYC signalling (Jovanovic et al. 2018). Thus, the identification of druggable targets laying upstream of MYC represents an attractive strategy to overcome the difficulty of directly inhibiting MYC. The same applies for LIN28B, which represents an established oncogene, but might be likewise challenging to target due to the lack of an active site. Moreover, OTUD6B loss did not only significantly decreased MYC mRNA levels but also led to strong accumulation of p27 in MM cells (Figure 43-Figure 46). Importantly, increased proteasomal degradation of p27 can be frequently observed in cancer resulting in downregulation of p27 and poor outcome (Catzavelos et al. 1997; Loda et al. 1997; Otto and Sicinski 2017; Porter et al. 1997). Consequently, selective inhibition of OTUD6B might induce a cell cycle arrest by the induction of p27 in patients, thereby blocking cell proliferation of cancer cells, as observed for MM cell lines in this study.

The current treatment of MM patients includes the administration of proteasomal inhibitors like bortezomib. In search for components of the UPS, which might contribute to the anti-cancer activity of proteasome inhibitors, a CRISPR/Cas9 screen was performed in the presence and absence of bortezomib. Importantly, sgRNAs targeting OTUD6B were depleted in both conditions, however, the anti-proliferative effect of OTUD6B loss was enhanced upon treatment with bortezomib. Future studies have to clarify whether OTUD6B indeed confers resistance to bortezomib or whether OTUD6B in general mediates stress resistance. However, the findings of the screen suggest that a combination therapy of bortezomib with a selective OTUD6B inhibitor might increase the response rate in patients. Furthermore, combination therapy of palbociclib, a CDK4/6 inhibitor, with bortezomib and dexamethasone attained a moderate response rate in relapsed/refractory multiple myeloma according to a phase 1/2 study (Niesvizky et al. 2015). With regard to the induction of a cell cycle arrest at late G1 and the failure of releasing from a palbociclib-mediated block into S phase, both induced by OTUD6B depletion (Figure 23, Figure 24, Figure 43), OTUD6B inhibition might represent a conceivable option for combination therapy with palbociclib in order to improve the response. Hence, further studies need to analyse whether OTUD6B depletion sensitizes MM cell to the treatment with palbociclib.

Taken together, this study provides strong evidences for the role of OTUD6B as an oncogene in MM and other malignancies and for being a valid vulnerability and target for future drug development.

7 Results II

This study represents a joint project, which was conducted in the research group of Prof. Dr. Florian Bassermann at Klinikum rechts der Isar (Technical University of Munich) in collaboration with Ella Fung and Vincenzo d'Angiolella at the Department of Radiation Oncology and Biology at the University of Oxford. Complementary data were already presented in the doctoral thesis of Ella Fung (Fung 2017). For comprehensive reasons, contributions by these collaborators are included in this thesis and respective parts are indicated in the text and figure legends.

7.1 FBXL13 interacts with CEP192 and CEP152

7.1.1 FBXL13 binds to CEP192 and CEP152

FBXL13 is an orphan F-box protein, for which no function has been described so far. However, published data exist, which link FBXL13 to genomic stability (Paulsen et al. 2009), suggesting a role in cancer development. In addition, a gene segment of 7q22, which includes the gene of *FBXL13*, has been found to be commonly deleted in myeloid tumours (Curtiss et al. 2005), indicating a potential tumour suppressor role for FBXL13. In contrast, FBXL13 has also been reported to be amplified or mutated in various solid tumours (cBioPortal) and cancer lines (Barretina et al. 2012), which rather suggests an oncogenic implication of FBXL13 in cancer. Nevertheless, these data indicate that FBXL13 plays a role in various malignancies, however, its role as a tumour suppressor or an oncogene might be cell type- and substrate-dependent.

In order to identify interactors and thus potential substrates of FBXL13, E. Fung and Prof. B. Kessler at the Department of Radiation Oncology and Biology and at the Target Discovery Institute (University of Oxford), respectively, performed mass spectrometry-based analyses of FLAG-FBXL13 immunoprecipitates from HEK293T cells. Here, they identified the centrosomal proteins Centrin-2, Centrin-3 and CEP152 as interacting partners of FBXL13 (Fung 2017). Importantly, they also found two components of the SCF complex, SKP1 and CUL1, providing evidence that FBXL13 forms a functional SCF ubiquitin E3 ligase complex. Together, these data suggest a role for FBXL13 in centrosome homeostasis by ubiquitylation of one or more centrosomal proteins. To test this hypothesis, binding of FBXL13 to CEP152 was validated in HEK293T cells by transfecting the cells with FLAG-FBXL13 or empty vector (EV) control and Myc-tagged CEP152 and subjecting the whole cell lysates (WCE) to FLAG-immunoprecipitation (IP). Indeed, Myc-CEP152 specifically co-immunoprecipitated with FLAG-FBXL13, confirming the results of the mass spectrometric analyses (Figure 49a). Importantly, this interaction could also be observed between FLAG-FBXL13 and endogenous CEP152 in HEK293T cells (Figure 49b). Of note, CEP152 has been previously reported to interact with CEP192, which is important for the recruitment of PLK4 to the centrosomes (Sonnen et al. 2013). Therefore, a potential interaction of FBXL13 and CEP192 was tested by performing analogous experiments to the CEP152 binding analyses. Strikingly, FLAG-FBXL13 strongly interacted with both Myc-tagged and endogenous CEP192 in FLAG-IP

experiments (Figure 49c, d). Surprisingly, the binding of FBXL13 to CEP192 was much stronger than to Myc-tagged or endogenous CEP152, suggesting that FBXL13 binds to CEP152 only indirectly.

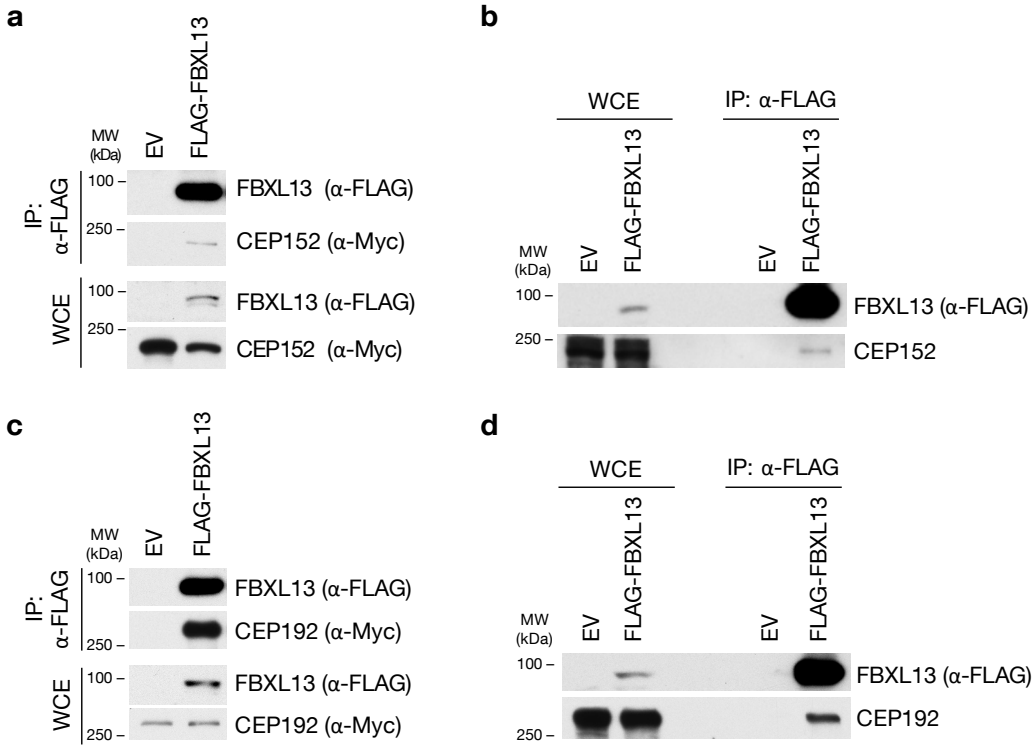

Figure 49: FBXL13 binds to CEP152 and CEP192. (a-d) Immunoprecipitation (IP) analysis of FLAG-FBXL13. HEK293T cells were transfected with FLAG-FBXL13 expression plasmid or empty vector (EV) alone **(b, d)** or together with constructs coding for Myc-CEP152 **(a)** or Myc-CEP192 **(c)** and lysates were subjected to FLAG-IP. Whole cell extracts (WCE) and IPs were analysed by immunoblotting using the indicated antibodies.

In order to analyse whether the binding of FBXL13 to CEP192 is of biological relevance, the interaction of endogenous proteins was analysed by performing endogenous immunoprecipitation of FBXL13. Notably, immunoblot analysis confirmed co-immunoprecipitation of endogenous CEP192 with FBXL13, but not with the IgG control antibody (Figure 50).

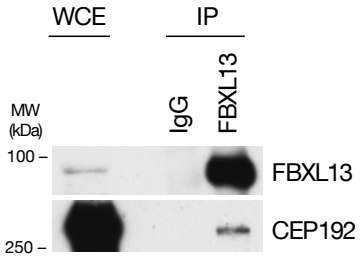

Figure 50: FBXL13 and CEP192 interact endogenously. Immunoprecipitation (IP) of endogenous FBXL13 from whole cell extract of HEK293T cells using a custom-made anti-FBXL13 peptide antibody or control rabbit IgG. WCE and immunoprecipitates were subjected to immunoblot analysis using the indicated antibodies.

7.1.2 FBXL13 binding to CEP192 is direct

CEP192 isoform 3 (UniProt: Q8TEP8-3), the longest isoform, is composed of 2537 amino acids (AA) and has been described to interact with centrioles and CEP152 via AA 603-2537, whereas AA 190-240 are responsible for PLK4 binding (Sonnen et al. 2013) (Figure 51a). Given a stronger binding of FBXL13 to CEP192 than to CEP152 (Figure 49), it is conceivable that the interaction between FBXL13 and CEP152 is mediated by CEP192 and thus indirect. To validate this assumption, HEK293T cells were transfected with siRNA targeting CEP152 (siCEP152) or non-targeting control (siGL) one day prior to transfection with FLAG-FBXL13 or empty vector (EV).

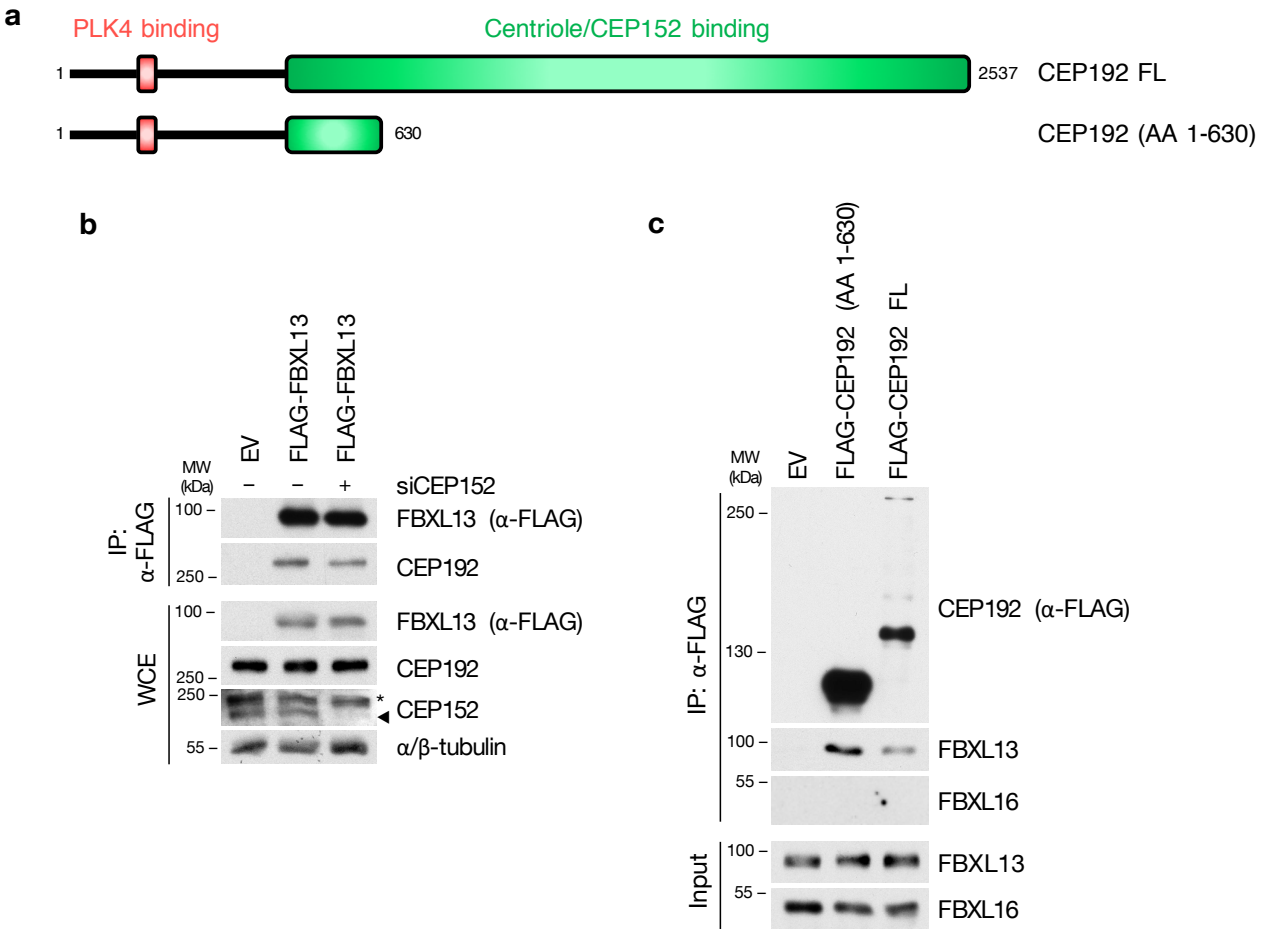

Figure 51: FBXL13 binding to CEP192 is direct. (a) Schematic overview of CEP192 isoform 3 (UniProt: Q8TEP8-3) full length (FL) and fragment (AA 1-630). AA, amino acid. **(b)** Immunoprecipitation (IP) analysis of FLAG-FBXL13. HEK293T cells were transfected with siRNA targeting CEP152 (siCEP152) or non-targeting siRNA (–) and one day later, cells were further transfected with constructs coding for FLAG-FBXL13 or empty vector (EV) control. Whole cell extracts (WCE) were subjected to FLAG immunoprecipitation (IP) and WCE and IP were analysed by immunoblotting using the indicated antibodies. α/β-tubulin served as a loading control. The asterisk marks an unspecific band and CEP152 is marked by an arrowhead. **(c)** *In vitro* binding assay of FBXL13 or FBXL16 and CEP192. *In vitro* synthesized FLAG-tagged CEP192 full length (FL) or AA 1-630 depicted in **a** using T7-coupled reticulocyte lysate were subjected to FLAG-IP and incubated with FBXL13 or FBXL16 proteins purified from insect cells. Input samples and immunoprecipitates were subjected to immunoblot analysis using the indicated antibodies.

The interaction of FLAG-FBXL13 with endogenous CEP192 was analysed in the CEP152 depleted or control cells by FLAG-IP. Importantly, CEP152 knockdown did not affect the binding of FBXL13 to CEP192 (Figure 51b), providing further evidence that FBXL13 binding to CEP192 is independent of CEP152.

To further investigate whether FBXL13 directly binds to CEP192, an *in vitro* binding assay was performed. To this end, FBXL13 and FBXL16, latter serving as a control, were expressed in and purified from insect cells and incubated with *in vitro* translated and transcribed FLAG-tagged CEP192 full length (FL) or fragment comprising AA 1-630. The fragment contained the PLK4 binding site and only very few amino acids of the part that is responsible for centriole and CEP152 binding (Figure 51a). Despite instability of full length CEP192, immunoblot analysis of FLAG-immunoprecipitated CEP192 FL revealed specific binding to FBXL13 but not to FBXL16 (Figure 51c). Moreover, FBXL13 but not FBXL16 interacted with immunoprecipitated FLAG-CEP192 AA 1-630, demonstrating that FBXL13 binds to the N-terminal part of CEP192. Notably, the N-terminal extension comprising AA 1-603 is only present in CEP192 isoform 3, suggesting that FBXL13 exclusively interacts with the longest isoform of CEP192. Taken together, these data provide evidence for a direct binding between FBXL13 and CEP192 and further support that the observed binding to CEP152 is mediated by CEP192, as the binding sites of FBXL13 and CE152 are located at different regions of CEP192.

7.1.3 CEP192 interacts with the leucine-rich repeat domain of FBXL13

FBXL13 consists of a N-terminal F-box domain, which is responsible for SKP1 binding (Fung 2017), and a C-terminal leucine-rich repeat (LRR) motif (Figure 52a). Latter is known to mediate protein-protein interactions and has been described to be the substrate binding site in other F-box proteins of the FBXL family (Cui et al. 2011; Raducu et al. 2016). In order to identify the binding regions of Centrin-2, Centrin-3 and CEP192 within FBXL13, mapping experiments were performed using FBXL13 fragments that contain either the F-box domain or the LRR motif or only the very N-terminal region (Figure 52a). Therefore, HEK293T cells were transfected with constructs coding for FLAG-tagged FBXL13 full length (FL) or fragments or an empty vector (EV) control and cell lysates were subjected to FLAG immunoprecipitation (IP). Immunoblot analysis showed that Centrin-2 and Centrin-3 specifically interacted with the very N-terminal part of FBXL13 comprising AA 1-151 whereas the binding site of CEP192 resided in the C-terminal region containing the LRR domain (Figure 52b). Given the different interaction sites of Centrin-2, Centrin-3 and CEP192, it is likely that CEP192 represents a ubiquitylation substrate whereas the binding to Centrin-2 and Centrin-3 might be important for the recruitment of FBXL13 to the centrosomes.

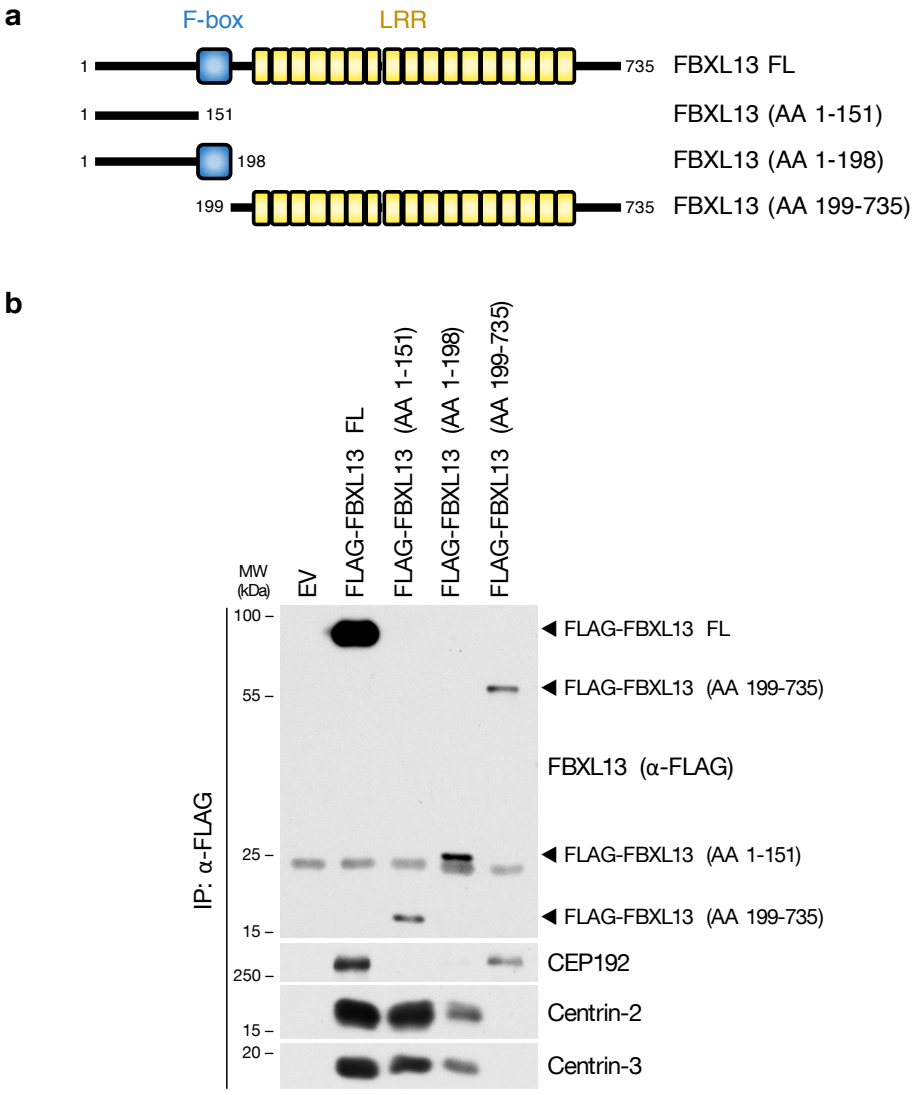

Figure 52: CEP192 binds to the leucine-rich repeat of FBXL13. (a) Schematic overview of FBXL13 full length (FL) and fragments. AA, amino acid; LRR, leucine-rich repeat. **(b)** Interaction analysis of FLAG-FBXL13 FL and fragments depicted in **a**. FLAG-FBXL13 coding constructs or empty vector (EV) control were expressed in HEK293T cells and lysates were subjected to FLAG-IP. Immunoprecipitates were analysed by immunoblotting using the indicated antibodies.

7.2 FBXL13 targets CEP192 for proteasomal degradation

7.2.1 FBXL13 destabilizes CEP192

Given a strong binding of CEP192 to the LRR domain of FBXL13, it is conceivable that CEP192 represents an ubiquitylation substrate of FBXL13 and thus CEP192 protein levels might be regulated by FBXL13. To test this hypothesis, U2OS cells were transfected with a construct coding for FBXL13, thereby inducing overexpression of FBXL13, or an empty vector control and CEP192 levels were analysed by immunoblotting. This revealed a strong reduction of CEP192 but not of Centrin-2 or Centrin-3 upon forced FBXL13 expression compared to the control (Figure 53a). Importantly, simultaneous addition of the proteasome inhibitor MG132 rescued the decrease

in CEP192 protein level, providing evidence that FBXL13 overexpression leads to the degradation of CEP192 by the proteasome. In contrast, when U2OS cells were transfected with vectors expressing shRNA targeting FBXL13 (shFBXL13) or scrambled control (shCtrl), the opposite could be observed. This time, CEP192 levels were stabilized upon FBXL13 silencing, leading to an accumulation of CEP192 in comparison to the control sample (Figure 53b). An efficient knockdown of FBXL13 was confirmed by qPCR analysis of FBXL13 mRNA level (Figure 53c).

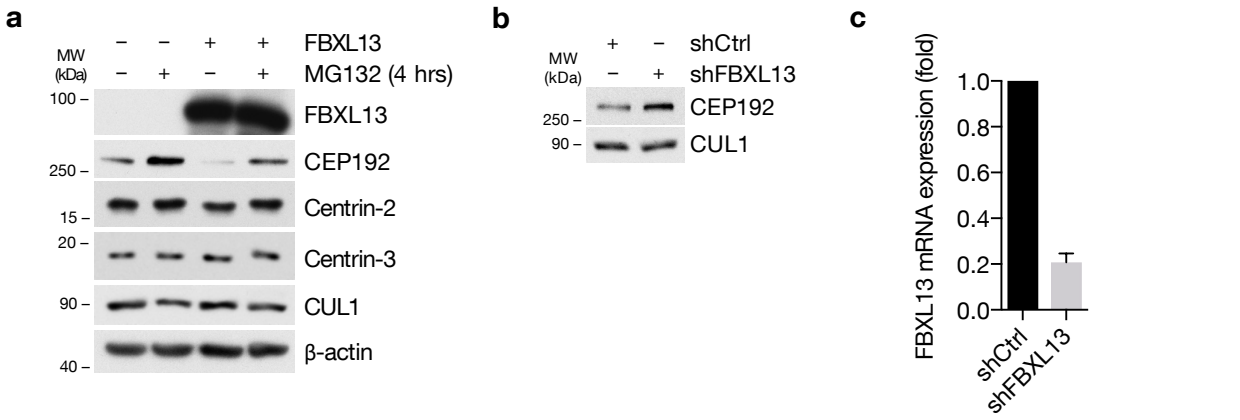

Figure 53: FBXL13 destabilizes CEP192. (a) Immunoblot analysis of U2OS cells transfected with FBXL13 expressing vector or empty vector (EV) control. One day after transfection, cells were treated with 10 µM MG132 or vehicle (DMSO) for 4 hrs prior to cell harvesting. Whole cell lysates were subjected to immunoblot analysis using the indicated antibodies. β-actin served as a loading control. **(b)** Immunoblot analysis of U2OS cells transfected with constructs coding for a shRNA targeting FBXL13 (shFBXL13) or non-targeting control (shCtrl). Cells were harvested 72 hrs post transfection and whole cell lysates were subjected to immunoblot analysis using the indicated antibodies. CUL1 served as a loading control. **(c)** Quantification of FBXL13 mRNA level from experiment depicted in **b** by qPCR analysis using specific primers for FBXL13 or RPLP0. The mRNA levels of FBXL13 were normalized to RPLP0 and the control shRNA transfected samples were set as 1 (n = 3 technical replicates, mean ± S.D.).

To further confirm that protein levels of CEP192 are regulated by FBXL13, a cycloheximide (CHX) experiment was performed, in which U2OS cells were transfected with either an FBXL13 expression plasmid or an empty vector control. Strikingly, overexpression of FBXL13 strongly reduced CEP192 protein level but did not affect half-lives of Centrin-2 and Centrin-3 (Figure 54). Moreover, quantification of CEP192 levels, which were normalized to β-actin signal, showed a reduction of about 75% upon 4 hrs CHX treatment and FBXL13 overexpression compared to 50% decrease in the control sample. Since starting levels of CEP192 (at 0 h CHX) were already reduced in FBXL13 overexpressing cells and FBXL13 itself decreased upon CHX treatment, CEP192 signal did not further decline at later time points of CHX incubation upon forced FBXL13 expression.

In line with the interaction studies, which showed binding of CEP192 to the LRR motif of FBXL13 (Figure 52), these experiments demonstrate that FBXL13 has an influence on CEP192 stability and thus support the assumption that CEP192 represents a bona fide substrate of FBXL13.

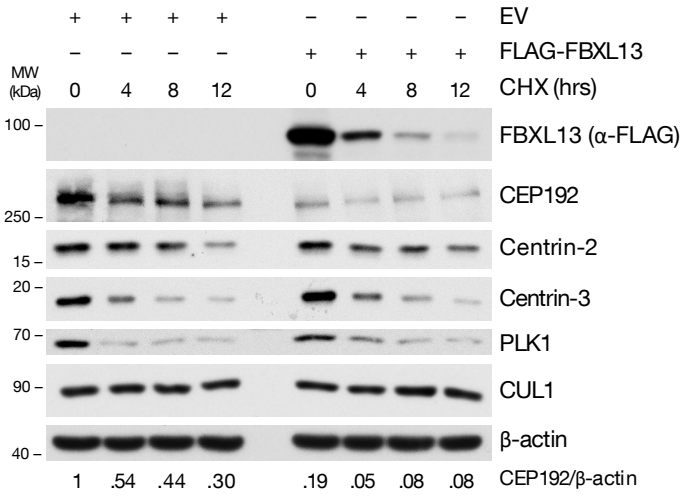

Figure 54: FBXL13 destabilizes CEP192 but not Centrin-2 and Centrin-3. Immunoblot analysis of U2OS cells transfected with FLAG-FBXL13 or empty vector (EV) control. One day after transfection, cells were treated with 100 µg/mL cycloheximide (CHX) and harvested at the indicated time points. Whole cell lysates were subjected to immunoblot analysis using the indicated antibodies. β-actin served as a loading control. Intensities of protein bands were measured using ImageJ and ratios of CEP192 to β-actin were calculated and normalized to the value of time point 0 hrs of the EV control.

7.2.2 FBXL13 ubiquitylates CEP192

The previous experiments provided evidence that CEP192 is a potential substrate of FBXL13 because CEP192 binds to the LRR motif of FBXL13 (Figure 52) and FBXL13 regulates CEP192 protein stability (Figure 53, Figure 54). To further confirm this assumption, the influence of FBXL13 loss on CEP192 ubiquitylation was investigated. Therefore, an *in vivo* ubiquitylation assay was performed, in which HEK293T cells were transfected with constructs encoding for HA-Ubiquitin and FLAG-CEP192 fragment comprising AA 1-630, which previously was shown to contain the binding site of FBXL13 (Figure 51b), or respective empty vectors. In addition, knockdown of FBXL13 was induced by expression of a respective shRNA and the effect of FBXL13 silencing was compared to cells expressing control shRNA. Moreover, cells were treated with the proteasome inhibitor MG132 to allow accumulation of ubiquitylated proteins. After lysis, whole cell extracts (WCEs) were denatured by addition of SDS and boiling in order to disrupt protein interactions with FLAG-CEP192 AA 1-630, thus ensuring to only analyse ubiquitylation of CEP192 and not auto-ubiquitylation of co-immunoprecipitated FBXL13. WCEs were subjected to FLAG-IP and ubiquitylation of CEP192 fragment could be detected by immunoblot analysis using an anti-HA antibody. Remarkably, ubiquitylation of CEP192 was strongly reduced upon FBXL13 downregulation (Figure 55), thus confirming the hypothesis that FBXL13 ubiquitylates and therefore targets CEP192 for proteasomal degradation.

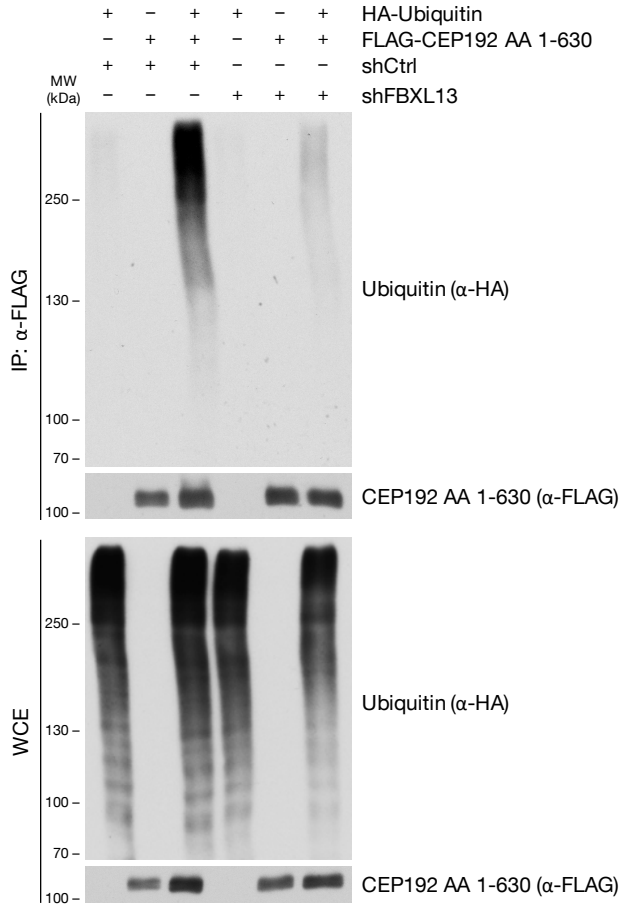

Figure 55: FBXL13 ubiquitylates CEP192. *In vivo* ubiquitylation assay of CEP192 in FBXL13 knockdown cells. HEK293T cells were transfected with indicated combinations of FLAG-CEP192, HA-Ubiquitin and empty vector together with constructs coding for shRNA targeting FBXL13 or a non-targeting control (shCtrl). Cells were treated with 10 µM MG132 for 3 hrs and denatured whole cell extracts (WCE) were subjected to FLAG immunoprecipitation (IP). WCE and IP were analysed by immunoblotting using the indicated antibodies.

7.3 FBXL13 negatively regulates microtubule arrays via CEP192 degradation

7.3.1 FBXL13 downregulates centrosomal CEP192 and γ-tubulin

Given that CEP192 represents an ubiquitylation substrate of FBXL13, it is likely that FBXL13 downregulates centrosomal CEP192 and thus has an influence on centrosome function. To validate this hypothesis, immunofluorescence (IF) studies of centrosomal CEP192 protein levels upon forced FBXL13 expression were performed by E. Fung (Fung 2017). To this end, U2OS cells transfected with an expression construct coding for FLAG-FBXL13 or empty vector control were subjected to confocal immunofluorescence microscopy using anti-FLAG and anti-CEP192 antibodies. Importantly, FLAG-FBXL13 could be detected at centrosomes colocalizing with endogenous CEP192 (Figure 56a). In accordance with the previous results, centrosomal levels of CEP192 were significantly reduced in FLAG-FBXL13 overexpressing cells (Figure 56a, b). Of note,

the antibody used for the detection of CEP192 recognizes all isoforms (Zhu et al. 2008) and since FBXL13 only interacts with CEP192 isoform 3, the remaining signal of CEP192 detected in the FBXL13 overexpressing sample could belong to other isoforms.

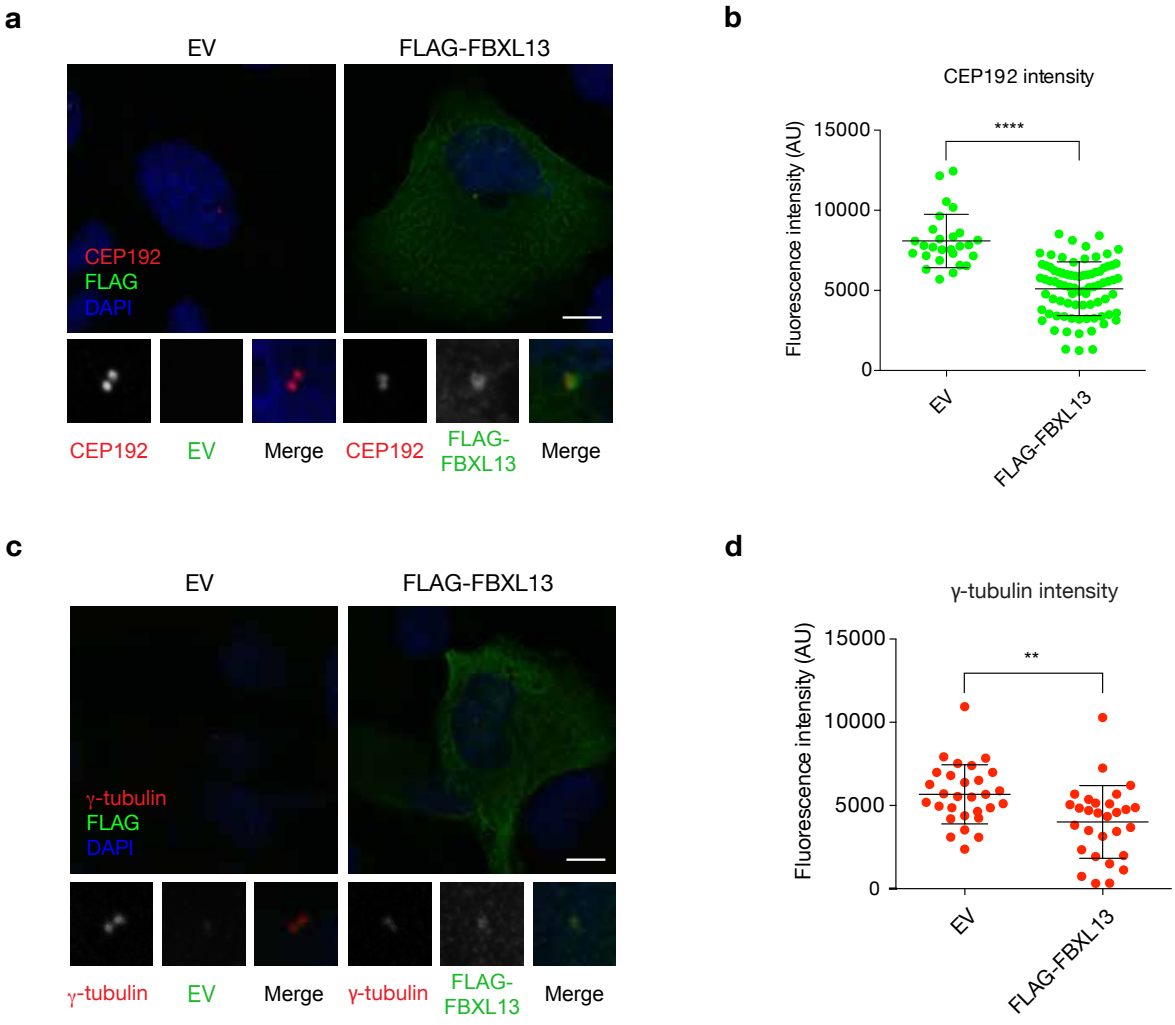

Figure 56: FBXL13 downregulates CEP192 and γ-tubulin at the centrosomes. (a, c) Representative images of immunofluorescence (IF) analyses of U2OS cells transfected with FLAG-FBXL13 expressing construct or empty vector (EV) control. Transfected cells were fixed with methanol and stained using anti-FLAG (FBXL13, green) and anti-CEP192 **(a)** or γ-tubulin **(b)** (red) antibodies. DNA was stained with DAPI (blue) and images were acquired by confocal microscopy. Scale bars represent 10 µm. **(b, d)** Quantification of experiments depicted in **a** and **c**. Fluorescence intensities of CEP192 **(b)** or γ-tubulin **(d)** signals at centrosomes in EV control and FLAG-FBXL13 expressing cells were measured (n = 3 independent experiments with n > 30 cells counted per experiment, mean ± S.D.). **, $P < 0.01$, ****; $P < 0.0001$ by Mann-Whitney test non-parametric. [Data provided by E. Fung (Fung 2017)].

CEP192 has been described to be important for centriole duplication and pericentriolar matrix (PCM) organization (Gomez-Ferreria et al. 2007; O'Rourke et al. 2014; Sonnen et al. 2013; Zhu et al. 2008). Therefore, it is conceivable that FBXL13 also plays a role in centrosome biology by targeting CEP192 for proteasomal degradation. To test this hypothesis, the effect of FBXL13 loss

on centrosome duplication was assessed in siRNA transfected U2OS cells by E. Fung. Indeed, this revealed that depletion of FBXL13 led to a small but significant increase in the number of cells containing overduplicated centrosomes (Fung 2017). However, these effects were rather small and given the involvement of CEP192 in γ-tubulin recruitment to centrosomes, it is possible that by controlling CEP192 protein level at the centrosomes, FBXL13 regulates PCM organization. To validate this assumption, U2OS cells were transfected with FLAG-FBXL13 expression construct or empty vector control and centrosomal γ-tubulin level were investigated by E. Fung. Strikingly, confocal microscopy of fixed and stained cells revealed a strong and significant reduction in γ-tubulin fluorescence signal upon forced FBXL13 expression (Figure 56c, d), suggesting that the observed reduction of centrosomal CEP192 level caused by FBXL13 overexpression has a profound effect on PCM recruitment.

7.3.2 FBXL13 is important for microtubule nucleation

Given the strong effect of forced FBXL13 expression on γ-tubulin recruitment to centrosomes (Figure 56c, d) and that the microtubule (MT) nucleation capacity highly depends on PCM integrity (Palazzo et al. 2000), FBXL13 overexpression might also influence centrosomal MT formation. To validate the impact of FBXL13 on MT nucleation capacity, microtubule re-growth after complete depolymerization was assessed in FBXL13 overexpressing cells by a MT nucleation assay. To this end, U2OS cells were transfected with FLAG-FBXL13 expression construct or empty vector control and depolymerization of MT was achieved by cold treatment of cells and the simultaneous

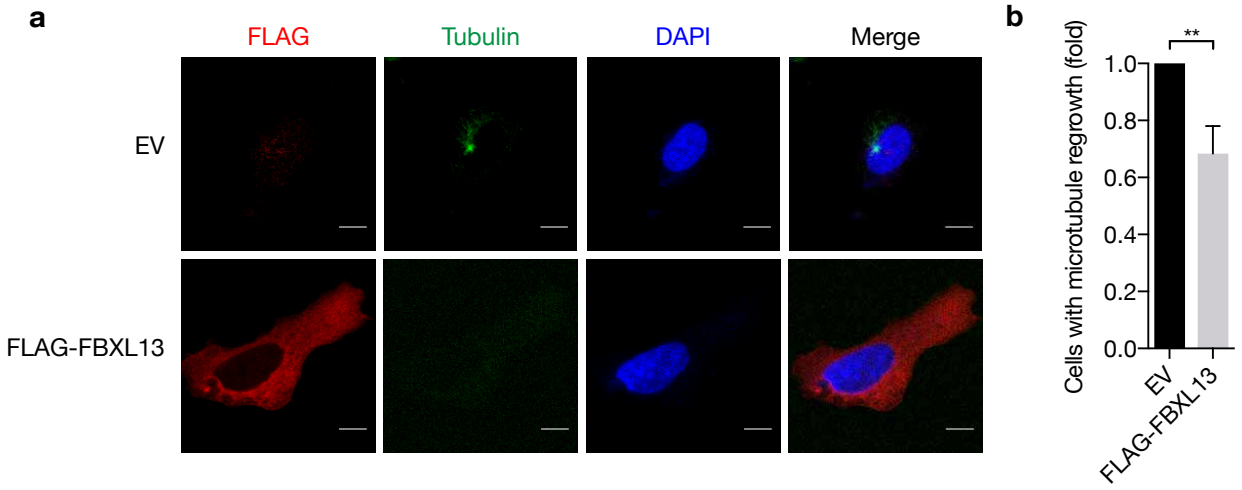

Figure 57: FBXL13 regulates centrosomal microtubule nucleation. (a) Representative images of microtubule regrowth assay in U2OS cells transfected with FLAG-FBXL13 expressing construct or empty vector (EV) control. Microtubules (MT) of transfected cells were completely depolymerized by treating cells with 10 µM nocodazole for 2 hrs at 4°C. Cells were re-warmed at 37°C and nocodazole was washed out to allow MT nucleation. Cells were fixed with methanol after 1 min and stained using anti-FLAG (FBXL13, red) and anti-α-tubulin (green) antibodies. DNA was stained with DAPI (blue) and images were acquired using an inverted fluorescence microscope. Scale bars represent 10 µm. **(b)** Quantification of experiment depicted in **a**. EV control and FLAG-FBXL13 expressing cells, in which MT nucleation took place, were counted and the number of EV expressing cells was set as 1 (n = 3 independent experiments with n = 100 cells counted per experiment, mean ± S.D.). **, $P < 0.01$ by one-sample t-test.

addition of nocodazole. After re-warming the cells, nocodazole was washed out to allow regrowth of MT and cells were fixed after 1 min. Immunofluorescence analysis revealed accumulation of α-tubulin at the site of centrosomes in empty vector cells (Figure 57a). As speculated, the number of cells, in which nucleation of MT took place, was indeed significantly reduced upon FBXL13 overexpression (Figure 57a, b). Overall, these data confirm the assumption that FBXL13 plays a role In PCM organization and therefore in MT nucleation.

7.4 FBXL13 regulates cell motility by controlling CEP192 protein level

7.4.1 FBXL13 is important for proper cell migration

Overduplication of centrosomes is commonly found in cancer and has been linked to metastasis (Chan 2011). Moreover, amplified centrosomes have been reported to promote invasion by increased nucleation of centrosomal microtubules (MT), which was dependent on CEP192 (Godinho et al. 2014). In addition, it was shown that CEP192 depletion impairs centrosomal MT arrays in interphase and causes extra-centrosomal MT nucleation, thereby modulating cell migration (O'Rourke et al. 2014). To investigate if FBXL13 regulates cell motility by controlling centrosomal CEP192 level, a 2-D scratch assay was conducted. Therefore, U2OS cells were transfected with siRNA targeting FBXL13 to induced FBXL13 knockdown or control siRNA (siGL) and subjected to wound healing assay. Strikingly, FBXL13 loss significantly reduced the capability of cells to migrate into the scratch zone, which could be rescued by co-expression of siRNA-resistant FBXL13 wildtype (Figure 58a, b). Of note, the slight overexpression of FBXL13, which was measured in the rescue setting by qPCR analysis, even increased the ability of cells to migrate compared to empty vector expressing control cells (Figure 58a-c), suggesting that FBXL13 promotes cell motility. Importantly, expression of FBXL13 lacking the F-box domain (ΔF-box) could not rescue the impaired migration phenotype caused by FBXL13 depletion despite stronger expression compared to the wildtype FBXL13 (Figure 58a-c). Together, these findings demonstrate that the ubiquitylation activity of FBXL13 is necessary for proper cell motility.

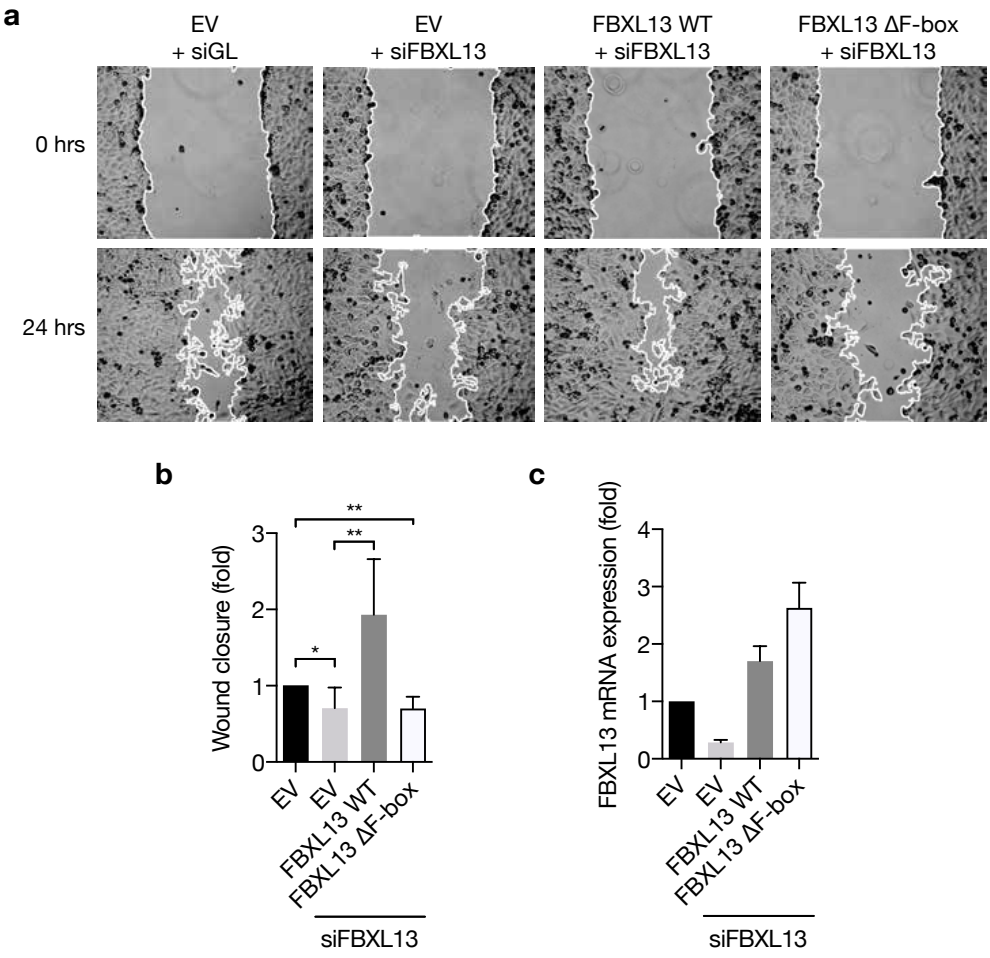

Figure 58: FBXL13 activity is essential for cell migration. (a) Representative images of wound healing assay of U2OS cells stably expressing siRNA-resistant FBXL13 wildtype (WT), FBXL13 lacking the F-box domain (ΔF-box) or empty vector (EV). Cells were transfected with siRNA targeting FBXL13 (siFBXL13) or a control siRNA (siGL) and 48 hrs later, cells were seeded into 6-well plates. After one day, when cells reached confluency, a linear wound was generated using a pipette tip and images were acquired at indicated time points using an inverted microscope. The wound edge is displayed by a white line. **(b)** Quantification of experiment depicted in **a**. Wound closure efficiency was calculated by the percentage of wound area closed after 24 hrs using the ImageJ software and the values for stably EV expressing cells transfected with siGL were set as 1 (n = 6, mean ± S.D.). *, $P < 0.05$; **, $P < 0.01$ by one-sample t-test. **(c)** Quantification of FBXL13 mRNA level from experiment depicted in **a** by qPCR analysis using specific primers for FBXL13 or RPLP0. The mRNA levels of FBXL13 were normalized to RPLP0 and the values for stably EV expressing cells transfected with siGL were set as 1 (n = 3, mean ± S.D.).

7.4.2 FBXL13 positively regulates cell motility by CEP192 degradation

The previous data indicate that FBXL13 positively regulates cell motility and that this depends on the ubiquitylation activity of FBXL13 (Figure 58). Given the negative effect of FBXL13 overexpression on CEP192 and γ-tubulin level at the centrosomes (Figure 56) and the role of CEP192 in cell motility (Godinho et al. 2014; O'Rourke et al. 2014), it is conceivable that the migration defect upon FBXL13 depletion is a consequence of CEP192 accumulation at the centrosomes. To test this hypothesis, the previously performed wound healing assay was repeated and cell migration was assessed upon single FBXL13 knockdown or FBXL13 and

CEP192 isoform 3 co-depletion. As expected, co-depletion of CEP192 rescued the migration defect caused by FBXL13 loss (Figure 59a-c), further providing evidence that the regulation of centrosomal CEP192 isoform 3 protein level by FBXL13 is important for proper cell motility.

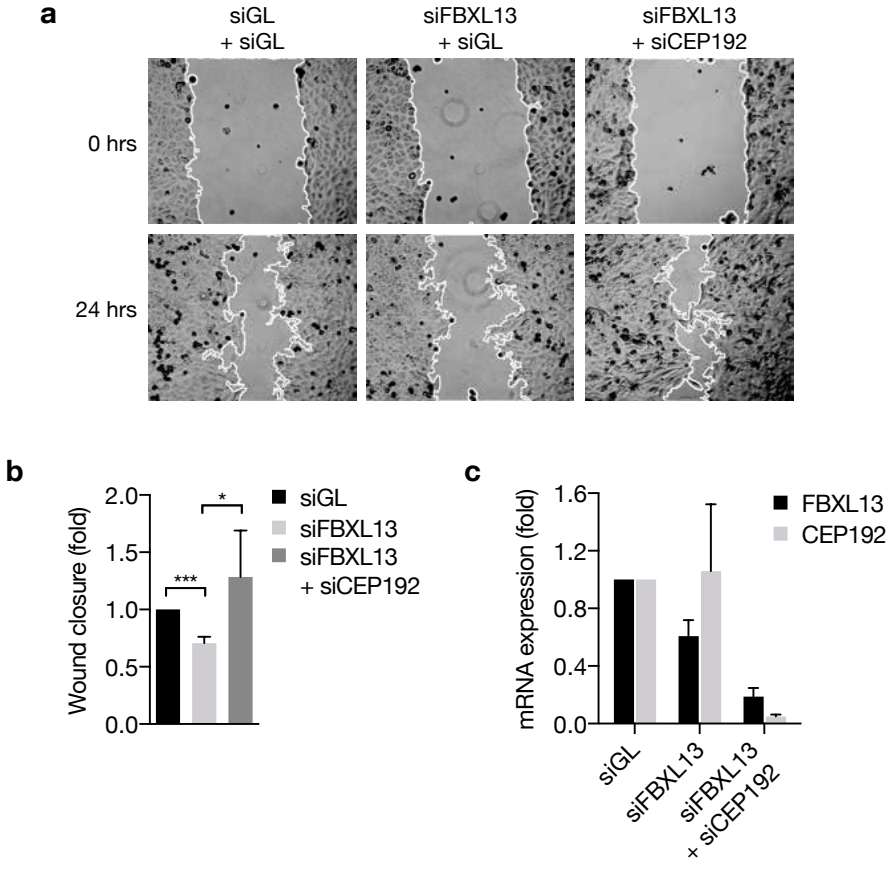

Figure 59: FBXL13 positively regulates cell motility by targeting CEP192 for degradation. Representative images of wound healing assays of U2OS cells transfected with the indicated combinations of siRNA targeting FBXL13 (siFBXL13), CEP192 isoform 3 (siCEP192) or a non-targeting control (siGL). Two days after transfection, cells were seeded into 6-well plates and the next day, when cells reached confluency, a linear wound was generated using a pipette tip and images were acquired at indicated time points using an inverted microscope. The wound edge is displayed by a white line. **(b)** Quantification of experiment depicted in **a**. Wound closure efficiency was calculated by the percentage of wound area closed after 24 hrs using the ImageJ software and the values for siGL expressing cells were set as 1 (n = 6, mean ± S.D.). *, $P < 0.05$; ***, $P < 0.001$ by one-sample t-test and differences between groups were analysed by unpaired Student's t-test. **(c)** Quantification of FBXL13 and CEP192 mRNA level from experiment depicted in **a** by qPCR analysis using specific primers for FBXL13, CEP192 or RPLP0. The mRNA levels of FBXL13 and CEP192 were normalized to RPLP0 and the values for siGL expressing cells were set as 1 (n = 3, mean ± S.D.).

8 Discussion II

By mediating ubiquitylation of numerous proteins involved in cell proliferation, apoptosis and metastasis, F-box proteins play a pivotal role in tumorigenesis and cancer progression. Despite large advances in the understanding of the functions of numerous F-box proteins over the last decades, the physiological role and the potential contribution to cancer development for many of the 69 F-box proteins remains unexplored. Further investigations are needed to shed light on the question, how unknown F-box proteins contribute to malignancies and hence represent targets for anti-cancer therapies. One orphan F-box protein is represented by FBXL13, for which no function has been described so far. However, data derived from recently published screens suggest an involvement of FBXL13 in tumorigenesis. For instance, FBXL13 has been found to be amplified or mutated in various solid tumours (cBioPortal) and cancer lines (Barretina et al. 2012). Additionally, loss of FBXL13 has been linked to genomic instability, further supporting a role for FBXL13 in cancer development. However, although these data indicate that FBXL13 plays a role in various malignancies, functional and mechanistic studies providing evidence for a direct involvement in tumorigenesis are missing.

The present study gives insight into the cellular role of FBXL13 and its potential implications in cancer. Starting from an unbiased affinity-based proteomic screen, the centrosomal proteins Centrin-2, Centrin-3 and CEP152 were identified as physical interactors of FBXL13 (Fung 2017). Based on the interaction with centrosomes, another centrosomal protein, CEP192, which is crucial for centriole duplication and centrosome maturation (Joukov, Walter, and De Nicolo 2014; Sonnen et al. 2013), could be found as a direct binding partner and bona fide substrate of FBXL13.

FBXL13 bound via its LRR domain to the N-terminal part of CEP192 isoform 3 containing the PLK4 binding site and mediated CEP192 polyubiquitylation, thereby targeting it for proteasomal degradation. A clear enrichment of ectopic FBXL13 could be observed at centrosomes leading to a significant reduction of centrosomal CEP192. In line with previously published data (Gomez-Ferreria et al. 2007), the reduction of CEP192 at centrosomes led to a strong decrease of γ-tubulin, suggesting an involvement of FBXL13 in centrosome homeostasis. Consequently, changes in the protein level of FBXL13 had a clear impact on the cellular capacity to nucleate centrosomal microtubules (MTs). First, ectopic expression of FBXL13 had a negative influence on the ability to nucleate centrosomal MTs after complete depolymerization and second, FBXL13 levels clearly correlated with microtubule arrays (Fung 2017).

While loss of FBXL13 caused only minor but significant effects on centriole overduplication (Fung 2017), this study demonstrates a clear correlation between FBXL13 and cell motility. Here, FBXL13 promoted cell migration, which was dependent on FBXL13-mediated ubiquitylation of CEP192.

The following chapters will discuss the interaction of FBXL13 with centrosomal proteins (8.1), the relevance of FBXL13-mediated ubiquitylation of CEP192 (8.2) and the function of FBXL13 in

cell migration (8.3). Moreover, a potential implication of FBXL13 in tumorigenesis and its role as an anti-cancer target will be discussed in the last section (8.4).

8.1 FBXL13 represents a novel centrosomal regulator

8.1.1 FBXL13 interacts with centrosomal proteins

F-box proteins have been implicated in centrosomal regulation, thereby playing an important role in the control of centrosome duplication and in the prevention of re-duplication. For instance, the $SCF^{CyclinF}$ complex mediates ubiquitin-dependent degradation of the centrosomal protein CP110 in G2 phase, which is required for bipolar spindle formation and hence for the maintenance of genomic integrity (D'Angiolella et al. 2010). Moreover, the degradation of PLK4 by $SCF^{\beta TrCP}$ has been shown to be crucial for prevention of centrosome overduplication during the cell cycle (Holland et al. 2010). In light of these findings, the current study provides evidence for a role of the previously uncharacterized F-box protein FBXL13 in centrosome physiology.

A proteome wide affinity-based mass spectrometry screening approach for FBXL13 binding partners found SKP1 and CUL1 as interactors and hence confirmed that FBXL13 builds a SCF complex (Fung 2017), supporting that FBXL13 is a bona fide ubiquitin E3 ligase. Additionally, the presence of multiple centrosomal proteins (Centrin-2, Centrin-3 and CEP152) suggested that FBXL13 interacts with centrosomes (Fung 2017). Interestingly, in search for interactors of F-box proteins belonging to the leucine rich repeat class (FBXLs), a previous publication has also found Centrin-2 and Centrin-3, two structural components of the centrosome, as binding partners of FBXL13, but no further functional studies were performed (Tan et al. 2013). However, in the same study, treatment with the proteasome inhibitor bortezomib or the neddylation inhibitor MLN4924, which inhibits SCF activity, did not increase the interaction of FBXL13 with Centrin-2 or Centrin-3, speaking against a ubiquitin-dependent regulation of these proteins by FBXL13. In line with these data, neither FBXL13 depletion (Figure 53a) nor forced expression of FBXL13 (Figure 54) had an influence on the protein stability of Centrin-2 and Centrin-3, confirming that FBXL13 does not regulate the levels of these proteins. However, binding studies confirmed a strong interaction of Centrin-2 and Centrin-3 with the N-terminal portion of FBXL13 (Figure 52), which does not correspond to the typical substrate binding site of FBXLs represented by the LRR domain, as previously reported for FBXL17 (Raducu et al. 2016). The relevance of this interaction could lie in the recruitment of FBXL13 to centrosomes, but further studies using N-terminal truncated mutants of FBXL13, which cannot bind to Centrin-2 and Centrin-3 anymore, are required to shed light on the functional outcome of this interactions.

Another centrosomal protein, which was found by the proteome-wide association approach, was CEP152 (Fung 2017). Together with CEP192, CEP152 plays a crucial role in centriole duplication by the recruitment and positioning of PLK4 (Kim, Park, et al. 2013; Sonnen et al. 2013). Moreover, CEP152 directly interacts with the large C-terminal portion of CEP192 present in all isoforms but not with the N-terminal extension of CEP192 isoform 3, which harbours the PLK4

binding site (Sonnen et al. 2013). Against this background, FBXL13 could interact and ubiquitylate either of these two proteins and indeed, direct comparison of the interaction between ectopically expressed proteins or semi-endogenous immunoprecipitation experiments revealed a stronger binding of FBXL13 to CEP192 than to CEP152 (Figure 49), suggesting that FBXL13 rather directly interacts with CEP192. Additional evidence for this assumption came from *in vitro* binding studies, which clearly proved that FBXL13 directly interacted with CEP192 independently of CEP152 (Figure 51c). Furthermore, knockdown of CEP152 did not interfere with FBXL13 binding to CEP192 (Figure 51b), however, *vice versa* CEP192 loss completely abolished the interaction between CEP152 and FBXL13 (Fung 2017), confirming that binding to CEP152 was only indirect. In this study, a custom-made peptide antibody against human FBXL13 was produced and successfully used for endogenous IP experiments from HEK293T cells, confirming the expression of endogenous FBXL13 in these cells. Importantly, this revealed that endogenous FBXL13 interacted with endogenous CEP192 (Figure 50), thereby excluding unspecific binding evoked by the overexpression of proteins. In contrast to Centrin-2 and Centrin-3, mapping analysis confirmed that FBXL13 interacts with CEP192 via its LRR domain, the typical substrate binding site, and not with the N-terminal portion containing the F-box domain (Figure 52). Together with the other findings, the distinct mode of interaction between FBXL13, Centrin-2, Centrin-3 and CEP192 implies that CEP192 represents the only centrosomal substrate of FBXL13 and hence the present study focused on the ubiquitylation-mediated regulation of CEP192 by FBXL13.

8.1.2 FBXL13 localizes at centrosomes

Given that FBXL13 interacts with centrosomal proteins and that CEP192 has been shown to be only present at centrosomes but not in the cytosol in S phase cells (Kim, Park, et al. 2013), regulation of CEP192 by FBXL13 requires a centrosomal localization of FBXL13. Indeed, ectopic FBXL13 was clearly enriched at centrosomes and co-localized with endogenous CEP192 (Figure 56a). Moreover, the staining of ectopic FBXL13 presumes a localization at the PCM, but a more precise evaluation using super-resolution 3D structured illumination microscopy, as previously used to analyse the spatial relationship of centriolar proteins and PCM components (Sonnen et al. 2012), would be required to make judgements of the exact position. Centrosomal localization of FBXL13 could be observed throughout the cell cycle (Fung 2017), but since overexpression of FBXL13 had a clear impact on centrosome function, this localization might not reflect the physiological situation and thus staining of endogenous FBXL13 would be necessary to investigate a cell cycle-dependent centrosomal localization. However, neither the antibody produced in this study nor the commercially available antibodies against FBXL13 could detect the native form of endogenous FBXL13 in immunofluorescence analysis. One possibility to overcome the need of a functional antibody to detect endogenous protein in the future, could be the use of CRISPR-mediated tagging of endogenous FBXL13 expressed from its physiological chromosomal context as used before for chromatin immunoprecipitation (ChIP) analyses, which also highly depend on suitable ChIP-seq grade antibodies (Savic et al. 2015). Since FBXL13 mRNA levels

measured by qPCR were rather low and also hardly detectable by immunoblot analysis in an asynchronous cell population, one could speculate that FBXL13 levels are indeed cell cycle-regulated, thereby only peaking at a certain cell cycle stage and being low in the other phases. However, a low expression of FBXL13 could also be explained by a limited need of protein amounts, because centrosomal proteins only act in a small cell compartment.

As discussed in the previous section (8.1.1), recruitment of FBXL13 to centrosomes could be mediated by binding to Centrin-2 and Centrin-3. Hence, it would be worth in future studies to analyse whether knockdown of Centrin-2 or Centrin-3 alters or abrogates the localization of FBXL13 at centrosomes. Alternatively, investigating the cellular localization of FBXL13 lacking the N-terminal part and thus the binding site for Centrin-2 and Centrin-3 could give further answers to the question how FBXL13 is recruited to centrosomes.

8.2 FBXL13 targets CEP192 for proteasomal degradation

The direct binding of FBXL13 to CEP192 as well as the nature of their interaction (discussed in 8.1.1) assumed that CEP192 represents an ubiquitylation substrate of FBXL13. This assumption could be confirmed by different experiments addressing protein stability (Figure 53, Figure 54) and ubiquitylation (Figure 55) of CEP192. Overexpression of FBXL13 strongly decreased CEP192 protein levels, which could be rescued by simultaneous inhibition of the proteasome (Figure 53a). Hence, FBXL13 seems to mediate degradative ubiquitylation, like most of the F-box proteins, at least in the context of CEP192. Likewise, loss of FBXL13 clearly led to an increase in CEP192 protein level, further providing evidence for the role of FBXL13 as ubiquitin E3 ligase of CEP192 (Figure 53b, c). Given that FBXL13 only interacted with and ubiquitylated the longest isoform of CEP192 (Figure 51c, Figure 55), the only isoform harbouring the PLK4 binding site (Figure 51a), it was conceivable that by targeting CEP192 for proteasomal degradation, FBXL13 regulates centrosome duplication, as previously described for the F-box protein Cyclin F (D'Angiolella et al. 2010). Although overexpression of FBXL13 did not affect centrosome duplication (Fung 2017), it has been reported that CEP192 cooperates with CEP152 in centriole duplication (Sonnen et al. 2013), so CEP152 might compensate for the downregulation of CEP192 caused by FBXL13 overexpression. Moreover, depletion of FBXL13 only slightly but significantly caused overduplication of centrosomes (Fung 2017). Despite its role in centriole duplication, overexpression of CEP192 did not give rise to additional MTOCs in previous publications, but caused amplification of loci containing γ-tubulin and pericentrin as well as abnormal mitotic spindles (Gomez-Ferreria et al. 2007; Moser et al. 2013). Hence, an increase in CEP192 protein level caused by FBXL13 loss might rather interfere with mitotic spindle assembly and thus should be analysed in future studies.

Another explanation for the minor effect on centriole duplication by FBXL13 alterations could be that FBXL13 does not restrict CEP192 levels in G2 phase, thereby preventing re-duplication of centrioles, but rather targets CEP192 at another cell cycle phase for degradation. In line with this hypothesis, FBXL13 overexpression indeed led to a reduced half-life of CEP192 level, but did not

cause a complete loss of CEP192 levels in cycloheximide experiments (Figure 54). Consequently, FBXL13 might not target the whole pool of CEP192 but rather degrades CEP192 at a certain time during the cell cycle, thus explaining the only partial reduction in CEP192 levels regarding to an asynchronous cell population. Indeed, CEP192 is not only required for centriole duplication in S phase but also for maturation of the PCM during mitosis (Gomez-Ferreria et al. 2007; Joukov, Walter, and De Nicolo 2014; Kim, Park, et al. 2013; Sonnen et al. 2013), and thus FBXL13 activity should be inhibited at this time. In fact, CEP192 accumulates in early mitosis and it has been shown that centrosomal CEP192 levels are the highest in prophase and metaphase followed by a subsequent decrease in anaphase and telophase (Gomez-Ferreria et al. 2007). However, the cellular mechanism by which CEP192 levels are downregulated at this cell cycle stage still remains unknown. It is thus imaginable, that FBXL13 is responsible for CEP192 degradation during mitotic exit, but further studies are necessary to shed light on a cell cycle-dependent regulation.

In this context, another open question remaining to be addressed is how the interaction and hence ubiquitylation of CEP192 by FBXL13 is regulated. Currently, it is unclear whether binding of CEP192 to FBXL13 depends on a certain stimulus, but it could be hypothesized, that CEP192 needs to be phosphorylated in order to be recognized by FBXL13. In fact, binding of most substrates by F-box proteins depends on phospho-degrons, thereby allowing a time-dependent degradation (Skaar, Pagan, and Pagano 2013). For instance, phosphorylated CDH1, an activator of the APC complex, is degraded by $SCF^{\beta\text{-}TrCP}$-mediated ubiquitylation in late G1, thereby allowing accumulation of another F-box protein SKP2 (Bashir et al. 2004; Fukushima et al. 2013; Wei et al. 2004). Upon phosphorylation by Cyclin E-CDK2, SKP2 in turn targets the CDK inhibitors p21 and p27 for proteasomal degradation (Bornstein et al. 2003; Carrano et al. 1999; Sheaff et al. 1997; Tsvetkov et al. 1999). These examples reflect the precise regulation of consecutive cell cycle events and since the centrosome cycle is highly coordinated with the cell cycle machinery, one could assume that FBXL13-mediated degradation of CEP192 might be regulated in a similar manner. Likewise, CEP192 has been reported to be targeted for proteasomal degradation by SCF^{SKP2} upon hydroxylation by PHD1, a hypoxia regulated protein (Moser et al. 2013). Alternatively, time-dependent degradation of CEP192 by FBXL13 could be achieved by alterations of its cellular localization, for instance by disrupting the binding to Centrin-2 and Centrin-3 as discussed in the previous section (8.1).

8.3 FBXL13 has a central role in cell motility

Centrosomes do not only play a role in mitotic spindle formation during mitosis, but also are involved in proper cell migration in interphase cells. Since alterations of FBXL13 had only minor effects on centrosome duplication (Fung 2017), during which FBXL13 activity should be low to maintain sufficient CEP192 levels, it can be assumed that FBXL13 plays a role in other centrosomal functions. As discussed before, it is not clear whether FBXL13 depletion or overexpression has an impact on proper assembly of a bipolar spindle and respective analyses should be part of future studies. However, the present study provided clear evidence for an

involvement of FBXL13 in cell motility, which depended on the ubiquitylation activity of FBXL13 (Figure 58). Moreover, impaired cell migration caused by FBXL13 loss could be rescued by simultaneous depletion of CEP192, confirming that the decrease in cell motility was caused by a failure in FBXL13-mediated degradation of CEP192 (Figure 59). Indeed, centrosomes are important regulators of cell polarity and thus cell migration, which is a crucial process involved in development, wound healing and immune response (Cheng et al. 2019; Franz, Jones, and Ridley 2002; Kushner et al. 2014; Martin et al. 2018; Wakida et al. 2010). Cell polarity is achieved by positioning the centrosomes in front of the nucleus, which generates an asymmetrical MT network, and is hence determined by the orientation of the nucleus-centrosome-axis (Elric and Etienne-Manneville 2014; Etienne-Manneville 2013). Here, centrosomal MTs are required for Golgi orientation and subsequent trafficking of vesicles to the leading edge (Luxton and Gundersen 2011; Petrie, Doyle, and Yamada 2009; Vinogradova et al. 2012; Yadav and Linstedt 2011). Given that FBXL13 overexpression on the one hand significantly reduced CEP192 and γ-tubulin levels at the centrosomes (Figure 56) and, on the other, impaired the capacity to nucleate centrosomal microtubules (Figure 57), FBXL13 alterations might interfere with the balance between centrosomal and acentrosomal MTs, which is important for directed cell migration (Figure 60), as previously reported (Cheng et al. 2019). Indeed, CEP192 plays a crucial role in the regulation of MT nucleation activity by recruiting γ-tubulin to centrosomes, which leads to an enrichment in γTuRCs (Gomez-Ferreria et al. 2007; Joukov, Walter, and De Nicolo 2014; Zhu et al. 2008). In line with this, FBXL13-mediated decrease of CEP192 levels resulted in reduced MT arrays (Fung 2017). Since FBXL13 overexpression increased the ability of cells to migrate, which was dependent on FBXL13 activity (Figure 58), it can be hypothesized that the resulting decrease in CEP192 level led to a shift towards acentrosomal MTs (Figure 60), which have been reported to favour cell motility (Cheng et al. 2019). In line with this, it has been shown that cell polarization rather depends on the presence of non-centrosomal MTs, whereas centrosomal MTs were dispensable in this publication (Martin et al. 2018). According to this assumption, it can be hypothesized that FBXL13 loss inhibited cell migration by increasing the centrosomal capacity to nucleate MTs at the cost of non-centrosomal MTs and as a consequence of impaired CEP192 degradation (Figure 59). Another observation that can be linked to altered cell motility is given by a decrease in the formation of microtubule arrays upon ectopic FBXL13 expression (Fung 2017), leading to a hyperpolarized cell shape and thus promoting cell migration (Figure 60). In accordance with these findings, CEP192 depletion causes an elongated cell shape (O'Rourke et al. 2014), which could be also observed in the present study (data not shown). However, the consequence of CEP192 loss in the previous publication was an inhibition of cell migration, although the same cellular system was used in the current study (O'Rourke et al. 2014). A possible explanation for the discrepancy could be the use of different siRNAs, since the present study only targeted the longest isoform of CEP192, which represented also the only isoform degraded by FBXL13, and not the others. Overall, the data of this study suggest that the physiological role of FBXL13 is to

control CEP192 levels, thereby keeping the balance between centrosomal and non-centrosomal MT nucleation activity in check (Figure 60).

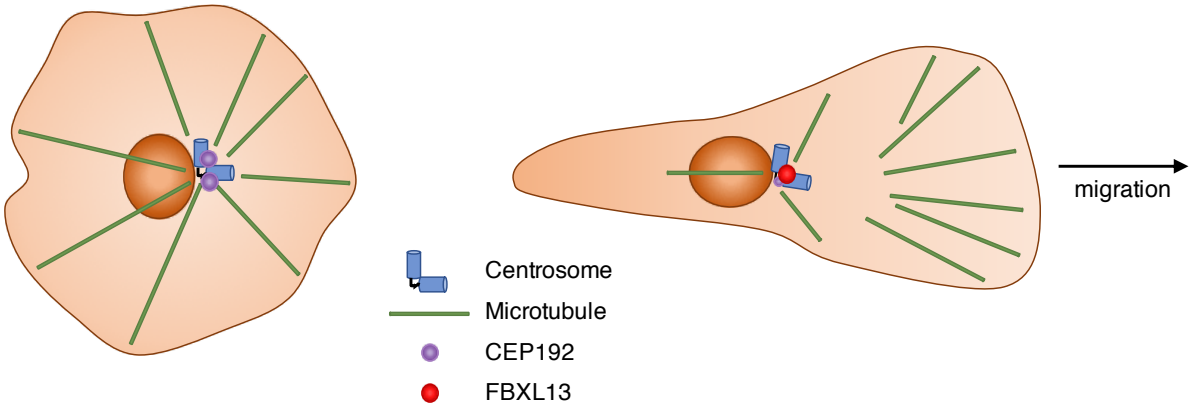

Figure 60: Model of FBXL13-mediated cell migration. Low levels of FBXL13 promote CEP192-mediated recruitment of γ-tubulin to centrosomes and thus an increase in microtubule (MT) arrays at the cost of acentrosomal MTs, leading to radial cell growth (left side). In contrast, enhanced expression of FBXL13 causes proteolytic degradation of CEP192 and a decrease in centrosomal MT nucleation activity. The subsequent shift towards the abundance of acentrosomal MTs leads to cell polarization and hence increased cell motility (right side).

8.4 FBXL13 as a potential anti-cancer target

Although the gene locus of *FBXL13* has been found to be commonly deleted in myeloid tumours (Curtiss et al. 2005), most studies provide evidence for an oncogenic role of FBXL13. However, whether FBXL13 acts as a tumour suppressor or as an oncogene might be cell context- and substrate-dependent, since F-box proteins generally target more than one substrate. Regarding a potential oncogenic role, one study performing a genome-wide siRNA screen revealed that FBXL13 depletion promotes genomic instability (Paulsen et al. 2009). Importantly, centrosomal abnormalities have been linked to genetic instability and thus cancer, mainly by causing aberrant mitotic spindle formation and interfering with proper cell division (Lingle et al. 2002; Nigg 2002; Pihan et al. 2001). However, since the current study did not focus on the impact of FBXL13 alterations on bipolar spindle assembly, it only can be speculated whether there is a potential connection. Other hints suggesting a potential oncogenic involvement of FBXL13 come from the observation that FBXL13 is frequently amplified or mutated in various solid tumours, such as head and neck, breast or non-epithelial prostate cancer (cBioPortal), and in different cancer cell lines (Barretina et al. 2012). A verification of a potential correlation between FBXL13 expression and tumorigenesis by analysing patient samples will be subject of future studies.

Many studies exist concerning the implication of numerical centrosomal aberrations, mostly centrosome amplification, leading to mis-segregation of chromosomes and genomic instability, in carcinogenesis, however, the consequences of structural centrosomal alterations are less well defined (Basto et al. 2008; D'Assoro et al. 2002; Ganem, Godinho, and Pellman 2009; Lingle et al. 2002). In fact, tissue integrity and cell polarity, particularly with regard to MT nucleation and

release, are largely associated with tumour progression (Schnerch and Nigg 2016). Additionally, alterations in MT-dependent processes evoked from aberrant centrosome structure have been also shown to have large impact on cell-cell adhesion and cell polarization (Schnerch and Nigg 2016). Against this background, it is conceivable that FBXL13 overexpression causes similar effects and increases cell invasiveness as a consequence of cell hyperpolarization and increased motility. Hence, future studies will address the question whether FBXL13 amplification promotes cell invasion and thus whether it could be used as a prognostic marker to predict the potential of a tumour to infiltrate other tissues and become metastatic. In this regard, the MCF10A cell line, a non-transformed human mammary epithelial cell line, could be used in a three-dimensional (3D) culture model in order to investigate the putative role of FBXL13 in the integrity of mammosphere structure, as used before in studies analysing the impact of numerical and structural centrosome aberrations on tissue architecture (Godinho et al. 2014; Schnerch and Nigg 2016).

Despite the lack of intrinsic enzymatic activity, F-box proteins have been considered as therapeutic targets by disrupting either substrate binding or by interfering with SCF complex formation (Chan et al. 2013; Wu et al. 2012). The present study focused on the functional characterization of the so far orphan F-box protein FBXL13 and provides a framework for future investigations, which may give further insight into the role of FBXL13 in tumour biology, including invasion, metastasis and uncontrolled proliferation. Besides its role as a positive regulator of cell migration (Figure 58), FBXL13 loss had a clear negative impact on cell proliferation (data not shown), thus representing an attractive new target for anti-cancer therapy. Nevertheless, a full understanding of the question how FBXL13-mediated degradation of CEP192 contribute to tumorigenesis will be necessary to elucidate the suitability of this protein as a prognostic marker or drug target. Overall, this study gave insight in the mechanistical function of an unknown F-box protein and its potential involvement in cancer development, thus providing a basis for further investigations.

9 Literature

Abal, M., M. Piel, V. Bouckson-Castaing, M. Mogensen, J. B. Sibarita, and M. Bornens. 2002. 'Microtubule release from the centrosome in migrating cells', *J Cell Biol*, 159: 731-7.

Abdul Rehman, S. A., Y. A. Kristariyanto, S. Y. Choi, P. J. Nkosi, S. Weidlich, K. Labib, K. Hofmann, and Y. Kulathu. 2016. 'MINDY-1 Is a Member of an Evolutionarily Conserved and Structurally Distinct New Family of Deubiquitinating Enzymes', *Mol Cell*, 63: 146-55.

Adams, J. 2004. 'The proteasome: a suitable antineoplastic target', *Nat Rev Cancer*, 4: 349-60.

Aguirre, A. J., R. M. Meyers, B. A. Weir, F. Vazquez, C. Z. Zhang, U. Ben-David, A. Cook, G. Ha, W. F. Harrington, M. B. Doshi, M. Kost-Alimova, S. Gill, H. Xu, L. D. Ali, G. Jiang, S. Pantel, Y. Lee, A. Goodale, A. D. Cherniack, C. Oh, G. Kryukov, G. S. Cowley, L. A. Garraway, K. Stegmaier, C. W. Roberts, T. R. Golub, M. Meyerson, D. E. Root, A. Tsherniak, and W. C. Hahn. 2016. 'Genomic Copy Number Dictates a Gene-Independent Cell Response to CRISPR/Cas9 Targeting', *Cancer Discov*, 6: 914-29.

Akaboshi, S., S. Watanabe, Y. Hino, Y. Sekita, Y. Xi, K. Araki, K. Yamamura, M. Oshima, T. Ito, H. Baba, and M. Nakao. 2009. 'HMGA1 is induced by Wnt/beta-catenin pathway and maintains cell proliferation in gastric cancer', *Am J Pathol*, 175: 1675-85.

Akhoondi, S., D. Sun, N. von der Lehr, S. Apostolidou, K. Klotz, A. Maljukova, D. Cepeda, H. Fiegl, D. Dafou, C. Marth, E. Mueller-Holzner, M. Corcoran, M. Dagnell, S. Z. Nejad, B. N. Nayer, M. R. Zali, J. Hansson, S. Egyhazi, F. Petersson, P. Sangfelt, H. Nordgren, D. Grander, S. I. Reed, M. Widschwendter, O. Sangfelt, and C. Spruck. 2007. 'FBXW7/hCDC4 is a general tumor suppressor in human cancer', *Cancer Res*, 67: 9006-12.

Anders, L., N. Ke, P. Hydbring, Y. J. Choi, H. R. Widlund, J. M. Chick, H. Zhai, M. Vidal, S. P. Gygi, P. Braun, and P. Sicinski. 2011. 'A systematic screen for CDK4/6 substrates links FOXM1 phosphorylation to senescence suppression in cancer cells', *Cancer Cell*, 20: 620-34.

Andersen, J. S., C. J. Wilkinson, T. Mayor, P. Mortensen, E. A. Nigg, and M. Mann. 2003. 'Proteomic characterization of the human centrosome by protein correlation profiling', *Nature*, 426: 570-4.

Aron, R., P. Pellegrini, E. W. Green, D. C. Maddison, K. Opoku-Nsiah, J. S. Wong, A. C. Daub, F. Giorgini, and S. Finkbeiner. 2018. 'Deubiquitinase Usp12 functions noncatalytically to induce autophagy and confer neuroprotection in models of Huntington's disease', *Nat Commun*, 9: 3191.

Arquint, C., A. M. Gabryjonczyk, and E. A. Nigg. 2014. 'Centrosomes as signalling centres', *Philos Trans R Soc Lond B Biol Sci*, 369.

Attal, M., J. L. Harousseau, A. M. Stoppa, J. J. Sotto, J. G. Fuzibet, J. F. Rossi, P. Casassus, H. Maisonneuve, T. Facon, N. Ifrah, C. Payen, and R. Bataille. 1996. 'A prospective, randomized trial of autologous bone marrow transplantation and chemotherapy in multiple myeloma. Intergroupe Francais du Myelome', *N Engl J Med*, 335: 91-7.

Avet-Loiseau, H., M. Attal, P. Moreau, C. Charbonnel, F. Garban, C. Hulin, S. Leyvraz, M. Michallet, I. Yakoub-Agha, L. Garderet, G. Marit, L. Michaux, L. Voillat, M. Renaud, B. Grosbois, G. Guillerm, L. Benboubker, M. Monconduit, C. Thieblemont, P. Casassus, D. Caillot, A. M.

Stoppa, J. J. Sotto, M. Wetterwald, C. Dumontet, J. G. Fuzibet, I. Azais, V. Dorvaux, M. Zandecki, R. Bataille, S. Minvielle, J. L. Harousseau, T. Facon, and C. Mathiot. 2007. 'Genetic abnormalities and survival in multiple myeloma: the experience of the Intergroupe Francophone du Myelome', *Blood*, 109: 3489-95.

Bai, C., R. Richman, and S. J. Elledge. 1994. 'Human cyclin F', *Embo j*, 13: 6087-98.

Bai, C., P. Sen, K. Hofmann, L. Ma, M. Goebl, J. W. Harper, and S. J. Elledge. 1996. 'SKP1 connects cell cycle regulators to the ubiquitin proteolysis machinery through a novel motif, the F-box', *Cell*, 86: 263-74.

Balzeau, J., M. R. Menezes, S. Cao, and J. P. Hagan. 2017. 'The LIN28/let-7 Pathway in Cancer', *Front Genet*, 8: 31.

Bard, J. A. M., E. A. Goodall, E. R. Greene, E. Jonsson, K. C. Dong, and A. Martin. 2018. 'Structure and Function of the 26S Proteasome', *Annu Rev Biochem*, 87: 697-724.

Barnum, K. J., and M. J. O'Connell. 2014. 'Cell cycle regulation by checkpoints', *Methods Mol Biol*, 1170: 29-40.

Barretina, J., G. Caponigro, N. Stransky, K. Venkatesan, A. A. Margolin, S. Kim, C. J. Wilson, J. Lehar, G. V. Kryukov, D. Sonkin, A. Reddy, M. Liu, L. Murray, M. F. Berger, J. E. Monahan, P. Morais, J. Meltzer, A. Korejwa, J. Jane-Valbuena, F. A. Mapa, J. Thibault, E. Bric-Furlong, P. Raman, A. Shipway, I. H. Engels, J. Cheng, G. K. Yu, J. Yu, P. Aspesi, Jr., M. de Silva, K. Jagtap, M. D. Jones, L. Wang, C. Hatton, E. Palescandolo, S. Gupta, S. Mahan, C. Sougnez, R. C. Onofrio, T. Liefeld, L. MacConaill, W. Winckler, M. Reich, N. Li, J. P. Mesirov, S. B. Gabriel, G. Getz, K. Ardlie, V. Chan, V. E. Myer, B. L. Weber, J. Porter, M. Warmuth, P. Finan, J. L. Harris, M. Meyerson, T. R. Golub, M. P. Morrissey, W. R. Sellers, R. Schlegel, and L. A. Garraway. 2012. 'The Cancer Cell Line Encyclopedia enables predictive modelling of anticancer drug sensitivity', *Nature*, 483: 603-7.

Bartek, J., C. Lukas, and J. Lukas. 2004. 'Checking on DNA damage in S phase', *Nat Rev Mol Cell Biol*, 5: 792-804.

Bashir, T., N. V. Dorrello, V. Amador, D. Guardavaccaro, and M. Pagano. 2004. 'Control of the SCF(Skp2-Cks1) ubiquitin ligase by the APC/C(Cdh1) ubiquitin ligase', *Nature*, 428: 190-3.

Basto, R., K. Brunk, T. Vinadogrova, N. Peel, A. Franz, A. Khodjakov, and J. W. Raff. 2008. 'Centrosome amplification can initiate tumorigenesis in flies', *Cell*, 133: 1032-42.

Batuman, V. 2012. 'The pathogenesis of acute kidney impairment in patients with multiple myeloma', *Adv Chronic Kidney Dis*, 19: 282-6.

Bazzi, H., and K. V. Anderson. 2014. 'Acentriolar mitosis activates a p53-dependent apoptosis pathway in the mouse embryo', *Proc Natl Acad Sci U S A*, 111: E1491-500.

Bergsagel, P. L., and W. M. Kuehl. 2001. 'Chromosome translocations in multiple myeloma', *Oncogene*, 20: 5611-22.

Bernstein, E., A. A. Caudy, S. M. Hammond, and G. J. Hannon. 2001. 'Role for a bidentate ribonuclease in the initiation step of RNA interference', *Nature*, 409: 363-6.

Beronja, S., P. Janki, E. Heller, W. H. Lien, B. E. Keyes, N. Oshimori, and E. Fuchs. 2013. 'RNAi screens in mice identify physiological regulators of oncogenic growth', *Nature*, 501: 185-90.

Besson, A., and V. W. Yong. 2001. 'Mitogenic signaling and the relationship to cell cycle regulation in astrocytomas', *J Neurooncol*, 51: 245-64.

Bettencourt-Dias, M., and D. M. Glover. 2007. 'Centrosome biogenesis and function: centrosomics brings new understanding', *Nat Rev Mol Cell Biol*, 8: 451-63.

Borissenko, L., and M. Groll. 2007. '20S proteasome and its inhibitors: crystallographic knowledge for drug development', *Chem Rev*, 107: 687-717.

Bornstein, G., J. Bloom, D. Sitry-Shevah, K. Nakayama, M. Pagano, and A. Hershko. 2003. 'Role of the SCFSkp2 ubiquitin ligase in the degradation of p21Cip1 in S phase', *J Biol Chem*, 278: 25752-7.

Borodovsky, A., B. M. Kessler, R. Casagrande, H. S. Overkleeft, K. D. Wilkinson, and H. L. Ploegh. 2001. 'A novel active site-directed probe specific for deubiquitylating enzymes reveals proteasome association of USP14', *Embo j*, 20: 5187-96.

Bour, S., C. Perrin, H. Akari, and K. Strebel. 2001. 'The human immunodeficiency virus type 1 Vpu protein inhibits NF-kappa B activation by interfering with beta TrCP-mediated degradation of Ikappa B', *J Biol Chem*, 276: 15920-8.

Bretones, G., J. C. Acosta, J. M. Caraballo, N. Ferrandiz, M. T. Gomez-Casares, M. Albajar, R. Blanco, P. Ruiz, W. C. Hung, M. P. Albero, I. Perez-Roger, and J. Leon. 2011. 'SKP2 oncogene is a direct MYC target gene and MYC down-regulates p27(KIP1) through SKP2 in human leukemia cells', *J Biol Chem*, 286: 9815-25.

Bruderer, R., M. H. Tatham, A. Plechanovova, I. Matic, A. K. Garg, and R. T. Hay. 2011. 'Purification and identification of endogenous polySUMO conjugates', *EMBO Rep*, 12: 142-8.

Buetow, L., and D. T. Huang. 2016. 'Structural insights into the catalysis and regulation of E3 ubiquitin ligases', *Nat Rev Mol Cell Biol*, 17: 626-42.

Carrano, A. C., E. Eytan, A. Hershko, and M. Pagano. 1999. 'SKP2 is required for ubiquitin-mediated degradation of the CDK inhibitor p27', *Nat Cell Biol*, 1: 193-9.

Castello, A., B. Fischer, K. Eichelbaum, R. Horos, B. M. Beckmann, C. Strein, N. E. Davey, D. T. Humphreys, T. Preiss, L. M. Steinmetz, J. Krijgsveld, and M. W. Hentze. 2012. 'Insights into RNA biology from an atlas of mammalian mRNA-binding proteins', *Cell*, 149: 1393-406.

Catzavelos, C., N. Bhattacharya, Y. C. Ung, J. A. Wilson, L. Roncari, C. Sandhu, P. Shaw, H. Yeger, I. Morava-Protzner, L. Kapusta, E. Franssen, K. I. Pritchard, and J. M. Slingerland. 1997. 'Decreased levels of the cell-cycle inhibitor p27Kip1 protein: prognostic implications in primary breast cancer', *Nat Med*, 3: 227-30.

Cenciarelli, C., D. S. Chiaur, D. Guardavaccaro, W. Parks, M. Vidal, and M. Pagano. 1999. 'Identification of a family of human F-box proteins', *Curr Biol*, 9: 1177-9.

Chan, C. H., C. F. Li, W. L. Yang, Y. Gao, S. W. Lee, Z. Feng, H. Y. Huang, K. K. Tsai, L. G. Flores, Y. Shao, J. D. Hazle, D. Yu, W. Wei, D. Sarbassov, M. C. Hung, K. I. Nakayama, and H. K. Lin.

2012. 'The Skp2-SCF E3 ligase regulates Akt ubiquitination, glycolysis, herceptin sensitivity, and tumorigenesis', *Cell*, 149: 1098-111.

Chan, C. H., J. K. Morrow, C. F. Li, Y. Gao, G. Jin, A. Moten, L. J. Stagg, J. E. Ladbury, Z. Cai, D. Xu, C. J. Logothetis, M. C. Hung, S. Zhang, and H. K. Lin. 2013. 'Pharmacological inactivation of Skp2 SCF ubiquitin ligase restricts cancer stem cell traits and cancer progression', *Cell*, 154: 556-68.

Chan, J. Y. 2011. 'A clinical overview of centrosome amplification in human cancers', *Int J Biol Sci*, 7: 1122-44.

Chang, T. C., L. R. Zeitels, H. W. Hwang, R. R. Chivukula, E. A. Wentzel, M. Dews, J. Jung, P. Gao, C. V. Dang, M. A. Beer, A. Thomas-Tikhonenko, and J. T. Mendell. 2009. 'Lin-28B transactivation is necessary for Myc-mediated let-7 repression and proliferation', *Proc Natl Acad Sci U S A*, 106: 3384-9.

Chapman, M. A., M. S. Lawrence, J. J. Keats, K. Cibulskis, C. Sougnez, A. C. Schinzel, C. L. Harview, J. P. Brunet, G. J. Ahmann, M. Adli, K. C. Anderson, K. G. Ardlie, D. Auclair, A. Baker, P. L. Bergsagel, B. E. Bernstein, Y. Drier, R. Fonseca, S. B. Gabriel, C. C. Hofmeister, S. Jagannath, A. J. Jakubowiak, A. Krishnan, J. Levy, T. Liefeld, S. Lonial, S. Mahan, B. Mfuko, S. Monti, L. M. Perkins, R. Onofrio, T. J. Pugh, S. V. Rajkumar, A. H. Ramos, D. S. Siegel, A. Sivachenko, A. K. Stewart, S. Trudel, R. Vij, D. Voet, W. Winckler, T. Zimmerman, J. Carpten, J. Trent, W. C. Hahn, L. A. Garraway, M. Meyerson, E. S. Lander, G. Getz, and T. R. Golub. 2011. 'Initial genome sequencing and analysis of multiple myeloma', *Nature*, 471: 467-72.

Chau, V., J. W. Tobias, A. Bachmair, D. Marriott, D. J. Ecker, D. K. Gonda, and A. Varshavsky. 1989. 'A multiubiquitin chain is confined to specific lysine in a targeted short-lived protein', *Science*, 243: 1576-83.

Cheng, H. W., C. T. Hsiao, Y. Q. Chen, C. M. Huang, S. I. Chan, A. Chiou, and J. C. Kuo. 2019. 'Centrosome guides spatial activation of Rac to control cell polarization and directed cell migration', *Life Sci Alliance*, 2.

Chernova, T. A., K. D. Allen, L. M. Wesoloski, J. R. Shanks, Y. O. Chernoff, and K. D. Wilkinson. 2003. 'Pleiotropic effects of Ubp6 loss on drug sensitivities and yeast prion are due to depletion of the free ubiquitin pool', *J Biol Chem*, 278: 52102-15.

Chesi, M., P. L. Bergsagel, L. A. Brents, C. M. Smith, D. S. Gerhard, and W. M. Kuehl. 1996. 'Dysregulation of cyclin D1 by translocation into an IgH gamma switch region in two multiple myeloma cell lines', *Blood*, 88: 674-81.

Chesi, M., P. L. Bergsagel, O. O. Shonukan, M. L. Martelli, L. A. Brents, T. Chen, E. Schrock, T. Ried, and W. M. Kuehl. 1998. 'Frequent dysregulation of the c-maf proto-oncogene at 16q23 by translocation to an Ig locus in multiple myeloma', *Blood*, 91: 4457-63.

Chesi, M., E. Nardini, L. A. Brents, E. Schrock, T. Ried, W. M. Kuehl, and P. L. Bergsagel. 1997. 'Frequent translocation t(4;14)(p16.3;q32.3) in multiple myeloma is associated with increased expression and activating mutations of fibroblast growth factor receptor 3', *Nat Genet*, 16: 260-4.

Chesi, M., D. F. Robbiani, M. Sebag, W. J. Chng, M. Affer, R. Tiedemann, R. Valdez, S. E. Palmer, S. S. Haas, A. K. Stewart, R. Fonseca, R. Kremer, G. Cattoretti, and P. L. Bergsagel. 2008. 'AID-

dependent activation of a MYC transgene induces multiple myeloma in a conditional mouse model of post-germinal center malignancies', *Cancer Cell*, 13: 167-80.

Chiecchio, L., G. P. Dagrada, R. K. Protheroe, D. M. Stockley, A. G. Smith, K. H. Orchard, N. C. Cross, C. J. Harrison, and F. M. Ross. 2009. 'Loss of 1p and rearrangement of MYC are associated with progression of smouldering myeloma to myeloma: sequential analysis of a single case', *Haematologica*, 94: 1024-8.

Chiecchio, L., G. P. Dagrada, H. E. White, M. R. Towsend, R. K. Protheroe, K. L. Cheung, D. M. Stockley, K. H. Orchard, N. C. Cross, C. J. Harrison, and F. M. Ross. 2009. 'Frequent upregulation of MYC in plasma cell leukemia', *Genes Chromosomes Cancer*, 48: 624-36.

Child, J. A., G. J. Morgan, F. E. Davies, R. G. Owen, S. E. Bell, K. Hawkins, J. Brown, M. T. Drayson, and P. J. Selby. 2003. 'High-dose chemotherapy with hematopoietic stem-cell rescue for multiple myeloma', *N Engl J Med*, 348: 1875-83.

Chng, W. J., G. F. Huang, T. H. Chung, S. B. Ng, N. Gonzalez-Paz, T. Troska-Price, G. Mulligan, M. Chesi, P. L. Bergsagel, and R. Fonseca. 2011. 'Clinical and biological implications of MYC activation: a common difference between MGUS and newly diagnosed multiple myeloma', *Leukemia*, 25: 1026-35.

Ciechanover, A., and R. Ben-Saadon. 2004. 'N-terminal ubiquitination: more protein substrates join in', *Trends Cell Biol*, 14: 103-6.

Clague, M. J., I. Barsukov, J. M. Coulson, H. Liu, D. J. Rigden, and S. Urbe. 2013. 'Deubiquitylases from genes to organism', *Physiol Rev*, 93: 1289-315.

Collins, G. A., and A. L. Goldberg. 2017. 'The Logic of the 26S Proteasome', *Cell*, 169: 792-806.

Comartin, D., G. D. Gupta, E. Fussner, E. Coyaud, M. Hasegan, M. Archinti, S. W. Cheung, D. Pinchev, S. Lawo, B. Raught, D. P. Bazett-Jones, J. Luders, and L. Pelletier. 2013. 'CEP120 and SPICE1 cooperate with CPAP in centriole elongation', *Curr Biol*, 23: 1360-6.

Conduit, P. T., A. Wainman, and J. W. Raff. 2015. 'Centrosome function and assembly in animal cells', *Nat Rev Mol Cell Biol*, 16: 611-24.

Cope, G. A., G. S. Suh, L. Aravind, S. E. Schwarz, S. L. Zipursky, E. V. Koonin, and R. J. Deshaies. 2002. 'Role of predicted metalloprotease motif of Jab1/Csn5 in cleavage of Nedd8 from Cul1', *Science*, 298: 608-11.

Copley, M. R., S. Babovic, C. Benz, D. J. Knapp, P. A. Beer, D. G. Kent, S. Wohrer, D. Q. Treloar, C. Day, K. Rowe, H. Mader, F. Kuchenbauer, R. K. Humphries, and C. J. Eaves. 2013. 'The Lin28b-let-7-Hmga2 axis determines the higher self-renewal potential of fetal haematopoietic stem cells', *Nat Cell Biol*, 15: 916-25.

Coux, O., K. Tanaka, and A. L. Goldberg. 1996. 'Structure and functions of the 20S and 26S proteasomes', *Annu Rev Biochem*, 65: 801-47.

Cron, K. R., K. Zhu, D. S. Kushwaha, G. Hsieh, D. Merzon, J. Rameseder, C. C. Chen, A. D. D'Andrea, and D. Kozono. 2013. 'Proteasome inhibitors block DNA repair and radiosensitize non-small cell lung cancer', *PLoS One*, 8: e73710.

Crosas, B., J. Hanna, D. S. Kirkpatrick, D. P. Zhang, Y. Tone, N. A. Hathaway, C. Buecker, D. S. Leggett, M. Schmidt, R. W. King, S. P. Gygi, and D. Finley. 2006. 'Ubiquitin chains are remodeled at the proteasome by opposing ubiquitin ligase and deubiquitinating activities', *Cell*, 127: 1401-13.

Cui, Y., S. He, C. Xing, K. Lu, J. Wang, G. Xing, A. Meng, S. Jia, F. He, and L. Zhang. 2011. 'SCFFBXL(1)(5) regulates BMP signalling by directing the degradation of HECT-type ubiquitin ligase Smurf1', *Embo j*, 30: 2675-89.

Cunha-Ferreira, I., A. Rodrigues-Martins, I. Bento, M. Riparbelli, W. Zhang, E. Laue, G. Callaini, D. M. Glover, and M. Bettencourt-Dias. 2009. 'The SCF/Slimb ubiquitin ligase limits centrosome amplification through degradation of SAK/PLK4', *Curr Biol*, 19: 43-9.

Curtiss, N. P., J. M. Bonifas, J. O. Lauchle, J. D. Balkman, C. P. Kratz, B. M. Emerling, E. D. Green, M. M. Le Beau, and K. M. Shannon. 2005. 'Isolation and analysis of candidate myeloid tumor suppressor genes from a commonly deleted segment of 7q22', *Genomics*, 85: 600-7.

D'Angiolella, V., V. Donato, S. Vijayakumar, A. Saraf, L. Florens, M. P. Washburn, B. Dynlacht, and M. Pagano. 2010. 'SCF(Cyclin F) controls centrosome homeostasis and mitotic fidelity through CP110 degradation', *Nature*, 466: 138-42.

D'Arcy, P., X. Wang, and S. Linder. 2015. 'Deubiquitinase inhibition as a cancer therapeutic strategy', *Pharmacol Ther*, 147: 32-54.

D'Assoro, A. B., S. L. Barrett, C. Folk, V. C. Negron, K. Boeneman, R. Busby, C. Whitehead, F. Stivala, W. L. Lingle, and J. L. Salisbury. 2002. 'Amplified centrosomes in breast cancer: a potential indicator of tumor aggressiveness', *Breast Cancer Res Treat*, 75: 25-34.

D'Errico, M., E. de Rinaldis, M. F. Blasi, V. Viti, M. Falchetti, A. Calcagnile, F. Sera, C. Saieva, L. Ottini, D. Palli, F. Palombo, A. Giuliani, and E. Dogliotti. 2009. 'Genome-wide expression profile of sporadic gastric cancers with microsatellite instability', *Eur J Cancer*, 45: 461-9.

Dammer, E. B., C. H. Na, P. Xu, N. T. Seyfried, D. M. Duong, D. Cheng, M. Gearing, H. Rees, J. J. Lah, A. I. Levey, J. Rush, and J. Peng. 2011. 'Polyubiquitin linkage profiles in three models of proteolytic stress suggest the etiology of Alzheimer disease', *J Biol Chem*, 286: 10457-65.

de Vasconcellos, J. F., R. M. Fasano, Y. T. Lee, M. Kaushal, C. Byrnes, E. R. Meier, M. Anderson, A. Rabel, R. Braylan, D. F. Stroncek, and J. L. Miller. 2014. 'LIN28A expression reduces sickling of cultured human erythrocytes', *PLoS One*, 9: e106924.

DeGregori, J., T. Kowalik, and J. R. Nevins. 1995. 'Cellular targets for activation by the E2F1 transcription factor include DNA synthesis- and G1/S-regulatory genes', *Mol Cell Biol*, 15: 4215-24.

Deng, L., C. Wang, E. Spencer, L. Yang, A. Braun, J. You, C. Slaughter, C. Pickart, and Z. J. Chen. 2000. 'Activation of the IkappaB kinase complex by TRAF6 requires a dimeric ubiquitin-conjugating enzyme complex and a unique polyubiquitin chain', *Cell*, 103: 351-61.

Deveraux, Q., V. Ustrell, C. Pickart, and M. Rechsteiner. 1994. 'A 26 S protease subunit that binds ubiquitin conjugates', *J Biol Chem*, 269: 7059-61.

Dhananjayan, S. C., A. Ismail, and Z. Nawaz. 2005. 'Ubiquitin and control of transcription', *Essays Biochem*, 41: 69-80.

Di Fonzo, A., M. C. Dekker, P. Montagna, A. Baruzzi, E. H. Yonova, L. Correia Guedes, A. Szczerbinska, T. Zhao, L. O. Dubbel-Hulsman, C. H. Wouters, E. de Graaff, W. J. Oyen, E. J. Simons, G. J. Breedveld, B. A. Oostra, M. W. Horstink, and V. Bonifati. 2009. 'FBXO7 mutations cause autosomal recessive, early-onset parkinsonian-pyramidal syndrome', *Neurology*, 72: 240-5.

Dick, L. R., and P. E. Fleming. 2010. 'Building on bortezomib: second-generation proteasome inhibitors as anti-cancer therapy', *Drug Discov Today*, 15: 243-9.

Dimopoulos, M. A., S. Lonial, K. A. Betts, C. Chen, M. L. Zichlin, A. Brun, J. E. Signorovitch, D. Makenbaeva, S. Mekan, O. Sy, K. Weisel, and P. G. Richardson. 2018. 'Elotuzumab plus lenalidomide and dexamethasone in relapsed/refractory multiple myeloma: Extended 4-year follow-up and analysis of relative progression-free survival from the randomized ELOQUENT-2 trial', *Cancer*, 124: 4032-43.

Dimopoulos, M. A., A. Oriol, H. Nahi, J. San-Miguel, N. J. Bahlis, S. Z. Usmani, N. Rabin, R. Z. Orlowski, M. Komarnicki, K. Suzuki, T. Plesner, S. S. Yoon, D. Ben Yehuda, P. G. Richardson, H. Goldschmidt, D. Reece, S. Lisby, N. Z. Khokhar, L. O'Rourke, C. Chiu, X. Qin, M. Guckert, T. Ahmadi, and P. Moreau. 2016. 'Daratumumab, Lenalidomide, and Dexamethasone for Multiple Myeloma', *N Engl J Med*, 375: 1319-31.

Dou, Q. P., and J. A. Zonder. 2014. 'Overview of proteasome inhibitor-based anti-cancer therapies: perspective on bortezomib and second generation proteasome inhibitors versus future generation inhibitors of ubiquitin-proteasome system', *Curr Cancer Drug Targets*, 14: 517-36.

Doxsey, S. 2001. 'Re-evaluating centrosome function', *Nat Rev Mol Cell Biol*, 2: 688-98.

Drexler, H. C. 1997. 'Activation of the cell death program by inhibition of proteasome function', *Proc Natl Acad Sci U S A*, 94: 855-60.

Drexler, H. C., W. Risau, and M. A. Konerding. 2000. 'Inhibition of proteasome function induces programmed cell death in proliferating endothelial cells', *Faseb j*, 14: 65-77.

Durie, B. G., A. Hoering, M. H. Abidi, S. V. Rajkumar, J. Epstein, S. P. Kahanic, M. Thakuri, F. Reu, C. M. Reynolds, R. Sexton, R. Z. Orlowski, B. Barlogie, and A. Dispenzieri. 2017. 'Bortezomib with lenalidomide and dexamethasone versus lenalidomide and dexamethasone alone in patients with newly diagnosed myeloma without intent for immediate autologous stem-cell transplant (SWOG S0777): a randomised, open-label, phase 3 trial', *Lancet*, 389: 519-27.

Durie, B. G., and S. E. Salmon. 1975. 'A clinical staging system for multiple myeloma. Correlation of measured myeloma cell mass with presenting clinical features, response to treatment, and survival', *Cancer*, 36: 842-54.

Dzhindzhev, N. S., G. Tzolovsky, Z. Lipinszki, S. Schneider, R. Lattao, J. Fu, J. Debski, M. Dadlez, and D. M. Glover. 2014. 'Plk4 phosphorylates Ana2 to trigger Sas6 recruitment and procentriole formation', *Curr Biol*, 24: 2526-32.

Eilers, M., and R. N. Eisenman. 2008. 'Myc's broad reach', *Genes Dev*, 22: 2755-66.

Elbashir, S. M., J. Harborth, W. Lendeckel, A. Yalcin, K. Weber, and T. Tuschl. 2001. 'Duplexes of 21-nucleotide RNAs mediate RNA interference in cultured mammalian cells', *Nature*, 411: 494-8.

Elric, J., and S. Etienne-Manneville. 2014. 'Centrosome positioning in polarized cells: common themes and variations', *Exp Cell Res*, 328: 240-8.

Etienne-Manneville, S. 2013. 'Microtubules in cell migration', *Annu Rev Cell Dev Biol*, 29: 471-99.

Ezhevsky, S. A., A. Ho, M. Becker-Hapak, P. K. Davis, and S. F. Dowdy. 2001. 'Differential regulation of retinoblastoma tumor suppressor protein by G(1) cyclin-dependent kinase complexes in vivo', *Mol Cell Biol*, 21: 4773-84.

Facon, T., J. Y. Mary, C. Hulin, L. Benboubker, M. Attal, B. Pegourie, M. Renaud, J. L. Harousseau, G. Guillerm, C. Chaleteix, M. Dib, L. Voillat, H. Maisonneuve, J. Troncy, V. Dorvaux, M. Monconduit, C. Martin, P. Casassus, J. Jaubert, H. Jardel, C. Doyen, B. Kolb, B. Anglaret, B. Grosbois, I. Yakoub-Agha, C. Mathiot, and H. Avet-Loiseau. 2007. 'Melphalan and prednisone plus thalidomide versus melphalan and prednisone alone or reduced-intensity autologous stem cell transplantation in elderly patients with multiple myeloma (IFM 99-06): a randomised trial', *Lancet*, 370: 1209-18.

Faesen, A. C., M. P. Luna-Vargas, P. P. Geurink, M. Clerici, R. Merkx, W. J. van Dijk, D. S. Hameed, F. El Oualid, H. Ovaa, and T. K. Sixma. 2011. 'The differential modulation of USP activity by internal regulatory domains, interactors and eight ubiquitin chain types', *Chem Biol*, 18: 1550-61.

Fang, S., K. L. Lorick, J. P. Jensen, and A. M. Weissman. 2003. 'RING finger ubiquitin protein ligases: implications for tumorigenesis, metastasis and for molecular targets in cancer', *Semin Cancer Biol*, 13: 5-14.

Felgner, P. L., T. R. Gadek, M. Holm, R. Roman, H. W. Chan, M. Wenz, J. P. Northrop, G. M. Ringold, and M. Danielsen. 1987. 'Lipofection: a highly efficient, lipid-mediated DNA-transfection procedure', *Proc Natl Acad Sci U S A*, 84: 7413-7.

Fernandez, P. C., S. R. Frank, L. Wang, M. Schroeder, S. Liu, J. Greene, A. Cocito, and B. Amati. 2003. 'Genomic targets of the human c-Myc protein', *Genes Dev*, 17: 1115-29.

Finley, D. 2009. 'Recognition and processing of ubiquitin-protein conjugates by the proteasome', *Annu Rev Biochem*, 78: 477-513.

Fong, K. W., Y. K. Choi, J. B. Rattner, and R. Z. Qi. 2008. 'CDK5RAP2 is a pericentriolar protein that functions in centrosomal attachment of the gamma-tubulin ring complex', *Mol Biol Cell*, 19: 115-25.

Fonseca, R., R. J. Bailey, G. J. Ahmann, S. V. Rajkumar, J. D. Hoyer, J. A. Lust, R. A. Kyle, M. A. Gertz, P. R. Greipp, and G. W. Dewald. 2002. 'Genomic abnormalities in monoclonal gammopathy of undetermined significance', *Blood*, 100: 1417-24.

Franz, C. M., G. E. Jones, and A. J. Ridley. 2002. 'Cell migration in development and disease', *Dev Cell*, 2: 153-8.

Frescas, D., and M. Pagano. 2008. 'Deregulated proteolysis by the F-box proteins SKP2 and beta-TrCP: tipping the scales of cancer', *Nat Rev Cancer*, 8: 438-49.

Fritah, A., C. Saucier, J. Mester, G. Redeuilh, and M. Sabbah. 2005. 'p21WAF1/CIP1 selectively controls the transcriptional activity of estrogen receptor alpha', *Mol Cell Biol*, 25: 2419-30.

Fuchs, S. Y., A. Chen, Y. Xiong, Z. Q. Pan, and Z. Ronai. 1999. 'HOS, a human homolog of Slimb, forms an SCF complex with Skp1 and Cullin1 and targets the phosphorylation-dependent degradation of IkappaB and beta-catenin', *Oncogene*, 18: 2039-46.

Fujita, N., S. Sato, K. Katayama, and T. Tsuruo. 2002. 'Akt-dependent phosphorylation of p27Kip1 promotes binding to 14-3-3 and cytoplasmic localization', *J Biol Chem*, 277: 28706-13.

Fujita, N., S. Sato, and T. Tsuruo. 2003. 'Phosphorylation of p27Kip1 at threonine 198 by p90 ribosomal protein S6 kinases promotes its binding to 14-3-3 and cytoplasmic localization', *J Biol Chem*, 278: 49254-60.

Fukushima, H., K. Ogura, L. Wan, Y. Lu, V. Li, D. Gao, P. Liu, A. W. Lau, T. Wu, M. W. Kirschner, H. Inuzuka, and W. Wei. 2013. 'SCF-mediated Cdh1 degradation defines a negative feedback system that coordinates cell-cycle progression', *Cell Rep*, 4: 803-16.

Fung, E. 2017. 'Fbxl13 regulates centrosome homeostasis and migration through ubiquitin mediated proteolysis', PhD thesis, University of Oxford.

Ganem, N. J., S. A. Godinho, and D. Pellman. 2009. 'A mechanism linking extra centrosomes to chromosomal instability', *Nature*, 460: 278-82.

Geng, L., B. Zhu, B. H. Dai, C. J. Sui, F. Xu, T. Kan, W. F. Shen, and J. M. Yang. 2011. 'A let-7/Fas double-negative feedback loop regulates human colon carcinoma cells sensitivity to Fas-related apoptosis', *Biochem Biophys Res Commun*, 408: 494-9.

Giuliani, N., V. Rizzoli, and G. D. Roodman. 2006. 'Multiple myeloma bone disease: Pathophysiology of osteoblast inhibition', *Blood*, 108: 3992-6.

Glickman, M. H., D. M. Rubin, O. Coux, I. Wefes, G. Pfeifer, Z. Cjeka, W. Baumeister, V. A. Fried, and D. Finley. 1998. 'A subcomplex of the proteasome regulatory particle required for ubiquitin-conjugate degradation and related to the COP9-signalosome and eIF3', *Cell*, 94: 615-23.

Glitza, I. C., G. Lu, R. Shah, Q. Bashir, N. Shah, R. E. Champlin, J. Shah, R. Z. Orlowski, and M. H. Qazilbash. 2015. 'Chromosome 8q24.1/c-MYC abnormality: a marker for high-risk myeloma', *Leuk Lymphoma*, 56: 602-7.

Godinho, S. A., R. Picone, M. Burute, R. Dagher, Y. Su, C. T. Leung, K. Polyak, J. S. Brugge, M. Thery, and D. Pellman. 2014. 'Oncogene-like induction of cellular invasion from centrosome amplification', *Nature*, 510: 167-71.

Gomez-Ferreria, M. A., M. Bashkurov, A. O. Helbig, B. Larsen, T. Pawson, A. C. Gingras, and L. Pelletier. 2012. 'Novel NEDD1 phosphorylation sites regulate gamma-tubulin binding and mitotic spindle assembly', *J Cell Sci*, 125: 3745-51.

Gomez-Ferreria, M. A., U. Rath, D. W. Buster, S. K. Chanda, J. S. Caldwell, D. R. Rines, and D. J. Sharp. 2007. 'Human Cep192 is required for mitotic centrosome and spindle assembly', *Curr Biol*, 17: 1960-6.

Graham, F. L., and A. J. van der Eb. 1973. 'A new technique for the assay of infectivity of human adenovirus 5 DNA', *Virology*, 52: 456-67.

Graser, S., Y. D. Stierhof, S. B. Lavoie, O. S. Gassner, S. Lamla, M. Le Clech, and E. A. Nigg. 2007. 'Cep164, a novel centriole appendage protein required for primary cilium formation', *J Cell Biol*, 179: 321-30.

Greipp, P. R., J. San Miguel, B. G. Durie, J. J. Crowley, B. Barlogie, J. Blade, M. Boccadoro, J. A. Child, H. Avet-Loiseau, R. A. Kyle, J. J. Lahuerta, H. Ludwig, G. Morgan, R. Powles, K. Shimizu, C. Shustik, P. Sonneveld, P. Tosi, I. Turesson, and J. Westin. 2005. 'International staging system for multiple myeloma', *J Clin Oncol*, 23: 3412-20.

Groll, M., L. Ditzel, J. Lowe, D. Stock, M. Bochtler, H. D. Bartunik, and R. Huber. 1997. 'Structure of 20S proteasome from yeast at 2.4 A resolution', *Nature*, 386: 463-71.

Guderian, G., J. Westendorf, A. Uldschmid, and E. A. Nigg. 2010. 'Plk4 trans-autophosphorylation regulates centriole number by controlling betaTrCP-mediated degradation', *J Cell Sci*, 123: 2163-9.

Guo, Y., Y. Chen, H. Ito, A. Watanabe, X. Ge, T. Kodama, and H. Aburatani. 2006. 'Identification and characterization of lin-28 homolog B (LIN28B) in human hepatocellular carcinoma', *Gene*, 384: 51-61.

Habedanck, R., Y. D. Stierhof, C. J. Wilkinson, and E. A. Nigg. 2005. 'The Polo kinase Plk4 functions in centriole duplication', *Nat Cell Biol*, 7: 1140-6.

Hafner, M., K. E. Max, P. Bandaru, P. Morozov, S. Gerstberger, M. Brown, H. Molina, and T. Tuschl. 2013. 'Identification of mRNAs bound and regulated by human LIN28 proteins and molecular requirements for RNA recognition', *Rna*, 19: 613-26.

Hagan, J. P., E. Piskounova, and R. I. Gregory. 2009. 'Lin28 recruits the TUTase Zcchc11 to inhibit let-7 maturation in mouse embryonic stem cells', *Nat Struct Mol Biol*, 16: 1021-5.

Haglund, K., and I. Dikic. 2005. 'Ubiquitylation and cell signaling', *Embo j*, 24: 3353-9.

Hanamura, I., J. P. Stewart, Y. Huang, F. Zhan, M. Santra, J. R. Sawyer, K. Hollmig, M. Zangarri, M. Pineda-Roman, F. van Rhee, F. Cavallo, B. Burington, J. Crowley, G. Tricot, B. Barlogie, and J. D. Shaughnessy, Jr. 2006. 'Frequent gain of chromosome band 1q21 in plasma-cell dyscrasias detected by fluorescence in situ hybridization: incidence increases from MGUS to relapsed myeloma and is related to prognosis and disease progression following tandem stem-cell transplantation', *Blood*, 108: 1724-32.

Hanna, J., K. Saha, B. Pando, J. van Zon, C. J. Lengner, M. P. Creyghton, A. van Oudenaarden, and R. Jaenisch. 2009. 'Direct cell reprogramming is a stochastic process amenable to acceleration', *Nature*, 462: 595-601.

Hao, R., P. Nanduri, Y. Rao, R. S. Panichelli, A. Ito, M. Yoshida, and T. P. Yao. 2013. 'Proteasomes activate aggresome disassembly and clearance by producing unanchored ubiquitin chains', *Mol Cell*, 51: 819-28.

Harbour, J. W., R. X. Luo, A. Dei Santi, A. A. Postigo, and D. C. Dean. 1999. 'Cdk phosphorylation triggers sequential intramolecular interactions that progressively block Rb functions as cells move through G1', *Cell*, 98: 859-69.

Haren, L., T. Stearns, and J. Luders. 2009. 'Plk1-dependent recruitment of gamma-tubulin complexes to mitotic centrosomes involves multiple PCM components', *PLoS One*, 4: e5976.

Hata, A., and J. Lieberman. 2015. 'Dysregulation of microRNA biogenesis and gene silencing in cancer', *Sci Signal*, 8: re3.

He, J., K. Kulkarni, P. C. da Fonseca, D. Krutauz, M. H. Glickman, D. Barford, and E. P. Morris. 2012. 'The structure of the 26S proteasome subunit Rpn2 reveals its PC repeat domain as a closed toroid of two concentric alpha-helical rings', *Structure*, 20: 513-21.

Henry, K. W., A. Wyce, W. S. Lo, L. J. Duggan, N. C. Emre, C. F. Kao, L. Pillus, A. Shilatifard, M. A. Osley, and S. L. Berger. 2003. 'Transcriptional activation via sequential histone H2B ubiquitylation and deubiquitylation, mediated by SAGA-associated Ubp8', *Genes Dev*, 17: 2648-63.

Heo, I., C. Joo, J. Cho, M. Ha, J. Han, and V. N. Kim. 2008. 'Lin28 mediates the terminal uridylation of let-7 precursor MicroRNA', *Mol Cell*, 32: 276-84.

Heo, I., C. Joo, Y. K. Kim, M. Ha, M. J. Yoon, J. Cho, K. H. Yeom, J. Han, and V. N. Kim. 2009. 'TUT4 in concert with Lin28 suppresses microRNA biogenesis through pre-microRNA uridylation', *Cell*, 138: 696-708.

Herhaus, L., A. B. Perez-Oliva, G. Cozza, R. Gourlay, S. Weidlich, D. G. Campbell, L. A. Pinna, and G. P. Sapkota. 2015. 'Casein kinase 2 (CK2) phosphorylates the deubiquitylase OTUB1 at Ser16 to trigger its nuclear localization', *Sci Signal*, 8: ra35.

Hershko, A. 1999. 'Mechanisms and regulation of the degradation of cyclin B', *Philos Trans R Soc Lond B Biol Sci*, 354: 1571-5; discussion 75-6.

Hershko, A., and A. Ciechanover. 1998. 'The ubiquitin system', *Annu Rev Biochem*, 67: 425-79.

Hideshima, T., C. Mitsiades, G. Tonon, P. G. Richardson, and K. C. Anderson. 2007. 'Understanding multiple myeloma pathogenesis in the bone marrow to identify new therapeutic targets', *Nat Rev Cancer*, 7: 585-98.

Hinchcliffe, E. H., and G. Sluder. 2001. '"It takes two to tango": understanding how centrosome duplication is regulated throughout the cell cycle', *Genes Dev*, 15: 1167-81.

Hinds, P. W., S. Mittnacht, V. Dulic, A. Arnold, S. I. Reed, and R. A. Weinberg. 1992. 'Regulation of retinoblastoma protein functions by ectopic expression of human cyclins', *Cell*, 70: 993-1006.

Hobbs, G. A., C. J. Der, and K. L. Rossman. 2016. 'RAS isoforms and mutations in cancer at a glance', *J Cell Sci*, 129: 1287-92.

Hochegger, H., S. Takeda, and T. Hunt. 2008. 'Cyclin-dependent kinases and cell-cycle transitions: does one fit all?', *Nat Rev Mol Cell Biol*, 9: 910-6.

Hochstrasser, M. 2009. 'Origin and function of ubiquitin-like proteins', *Nature*, 458: 422-9.

Hoffman, B., and D. A. Liebermann. 2008. 'Apoptotic signaling by c-MYC', *Oncogene*, 27: 6462-72.

Holland, A. J., W. Lan, S. Niessen, H. Hoover, and D. W. Cleveland. 2010. 'Polo-like kinase 4 kinase activity limits centrosome overduplication by autoregulating its own stability', *J Cell Biol*, 188: 191-8.

Honda, R., E. D. Lowe, E. Dubinina, V. Skamnaki, A. Cook, N. R. Brown, and L. N. Johnson. 2005. 'The structure of cyclin E1/CDK2: implications for CDK2 activation and CDK2-independent roles', *Embo j*, 24: 452-63.

Huang, O. W., X. Ma, J. Yin, J. Flinders, T. Maurer, N. Kayagaki, Q. Phung, I. Bosanac, D. Arnott, V. M. Dixit, S. G. Hymowitz, M. A. Starovasnik, and A. G. Cochran. 2012. 'Phosphorylation-dependent activity of the deubiquitinase DUBA', *Nat Struct Mol Biol*, 19: 171-5.

Huang, T. T., and A. D. D'Andrea. 2006. 'Regulation of DNA repair by ubiquitylation', *Nat Rev Mol Cell Biol*, 7: 323-34.

Huang, X., M. Di Liberto, D. Jayabalan, J. Liang, S. Ely, J. Bretz, A. L. Shaffer, 3rd, T. Louie, I. Chen, S. Randolph, W. C. Hahn, L. M. Staudt, R. Niesvizky, M. A. Moore, and S. Chen-Kiang. 2012. 'Prolonged early G(1) arrest by selective CDK4/CDK6 inhibition sensitizes myeloma cells to cytotoxic killing through cell cycle-coupled loss of IRF4', *Blood*, 120: 1095-106.

Hurt, E. M., A. Wiestner, A. Rosenwald, A. L. Shaffer, E. Campo, T. Grogan, P. L. Bergsagel, W. M. Kuehl, and L. M. Staudt. 2004. 'Overexpression of c-maf is a frequent oncogenic event in multiple myeloma that promotes proliferation and pathological interactions with bone marrow stroma', *Cancer Cell*, 5: 191-9.

Husnjak, K., S. Elsasser, N. Zhang, X. Chen, L. Randles, Y. Shi, K. Hofmann, K. J. Walters, D. Finley, and I. Dikic. 2008. 'Proteasome subunit Rpn13 is a novel ubiquitin receptor', *Nature*, 453: 481-8.

Hutvagner, G., J. McLachlan, A. E. Pasquinelli, E. Balint, T. Tuschl, and P. D. Zamore. 2001. 'A cellular function for the RNA-interference enzyme Dicer in the maturation of the let-7 small temporal RNA', *Science*, 293: 834-8.

Jahan, A. S., M. Lestra, L. K. Swee, Y. Fan, M. M. Lamers, F. G. Tafesse, C. S. Theile, E. Spooner, R. Bruzzone, H. L. Ploegh, and S. Sanyal. 2016. 'Usp12 stabilizes the T-cell receptor complex at the cell surface during signaling', *Proc Natl Acad Sci U S A*, 113: E705-14.

Jiang, Y. H., and A. L. Beaudet. 2004. 'Human disorders of ubiquitination and proteasomal degradation', *Curr Opin Pediatr*, 16: 419-26.

Jin, J., T. Cardozo, R. C. Lovering, S. J. Elledge, M. Pagano, and J. W. Harper. 2004. 'Systematic analysis and nomenclature of mammalian F-box proteins', *Genes Dev*, 18: 2573-80.

Jin, L., A. Williamson, S. Banerjee, I. Philipp, and M. Rape. 2008. 'Mechanism of ubiquitin-chain formation by the human anaphase-promoting complex', *Cell*, 133: 653-65.

Johnson, C. D., A. Esquela-Kerscher, G. Stefani, M. Byrom, K. Kelnar, D. Ovcharenko, M. Wilson, X. Wang, J. Shelton, J. Shingara, L. Chin, D. Brown, and F. J. Slack. 2007. 'The let-7 microRNA represses cell proliferation pathways in human cells', *Cancer Res*, 67: 7713-22.

Johnson, S. M., H. Grosshans, J. Shingara, M. Byrom, R. Jarvis, A. Cheng, E. Labourier, K. L. Reinert, D. Brown, and F. J. Slack. 2005. 'RAS is regulated by the let-7 microRNA family', *Cell*, 120: 635-47.

Joukov, V., J. C. Walter, and A. De Nicolo. 2014. 'The Cep192-organized aurora A-Plk1 cascade is essential for centrosome cycle and bipolar spindle assembly', *Mol Cell*, 55: 578-91.

Jovanovic, K. K., C. Roche-Lestienne, I. M. Ghobrial, T. Facon, B. Quesnel, and S. Manier. 2018. 'Targeting MYC in multiple myeloma', *Leukemia*, 32: 1295-306.

Kaiser, S., Y. K. Park, J. L. Franklin, R. B. Halberg, M. Yu, W. J. Jessen, J. Freudenberg, X. Chen, K. Haigis, A. G. Jegga, S. Kong, B. Sakthivel, H. Xu, T. Reichling, M. Azhar, G. P. Boivin, R. B. Roberts, A. C. Bissahoyo, F. Gonzales, G. C. Bloom, S. Eschrich, S. L. Carter, J. E. Aronow, J. Kleimeyer, M. Kleimeyer, V. Ramaswamy, S. H. Settle, B. Boone, S. Levy, J. M. Graff, T. Doetschman, J. Groden, W. F. Dove, D. W. Threadgill, T. J. Yeatman, R. J. Coffey, Jr., and B. J. Aronow. 2007. 'Transcriptional recapitulation and subversion of embryonic colon development by mouse colon tumor models and human colon cancer', *Genome Biol*, 8: R131.

Kastan, M. B., and J. Bartek. 2004. 'Cell-cycle checkpoints and cancer', *Nature*, 432: 316-23.

Katsuno, Y., A. Suzuki, K. Sugimura, K. Okumura, D. H. Zineldeen, M. Shimada, H. Niida, T. Mizuno, F. Hanaoka, and M. Nakanishi. 2009. 'Cyclin A-Cdk1 regulates the origin firing program in mammalian cells', *Proc Natl Acad Sci U S A*, 106: 3184-9.

Keller, U. B., J. B. Old, F. C. Dorsey, J. A. Nilsson, L. Nilsson, K. H. MacLean, L. Chung, C. Yang, C. Spruck, K. Boyd, S. I. Reed, and J. L. Cleveland. 2007. 'Myc targets Cks1 to provoke the suppression of p27Kip1, proliferation and lymphomagenesis', *Embo j*, 26: 2562-74.

Kim, D. I., S. C. Jensen, K. A. Noble, B. Kc, K. H. Roux, K. Motamedchaboki, and K. J. Roux. 2016. 'An improved smaller biotin ligase for BioID proximity labeling', *Mol Biol Cell*, 27: 1188-96.

Kim, J. B., S. Y. Kim, B. M. Kim, H. Lee, I. Kim, J. Yun, Y. Jo, T. Oh, Y. Jo, H. D. Chae, and D. Y. Shin. 2013. 'Identification of a novel anti-apoptotic E3 ubiquitin ligase that ubiquitinates antagonists of inhibitor of apoptosis proteins SMAC, HtrA2, and ARTS', *J Biol Chem*, 288: 12014-21.

Kim, T. S., J. E. Park, A. Shukla, S. Choi, R. N. Murugan, J. H. Lee, M. Ahn, K. Rhee, J. K. Bang, B. Y. Kim, J. Loncarek, R. L. Erikson, and K. S. Lee. 2013. 'Hierarchical recruitment of Plk4 and regulation of centriole biogenesis by two centrosomal scaffolds, Cep192 and Cep152', *Proc Natl Acad Sci U S A*, 110: E4849-57.

Kim, V. N. 2004. 'MicroRNA precursors in motion: exportin-5 mediates their nuclear export', *Trends Cell Biol*, 14: 156-9.

Kim, V. N., J. Han, and M. C. Siomi. 2009. 'Biogenesis of small RNAs in animals', *Nat Rev Mol Cell Biol*, 10: 126-39.

Kim, W., E. J. Bennett, E. L. Huttlin, A. Guo, J. Li, A. Possemato, M. E. Sowa, R. Rad, J. Rush, M. J. Comb, J. W. Harper, and S. P. Gygi. 2011. 'Systematic and quantitative assessment of the ubiquitin-modified proteome', *Mol Cell*, 44: 325-40.

King, C. E., M. Cuatrecasas, A. Castells, A. R. Sepulveda, J. S. Lee, and A. K. Rustgi. 2011. 'LIN28B promotes colon cancer progression and metastasis', *Cancer Res*, 71: 4260-8.

Kingston, R. E., C. A. Chen, and J. K. Rose. 2003. 'Calcium phosphate transfection', *Curr Protoc Mol Biol*, Chapter 9: Unit 9.1.

Kinoshita, K., T. L. Noetzel, L. Pelletier, K. Mechtler, D. N. Drechsel, A. Schwager, M. Lee, J. W. Raff, and A. A. Hyman. 2005. 'Aurora A phosphorylation of TACC3/maskin is required for centrosome-dependent microtubule assembly in mitosis', *J Cell Biol*, 170: 1047-55.

Kirisako, T., K. Kamei, S. Murata, M. Kato, H. Fukumoto, M. Kanie, S. Sano, F. Tokunaga, K. Tanaka, and K. Iwai. 2006. 'A ubiquitin ligase complex assembles linear polyubiquitin chains', *Embo j*, 25: 4877-87.

Kisselev, A. F., T. N. Akopian, K. M. Woo, and A. L. Goldberg. 1999. 'The sizes of peptides generated from protein by mammalian 26 and 20 S proteasomes. Implications for understanding the degradative mechanism and antigen presentation', *J Biol Chem*, 274: 3363-71.

Kitagawa, D., I. Vakonakis, N. Olieric, M. Hilbert, D. Keller, V. Olieric, M. Bortfeld, M. C. Erat, I. Fluckiger, P. Gonczy, and M. O. Steinmetz. 2011. 'Structural basis of the 9-fold symmetry of centrioles', *Cell*, 144: 364-75.

Kitagawa, M., S. Hatakeyama, M. Shirane, M. Matsumoto, N. Ishida, K. Hattori, I. Nakamichi, A. Kikuchi, K. Nakayama, and K. Nakayama. 1999. 'An F-box protein, FWD1, mediates ubiquitin-dependent proteolysis of beta-catenin', *Embo j*, 18: 2401-10.

Koepp, D. M., L. K. Schaefer, X. Ye, K. Keyomarsi, C. Chu, J. W. Harper, and S. J. Elledge. 2001. 'Phosphorylation-dependent ubiquitination of cyclin E by the SCFFbw7 ubiquitin ligase', *Science*, 294: 173-7.

Komander, D., and M. Rape. 2012. 'The ubiquitin code', *Annu Rev Biochem*, 81: 203-29.

Komander, D., F. Reyes-Turcu, J. D. Licchesi, P. Odenwaelder, K. D. Wilkinson, and D. Barford. 2009. 'Molecular discrimination of structurally equivalent Lys 63-linked and linear polyubiquitin chains', *EMBO Rep*, 10: 466-73.

Kops, G. J., B. A. Weaver, and D. W. Cleveland. 2005. 'On the road to cancer: aneuploidy and the mitotic checkpoint', *Nat Rev Cancer*, 5: 773-85.

Koscielny, G., G. Yaikhom, V. Iyer, T. F. Meehan, H. Morgan, J. Atienza-Herrero, A. Blake, C. K. Chen, R. Easty, A. Di Fenza, T. Fiegel, M. Grifiths, A. Horne, N. A. Karp, N. Kurbatova, J. C. Mason, P. Matthews, D. J. Oakley, A. Qazi, J. Regnart, A. Retha, L. A. Santos, D. J. Sneddon, J. Warren, H. Westerberg, R. J. Wilson, D. G. Melvin, D. Smedley, S. D. Brown, P. Flicek, W. C. Skarnes, A. M. Mallon, and H. Parkinson. 2014. 'The International Mouse Phenotyping Consortium Web Portal, a unified point of access for knockout mice and related phenotyping data', *Nucleic Acids Res*, 42: D802-9.

Kossatz, U., J. Vervoorts, I. Nickeleit, H. A. Sundberg, J. S. Arthur, M. P. Manns, and N. P. Malek. 2006. 'C-terminal phosphorylation controls the stability and function of p27kip1', *Embo j*, 25: 5159-70.

Kuehl, W. M., and P. L. Bergsagel. 2002. 'Multiple myeloma: evolving genetic events and host interactions', *Nat Rev Cancer*, 2: 175-87.

Kuehl, W. M., and P. L. Bergsagel. 2012. 'MYC addiction: a potential therapeutic target in MM', *Blood*, 120: 2351-2.

Kumar, S. K., V. Rajkumar, R. A. Kyle, M. van Duin, P. Sonneveld, M. V. Mateos, F. Gay, and K. C. Anderson. 2017. 'Multiple myeloma', *Nat Rev Dis Primers*, 3: 17046.

Kushner, E. J., L. S. Ferro, J. Y. Liu, J. R. Durrant, S. L. Rogers, A. C. Dudley, and V. L. Bautch. 2014. 'Excess centrosomes disrupt endothelial cell migration via centrosome scattering', *J Cell Biol*, 206: 257-72.

Kyle, R. A., and S. V. Rajkumar. 1999. 'Monoclonal gammopathies of undetermined significance', *Hematol Oncol Clin North Am*, 13: 1181-202.

Kyle, R. A., and S. V. Rajkumar. 2009. 'Criteria for diagnosis, staging, risk stratification and response assessment of multiple myeloma', *Leukemia*, 23: 3-9.

Kyle, R. A., E. D. Remstein, T. M. Therneau, A. Dispenzieri, P. J. Kurtin, J. M. Hodnefield, D. R. Larson, M. F. Plevak, D. F. Jelinek, R. Fonseca, L. J. Melton, 3rd, and S. V. Rajkumar. 2007. 'Clinical course and prognosis of smoldering (asymptomatic) multiple myeloma', *N Engl J Med*, 356: 2582-90.

Lambrus, B. G., Y. Uetake, K. M. Clutario, V. Daggubati, M. Snyder, G. Sluder, and A. J. Holland. 2015. 'p53 protects against genome instability following centriole duplication failure', *J Cell Biol*, 210: 63-77.

Lara-Gonzalez, P., F. G. Westhorpe, and S. S. Taylor. 2012. 'The spindle assembly checkpoint', *Curr Biol*, 22: R966-80.

Lawo, S., M. Hasegan, G. D. Gupta, and L. Pelletier. 2012. 'Subdiffraction imaging of centrosomes reveals higher-order organizational features of pericentriolar material', *Nat Cell Biol*, 14: 1148-58.

Lee, K., and K. Rhee. 2011. 'PLK1 phosphorylation of pericentrin initiates centrosome maturation at the onset of mitosis', *J Cell Biol*, 195: 1093-101.

Lee, Y., C. Ahn, J. Han, H. Choi, J. Kim, J. Yim, J. Lee, P. Provost, O. Radmark, S. Kim, and V. N. Kim. 2003. 'The nuclear RNase III Drosha initiates microRNA processing', *Nature*, 425: 415-9.

Lee, Y., K. Jeon, J. T. Lee, S. Kim, and V. N. Kim. 2002. 'MicroRNA maturation: stepwise processing and subcellular localization', *Embo j*, 21: 4663-70.

Li, M., D. Chen, A. Shiloh, J. Luo, A. Y. Nikolaev, J. Qin, and W. Gu. 2002. 'Deubiquitination of p53 by HAUSP is an important pathway for p53 stabilization', *Nature*, 416: 648-53.

Liang, J., S. H. Shao, Z. X. Xu, B. Hennessy, Z. Ding, M. Larrea, S. Kondo, D. J. Dumont, J. U. Gutterman, C. L. Walker, J. M. Slingerland, and G. B. Mills. 2007. 'The energy sensing LKB1-AMPK pathway regulates p27(kip1) phosphorylation mediating the decision to enter autophagy or apoptosis', *Nat Cell Biol*, 9: 218-24.

Lin, Y. C., C. W. Chang, W. B. Hsu, C. J. Tang, Y. N. Lin, E. J. Chou, C. T. Wu, and T. K. Tang. 2013. 'Human microcephaly protein CEP135 binds to hSAS-6 and CPAP, and is required for centriole assembly', *Embo j*, 32: 1141-54.

Lingle, W. L., S. L. Barrett, V. C. Negron, A. B. D'Assoro, K. Boeneman, W. Liu, C. M. Whitehead, C. Reynolds, and J. L. Salisbury. 2002. 'Centrosome amplification drives chromosomal instability in breast tumor development', *Proc Natl Acad Sci U S A*, 99: 1978-83.

Livak, K. J., and T. D. Schmittgen. 2001. 'Analysis of relative gene expression data using real-time quantitative PCR and the 2(-Delta Delta C(T)) Method', *Methods*, 25: 402-8.

Loda, M., B. Cukor, S. W. Tam, P. Lavin, M. Fiorentino, G. F. Draetta, J. M. Jessup, and M. Pagano. 1997. 'Increased proteasome-dependent degradation of the cyclin-dependent kinase inhibitor p27 in aggressive colorectal carcinomas', *Nat Med*, 3: 231-4.

Loughlin, F. E., L. F. Gebert, H. Towbin, A. Brunschweiger, J. Hall, and F. H. Allain. 2011. 'Structural basis of pre-let-7 miRNA recognition by the zinc knuckles of pluripotency factor Lin28', *Nat Struct Mol Biol*, 19: 84-9.

Lowry, O. H., N. J. Rosebrough, A. L. Farr, and R. J. Randall. 1951. 'Protein measurement with the Folin phenol reagent', *J Biol Chem*, 193: 265-75.

Lundberg, A. S., and R. A. Weinberg. 1998. 'Functional inactivation of the retinoblastoma protein requires sequential modification by at least two distinct cyclin-cdk complexes', *Mol Cell Biol*, 18: 753-61.

Luxton, G. W., and G. G. Gundersen. 2011. 'Orientation and function of the nuclear-centrosomal axis during cell migration', *Curr Opin Cell Biol*, 23: 579-88.

Ma, X., C. Li, L. Sun, D. Huang, T. Li, X. He, G. Wu, Z. Yang, X. Zhong, L. Song, P. Gao, and H. Zhang. 2014. 'Lin28/let-7 axis regulates aerobic glycolysis and cancer progression via PDK1', *Nat Commun*, 5: 5212.

Malek, E., M. A. Abdel-Malek, S. Jagannathan, N. Vad, R. Karns, A. G. Jegga, A. Broyl, M. van Duin, P. Sonneveld, F. Cottini, K. C. Anderson, and J. J. Driscoll. 2017. 'Pharmacogenomics and chemical library screens reveal a novel SCF(SKP2) inhibitor that overcomes Bortezomib resistance in multiple myeloma', *Leukemia*, 31: 645-53.

Malumbres, M. 2014. 'Cyclin-dependent kinases', *Genome Biol*, 15: 122.

Malumbres, M., and M. Barbacid. 2001. 'To cycle or not to cycle: a critical decision in cancer', *Nat Rev Cancer*, 1: 222-31.

Malumbres, M., and M. Barbacid. 2009. 'Cell cycle, CDKs and cancer: a changing paradigm', *Nat Rev Cancer*, 9: 153-66.

Manier, S., J. T. Powers, A. Sacco, S. V. Glavey, D. Huynh, M. R. Reagan, K. Z. Salem, M. Moschetta, J. Shi, Y. Mishima, C. Roche-Lestienne, X. Leleu, A. M. Roccaro, G. Q. Daley, and I. M. Ghobrial. 2017. 'The LIN28B/let-7 axis is a novel therapeutic pathway in multiple myeloma', *Leukemia*, 31: 853-60.

Mao, J., J. Ladd, E. Gad, L. Rastetter, M. M. Johnson, E. Marzbani, J. S. Childs, H. Lu, Y. Dang, E. Broussard, S. E. Stanton, S. M. Hanash, and M. L. Disis. 2014. 'Mining the pre-diagnostic

antibody repertoire of TgMMTV-neu mice to identify autoantibodies useful for the early detection of human breast cancer', *J Transl Med*, 12: 121.

Martin, M., A. Veloso, J. Wu, E. A. Katrukha, and A. Akhmanova. 2018. 'Control of endothelial cell polarity and sprouting angiogenesis by non-centrosomal microtubules', *Elife*, 7.

Martinez, J., A. Patkaniowska, H. Urlaub, R. Luhrmann, and T. Tuschl. 2002. 'Single-stranded antisense siRNAs guide target RNA cleavage in RNAi', *Cell*, 110: 563-74.

Masdehors, P., S. Omura, H. Merle-Beral, F. Mentz, J. M. Cosset, J. Dumont, H. Magdelenat, and J. Delic. 1999. 'Increased sensitivity of CLL-derived lymphocytes to apoptotic death activation by the proteasome-specific inhibitor lactacystin', *Br J Haematol*, 105: 752-7.

Mateyak, M. K., A. J. Obaya, and J. M. Sedivy. 1999. 'c-Myc regulates cyclin D-Cdk4 and -Cdk6 activity but affects cell cycle progression at multiple independent points', *Mol Cell Biol*, 19: 4672-83.

Matsumoto, M. L., K. E. Wickliffe, K. C. Dong, C. Yu, I. Bosanac, D. Bustos, L. Phu, D. S. Kirkpatrick, S. G. Hymowitz, M. Rape, R. F. Kelley, and V. M. Dixit. 2010. 'K11-linked polyubiquitination in cell cycle control revealed by a K11 linkage-specific antibody', *Mol Cell*, 39: 477-84.

Mayr, C., M. T. Hemann, and D. P. Bartel. 2007. 'Disrupting the pairing between let-7 and Hmga2 enhances oncogenic transformation', *Science*, 315: 1576-9.

Mayr, F., A. Schutz, N. Doge, and U. Heinemann. 2012. 'The Lin28 cold-shock domain remodels pre-let-7 microRNA', *Nucleic Acids Res*, 40: 7492-506.

McCarthy, P. L., S. A. Holstein, M. T. Petrucci, P. G. Richardson, C. Hulin, P. Tosi, S. Bringhen, P. Musto, K. C. Anderson, D. Caillot, F. Gay, P. Moreau, G. Marit, S. H. Jung, Z. Yu, B. Winograd, R. D. Knight, A. Palumbo, and M. Attal. 2017. 'Lenalidomide Maintenance After Autologous Stem-Cell Transplantation in Newly Diagnosed Multiple Myeloma: A Meta-Analysis', *J Clin Oncol*, 35: 3279-89.

Mellacheruvu, D., Z. Wright, A. L. Couzens, J. P. Lambert, N. A. St-Denis, T. Li, Y. V. Miteva, S. Hauri, M. E. Sardiu, T. Y. Low, V. A. Halim, R. D. Bagshaw, N. C. Hubner, A. Al-Hakim, A. Bouchard, D. Faubert, D. Fermin, W. H. Dunham, M. Goudreault, Z. Y. Lin, B. G. Badillo, T. Pawson, D. Durocher, B. Coulombe, R. Aebersold, G. Superti-Furga, J. Colinge, A. J. Heck, H. Choi, M. Gstaiger, S. Mohammed, I. M. Cristea, K. L. Bennett, M. P. Washburn, B. Raught, R. M. Ewing, A. C. Gingras, and A. I. Nesvizhskii. 2013. 'The CRAPome: a contaminant repository for affinity purification-mass spectrometry data', *Nat Methods*, 10: 730-6.

Metzger, M. B., V. A. Hristova, and A. M. Weissman. 2012. 'HECT and RING finger families of E3 ubiquitin ligases at a glance', *J Cell Sci*, 125: 531-7.

Mevissen, T. E., M. K. Hospenthal, P. P. Geurink, P. R. Elliott, M. Akutsu, N. Arnaudo, R. Ekkebus, Y. Kulathu, T. Wauer, F. El Oualid, S. M. Freund, H. Ovaa, and D. Komander. 2013. 'OTU deubiquitinases reveal mechanisms of linkage specificity and enable ubiquitin chain restriction analysis', *Cell*, 154: 169-84.

Mevissen, T. E. T., and D. Komander. 2017. 'Mechanisms of Deubiquitinase Specificity and Regulation', *Annu Rev Biochem*, 86: 159-92.

Mittelman, M. 2003. 'The implications of anemia in multiple myeloma', *Clin Lymphoma*, 4 Suppl 1: S23-9.

Morita, K., and M. Han. 2006. 'Multiple mechanisms are involved in regulating the expression of the developmental timing regulator lin-28 in Caenorhabditis elegans', *Embo j*, 25: 5794-804.

Moritz, M., M. B. Braunfeld, J. W. Sedat, B. Alberts, and D. A. Agard. 1995. 'Microtubule nucleation by gamma-tubulin-containing rings in the centrosome', *Nature*, 378: 638-40.

Morris, E. J., and N. J. Dyson. 2001. 'Retinoblastoma protein partners', *Adv Cancer Res*, 82: 1-54.

Moser, S. C., D. Bensaddek, B. Ortmann, J. F. Maure, S. Mudie, J. J. Blow, A. I. Lamond, J. R. Swedlow, and S. Rocha. 2013. 'PHD1 links cell-cycle progression to oxygen sensing through hydroxylation of the centrosomal protein Cep192', *Dev Cell*, 26: 381-92.

Moss, E. G., R. C. Lee, and V. Ambros. 1997. 'The cold shock domain protein LIN-28 controls developmental timing in C. elegans and is regulated by the lin-4 RNA', *Cell*, 88: 637-46.

Moss, E. G., and L. Tang. 2003. 'Conservation of the heterochronic regulator Lin-28, its developmental expression and microRNA complementary sites', *Dev Biol*, 258: 432-42.

Mukhopadhyay, D., and H. Riezman. 2007. 'Proteasome-independent functions of ubiquitin in endocytosis and signaling', *Science*, 315: 201-5.

Mundy, G. R., L. G. Raisz, R. A. Cooper, G. P. Schechter, and S. E. Salmon. 1974. 'Evidence for the secretion of an osteoclast stimulating factor in myeloma', *N Engl J Med*, 291: 1041-6.

Munoz, D. M., P. J. Cassiani, L. Li, E. Billy, J. M. Korn, M. D. Jones, J. Golji, D. A. Ruddy, K. Yu, G. McAllister, A. DeWeck, D. Abramowski, J. Wan, M. D. Shirley, S. Y. Neshat, D. Rakiec, R. de Beaumont, O. Weber, A. Kauffmann, E. R. McDonald, 3rd, N. Keen, F. Hofmann, W. R. Sellers, T. Schmelzle, F. Stegmeier, and M. R. Schlabach. 2016. 'CRISPR Screens Provide a Comprehensive Assessment of Cancer Vulnerabilities but Generate False-Positive Hits for Highly Amplified Genomic Regions', *Cancer Discov*, 6: 900-13.

Nakayama, K. I., and K. Nakayama. 2005. 'Regulation of the cell cycle by SCF-type ubiquitin ligases', *Semin Cell Dev Biol*, 16: 323-33.

Nakayama, K. I., and K. Nakayama. 2006. 'Ubiquitin ligases: cell-cycle control and cancer', *Nat Rev Cancer*, 6: 369-81.

Nam, Y., C. Chen, R. I. Gregory, J. J. Chou, and P. Sliz. 2011. 'Molecular basis for interaction of let-7 microRNAs with Lin28', *Cell*, 147: 1080-91.

Naymagon, L., and M. Abdul-Hay. 2016. 'Novel agents in the treatment of multiple myeloma: a review about the future', *J Hematol Oncol*, 9: 52.

Neben, K., A. Jauch, T. Hielscher, J. Hillengass, N. Lehners, A. Seckinger, M. Granzow, M. S. Raab, A. D. Ho, H. Goldschmidt, and D. Hose. 2013. 'Progression in smoldering myeloma is independently determined by the chromosomal abnormalities del(17p), t(4;14), gain 1q, hyperdiploidy, and tumor load', *J Clin Oncol*, 31: 4325-32.

Newman, M. A., J. M. Thomson, and S. M. Hammond. 2008. 'Lin-28 interaction with the Let-7 precursor loop mediates regulated microRNA processing', *Rna*, 14: 1539-49.

Niesvizky, R., A. Z. Badros, L. J. Costa, S. A. Ely, S. B. Singhal, E. A. Stadtmauer, N. A. Haideri, A. Yacoub, G. Hess, S. Lentzsch, I. Spicka, A. A. Chanan-Khan, M. S. Raab, S. Tarantolo, R. Vij, J. A. Zonder, X. Huang, D. Jayabalan, M. Di Liberto, X. Huang, Y. Jiang, S. T. Kim, S. Randolph, and S. Chen-Kiang. 2015. 'Phase 1/2 study of cyclin-dependent kinase (CDK)4/6 inhibitor palbociclib (PD-0332991) with bortezomib and dexamethasone in relapsed/refractory multiple myeloma', *Leuk Lymphoma*, 56: 3320-8.

Nigg, E. A. 2002. 'Centrosome aberrations: cause or consequence of cancer progression?', *Nat Rev Cancer*, 2: 815-25.

Noble, C. G., and H. Song. 2007. 'MLN51 stimulates the RNA-helicase activity of eIF4AIII', *PLoS One*, 2: e303.

Novak, B., O. Kapuy, M. R. Domingo-Sananes, and J. J. Tyson. 2010. 'Regulated protein kinases and phosphatases in cell cycle decisions', *Curr Opin Cell Biol*, 22: 801-8.

Nutt, S. L., P. D. Hodgkin, D. M. Tarlinton, and L. M. Corcoran. 2015. 'The generation of antibody-secreting plasma cells', *Nat Rev Immunol*, 15: 160-71.

O'Connor, B. P., M. W. Gleeson, R. J. Noelle, and L. D. Erickson. 2003. 'The rise and fall of long-lived humoral immunity: terminal differentiation of plasma cells in health and disease', *Immunol Rev*, 194: 61-76.

O'Rourke, B. P., M. A. Gomez-Ferreria, R. H. Berk, A. M. Hackl, M. P. Nicholas, S. C. O'Rourke, L. Pelletier, and D. J. Sharp. 2014. 'Cep192 controls the balance of centrosome and non-centrosomal microtubules during interphase', *PLoS One*, 9: e101001.

Ohta, M., T. Ashikawa, Y. Nozaki, H. Kozuka-Hata, H. Goto, M. Inagaki, M. Oyama, and D. Kitagawa. 2014. 'Direct interaction of Plk4 with STIL ensures formation of a single procentriole per parental centriole', *Nat Commun*, 5: 5267.

Okazuka, K., and T. Ishida. 2018. 'Proteasome inhibitors for multiple myeloma', *Jpn J Clin Oncol*, 48: 785-93.

Oranger, A., C. Carbone, M. Izzo, and M. Grano. 2013. 'Cellular mechanisms of multiple myeloma bone disease', *Clin Dev Immunol*, 2013: 289458.

Ortega, S., M. Malumbres, and M. Barbacid. 2002. 'Cyclin D-dependent kinases, INK4 inhibitors and cancer', *Biochim Biophys Acta*, 1602: 73-87.

Otto, T., and P. Sicinski. 2017. 'Cell cycle proteins as promising targets in cancer therapy', *Nat Rev Cancer*, 17: 93-115.

Pagano, M., R. Pepperkok, F. Verde, W. Ansorge, and G. Draetta. 1992. 'Cyclin A is required at two points in the human cell cycle', *Embo j*, 11: 961-71.

Paintrand, M., M. Moudjou, H. Delacroix, and M. Bornens. 1992. 'Centrosome organization and centriole architecture: their sensitivity to divalent cations', *J Struct Biol*, 108: 107-28.

Palazzo, R. E., J. M. Vogel, B. J. Schnackenberg, D. R. Hull, and X. Wu. 2000. 'Centrosome maturation', *Curr Top Dev Biol*, 49: 449-70.

Palumbo, A., H. Avet-Loiseau, S. Oliva, H. M. Lokhorst, H. Goldschmidt, L. Rosinol, P. Richardson, S. Caltagirone, J. J. Lahuerta, T. Facon, S. Bringhen, F. Gay, M. Attal, R. Passera, A. Spencer, M. Offidani, S. Kumar, P. Musto, S. Lonial, M. T. Petrucci, R. Z. Orlowski, E. Zamagni, G. Morgan, M. A. Dimopoulos, B. G. Durie, K. C. Anderson, P. Sonneveld, J. San Miguel, M. Cavo, S. V. Rajkumar, and P. Moreau. 2015. 'Revised International Staging System for Multiple Myeloma: A Report From International Myeloma Working Group', *J Clin Oncol*, 33: 2863-9.

Palumbo, A., S. Bringhen, T. Caravita, E. Merla, V. Capparella, V. Callea, C. Cangialosi, M. Grasso, F. Rossini, M. Galli, L. Catalano, E. Zamagni, M. T. Petrucci, V. De Stefano, M. Ceccarelli, M. T. Ambrosini, I. Avonto, P. Falco, G. Ciccone, A. M. Liberati, P. Musto, and M. Boccadoro. 2006. 'Oral melphalan and prednisone chemotherapy plus thalidomide compared with melphalan and prednisone alone in elderly patients with multiple myeloma: randomised controlled trial', *Lancet*, 367: 825-31.

Palumbo, A., A. Chanan-Khan, K. Weisel, A. K. Nooka, T. Masszi, M. Beksac, I. Spicka, V. Hungria, M. Munder, M. V. Mateos, T. M. Mark, M. Qi, J. Schecter, H. Amin, X. Qin, W. Deraedt, T. Ahmadi, A. Spencer, and P. Sonneveld. 2016. 'Daratumumab, Bortezomib, and Dexamethasone for Multiple Myeloma', *N Engl J Med*, 375: 754-66.

Pasquinelli, A. E., B. J. Reinhart, F. Slack, M. Q. Martindale, M. I. Kuroda, B. Maller, D. C. Hayward, E. E. Ball, B. Degnan, P. Muller, J. Spring, A. Srinivasan, M. Fishman, J. Finnerty, J. Corbo, M. Levine, P. Leahy, E. Davidson, and G. Ruvkun. 2000. 'Conservation of the sequence and temporal expression of let-7 heterochronic regulatory RNA', *Nature*, 408: 86-9.

Paulsen, R. D., D. V. Soni, R. Wollman, A. T. Hahn, M. C. Yee, A. Guan, J. A. Hesley, S. C. Miller, E. F. Cromwell, D. E. Solow-Cordero, T. Meyer, and K. A. Cimprich. 2009. 'A genome-wide siRNA screen reveals diverse cellular processes and pathways that mediate genome stability', *Mol Cell*, 35: 228-39.

Pazour, G. J., and G. B. Witman. 2003. 'The vertebrate primary cilium is a sensory organelle', *Curr Opin Cell Biol*, 15: 105-10.

Petrie, R. J., A. D. Doyle, and K. M. Yamada. 2009. 'Random versus directionally persistent cell migration', *Nat Rev Mol Cell Biol*, 10: 538-49.

Petroski, M. D., and R. J. Deshaies. 2005. 'Function and regulation of cullin-RING ubiquitin ligases', *Nat Rev Mol Cell Biol*, 6: 9-20.

Piel, M., P. Meyer, A. Khodjakov, C. L. Rieder, and M. Bornens. 2000. 'The respective contributions of the mother and daughter centrioles to centrosome activity and behavior in vertebrate cells', *J Cell Biol*, 149: 317-30.

Pihan, G. A., A. Purohit, J. Wallace, R. Malhotra, L. Liotta, and S. J. Doxsey. 2001. 'Centrosome defects can account for cellular and genetic changes that characterize prostate cancer progression', *Cancer Res*, 61: 2212-9.

Piskounova, E., C. Polytarchou, J. E. Thornton, R. J. LaPierre, C. Pothoulakis, J. P. Hagan, D. Iliopoulos, and R. I. Gregory. 2011. 'Lin28A and Lin28B inhibit let-7 microRNA biogenesis by distinct mechanisms', *Cell*, 147: 1066-79.

Podar, K., Y. T. Tai, F. E. Davies, S. Lentzsch, M. Sattler, T. Hideshima, B. K. Lin, D. Gupta, Y. Shima, D. Chauhan, C. Mitsiades, N. Raje, P. Richardson, and K. C. Anderson. 2001. 'Vascular endothelial growth factor triggers signaling cascades mediating multiple myeloma cell growth and migration', *Blood*, 98: 428-35.

Podar, K., Y. T. Tai, B. K. Lin, R. P. Narsimhan, M. Sattler, T. Kijima, R. Salgia, D. Gupta, D. Chauhan, and K. C. Anderson. 2002. 'Vascular endothelial growth factor-induced migration of multiple myeloma cells is associated with beta 1 integrin- and phosphatidylinositol 3-kinase-dependent PKC alpha activation', *J Biol Chem*, 277: 7875-81.

Polesskaya, A., S. Cuvellier, I. Naguibneva, A. Duquet, E. G. Moss, and A. Harel-Bellan. 2007. 'Lin-28 binds IGF-2 mRNA and participates in skeletal myogenesis by increasing translation efficiency', *Genes Dev*, 21: 1125-38.

Polyak, K., J. Y. Kato, M. J. Solomon, C. J. Sherr, J. Massague, J. M. Roberts, and A. Koff. 1994. 'p27Kip1, a cyclin-Cdk inhibitor, links transforming growth factor-beta and contact inhibition to cell cycle arrest', *Genes Dev*, 8: 9-22.

Porter, P. L., K. E. Malone, P. J. Heagerty, G. M. Alexander, L. A. Gatti, E. J. Firpo, J. R. Daling, and J. M. Roberts. 1997. 'Expression of cell-cycle regulators p27Kip1 and cyclin E, alone and in combination, correlate with survival in young breast cancer patients', *Nat Med*, 3: 222-5.

Prochownik, E. V. 2008. 'c-Myc: linking transformation and genomic instability', *Curr Mol Med*, 8: 446-58.

Qin, R., J. Zhou, C. Chen, T. Xu, Y. Yan, Y. Ma, Z. Zheng, Y. Shen, Y. Lu, D. Fu, and J. Chen. 2014. 'LIN28 is involved in glioma carcinogenesis and predicts outcomes of glioblastoma multiforme patients', *PLoS One*, 9: e86446.

Raducu, M., E. Fung, S. Serres, P. Infante, A. Barberis, R. Fischer, C. Bristow, M. L. Thezenas, C. Finta, J. C. Christianson, F. M. Buffa, B. M. Kessler, N. R. Sibson, L. Di Marcotullio, R. Toftgard, and V. D'Angiolella. 2016. 'SCF (Fbxl17) ubiquitylation of Sufu regulates Hedgehog signaling and medulloblastoma development', *Embo j*, 35: 1400-16.

Rahighi, S., F. Ikeda, M. Kawasaki, M. Akutsu, N. Suzuki, R. Kato, T. Kensche, T. Uejima, S. Bloor, D. Komander, F. Randow, S. Wakatsuki, and I. Dikic. 2009. 'Specific recognition of linear ubiquitin chains by NEMO is important for NF-kappaB activation', *Cell*, 136: 1098-109.

Rajan, A. M., and S. V. Rajkumar. 2015. 'Interpretation of cytogenetic results in multiple myeloma for clinical practice', *Blood Cancer J*, 5: e365.

Rajkumar, S. V., M. A. Dimopoulos, A. Palumbo, J. Blade, G. Merlini, M. V. Mateos, S. Kumar, J. Hillengass, E. Kastritis, P. Richardson, O. Landgren, B. Paiva, A. Dispenzieri, B. Weiss, X. LeLeu, S. Zweegman, S. Lonial, L. Rosinol, E. Zamagni, S. Jagannath, O. Sezer, S. Y. Kristinsson, J. Caers, S. Z. Usmani, J. J. Lahuerta, H. E. Johnsen, M. Beksac, M. Cavo, H. Goldschmidt, E. Terpos, R. A. Kyle, K. C. Anderson, B. G. Durie, and J. F. Miguel. 2014. 'International Myeloma Working Group updated criteria for the diagnosis of multiple myeloma', *Lancet Oncol*, 15: e538-48.

Rajkumar, S. V., V. Gupta, R. Fonseca, A. Dispenzieri, W. I. Gonsalves, D. Larson, R. P. Ketterling, J. A. Lust, R. A. Kyle, and S. K. Kumar. 2013. 'Impact of primary molecular cytogenetic abnormalities and risk of progression in smoldering multiple myeloma', *Leukemia*, 27: 1738-44.

Rajkumar, S. V., and S. Kumar. 2016. 'Multiple Myeloma: Diagnosis and Treatment', *Mayo Clin Proc*, 91: 101-19.

Ravid, T., and M. Hochstrasser. 2008. 'Diversity of degradation signals in the ubiquitin-proteasome system', *Nat Rev Mol Cell Biol*, 9: 679-90.

Regelink, J. C., M. C. Minnema, E. Terpos, M. H. Kamphuis, P. G. Raijmakers, I. C. Pieters-van den Bos, B. G. Heggelman, R. J. Nievelstein, R. H. Otten, D. van Lammeren-Venema, J. M. Zijlstra, A. I. Arens, J. W. de Rooy, O. S. Hoekstra, R. Raymakers, P. Sonneveld, R. W. Ostelo, and S. Zweegman. 2013. 'Comparison of modern and conventional imaging techniques in establishing multiple myeloma-related bone disease: a systematic review', *Br J Haematol*, 162: 50-61.

Reinhart, B. J., F. J. Slack, M. Basson, A. E. Pasquinelli, J. C. Bettinger, A. E. Rougvie, H. R. Horvitz, and G. Ruvkun. 2000. 'The 21-nucleotide let-7 RNA regulates developmental timing in Caenorhabditis elegans', *Nature*, 403: 901-6.

Reyes-Turcu, F. E., K. H. Ventii, and K. D. Wilkinson. 2009. 'Regulation and cellular roles of ubiquitin-specific deubiquitinating enzymes', *Annu Rev Biochem*, 78: 363-97.

Richards, M., S. P. Tan, J. H. Tan, W. K. Chan, and A. Bongso. 2004. 'The transcriptome profile of human embryonic stem cells as defined by SAGE', *Stem Cells*, 22: 51-64.

Richardson, A. L., Z. C. Wang, A. De Nicolo, X. Lu, M. Brown, A. Miron, X. Liao, J. D. Iglehart, D. M. Livingston, and S. Ganesan. 2006. 'X chromosomal abnormalities in basal-like human breast cancer', *Cancer Cell*, 9: 121-32.

Ritorto, M. S., R. Ewan, A. B. Perez-Oliva, A. Knebel, S. J. Buhrlage, M. Wightman, S. M. Kelly, N. T. Wood, S. Virdee, N. S. Gray, N. A. Morrice, D. R. Alessi, and M. Trost. 2014. 'Screening of DUB activity and specificity by MALDI-TOF mass spectrometry', *Nat Commun*, 5: 4763.

Roodman, G. D. 2009. 'Pathogenesis of myeloma bone disease', *Leukemia*, 23: 435-41.

Roux, K. J., D. I. Kim, M. Raida, and B. Burke. 2012. 'A promiscuous biotin ligase fusion protein identifies proximal and interacting proteins in mammalian cells', *J Cell Biol*, 196: 801-10.

Rybak, A., H. Fuchs, L. Smirnova, C. Brandt, E. E. Pohl, R. Nitsch, and F. G. Wulczyn. 2008. 'A feedback loop comprising lin-28 and let-7 controls pre-let-7 maturation during neural stem-cell commitment', *Nat Cell Biol*, 10: 987-93.

Saeki, Y., and K. Tanaka. 2012. 'Assembly and function of the proteasome', *Methods Mol Biol*, 832: 315-37.

Sahtoe, D. D., and T. K. Sixma. 2015. 'Layers of DUB regulation', *Trends Biochem Sci*, 40: 456-67.

Sampson, V. B., N. H. Rong, J. Han, Q. Yang, V. Aris, P. Soteropoulos, N. J. Petrelli, S. P. Dunn, and L. J. Krueger. 2007. 'MicroRNA let-7a down-regulates MYC and reverts MYC-induced growth in Burkitt lymphoma cells', *Cancer Res*, 67: 9762-70.

San Miguel, J. F., R. Schlag, N. K. Khuageva, M. A. Dimopoulos, O. Shpilberg, M. Kropff, I. Spicka, M. T. Petrucci, A. Palumbo, O. S. Samoilova, A. Dmoszynska, K. M. Abdulkadyrov, R. Schots, B. Jiang, M. V. Mateos, K. C. Anderson, D. L. Esseltine, K. Liu, A. Cakana, H. van de Velde, and P.

G. Richardson. 2008. 'Bortezomib plus melphalan and prednisone for initial treatment of multiple myeloma', *N Engl J Med*, 359: 906-17.

Sanjana, N. E., O. Shalem, and F. Zhang. 2014. 'Improved vectors and genome-wide libraries for CRISPR screening', *Nat Methods*, 11: 783-84.

Santiago-Sim, T., L. C. Burrage, F. Ebstein, M. J. Tokita, M. Miller, W. Bi, A. A. Braxton, J. A. Rosenfeld, M. Shahrour, A. Lehmann, B. Cogne, S. Kury, T. Besnard, B. Isidor, S. Bezieau, I. Hazart, H. Nagakura, L. L. Immken, R. O. Littlejohn, E. Roeder, B. Kara, K. Hardies, S. Weckhuysen, P. May, J. R. Lemke, O. Elpeleg, B. Abu-Libdeh, K. N. James, J. L. Silhavy, M. Y. Issa, M. S. Zaki, J. G. Gleeson, J. R. Seavitt, M. E. Dickinson, M. C. Ljungberg, S. Wells, S. J. Johnson, L. Teboul, C. M. Eng, Y. Yang, P. M. Kloetzel, J. D. Heaney, and M. A. Walkiewicz. 2017. 'Biallelic Variants in OTUD6B Cause an Intellectual Disability Syndrome Associated with Seizures and Dysmorphic Features', *Am J Hum Genet*, 100: 676-88.

Sauer, R. T., D. N. Bolon, B. M. Burton, R. E. Burton, J. M. Flynn, R. A. Grant, G. L. Hersch, S. A. Joshi, J. A. Kenniston, I. Levchenko, S. B. Neher, E. S. Oakes, S. M. Siddiqui, D. A. Wah, and T. A. Baker. 2004. 'Sculpting the proteome with AAA(+) proteases and disassembly machines', *Cell*, 119: 9-18.

Savic, D., E. C. Partridge, K. M. Newberry, S. B. Smith, S. K. Meadows, B. S. Roberts, M. Mackiewicz, E. M. Mendenhall, and R. M. Myers. 2015. 'CETCh-seq: CRISPR epitope tagging ChIP-seq of DNA-binding proteins', *Genome Res*, 25: 1581-9.

Scheffner, M., U. Nuber, and J. M. Huibregtse. 1995. 'Protein ubiquitination involving an E1-E2-E3 enzyme ubiquitin thioester cascade', *Nature*, 373: 81-3.

Scheuermann, J. C., A. G. de Ayala Alonso, K. Oktaba, N. Ly-Hartig, R. K. McGinty, S. Fraterman, M. Wilm, T. W. Muir, and J. Muller. 2010. 'Histone H2A deubiquitinase activity of the Polycomb repressive complex PR-DUB', *Nature*, 465: 243-7.

Schnerch, D., and E. A. Nigg. 2016. 'Structural centrosome aberrations favor proliferation by abrogating microtubule-dependent tissue integrity of breast epithelial mammospheres', *Oncogene*, 35: 2711-22.

Schockel, L., M. Mockel, B. Mayer, D. Boos, and O. Stemmann. 2011. 'Cleavage of cohesin rings coordinates the separation of centrioles and chromatids', *Nat Cell Biol*, 13: 966-72.

Schulman, B. A., and J. W. Harper. 2009. 'Ubiquitin-like protein activation by E1 enzymes: the apex for downstream signalling pathways', *Nat Rev Mol Cell Biol*, 10: 319-31.

Schulz, S., G. Chachami, L. Kozaczkiewicz, U. Winter, N. Stankovic-Valentin, P. Haas, K. Hofmann, H. Urlaub, H. Ovaa, J. Wittbrodt, E. Meulmeester, and F. Melchior. 2012. 'Ubiquitin-specific protease-like 1 (USPL1) is a SUMO isopeptidase with essential, non-catalytic functions', *EMBO Rep*, 13: 930-8.

Sdelci, S., M. Schutz, R. Pinyol, M. T. Bertran, L. Regue, C. Caelles, I. Vernos, and J. Roig. 2012. 'Nek9 phosphorylation of NEDD1/GCP-WD contributes to Plk1 control of gamma-tubulin recruitment to the mitotic centrosome', *Curr Biol*, 22: 1516-23.

Sears, R., G. Leone, J. DeGregori, and J. R. Nevins. 1999. 'Ras enhances Myc protein stability', *Mol Cell*, 3: 169-79.

Sears, R., F. Nuckolls, E. Haura, Y. Taya, K. Tamai, and J. R. Nevins. 2000. 'Multiple Ras-dependent phosphorylation pathways regulate Myc protein stability', *Genes Dev*, 14: 2501-14.

Segalla, S., S. Pivetti, K. Todoerti, M. A. Chudzik, E. C. Giuliani, F. Lazzaro, V. Volta, D. Lazarevic, G. Musco, M. Muzi-Falconi, A. Neri, S. Biffo, and G. Tonon. 2015. 'The ribonuclease DIS3 promotes let-7 miRNA maturation by degrading the pluripotency factor LIN28B mRNA', *Nucleic Acids Res*, 43: 5182-93.

Shalem, O., N. E. Sanjana, E. Hartenian, X. Shi, D. A. Scott, T. Mikkelson, D. Heckl, B. L. Ebert, D. E. Root, J. G. Doench, and F. Zhang. 2014. 'Genome-scale CRISPR-Cas9 knockout screening in human cells', *Science*, 343: 84-87.

Sheaff, R. J., M. Groudine, M. Gordon, J. M. Roberts, and B. E. Clurman. 1997. 'Cyclin E-CDK2 is a regulator of p27Kip1', *Genes Dev*, 11: 1464-78.

Shen, M., S. Schmitt, D. Buac, and Q. P. Dou. 2013. 'Targeting the ubiquitin-proteasome system for cancer therapy', *Expert Opin Ther Targets*, 17: 1091-108.

Sherr, C. J., and J. M. Roberts. 2004. 'Living with or without cyclins and cyclin-dependent kinases', *Genes Dev*, 18: 2699-711.

Shi, Y., X. Chen, S. Elsasser, B. B. Stocks, G. Tian, B. H. Lee, Y. Shi, N. Zhang, S. A. de Poot, F. Tuebing, S. Sun, J. Vannoy, S. G. Tarasov, J. R. Engen, D. Finley, and K. J. Walters. 2016. 'Rpn1 provides adjacent receptor sites for substrate binding and deubiquitination by the proteasome', *Science*, 351.

Shinoda, G., N. Shyh-Chang, T. Y. Soysa, H. Zhu, M. T. Seligson, S. P. Shah, N. Abo-Sido, A. Yabuuchi, J. P. Hagan, R. I. Gregory, J. M. Asara, L. C. Cantley, E. G. Moss, and G. Q. Daley. 2013. 'Fetal deficiency of lin28 programs life-long aberrations in growth and glucose metabolism', *Stem Cells*, 31: 1563-73.

Shirane, M., S. Hatakeyama, K. Hattori, K. Nakayama, and K. Nakayama. 1999. 'Common pathway for the ubiquitination of IkappaBalpha, IkappaBbeta, and IkappaBepsilon mediated by the F-box protein FWD1', *J Biol Chem*, 274: 28169-74.

Shyh-Chang, N., and G. Q. Daley. 2013. 'Lin28: primal regulator of growth and metabolism in stem cells', *Cell Stem Cell*, 12: 395-406.

Siegel, R. L., K. D. Miller, and A. Jemal. 2016. 'Cancer statistics, 2016', *CA Cancer J Clin*, 66: 7-30.

Skaar, J. R., J. K. Pagan, and M. Pagano. 2013. 'Mechanisms and function of substrate recruitment by F-box proteins', *Nat Rev Mol Cell Biol*, 14: 369-81.

Sobol, A., C. Askonas, S. Alani, M. J. Weber, V. Ananthanarayanan, C. Osipo, and M. Bocchetta. 2017. 'Deubiquitinase OTUD6B Isoforms Are Important Regulators of Growth and Proliferation', *Mol Cancer Res*, 15: 117-27.

Song, A., J. Ye, K. Zhang, L. Sun, Y. Zhao, and H. Yu. 2013. 'Lentiviral vector-mediated siRNA knockdown of c-MYC: cell growth inhibition and cell cycle arrest at G2/M phase in Jijoye cells', *Biochem Genet*, 51: 603-17.

Sonnen, K. F., A. M. Gabryjonczyk, E. Anselm, Y. D. Stierhof, and E. A. Nigg. 2013. 'Human Cep192 and Cep152 cooperate in Plk4 recruitment and centriole duplication', *J Cell Sci*, 126: 3223-33.

Sonnen, K. F., L. Schermelleh, H. Leonhardt, and E. A. Nigg. 2012. '3D-structured illumination microscopy provides novel insight into architecture of human centrosomes', *Biol Open*, 1: 965-76.

Sonneveld, P., I. G. Schmidt-Wolf, B. van der Holt, L. El Jarari, U. Bertsch, H. Salwender, S. Zweegman, E. Vellenga, A. Broyl, I. W. Blau, K. C. Weisel, S. Wittebol, G. M. Bos, M. Stevens-Kroef, C. Scheid, M. Pfreundschuh, D. Hose, A. Jauch, H. van der Velde, R. Raymakers, M. R. Schaafsma, M. J. Kersten, M. van Marwijk-Kooy, U. Duehrsen, W. Lindemann, P. W. Wijermans, H. M. Lokhorst, and H. M. Goldschmidt. 2012. 'Bortezomib induction and maintenance treatment in patients with newly diagnosed multiple myeloma: results of the randomized phase III HOVON-65/ GMMG-HD4 trial', *J Clin Oncol*, 30: 2946-55.

Sowa, M. E., E. J. Bennett, S. P. Gygi, and J. W. Harper. 2009. 'Defining the human deubiquitinating enzyme interaction landscape', *Cell*, 138: 389-403.

Stewart, M. D., T. Ritterhoff, R. E. Klevit, and P. S. Brzovic. 2016. 'E2 enzymes: more than just middle men', *Cell Res*, 26: 423-40.

Stone, M., R. Hartmann-Petersen, M. Seeger, D. Bech-Otschir, M. Wallace, and C. Gordon. 2004. 'Uch2/Uch37 is the major deubiquitinating enzyme associated with the 26S proteasome in fission yeast', *J Mol Biol*, 344: 697-706.

Straniero, L., V. Rimoldi, G. Solda, M. Bellini, G. Biasucci, R. Asselta, and S. Duga. 2018. 'First Replication of the Involvement of OTUD6B in Intellectual Disability Syndrome With Seizures and Dysmorphic Features', *Front Genet*, 9: 464.

Sutterluty, H., E. Chatelain, A. Marti, C. Wirbelauer, M. Senften, U. Muller, and W. Krek. 1999. 'p45SKP2 promotes p27Kip1 degradation and induces S phase in quiescent cells', *Nat Cell Biol*, 1: 207-14.

Swatek, K. N., and D. Komander. 2016. 'Ubiquitin modifications', *Cell Res*, 26: 399-422.

Takashima, K., H. Oshiumi, H. Takaki, M. Matsumoto, and T. Seya. 2015. 'RIOK3-mediated phosphorylation of MDA5 interferes with its assembly and attenuates the innate immune response', *Cell Rep*, 11: 192-200.

Tan, M. K., H. J. Lim, E. J. Bennett, Y. Shi, and J. W. Harper. 2013. 'Parallel SCF adaptor capture proteomics reveals a role for SCFFBXL17 in NRF2 activation via BACH1 repressor turnover', *Mol Cell*, 52: 9-24.

Tang, C. J., R. H. Fu, K. S. Wu, W. B. Hsu, and T. K. Tang. 2009. 'CPAP is a cell-cycle regulated protein that controls centriole length', *Nat Cell Biol*, 11: 825-31.

Tang, C. J., S. Y. Lin, W. B. Hsu, Y. N. Lin, C. T. Wu, Y. C. Lin, C. W. Chang, K. S. Wu, and T. K. Tang. 2011. 'The human microcephaly protein STIL interacts with CPAP and is required for procentriole formation', *Embo j*, 30: 4790-804.

Tang, L. J., Y. Li, Y. L. Liu, J. M. Wang, D. W. Liu, and Q. B. Tian. 2016. 'USP12 regulates cell cycle progression by involving c-Myc, cyclin D2 and BMI-1', *Gene*, 578: 92-9.

Tang, N., and W. F. Marshall. 2012. 'Centrosome positioning in vertebrate development', *J Cell Sci*, 125: 4951-61.

Teras, L. R., C. E. DeSantis, J. R. Cerhan, L. M. Morton, A. Jemal, and C. R. Flowers. 2016. '2016 US lymphoid malignancy statistics by World Health Organization subtypes', *CA Cancer J Clin*.

Thornton, J. E., H. M. Chang, E. Piskounova, and R. I. Gregory. 2012. 'Lin28-mediated control of let-7 microRNA expression by alternative TUTases Zcchc11 (TUT4) and Zcchc6 (TUT7)', *Rna*, 18: 1875-85.

Tian, N., Z. Han, Z. Li, M. Zhou, and C. Fan. 2014. 'Lin28/let-7/Bcl-xL pathway: the underlying mechanism of drug resistance in Hep3B cells', *Oncol Rep*, 32: 1050-6.

Tian, Z., P. D'Arcy, X. Wang, A. Ray, Y. T. Tai, Y. Hu, R. D. Carrasco, P. Richardson, S. Linder, D. Chauhan, and K. C. Anderson. 2014. 'A novel small molecule inhibitor of deubiquitylating enzyme USP14 and UCHL5 induces apoptosis in multiple myeloma and overcomes bortezomib resistance', *Blood*, 123: 706-16.

Tricot, G., B. Barlogie, S. Jagannath, D. Bracy, S. Mattox, D. H. Vesole, S. Naucke, and J. R. Sawyer. 1995. 'Poor prognosis in multiple myeloma is associated only with partial or complete deletions of chromosome 13 or abnormalities involving 11q and not with other karyotype abnormalities', *Blood*, 86: 4250-6.

Tsialikas, J., and J. Romer-Seibert. 2015. 'LIN28: roles and regulation in development and beyond', *Development*, 142: 2397-404.

Tsou, M. F., and T. Stearns. 2006. 'Mechanism limiting centrosome duplication to once per cell cycle', *Nature*, 442: 947-51.

Tsvetkov, L. M., K. H. Yeh, S. J. Lee, H. Sun, and H. Zhang. 1999. 'p27(Kip1) ubiquitination and degradation is regulated by the SCF(Skp2) complex through phosphorylated Thr187 in p27', *Curr Biol*, 9: 661-4.

Urbe, S., H. Liu, S. D. Hayes, C. Heride, D. J. Rigden, and M. J. Clague. 2012. 'Systematic survey of deubiquitinase localization identifies USP21 as a regulator of centrosome- and microtubule-associated functions', *Mol Biol Cell*, 23: 1095-103.

van Breugel, M., M. Hirono, A. Andreeva, H. A. Yanagisawa, S. Yamaguchi, Y. Nakazawa, N. Morgner, M. Petrovich, I. O. Ebong, C. V. Robinson, C. M. Johnson, D. Veprintsev, and B. Zuber. 2011. 'Structures of SAS-6 suggest its organization in centrioles', *Science*, 331: 1196-9.

Vigneron, S., L. Sundermann, J. C. Labbe, L. Pintard, O. Radulescu, A. Castro, and T. Lorca. 2018. 'Cyclin A-cdk1-Dependent Phosphorylation of Bora Is the Triggering Factor Promoting Mitotic Entry', *Dev Cell*, 45: 637-50.e7.

Vincent Rajkumar, S. 2014. 'Multiple myeloma: 2014 Update on diagnosis, risk-stratification, and management', *Am J Hematol*, 89: 999-1009.

Vinogradova, T., R. Paul, A. D. Grimaldi, J. Loncarek, P. M. Miller, D. Yampolsky, V. Magidson, A. Khodjakov, A. Mogilner, and I. Kaverina. 2012. 'Concerted effort of centrosomal and Golgi-derived

microtubules is required for proper Golgi complex assembly but not for maintenance', *Mol Biol Cell*, 23: 820-33.

Viswanathan, S. R., G. Q. Daley, and R. I. Gregory. 2008. 'Selective blockade of microRNA processing by Lin28', *Science*, 320: 97-100.

Viswanathan, S. R., J. T. Powers, W. Einhorn, Y. Hoshida, T. L. Ng, S. Toffanin, M. O'Sullivan, J. Lu, L. A. Phillips, V. L. Lockhart, S. P. Shah, P. S. Tanwar, C. H. Mermel, R. Beroukhim, M. Azam, J. Teixeira, M. Meyerson, T. P. Hughes, J. M. Llovet, J. Radich, C. G. Mullighan, T. R. Golub, P. H. Sorensen, and G. Q. Daley. 2009. 'Lin28 promotes transformation and is associated with advanced human malignancies', *Nat Genet*, 41: 843-8.

Vlach, J., S. Hennecke, K. Alevizopoulos, D. Conti, and B. Amati. 1996. 'Growth arrest by the cyclin-dependent kinase inhibitor p27Kip1 is abrogated by c-Myc', *Embo j*, 15: 6595-604.

Vorobjev, I. A., and S. Chentsov Yu. 1982. 'Centrioles in the cell cycle. I. Epithelial cells', *J Cell Biol*, 93: 938-49.

Wakida, N. M., E. L. Botvinick, J. Lin, and M. W. Berns. 2010. 'An intact centrosome is required for the maintenance of polarization during directional cell migration', *PLoS One*, 5: e15462.

Walzik, M. 2017. 'Characterization of deubiquitylating enzymes in the pathogenesis of multiple myeloma', Technical University of Munich.

Wang, J., J. Li, J. Gu, J. Yu, S. Guo, Y. Zhu, and D. Ye. 2015. 'Abnormal methylation status of FBXW10 and SMPD3, and associations with clinical characteristics in clear cell renal cell carcinoma', *Oncol Lett*, 10: 3073-80.

Wang, L., C. Yuan, K. Lv, S. Xie, P. Fu, X. Liu, Y. Chen, C. Qin, W. Deng, and W. Hu. 2013. 'Lin28 mediates radiation resistance of breast cancer cells via regulation of caspase, H2A.X and Let-7 signaling', *PLoS One*, 8: e67373.

Wang, S., J. Juan, Z. Zhang, Y. Du, Y. Xu, J. Tong, B. Cao, M. F. Moran, Y. Zeng, and X. Mao. 2017. 'Inhibition of the deubiquitinase USP5 leads to c-Maf protein degradation and myeloma cell apoptosis', *Cell Death Dis*, 8: e3058.

Wang, T., G. Wang, D. Hao, X. Liu, D. Wang, N. Ning, and X. Li. 2015. 'Aberrant regulation of the LIN28A/LIN28B and let-7 loop in human malignant tumors and its effects on the hallmarks of cancer', *Mol Cancer*, 14: 125.

Wang, Y., J. Li, S. Guo, Y. Ouyang, L. Yin, S. Liu, Z. Zhao, J. Yang, W. Huang, H. Qin, X. Zhao, B. Ni, and H. Wang. 2017. 'Lin28B facilitates the progression and metastasis of pancreatic ductal adenocarcinoma', *Oncotarget*, 8: 60414-28.

Wang, Z., P. Liu, H. Inuzuka, and W. Wei. 2014. 'Roles of F-box proteins in cancer', *Nat Rev Cancer*, 14: 233-47.

Wei, W., N. G. Ayad, Y. Wan, G. J. Zhang, M. W. Kirschner, and W. G. Kaelin, Jr. 2004. 'Degradation of the SCF component Skp2 in cell-cycle phase G1 by the anaphase-promoting complex', *Nature*, 428: 194-8.

Winston, J. T., D. M. Koepp, C. Zhu, S. J. Elledge, and J. W. Harper. 1999. 'A family of mammalian F-box proteins', *Curr Biol*, 9: 1180-2.

Wong, Y. L., J. V. Anzola, R. L. Davis, M. Yoon, A. Motamedi, A. Kroll, C. P. Seo, J. E. Hsia, S. K. Kim, J. W. Mitchell, B. J. Mitchell, A. Desai, T. C. Gahman, A. K. Shiau, and K. Oegema. 2015. 'Cell biology. Reversible centriole depletion with an inhibitor of Polo-like kinase 4', *Science*, 348: 1155-60.

Woodruff, J. B., O. Wueseke, and A. A. Hyman. 2014. 'Pericentriolar material structure and dynamics', *Philos Trans R Soc Lond B Biol Sci*, 369.

Wu, L., A. V. Grigoryan, Y. Li, B. Hao, M. Pagano, and T. J. Cardozo. 2012. 'Specific small molecule inhibitors of Skp2-mediated p27 degradation', *Chem Biol*, 19: 1515-24.

Wurmbach, E., Y. B. Chen, G. Khitrov, W. Zhang, S. Roayaie, M. Schwartz, I. Fiel, S. Thung, V. Mazzaferro, J. Bruix, E. Bottinger, S. Friedman, S. Waxman, and J. M. Llovet. 2007. 'Genome-wide molecular profiles of HCV-induced dysplasia and hepatocellular carcinoma', *Hepatology*, 45: 938-47.

Xu, B., and Y. Huang. 2009. 'Histone H2a mRNA interacts with Lin28 and contains a Lin28-dependent posttranscriptional regulatory element', *Nucleic Acids Res*, 37: 4256-63.

Xu, B., K. Zhang, and Y. Huang. 2009. 'Lin28 modulates cell growth and associates with a subset of cell cycle regulator mRNAs in mouse embryonic stem cells', *Rna*, 15: 357-61.

Xu, P., D. M. Duong, N. T. Seyfried, D. Cheng, Y. Xie, J. Robert, J. Rush, M. Hochstrasser, D. Finley, and J. Peng. 2009. 'Quantitative proteomics reveals the function of unconventional ubiquitin chains in proteasomal degradation', *Cell*, 137: 133-45.

Xu, Z., Y. Zheng, Y. Zhu, X. Kong, and L. Hu. 2011. 'Evidence for OTUD-6B participation in B lymphocytes cell cycle after cytokine stimulation', *PLoS One*, 6: e14514.

Yaccoby, S., R. N. Pearse, C. L. Johnson, B. Barlogie, Y. Choi, and J. Epstein. 2002. 'Myeloma interacts with the bone marrow microenvironment to induce osteoclastogenesis and is dependent on osteoclast activity', *Br J Haematol*, 116: 278-90.

Yada, M., S. Hatakeyama, T. Kamura, M. Nishiyama, R. Tsunematsu, H. Imaki, N. Ishida, F. Okumura, K. Nakayama, and K. I. Nakayama. 2004. 'Phosphorylation-dependent degradation of c-Myc is mediated by the F-box protein Fbw7', *Embo j*, 23: 2116-25.

Yadav, S., and A. D. Linstedt. 2011. 'Golgi positioning', *Cold Spring Harb Perspect Biol*, 3.

Yang, D. H., and E. G. Moss. 2003. 'Temporally regulated expression of Lin-28 in diverse tissues of the developing mouse', *Gene Expr Patterns*, 3: 719-26.

Yang, J., B. D. Bennett, S. Luo, K. Inoue, S. A. Grimm, G. P. Schroth, P. R. Bushel, H. K. Kinyamu, and T. K. Archer. 2015. 'LIN28A Modulates Splicing and Gene Expression Programs in Breast Cancer Cells', *Mol Cell Biol*, 35: 3225-43.

Yang, M., S. L. Yang, S. Herrlinger, C. Liang, M. Dzieciatkowska, K. C. Hansen, R. Desai, A. Nagy, L. Niswander, E. G. Moss, and J. F. Chen. 2015. 'Lin28 promotes the proliferative capacity of neural progenitor cells in brain development', *Development*, 142: 1616-27.

Yang, W., J. Shen, M. Wu, M. Arsura, M. FitzGerald, Z. Suldan, D. W. Kim, C. S. Hofmann, S. Pianetti, R. Romieu-Mourez, L. P. Freedman, and G. E. Sonenshein. 2001. 'Repression of

transcription of the p27(Kip1) cyclin-dependent kinase inhibitor gene by c-Myc', *Oncogene*, 20: 1688-702.

Yang, Y., K. Xue, Z. Li, W. Zheng, W. Dong, J. Song, S. Sun, T. Ma, and W. Li. 2018. 'c-Myc regulates the CDK1/cyclin B1 dependentG2/M cell cycle progression by histone H4 acetylation in Raji cells', *Int J Mol Med*, 41: 3366-78.

Yao, F., Z. Zhou, J. Kim, Q. Hang, Z. Xiao, B. N. Ton, L. Chang, N. Liu, L. Zeng, W. Wang, Y. Wang, P. Zhang, X. Hu, X. Su, H. Liang, Y. Sun, and L. Ma. 2018. 'SKP2- and OTUD1-regulated non-proteolytic ubiquitination of YAP promotes YAP nuclear localization and activity', *Nat Commun*, 9: 2269.

Yao, T., and R. E. Cohen. 2002. 'A cryptic protease couples deubiquitination and degradation by the proteasome', *Nature*, 419: 403-7.

Yin, J., T. H. Kim, N. Park, D. Shin, H. I. Choi, S. Cho, J. B. Park, and J. H. Kim. 2016. 'TRIM71 suppresses tumorigenesis via modulation of Lin28B-let-7-HMGA2 signaling', *Oncotarget*, 7: 79854-68.

Yoshihara, K., A. Tajima, D. Komata, T. Yamamoto, S. Kodama, H. Fujiwara, M. Suzuki, Y. Onishi, M. Hatae, K. Sueyoshi, H. Fujiwara, Y. Kudo, I. Inoue, and K. Tanaka. 2009. 'Gene expression profiling of advanced-stage serous ovarian cancers distinguishes novel subclasses and implicates ZEB2 in tumor progression and prognosis', *Cancer Sci*, 100: 1421-8.

Yu, J., M. A. Vodyanik, K. Smuga-Otto, J. Antosiewicz-Bourget, J. L. Frane, S. Tian, J. Nie, G. A. Jonsdottir, V. Ruotti, R. Stewart, Slukvin, II, and J. A. Thomson. 2007. 'Induced pluripotent stem cell lines derived from human somatic cells', *Science*, 318: 1917-20.

Yu, Z. K., J. L. Gervais, and H. Zhang. 1998. 'Human CUL-1 associates with the SKP1/SKP2 complex and regulates p21(CIP1/WAF1) and cyclin D proteins', *Proc Natl Acad Sci U S A*, 95: 11324-9.

Zhan, F., B. Barlogie, V. Arzoumanian, Y. Huang, D. R. Williams, K. Hollmig, M. Pineda-Roman, G. Tricot, F. van Rhee, M. Zangari, M. Dhodapkar, and J. D. Shaughnessy, Jr. 2007. 'Gene-expression signature of benign monoclonal gammopathy evident in multiple myeloma is linked to good prognosis', *Blood*, 109: 1692-700.

Zhang, D., K. Zaugg, T. W. Mak, and S. J. Elledge. 2006. 'A role for the deubiquitinating enzyme USP28 in control of the DNA-damage response', *Cell*, 126: 529-42.

Zhang, Q., D. Karnak, M. Tan, T. S. Lawrence, M. A. Morgan, and Y. Sun. 2016. 'FBXW7 Facilitates Nonhomologous End-Joining via K63-Linked Polyubiquitylation of XRCC4', *Mol Cell*, 61: 419-33.

Zhu, F., S. Lawo, A. Bird, D. Pinchev, A. Ralph, C. Richter, T. Muller-Reichert, R. Kittler, A. A. Hyman, and L. Pelletier. 2008. 'The mammalian SPD-2 ortholog Cep192 regulates centrosome biogenesis', *Curr Biol*, 18: 136-41.

Zimmerman, W. C., J. Sillibourne, J. Rosa, and S. J. Doxsey. 2004. 'Mitosis-specific anchoring of gamma tubulin complexes by pericentrin controls spindle organization and mitotic entry', *Mol Biol Cell*, 15: 3642-57.

10 List of figures and tables

10.1 List of figures

Figure 1: Development of multiple myeloma 4
Figure 2: Overview of ubiquitin modifications and their cellular outcomes 8
Figure 3: Enzymatic cascade of the ubiquitin system 10
Figure 4: SCF complex-mediated ubiquitylation 11
Figure 5: Schematic overview of FBXL13 12
Figure 6: Schematic overview of OTUD6B isoforms 14
Figure 7: Overview of the LIN28 family 17
Figure 8: Oncogenic role of LIN28 19
Figure 9: Overview of cell cycle regulation 20
Figure 10: Generation of stable MM1.S Cas9 cells 67
Figure 11: CRISPR/Cas9-mediated knockout in MM1.S Cas9 cells 67
Figure 12: Analysis of infection rates and bortezomib response in MM1.S Cas9 cells 68
Figure 13: Workflow of CRISPR/Cas9 sgRNA library preparation 69
Figure 14: Quantification of sgRNA libraries 70
Figure 15: Workflow of CRISPR/Cas9 screen in MM1.S Cas9 cells 71
Figure 16: CRISPR/Cas9 screen of F-box proteins in MM1.S Cas9 cells 72
Figure 17: CRISPR-mediated knockout of FBXW10 leads to a growth disadvantage 73
Figure 18: CRISPR/Cas9 screen of DUBs in MM1.S Cas9 cells 75
Figure 19: CRISPR/Cas9-mediated knockout of OTUD6B in MM1.S cells has an anti-proliferative effect 76
Figure 20: OTUD6B is essential for multiple myeloma proliferation 77
Figure 21: OTUD6B knockdown in MM cell lines has an anti-proliferative effect 78
Figure 22: OTUD6B is essential for proliferation of various cancer types 79
Figure 23: OTUD6B is essential for cell cycle progression 80
Figure 24: OTUD6B is important for G1/S transition 81
Figure 25: OTUD6B is an active cysteine protease DUB 82
Figure 26: OTUD6B activity peaks at G1/S transition 83
Figure 27: Mass spectrometric analysis of FLAG-purified OTUD6B 85
Figure 28: Mass spectrometric analysis of OTUD6B BioID2 purification 87
Figure 29: OTUD6B binds to LIN28B 88
Figure 30: OTUD6B isoform 1 binding to LIN28B is independent of its catalytic activity 89
Figure 31: OTUD6B binds to the cold shock domain of LIN28B 90
Figure 32: OTUD6B binding to LIN28B is phosphorylation-dependent 92
Figure 33: OTUD6B binds to RIOK3 93
Figure 34: RIOK3 promotes binding of OTUD6B to LIN28B 94
Figure 35: OTUD6B deubiquitylates LIN28B *in vivo* 95
Figure 36: OTUD6B removes K48 ubiquitylation from LIN28B 97
Figure 37: LIN28B protein levels are cell cycle regulated 98
Figure 38: OTUD6B stabilizes LIN28B at G1/S transition 99
Figure 39: OTUD6B prevents proteasomal degradation of LIN28B at G1/S transition 99
Figure 40: OTUD6B and LIN28B expression in various MM cell lines 100
Figure 41: Overexpression of LIN28B partially counteracts the proliferation defect caused by OTUD6B depletion 101

Figure 42: OTUD6B is essential for proliferation of LIN28B expressing DLBCL cells 102
Figure 43: OTUD6B and LIN28B are essential for G1/S transition in MM cells 103
Figure 44: OTUD6B promotes MYC expression in MM cells 104
Figure 45: OTUD6B regulates MYC targets 105
Figure 46: LIN28B and OTUD6B are part of the same signalling pathway 106
Figure 47: MYC and OTUD6B mRNA levels correlate in primary MM patient cells 106
Figure 48: Model of OTUD6B-mediated entry into S phase 117
Figure 49: FBXL13 binds to CEP152 and CEP192 121
Figure 50: FBXL13 and CEP192 interact endogenously 121
Figure 51: FBXL13 binding to CEP192 is direct 122
Figure 52: CEP192 binds to the leucine-rich repeat of FBXL13 124
Figure 53: FBXL13 destabilizes CEP192 125
Figure 54: FBXL13 destabilizes CEP192 but not Centrin-2 and Centrin-3 126
Figure 55: FBXL13 ubiquitylates CEP192 127
Figure 56: FBXL13 downregulates CEP192 and γ-tubulin at the centrosomes 128
Figure 57: FBXL13 regulates centrosomal microtubule nucleation 129
Figure 58: FBXL13 activity is essential for cell migration 131
Figure 59: FBXL13 positively regulates cell motility by targeting CEP192 for degradation 132
Figure 60: Model of FBXL13-mediated cell migration 139

10.2 List of tables

Table 1: Two-step PCR program for NGS sample preparation 49

11 Appendix

11.1 Sequences of sgRNA libraries

11.1.1 Sequences of F-box protein sgRNAs

F-box protein	Sequence (forward)	F-box protein	Sequence (forward)
BTRC	TGGTACCGAGTGACCTCTGA	FBXO31	CGAGCCGGACACAGACCCCG
BTRC	CCTACTGAAAGCTCGGGGAT	FBXO31	GCGCATCGAGGCTAGCGCCG
BTRC	GTATGATTGTGCCCAAGCAA	FBXO31	CGGCGCCGACATCCGCGCGA
CCNF	ACTTACGGCCTTCATTGTAG	FBXO33	ACCAGCCGCACTTGCGCATG
CCNF	GCTTCTTCAGTCTCGCTGAG	FBXO33	GCCGCCGAGAACTATCTGAG
CCNF	ATAGCCTACCTCTACAATGA	FBXO33	AACCCAGTATACCACTAGAG
ECT2L	GACGTTGCTTGTTAGTCCAG	FBXO34	TAACAGCTTCCGTCGAAATG
ECT2L	TTTCTATGAGTAACCGATGA	FBXO34	AGATGATGCTTTACCGAGAG
ECT2L	TTCGAAGTACTGACAGCCAT	FBXO34	TCGAGATCCACGCTATAGAG
FBXL12	GGGATGCCATGTACCTTCGA	FBXO36	GGCGTCCCAAGATGGCGTCG
FBXL12	CGGCGGGATCATGGCGACTT	FBXO36	TAATAGTCTTTGCTAGGCGG
FBXL12	TGTCGACCTGACGCTCTACA	FBXO36	AATTATAGGTAATCTTTAGA
FBXL13	TTCCTTCAGATATTCTATTG	FBXO38	TAACGCCGAGTACCGTTCTT
FBXL13	TAACCATTATCCTAACAAAA	FBXO38	CCAATCGAGTCCATCTTGAG
FBXL13	AAAAATCTGTATTTCATCAC	FBXO38	TGGTTGATATCAACCTAGTA
FBXL14	CGATCTCCTGCACAAACGCG	FBXO39	GCTCCTCGTCGAGTGACTCA
FBXL14	TCCCACTGCAGGAGGCACGA	FBXO39	CAACCATGAGTCACTCGACG
FBXL14	CCGCCTACCACAAGTCGGTG	FBXO39	GATCATGAAGTACGAACGCT
FBXL15	TGCCTCCGCGTCGGAAGCGA	FBXO4	GGTCCAAACATAGCAAATCG
FBXL15	TGGCGCGGAATCCGCAGCTG	FBXO4	GAACCACGATTTGCTATGTT
FBXL15	ACAGCCGATGGAGCCACCGA	FBXO4	CCCAACTGACACAGATCATG
FBXL16	CACGGCGCTGGCCTACTTCA	FBXO40	TAGGAGACGTATCTTCCTCG
FBXL16	CACGAGCTCCACGCCGTCGT	FBXO40	CCGTGCCTCAACTCCGAATA
FBXL16	CCACAGGTGTGTACGCATCA	FBXO40	GCAGGACGTTCGTACAGCCA
FBXL17	GCGTTGCCTTTCCGCATCAT	FBXO41	GGACCGCTCTGAGCCCCCGT
FBXL17	CCAGTTCAGTGATATGACGT	FBXO41	GTATTCTGCAGCCCGCCCCG
FBXL17	AGGGCTGTCTGAAATTACAA	FBXO41	ACCCCGCCGACACAGCACTG
FBXL18	TCAGAATCAGATCTGTGCTG	FBXO42	AGCAACTCTGGTCGTGTACA
FBXL18	TGAACGTCCGGCGTACCTGT	FBXO42	CGGCCCTTGTCTGCAAACAG
FBXL18	CAGCACGACATTGCGCGCCA	FBXO42	CATCTCTTACCTGAAGCCAA
FBXL19	GGCCGCCGTAGGGCCGACAA	FBXO43	GACTCCGATAAGTAATCTTG
FBXL19	CCTCGCCGTTGTCGGCCCTA	FBXO43	CTTAGATGTCAAAGTTACGT
FBXL19	ACAGCTGTGTGCCTCTTGTG	FBXO43	ACAACTGAAAACAGATTCTG
FBXL2	CTTCCAGAATTGCCACGAAT	FBXO44	GCCAGAGGCTGCAGACCAGG

FBXL2	CCTTGGAAATCTGTGCACAT
FBXL2	TAAAACCTGCGTCAGTCAAA
FBXL20	TTACCGTAACAGGAGTTCTT
FBXL20	TTCCCAAAGAACTCCTGTTA
FBXL20	CCCTGGAGACCTGAGCACAG
FBXL21	ACACGGTTCTTCTAGACTGG
FBXL21	GCACAGGCCCGATCTAGTAA
FBXL21	CAACCAGACTCATACACACA
FBXL22	GATTTCGGTCCAACGGCGAT
FBXL22	CGTCACCCCCGAGCGCAAGT
FBXL22	CCAGCTCCACGACGTGTTTG
FBXL3	CGGAATAGGATGAAACGAGG
FBXL3	TTCCCGACATGATGCCCACT
FBXL3	TCCTGACCAAAAGTATAGTT
FBXL4	CAATTCAAGGCGTACTAATT
FBXL4	GATAGAGAACAAGTCGTTTA
FBXL4	TGGGAAGCATTCACCTTCGT
FBXL5	CTGCATCGACATAACTCTTG
FBXL5	TCCTTAGAGGTCTTAGCCTA
FBXL5	GATGCTTAGCCTCTTTGAAA
FBXL6	GAGCGTCAGCAGTCACACCG
FBXL6	TCCCCTTCAGCTGCCTGTCG
FBXL6	GCTGAAGGGGAATGCTATTA
FBXL7	TGCGTCCGCCTGACCGACGA
FBXL7	CGACGTGGGCATCCGCTACG
FBXL7	CTGGAGGACTATCCGCCTGA
FBXL8	TCGCGGCCCGCGTCGAAGAG
FBXL8	CTGCTACCTGCAGCGCCGTG
FBXL8	CCCAATCACGCCACGAGCGT
FBXO10	TCATGCGCCACAGCTCCAAG
FBXO10	GAACGACGTACCCTGAGTGT
FBXO10	GCGGTGTATACATAATAGCA
FBXO11	GGAGACCCAGGCGAGTGTCG
FBXO11	ACTCCGTCCGAGCCGCCAAC
FBXO11	GTGTCCCACAAAGAACAGTA
FBXO15	TTACTTTCAGAAAGGGGCCA
FBXO15	CTATGGCGACTGGACGCGGT
FBXO15	TCACACATCCAGTACACAGA
FBXO16	GAGGACCGAAAAGCTGATAA
FBXO16	GTGCTTATCAGAAGATCGCC
FBXO16	TTACCTGTGCACAACGACAA
FBXO17	TGGGGCGCTCGAGAGAACTG
FBXO44	CGGCGTGGACACTCATTACT
FBXO44	TGGTGGACCTCAAGGCCGAA
FBXO45	AGCCACTGTCATCCGTCCAA
FBXO45	GCACGGCGATGAGAACAGCG
FBXO45	TGATTGGAATTGCCACAAAA
FBXO46	AACGTCCGTAAGGCAGGTCA
FBXO46	CGGAGCGTCAGGCTTCCACG
FBXO46	ACTGTTTGCACGGATCATCG
FBXO47	TCTCTGCCGCAAGATACAAA
FBXO47	CTGGAGCACTACAGATCTCT
FBXO47	ATAAGAAATTATAAACGCGA
FBXO48	CCCCATGTATCTGCATCCAT
FBXO48	TCACACAGAAGCGAACTCTG
FBXO48	AGAGTAAAGTGAAACACGAA
FBXO5	CACTCACTATCCGAGGGTCG
FBXO5	GTTTAAGTCCGGAATGAACA
FBXO5	TGTCTAAAGTGAGCACAACT
FBXO6	CAACACGAAGTAGTCAGCCG
FBXO6	CTCGGCTGACTACTTCGTGT
FBXO6	GGTCAGGAAAATCTGTCCCG
FBXO7	CACCGATTCACTACAGAGCA
FBXO7	GTTGATACATCTTCTCATGT
FBXO7	ATCCGTAGTTTCAGTTCCAA
FBXO8	CCTGATTTAATGCGAGAACT
FBXO8	TATCCTGGATGATTCGCCAA
FBXO8	CTTTAATGCCAACCCAGATG
FBXO9	ATGTACATCAGGACCTCCAT
FBXO9	AGGCTCTCTCCAGAAAACAT
FBXO9	AGTCACTAGACACCACCCAT
FBXW10	CTTCTCACAACGAAAATAGG
FBXW10	GATCCTGCAGAACCACTCTT
FBXW10	CCAGAAAATGAACACTTGCT
FBXW11	CGAATGTGTCATTATCAGCA
FBXW11	GTGGTCTGAATCAGATCAAG
FBXW11	GTCAAAGTCTACTACATTGA
FBXW12	AAACCTGCAGCAAGCCGAAC
FBXW12	CTCTCCCATAGCATTGGAAT
FBXW12	CTCAGGAAATAGACTTACAG
FBXW2	ATATGCACTAGTATTTAGCG
FBXW2	ACTTCACCGCTGCACAAGTG
FBXW2	CAGTTGATTTCTCTCCCAAT
FBXW4	TGCACTAACAATATGCGAGT

FBXO17	ACTGCTCAAAAGATACGTAG
FBXO17	CTTGTGGACCTGGTGATGGA
FBXO18	ACCATCACTCATGAGCTACG
FBXO18	GTGCCTGAGTCATGTGATAA
FBXO18	CGATGGTACAGCTTCTTCCA
FBXO2	AACCTTCTGCGTAACCCGTG
FBXO2	TACTCGGGCCGCAGCGACGC
FBXO2	GGGCAGCTCGTCCAGGTACG
FBXO21	GGCGACTGTTTATGCCCCGA
FBXO21	GCCCCACCGACTACGTCAAT
FBXO21	TTCCAACCAATTGACGTAGT
FBXO22	AGATCCAGGTTACGCTCCGA
FBXO22	GGGGCATTGCTTGGTTCGCG
FBXO22	GAGTGTCGTGGCCATAAGAG
FBXO24	TGACCAGCCACGCTCCTACA
FBXO24	TTTGGCCGAATCTTCATGCA
FBXO24	GGTCCATACCTGTGACGTAG
FBXO25	TCAGAAACATTACCCAGCGA
FBXO25	TCCCAGTTAACTTCATTGAG
FBXO25	ATGAATATGCATCGAAAAAA
FBXO27	GCGAATAAGGTTGCGTCCGA
FBXO27	ACATACAGCCGCTGTCGTGT
FBXO27	TGGGGAGCCCGACACGACAG
FBXO28	GCCTCAAAACAACACGCTTG
FBXO28	AAGAGGAACCGCCGTCGCCT
FBXO28	CTGCATGACGAGCTAATGAA
FBXO3	TGTTCATACCGAATTCACAA
FBXO3	CTTTATAGAGGGTGCTCGAG
FBXO3	AAATAAAATACCTGAAAATT
FBXO30	TAGTATTGGAATGTGTCGCT
FBXO30	TCTCGTGTCACACACATACA
FBXO30	ACACGAGAACTCACTAAAGA
FBXW4	AGCCGAGTACTTGACAGTGA
FBXW4	AAAGGGGGCATCATTGTGAG
FBXW5	GCGAGTCGTCCTTGTTGAAC
FBXW5	CCAGTTCGCGTCCTGCTCCA
FBXW5	CACGCGGGACAGCAGCGCGA
FBXW7	CTTACCCGTCTTCGACAAAA
FBXW7	TGTATGTGTGTCCCGAGAAG
FBXW7	CTCAGTATCAAACCGCTTCT
FBXW8	CAGCCAGGACGATGCAACCG
FBXW8	CGAGCTGTTTATCCTCACAA
FBXW8	GAGACGTCTAGACATGTGAC
FBXW9	GAGATCGCAACGTCAACTTG
FBXW9	CGTACGCGCGCCCTACCCAG
FBXW9	CCCACCTCTGGGGTCGTAGA
KDM2A	ACGCTACTATGAGACCCCAG
KDM2A	TATGGCAGGGAGTCGTCGCA
KDM2A	TCAGAATTCTTGAAAATCAG
KDM2B	GCGTTACTACGAGACGCCCG
KDM2B	CTTGGTCAAGCGTCCGACTG
KDM2B	CCAGCGATACGACGAGAACG
LMO7	CTACTTACCAATCCTGCTAT
LMO7	TTTCGAGCCTCTCTAGAAAA
LMO7	TTGAAAGCTTGTGAACAGAT
LRRC29	CTGTGTCCAGTCCCGCTTCG
LRRC29	GGCCCACTGCTCTTCATTGA
LRRC29	GGTCAGCCCCTCCCACGAAG
SKP2	TCAGGTCTGGAATCTCCTGG
SKP2	GTCGGGCTCCTCTTTCTCCA
SKP2	GGTTTGAGAGCAGTTCCTGG

11.1.2 Sequences of DUB sgRNAs

DUB	Sequence (forward)
ATXN3	TGCCTGAATAACTTATTGCA
ATXN3	TCAACAGTCCAGAGTATCAG
ATXN3	CTGTCATCCATATTTCCAGA
ATXN3L	ATCGAGCCAAGAAATTTGCA
ATXN3L	ACAGTTCATACCTACACGAA
USP18	GGAGTGATCACGAATGAGCA
USP18	CATTACGAACACCTGAATCA
USP18	AAGATCTGCCGGGGACTGCG
USP19	GGCCCCACACCACCTTCCGT
USP19	AGACGCCCACCAGTCCCTAG

ATXN3L	ATTGCTCTCGAACTTGTTGT
BAP1	ACCCACCCTGAGTCGCATGA
BAP1	GGAAGATAAATCCATATACA
BAP1	TCAAATGGATCGAAGAGCGC
BRCC3	TCTAGTTGAACGATGATACA
BRCC3	ATACTTACTCTGAACTCTTT
BRCC3	ACAAGCCATGTACCAGATGA
COPS5	CTTACCACCACTGCTACAAA
COPS5	TATCATAGCCACCCTGGCTA
COPS5	GGCTACAAACCTCCTGATGA
CYLD	TAGAACCTTTGCTAAAAATA
CYLD	AAGCTCCTTAAAGTACCGAA
CYLD	CTTCACCCTACTGGGAAGAG
JOSD1	TGAAGCCCATGACGTTAGTG
JOSD1	GCACTGGATCTGTGTTCGAG
JOSD1	TAGGTTGTCTCCAAACACCA
JOSD2	CTGCCGTTCGTGGTACACGG
JOSD2	CACCCACCGTGTACCACGAA
JOSD2	CTATGATGTCAATGTGATCA
MPND	ACGTACCTCATCAGCAGCCG
MPND	AGTCTGACCTGGCCAAGTCG
MPND	TCTCAGCAGAGGACAAGAGT
MYSM1	AGGCTAAATTTGGCCGAAGA
MYSM1	TGTGGATATCGAAGGGGACG
MYSM1	TCCCATCATGGCGGCTGAAG
OTUB1	CCTTCGGAGTCGCTGCCCAG
OTUB1	GCGCTGTTTAAAGATGGCGG
OTUB1	CCCTCACCTCTTGCTGAATT
OTUB2	ACCGCCATCCGCAAGACCAA
OTUB2	TTCAGGATGGTCCCGAAGAA
OTUB2	CTCCAGGTAGGAATAGCCCA
OTUD1	CCGTGTCGCGTCCAAGCCCG
OTUD1	GCCAAGTGCTCTTCGCCCCA
OTUD1	CTCCGCCGCACTACTCGGGG
OTUD3	TTACACATCGCATATCGGTA
OTUD3	AGCACTACGACAGTGTTCGG
OTUD3	AGGTGACCTACCTGCCACAA
OTUD4	TTTACCTGTACATAAGAGAA
OTUD4	GAACAGAGAGAAATTTGAAG
OTUD4	ACAGGAATGGGTAGGACAAG
OTUD5	CCATTCGTGTTAGCTACCAT
OTUD5	CCGATGGTAGCTAACACGAA
USP19	ATTCCTAGACCGCTCCTTTG
USP2	AAAAACTCACCGTGTTCCCA
USP2	AGTCGAACCGGGCACAAGCA
USP2	TACATGCGGGACCTGCACCA
USP20	GGACTTGCTGCTCAAATCTA
USP20	GGTCACCGGACCAAACCTAT
USP20	GGATTCTCCGCAGCCAACAT
USP21	CTCAGACAGAAGTCCCGAAG
USP21	TGAGCAGCACTCGACCTCTT
USP21	ATGACCGAGCCAACCTAATG
USP22	AGTCCCGCAGAAGTGGCGTG
USP22	CTGCGTGGGCTGATCAACCT
USP22	GCCTCCGTACATCAGATCAA
USP24	TTGGGCAGAAGTGTTTGGAG
USP24	CATCAAGTGCTGTTCACAAG
USP24	TCTACAATTCTCATCAGACT
USP25	GAATCCCTCCAAACTTCTGT
USP25	TCTTAGCATTCTTCGCAGTA
USP25	CCCGTTGGGCTAAAGAATGT
USP26	ATGGCTGCCCTATTCCTACG
USP26	TACGATGATATGCGGGTGTT
USP26	GACAACACTAATGAGCCGGT
USP27X	CGCGGCGCACGACTGCGACG
USP27X	ACTGCTTGCGGAGGTTTACG
USP27X	CTCGATGCCAGTTGTAGTAT
USP28	TGAGCGTTTAGTTTCTGCAG
USP28	CTCCAGTAGACTCAAAGCAA
USP28	CTGCTGCAGCTCCGCAGTCA
USP29	AATTTGGGGAGCTCCCGATA
USP29	TTGAGCAGTAGTGCACCTGT
USP29	TGTCGAGGTTCATCTTCAAG
USP3	CGCCCTGAAGTTCCAAGTGT
USP3	CGCTTACTTCTGAACTGACT
USP3	TTCCCGCTCAGCAATTCTGC
USP30	TCGCTCATCTTCCAATGACG
USP30	ATGAGCGAGACCGCCAGCCT
USP30	CTTAGATGCAAGCTGCTTGT
USP31	CAATTCCTCTGCCCCACACA
USP31	TCTTACCTTGTGTGGGGCAG
USP31	AGACTTATTACCTGATCAGT
USP32	TGTAGAGCTAAAACGACTGA
USP32	AGAATGCTCCACGTGGTGGA

OTUD5	GAGGCTGAACTCCGCTGCCG
OTUD6A	CGACAACATCGTGCGCACCA
OTUD6A	CGGAGTTGTAGTGCTCGCCG
OTUD6A	CCTGGCCGGCTTCAAGCGCG
OTUD6B	CTCAGCGGTCTGACTTCTCA
OTUD6B	TACATACAGTGGCCATCAGA
OTUD6B	GAAGCAACTCACCGAAGATG
OTUD7A	AGACCTGAGCGTGTACAGCG
OTUD7A	CTGTGTGCACGAGCTGTAAA
OTUD7A	ATTTCAGGAGCTTCATCGAG
OTUD7B	TTGAGAAGGAAGCGTTGAAA
OTUD7B	CTAGCGCGAGATCTCCTAGA
OTUD7B	GCAGCATCAAGTCCCGATCA
PAN2	CCCCACGGGCCATATACTTG
PAN2	GACAGCAGCACTCTACTCGT
PAN2	TCTCCTCGTGCAAGTCAAAG
PRPF8	CCAGGGAATCTCATTGACGA
PRPF8	AGGTTGATGTCTCGAACAAG
PRPF8	TCTATGACCACCAGCCGTTG
PSMD14	TGCCACAGCTCTCTCCGACA
PSMD14	TTCAGGCCGGAGATGGTTGT
PSMD14	ATCAAACCCATAACTTCCAT
STAMBP	ATGGCGCAATCCATCGATTG
STAMBP	TGGCCCGCTAGTGCCTGACT
STAMBP	TTTACAGTTCCCACAATCGA
STAMBPL1	CCAGACCTAAAGTAACGTCG
STAMBPL1	ACCAGAGAATTCACAGTAAA
STAMBPL1	CACATTGCTGGTAATCTCGA
TNFAIP3	CTGTCATAGCCGAGAACAAT
TNFAIP3	TGGATGATCTCCCGAAACTG
TNFAIP3	CTTGTGGCGCTGAAAACGAA
UCHL1	AATCGGACTTATTCACGCAG
UCHL1	ACAGGCAGCCCATGATGCCG
UCHL1	CGCCGGCCAGTGGCGCTTCG
UCHL3	TCTACTTTCTCATCTATACT
UCHL3	CAAACAATCAGCAATGCCTG
UCHL3	ATTGCATTAGTTCATGTAGA
UCHL5	CTGATAATGTCTCGCCTAAA
UCHL5	GAGCCCAAGTAGAAGAAATA
UCHL5	GTTCAGTAACACACTCACTA
USP1	AGTGTGTTAAGCAGTCGCCT
USP1	CTGTTCAACCGAAATGATTA
USP32	ATTATTGAAGTGCAGCCCTT
USP33	TCACCAACTGAATCCAAATG
USP33	TATATCCAGATCATCAAATA
USP33	TGATGATCTGGATATAGAAG
USP34	AAATGGCCTTTCTCTCATGA
USP34	ATTTCAGTATCAGATGTAGA
USP34	AACGCATGTGCTATAAGAAA
USP35	CACACGACTCGCAGTAGTAG
USP35	CTACTACTGCTATGCCCGTG
USP35	TTCGCTCACCAAAATTGAGA
USP36	ATCGCCCGACACTTCCGCTT
USP36	CTTGATGGCGTTGCCGCTGT
USP36	CTCCAGCGCGACGTCCAAGT
USP37	CGGCTTTGTTTCGCTCCACT
USP37	AAACTACCAGACCCCTGAGA
USP37	TATTGACAAAGTACCAAGTA
USP38	CTAAAGAGATCCAGCACCGA
USP38	GCTAGACGAGGCGCAGTGCG
USP38	AGGCTTGCCAATGCTACAGA
USP39	ACACAACTCGATGCTTACGG
USP39	CCTATTACCAGAAAAAAGAT
USP39	TTCAGCAAAGAATGGCCGAG
USP4	CTATGTATTGGTCCCTACCG
USP4	TCCCTGCGGAGCGTGAAACA
USP4	TAGTAGTTTATTCCACGCCT
USP40	TCCACCCAAAGCTGTCAGTG
USP40	AATGTAAGAACGTTAGCGAG
USP40	AACAAGCGCTGTAACTGTAA
USP41	GTATGTCACTGTGGGCCTCA
USP41	GTACATGTGTATGTCACTGT
USP41	AAAATGACAGGGGATCCATG
USP42	TCCAATGTTATATCAAGATA
USP42	TAGCATCAACAGTGTATTGA
USP42	TCCATATCTTGATATAACAT
USP43	ATACACGCCCCAACTTTCCG
USP43	GCCACTTTCAAGCACAATAT
USP43	TGCACAAAGCTTTGACCTAG
USP44	CTTTATCTATGACTTGTCCG
USP44	CGTAATAACCGAGAGAAGAT
USP44	CTACAGACCTGAATCGTTTG
USP45	TTATAATTAATCTGAGCACA
USP45	TCAGATTAATTATAATACAA

USP1	GTCATACCTAGTGAAAGTAA
USP10	CTTACCTCAACTGAAGATCG
USP10	CGGCGGCTACCTGCGGGCTG
USP10	GTGCAGCTTCCTCCATACAG
USP11	CCATTATACCTTGCGTTCAA
USP11	TTCAGCCATACCGATTCTAT
USP11	CCAGCCACCCATTGAACGCA
USP12	TTTATAGGGCGCCAATGCTT
USP12	GCCACCTACCATGGTACAGA
USP12	ATTCGCCTCCATCTGTACCA
USP13	GCTGGTAACTCCTCAATATT
USP13	CCTGAAAAGACATGTGCGAG
USP13	TTCAACATGTTCCCTTCCAA
USP14	AGAACGAATACACTGAACTG
USP14	GCGAGTATTGCAACAGAAAT
USP14	GAATACAGATGAACCTCCAA
USP15	AAATGTACCTTTCGTGCTAT
USP15	TGGTGATGCCCAGTCACTTA
USP15	TTTAGCAAAGCTGACACAAT
USP16	GCATTACACTGCCTATGCCA
USP16	TGGCGTCAGATAGTGCTTCA
USP16	AAGTGCTTACTTGTTCCAGA
USP17L10	TTCTTGAGCTTTGACATAAG
USP17L10	TTCAACGTCAGAAGAGTCGA
USP17L10	GGCACACTCGCTTCCCTACG
USP17L11	GCTGTGTTTGTTCTTCCCTT
USP17L11	GGAGGACGACTCACTCTACT
USP17L11	CCACGTCATCCAGCCCTCAC
USP17L12	CGATGCAAGCTCACATCACA
USP17L12	GGAGGAAGACTCACTCTACT
USP17L12	CACCAAGTGCTCGTCCAACT
USP17L13	AGGAAAGCACCTTAGACCGC
USP17L13	CTATGCAAGCTCACATCACA
USP17L13	GGAGGAGGACTCACTCTACT
USP17L15	TACATGTCTCAGACGAACTC
USP17L15	ACATGTATAGCTTCATGTCA
USP17L15	TCACACGCAAACCTACACGT
USP17L2	GAAGTCACCACTCTCATCTG
USP17L2	TCCTCCCTTGCAGAGAAGCG
USP17L2	GGATGACATGACCAGGACTG
USP17L27	GCTGTGTTTGTTCTTCCCTT
USP17L27	TCCTTGCGTTGCTCGCCTGT
USP45	TTCTCAGGTAAAGCTTTAGT
USP46	CCTAAAGCGGTTCAAGTACA
USP46	CACCAAGCTGTCTTACCGTG
USP46	AGTTCATATACCTTAGACAG
USP47	CTTTGGATGGGATAGTAGTG
USP47	AAAGCTCCTTGTAACATCTG
USP47	CAGAGTCATGTTTGATGCTT
USP48	TCGATGATCCCAACTGTGAG
USP48	ACAGACTTACACAGTTACAT
USP48	CCCCTTAGACGAAACTGCAA
USP49	CCCGTGATGCATGACCACTG
USP49	ATACCTGGTCAAAGACGACA
USP49	CTAAGCAGCACCACTTCTGA
USP5	GAAGAAGCGGCAAGCCGAAG
USP5	CTCACCAATAGCCAGCCGCG
USP5	CACCCCGGAAGAAGCCCACG
USP50	CTATGATACCCTTCCAGTTA
USP50	TCATTACCCACTCACTAACT
USP50	GTGAGGTCCAAGTTAGTGAG
USP51	GCGGGCTCACGCTCTTGTAA
USP51	TGATCTACCAGCGTTTCGTT
USP51	GTCTTCGAGACGTGAAGCCG
USP53	ACTCCGCAGCATCATCCATA
USP53	TAGTGTGTGTGTCGTAGCTG
USP53	GATGAGCAGCGATTTCAACT
USP54	TTCAAACAAAGATTCGCAAA
USP54	CAATCTGAACTGTACTTAGT
USP54	TAAGCTGCCTAAAGCTACGT
USP6	AGCTGCCTCCTGTGACTGCA
USP6	GACAAGGGGCCTGAGCCCGT
USP6	CATACTTATGAAGTATGACA
USP6NL	AATCCTACCTTCCTTCACTG
USP6NL	GGAGCTCCCAGATCATAATG
USP6NL	TTTCATAGGCGAATTTACAA
USP7	AGACACCAGTTGGCGCTCCG
USP7	GAGTGATGGACACAACACCG
USP7	AGACCACACCAAAAAAGCGT
USP8	CACATTGGCTAAAGGCTCTT
USP8	CCAAGGAGCAATCACAGCAA
USP8	CACAGCGGCTACAACAAAAA
USP9X	CAACACACCTTTGGTGATCG
USP9X	AAAACTGGAACCACCCATCG

USP17L27	CACCAAGTGCTCGTCCAACT
USP17L3	GGGGGATGACTCACTCTACT
USP17L3	GCCAGAAGCCAATGCCTGTG
USP17L3	TTGGCTTCTGGCTTCCATAG
USP17L4	TGTCTGTGTCTTCAGCGCCA
USP17L4	GGGGGACGACTCACTCTACT
USP17L4	TTGAGCTCTCCTTGCGTTGC
USP17L5	GCGAAGCCCGAAGAACTCAA
USP17L5	CTATGCAAGCTCACATCACA
USP17L5	GACGACTCACTCTACTTGAG
USP17L7	AGAAGGTATTTCCTATCTTC
USP17L7	TTCGACGAAACCGACAGATC
USP17L7	CTGTCGGTTTCGTCGAAGAG
USP17L8	CTCTGGAGACAAAGACCGCA
USP17L8	AGACCAGCCCCCACAGCAGC
USP17L8	CTTGCGGTCTTTGTCTCCAG
USP9X	GTTGATCATGTCATCCAACT
USP9Y	AGTTGCTACGGAATTCTCAT
USP9Y	GCTATTGATCTTAGTGTAAA
USP9Y	AATCCTTAGGCCTCGATGGG
USPL1	GACTTTGAATGTTCGCAGTG
USPL1	CTTCGAGCACAGTCCAGTCA
USPL1	TTGCCCTGCTTGTAGAGAGA
VCPIP1	GCTCTGTACTTTGATCCCGA
VCPIP1	GTCTTACAGGAGAAGATGTA
VCPIP1	CTCGATGCTGACAGAACCGG
YOD1	GGCGGTCAGCGAATCCTCGT
YOD1	ACTCGGGAGGGTATCCGACG
YOD1	AGTGTGTACTATGTCGTCGA
ZRANB1	CTTGGAATTGGCTACACGTT
ZRANB1	CAGCAAGCGTACTTCATCTG
ZRANB1	GCTAGCAATATTGCTTACAG

11.1.3 Sequences of non-targeting and positive control sgRNAs

Non-targeting	Sequence (forward)
NT-1	ACGGAGGCTAAGCGTCGCAA
NT-2	CGCTTCCGCGGCCCGTTCAA
NT-3	ATCGTTTCCGCTTAACGGCG
NT-4	GTAGGCGCGCCGCTCTCTAC
NT-5	CCATATCGGGGCGAGACATG
NT-6	TACTAACGCCGCTCCTACAG
NT-7	CGGAGTAACAAGCGGACGGA
NT-8	GGGCCCGCATAGGATATCGC
NT-9	GTGTCGGATTCCGCCGCTTA
NT-10	ACGGGCGGCTATCGCTGACT
NT-11	CGCGGAAATTTTACCGACGA
NT-12	CTTACAATCGTCGGTCCAAT

Positive control	Sequence (forward)
POLR2I	CAACAAGATCACGCACGAAG
POLR2I	GAACCGCATTCTGCTCTACG
POLR2I	CCCTCTCAGGTGCGGCCACA
RPA3	TACGGGTTCCATCAACTCGA
RPA3	GGTTGGAAGAGTAACCGCCA
RPA3	GATGAATTGAGCTAGCATGC
RPL32	GCGCAGTGAAGAAAATGAGT
RPL32	AGACCGATATGTCAAAATTA
RPL32	GTTGCTTCCATAACCAATGT
RPL8	TGGTCTTCCGGGATCCGTAT
RPL8	GTCCGCTTCTTAAACCGATA
RPL8	CTTGCAGCCCAGCTCAACAT
RPS19	TACCCCCAGCTTCCACAGCG
RPS19	CTGACGTCCCCCATAGATCT
RPS19	TCCAGATCTCTTTGTCCCTG

11.2 Results of CRISPR/Cas9 screens

11.2.1 CRISPR/Cas9 screen of F-box proteins

Depleted targets	untreated/ $T_0 < 0$	Enriched targets	untreated/ $T_0 > 0$	Depleted targets	Bortezomib/ $T_0 < 0$	Enriched targets	Bortezomib/ $T_0 > 0$
RPS19_1	0.007	FBXL13_3	1.000	POLR2I_2	0.006	FBXW2_2	1.004
RPL8_3	0.012	FBXL12_1	1.001	RPS19_3	0.016	FBXL5_1	1.004
RPS19_3	0.014	FBXO15_1	1.001	RPA3_3	0.025	FBXO44_2	1.005
POLR2I_2	0.018	FBXO41_1	1.007	RPL8_3	0.030	FBXO45_3	1.005
RPL32_1	0.039	FBXL21_3	1.011	RPL32_3	0.048	LMO7_1	1.013
RPA3_3	0.080	SKP2_1	1.013	RPL32_1	0.051	FBXW4_2	1.014
RPA3_2	0.087	FBXO17_1	1.016	RPS19_1	0.081	FBXO34_2	1.019
RPL32_3	0.114	FBXO43_3	1.018	RPL8_1	0.084	FBXL22_3	1.019
POLR2I_1	0.125	FBXO5_2	1.020	RPA3_2	0.094	FBXL8_1	1.020
RPL8_2	0.131	FBXO32_2	1.021	POLR2I_1	0.141	FBXL7_2	1.023
RPL8_1	0.133	FBXO32_1	1.022	FBXW10_1	0.182	SKP2_1	1.027
FBXW11_2	0.197	FBXL14_2	1.030	FBXW11_2	0.186	FBXO39_3	1.027
SKP2_2	0.275	NT_6	1.037	RPL8_2	0.240	LRRC29_3	1.031
POLR2I_3	0.298	FBXL17_1	1.041	POLR2I_3	0.355	FBXL14_3	1.037
RPA3_1	0.332	LMO7_2	1.048	RPA3_1	0.426	FBXW12_1	1.038
FBXW11_3	0.377	FBXO4_3	1.052	FBXW10_2	0.441	FBXO38_2	1.048
FBXO42_1	0.400	FBXL20_1	1.053	FBXO42_3	0.455	FBXO46_3	1.050
FBXO43_2	0.410	FBXO34_2	1.060	FBXO9_2	0.480	FBXL21_3	1.052
RPS19_2	0.420	FBXL20_3	1.068	FBXO7_3	0.483	KDM2A_3	1.053
FBXW10_1	0.451	FBXO30_3	1.068	FBXO21_3	0.498	FBXW8_1	1.056
CCNF_1	0.457	FBXO46_3	1.068	SKP2_3	0.505	FBXO46_1	1.057
FBXO7_3	0.466	FBXO32_3	1.069	CCNF_2	0.508	KDM2A_2	1.062
FBXL5_3	0.571	FBXW7_2	1.070	FBXL21_1	0.517	FBXL12_2	1.065
FBXL5_2	0.585	FBXO39_2	1.080	RPS19_2	0.523	FBXO30_3	1.065
FBXO11_2	0.601	KDM2B_3	1.086	CCNF_1	0.524	FBXW5_3	1.072
FBXO2_2	0.614	LRRC29_2	1.087	FBXO41_1	0.529	FBXL18_2	1.087
FBXO33_2	0.619	FBXO22_1	1.089	FBXW11_3	0.539	FBXL13_3	1.088
KDM2A_1	0.622	FBXO34_1	1.090	FBXL6_1	0.562	FBXO16_3	1.089
CCNF_2	0.626	FBXO10_3	1.093	FBXO5_3	0.567	FBXO32_3	1.092
FBXW10_2	0.651	FBXO3_2	1.103	FBXL5_2	0.602	FBXL19_2	1.093
FBXO34_3	0.689	FBXO28_2	1.105	FBXO40_1	0.606	KDM2B_1	1.101
FBXO44_2	0.694	FBXO21_3	1.111	FBXL18_1	0.617	NT_1	1.103
FBXL16_3	0.702	ECT2L_2	1.112	FBXO24_2	0.619	FBXW11_1	1.104
FBXW9_3	0.702	KDM2B_1	1.112	CCNF_3	0.626	FBXL2_1	1.111
FBXL12_2	0.702	FBXO28_3	1.113	FBXL17_3	0.634	FBXW7_1	1.113
FBXO11_3	0.707	FBXL3_3	1.114	SKP2_2	0.636	NT_4	1.115

KDM2A_2	0.708	RPL32_2	1.118	FBXO3_1	0.669	FBXO43_1	1.127
FBXO2_3	0.711	FBXL14_1	1.120	FBXO32_1	0.672	FBXO11_3	1.133
FBXO42_2	0.719	FBXW8_3	1.123	FBXW9_2	0.707	FBXO36_3	1.138
FBXO10_2	0.723	FBXL14_3	1.124	FBXL16_3	0.712	FBXL12_1	1.147
SKP2_3	0.749	FBXO18_2	1.124	FBXO4_3	0.738	FBXO28_3	1.150
FBXL8_1	0.761	FBXW5_2	1.127	FBXL8_3	0.741	FBXO24_1	1.154
FBXO16_1	0.769	FBXL17_2	1.127	FBXO42_2	0.753	FBXL18_3	1.159
FBXL6_2	0.772	ECT2L_3	1.128	FBXO42_1	0.757	FBXO34_3	1.161
FBXO22_2	0.773	NT_12	1.128	FBXL4_3	0.766	NT_11	1.169
FBXO9_2	0.786	FBXL15_1	1.130	FBXO2_2	0.777	FBXO25_3	1.183
FBXO41_2	0.789	NT_10	1.133	FBXO7_1	0.783	FBXL3_3	1.186
FBXL7_2	0.789	FBXL22_3	1.134	FBXO9_3	0.785	FBXO45_2	1.187
FBXL4_2	0.798	FBXL2_1	1.136	FBXO43_2	0.787	FBXO6_1	1.188
FBXO46_2	0.800	FBXL2_3	1.139	FBXO10_1	0.794	FBXL15_1	1.194
FBXL12_3	0.811	FBXO7_1	1.146	FBXO36_2	0.803	FBXL20_1	1.197
FBXL6_1	0.812	FBXL6_3	1.150	FBXL15_2	0.825	FBXW5_1	1.204
FBXO39_3	0.813	FBXL7_1	1.151	FBXW2_1	0.828	FBXO24_3	1.205
FBXL18_2	0.813	FBXO45_1	1.160	BTRC_2	0.838	FBXO15_1	1.212
BTRC_2	0.823	NT_9	1.168	FBXL17_1	0.847	FBXO6_3	1.215
FBXO36_2	0.824	FBXO28_1	1.171	FBXO48_3	0.859	NT_12	1.220
FBXO18_1	0.824	FBXO44_1	1.173	FBXO10_2	0.864	FBXO27_1	1.221
FBXO30_1	0.825	FBXO8_2	1.173	FBXO40_2	0.864	FBXL5_3	1.223
FBXO31_2	0.839	FBXO17_2	1.173	FBXL20_3	0.865	FBXO25_1	1.225
FBXO6_2	0.842	NT_8	1.178	FBXO32_2	0.870	FBXO30_1	1.227
BTRC_1	0.843	FBXO24_1	1.179	FBXO9_1	0.884	FBXL2_2	1.227
FBXW2_1	0.848	FBXW4_2	1.188	FBXO18_1	0.888	FBXW9_1	1.227
FBXO16_3	0.848	FBXL2_2	1.192	FBXO16_1	0.893	FBXO22_2	1.231
FBXO42_3	0.850	FBXO16_2	1.206	FBXO21_1	0.894	BTRC_1	1.233
FBXL4_3	0.859	FBXO36_3	1.214	FBXO33_2	0.897	FBXW8_3	1.234
FBXO44_3	0.861	KDM2B_2	1.215	LRRC29_1	0.898	FBXL20_2	1.235
FBXL5_1	0.864	FBXL19_2	1.225	FBXO8_2	0.899	FBXW10_3	1.235
FBXO9_1	0.867	FBXW5_1	1.233	FBXL2_3	0.899	FBXL22_2	1.235
FBXL18_1	0.870	FBXO5_1	1.241	FBXO5_2	0.902	FBXO47_1	1.236
FBXO5_3	0.873	NT_4	1.242	FBXL6_2	0.903	FBXL14_1	1.237
FBXO22_3	0.877	FBXO31_1	1.248	FBXL4_2	0.904	LMO7_2	1.238
FBXO15_3	0.878	FBXW5_3	1.250	FBXL16_1	0.911	FBXO22_3	1.249
FBXO25_1	0.879	FBXL22_2	1.253	FBXL14_2	0.912	FBXL12_3	1.252
FBXL17_3	0.892	FBXL8_3	1.259	KDM2B_3	0.921	FBXL17_2	1.254
FBXO27_3	0.895	FBXO6_3	1.260	FBXO34_1	0.924	FBXW4_3	1.254
FBXO15_2	0.902	FBXO27_1	1.260	FBXW4_1	0.926	FBXO25_2	1.256
FBXO17_3	0.906	FBXL3_2	1.266	FBXL3_2	0.926	NT_5	1.258
LRRC29_1	0.907	FBXL4_1	1.273	FBXL16_2	0.928	FBXL19_3	1.264

FBXO43_1	0.907	FBXO47_2	1.280	FBXO22_1	0.931	FBXW5_2	1.265
FBXL19_3	0.912	FBXO33_1	1.280	FBXO38_1	0.936	LMO7_3	1.265
FBXO40_2	0.912	FBXW2_2	1.285	FBXO7_2	0.938	FBXO44_1	1.265
FBXO6_1	0.914	FBXL16_2	1.285	FBXO15_3	0.942	NT_8	1.267
FBXO31_3	0.916	FBXO9_3	1.286	FBXO46_2	0.943	FBXO3_3	1.279
FBXO40_1	0.922	FBXO40_3	1.293	NT_10	0.948	FBXO17_2	1.290
FBXW9_2	0.931	FBXL15_3	1.300	ECT2L_1	0.952	FBXO27_2	1.292
CCNF_3	0.936	FBXO38_2	1.305	FBXL19_1	0.953	FBXL22_1	1.294
FBXO48_1	0.937	FBXL20_2	1.310	RPL32_2	0.959	BTRC_3	1.296
FBXO2_1	0.937	FBXO36_1	1.324	FBXO15_2	0.964	FBXO2_3	1.312
FBXO7_2	0.939	FBXW7_3	1.337	FBXO39_2	0.965	ECT2L_3	1.313
FBXL8_2	0.940	FBXO25_2	1.347	NT_9	0.965	FBXO21_2	1.320
FBXL18_3	0.941	FBXW10_3	1.351	FBXO36_1	0.965	FBXW7_2	1.320
FBXL16_1	0.944	FBXO24_2	1.357	FBXO31_1	0.966	FBXO27_3	1.330
KDM2A_3	0.945	FBXO25_3	1.362	FBXL6_3	0.966	FBXO45_1	1.331
FBXO3_1	0.945	FBXO33_3	1.370	NT_6	0.968	FBXL15_3	1.336
FBXL19_1	0.947	FBXW4_1	1.375	FBXO41_3	0.969	FBXO33_1	1.369
FBXW12_2	0.951	NT_5	1.379	FBXL8_2	0.972	FBXL13_1	1.396
FBXL15_2	0.953	FBXL21_2	1.426	FBXO6_2	0.973	FBXO18_2	1.403
FBXO48_3	0.956	FBXW9_1	1.443	KDM2B_2	0.979	FBXO11_2	1.404
FBXL21_1	0.966	FBXO8_1	1.443	FBXO17_1	0.981	FBXW12_3	1.416
LRRC29_3	0.969	FBXO47_3	1.444	LRRC29_2	0.985	FBXO5_1	1.418
FBXW12_1	0.970	FBXL22_1	1.452	FBXO31_2	0.987	FBXO3_2	1.425
FBXO21_1	0.971	FBXO30_2	1.455	FBXO41_2	0.987	FBXW2_3	1.432
FBXW11_1	0.974	FBXL3_1	1.457	ECT2L_2	0.988	KDM2A_1	1.436
FBXO10_1	0.980	FBXO21_2	1.479	FBXO17_3	0.989	FBXO2_1	1.450
FBXO41_3	0.985	LMO7_1	1.486	FBXL13_2	0.989	FBXO47_3	1.454
FBXO27_2	0.993	FBXO3_3	1.529	FBXO30_2	0.992	FBXO47_2	1.470
FBXW8_1	0.993	FBXO46_1	1.539	FBXO31_3	0.995	FBXO33_3	1.472
FBXO45_3	0.995	FBXW7_1	1.540	FBXO48_1	0.996	FBXL7_3	1.478
FBXL7_3	0.999	FBXW4_3	1.549	FBXL7_1	0.997	FBXO43_3	1.487
		FBXO47_1	1.554			FBXO8_1	1.497
		FBXO24_3	1.556			FBXO8_3	1.519
		NT_1	1.576			FBXO28_2	1.523
		FBXO4_1	1.577			FBXO38_3	1.524
		NT_11	1.583			FBXO44_3	1.543
		FBXL13_2	1.587			FBXL21_2	1.546
		ECT2L_1	1.605			FBXW9_3	1.563
		NT_7	1.610			FBXL3_1	1.565
		FBXO48_2	1.630			FBXO16_2	1.565
		NT_2	1.637			FBXL4_1	1.569
		FBXO39_1	1.647			FBXO28_1	1.585

FBXO45_2	1.716	NT_7	1.585
FBXO8_3	1.728	FBXO10_3	1.605
FBXO4_2	1.741	FBXO4_1	1.611
LMO7_3	1.767	FBXO4_2	1.659
FBXW2_3	1.779	FBXO39_1	1.659
FBXW8_2	1.781	FBXO48_2	1.683
FBXL13_1	1.829	FBXW8_2	1.687
BTRC_3	1.877	FBXW7_3	1.731
FBXO38_3	1.926	FBXO40_3	1.837
NT_3	1.939	NT_2	1.922
FBXO38_1	2.030	NT_3	1.980
FBXW12_3	2.188	FBXW12_2	1.983

11.2.2 CRISPR/Cas9 screen of DUBs

Depleted targets	untreated/ $T_0 < 0$	Enriched targets	untreated/ $T_0 > 0$	Depleted targets	Bortezomib/ $T_0 < 0$	Enriched targets	Bortezomib/ $T_0 > 0$
COPS5_2	0.012	OTUD1_1	1.000	RPL8_3	0.026	USP27X_2	1.000
RPL8_3	0.038	USP1_3	1.001	COPS5_2	0.026	PSMD14_3	1.002
USP17L15_3	0.048	PAN2_3	1.001	RPA3_3	0.047	UCHL3_2	1.004
RPL32_1	0.053	USP32_1	1.005	RPS19_3	0.052	USP42_3	1.006
USP17L11_1	0.067	USP38_1	1.006	POLR2I_2	0.056	USP53_2	1.007
USP17L27_1	0.076	PAN2_1	1.006	RPA3_2	0.078	UCHL5_1	1.021
RPS19_3	0.077	USP3_1	1.006	RPL32_1	0.082	USP19_3	1.027
PSMD14_1	0.085	OTUD7A_2	1.010	USP17L5_2	0.124	USP44_2	1.029
POLR2I_2	0.096	USP43_3	1.016	USP17L13_2	0.134	NT_12	1.031
RPL32_3	0.099	OTUB2_1	1.018	PSMD14_1	0.144	OTUB1_3	1.031
USP17L5_2	0.110	USP42_1	1.019	USP17L15_3	0.170	USP32_2	1.031
RPA3_3	0.112	USP41_3	1.021	RPA3_1	0.176	USP11_1	1.033
USP17L13_2	0.123	USP30_2	1.034	BAP1_1	0.186	USP54_1	1.036
POLR2I_1	0.126	OTUD3_3	1.038	OTUD6B_2	0.195	UCHL3_3	1.036
USP17L11_3	0.129	USP15_3	1.041	RPL32_3	0.221	NT_10	1.040
RPL8_1	0.134	USP21_1	1.042	PSMD14_2	0.226	USP9X_3	1.043
RPA3_2	0.145	STAMBP_1	1.046	USPL1_1	0.235	USP28_1	1.045
USPL1_1	0.148	OTUD5_2	1.049	USPL1_3	0.243	USP17L4_3	1.048
RPL8_2	0.186	USP39_3	1.051	USP5_1	0.274	STAMBP_3	1.051
PRPF8_2	0.196	USP6NL_2	1.052	USP17L11_3	0.279	USP39_1	1.055
RPA3_1	0.215	USP17L7_2	1.058	RPL8_2	0.281	USP17L2_3	1.060
USPL1_2	0.220	UCHL5_1	1.059	RPL8_1	0.293	OTUB1_1	1.064
USP17L5_1	0.251	USP16_3	1.061	USP19_2	0.325	USP6NL_1	1.064
POLR2I_3	0.255	STAMBPL1_2	1.070	USP17L11_1	0.336	USP17L12_3	1.065

USPL1_3	0.260	YOD1_3	1.071	USP17L27_1	0.340	USP10_2	1.067
USP17L11_2	0.268	USP51_3	1.071	USP17L5_1	0.363	USP2_3	1.069
USP10_3	0.316	JOSD1_2	1.074	VCPIP1_2	0.372	USP29_3	1.071
BAP1_3	0.317	COPS5_1	1.076	PRPF8_2	0.385	USP17L8_1	1.078
PSMD14_2	0.320	USP6_3	1.082	ZRANB1_2	0.387	OTUD3_2	1.083
COPS5_3	0.327	USP17L10_1	1.089	BAP1_2	0.392	USP26_1	1.087
OTUD5_1	0.382	USP35_2	1.090	JOSD2_1	0.412	USP36_1	1.089
USP5_3	0.383	OTUB2_2	1.091	USP17L11_2	0.419	BRCC3_3	1.090
BAP1_1	0.425	USP53_2	1.091	USPL1_2	0.425	USP50_3	1.090
USP12_2	0.438	USP27X_1	1.098	BAP1_3	0.452	USP13_1	1.092
PRPF8_1	0.453	USP30_3	1.113	USP14_1	0.457	USP47_2	1.095
USP12_3	0.471	USP26_1	1.113	COPS5_3	0.458	USP8_1	1.098
USP5_1	0.509	YOD1_1	1.115	OTUD6B_3	0.465	USP17L12_1	1.100
RPS19_2	0.523	USP17L15_2	1.119	RPS19_2	0.468	USP8_2	1.106
ZRANB1_2	0.525	OTUD4_3	1.121	USP5_3	0.473	USP46_2	1.109
USP17L3_3	0.533	NT_10	1.122	USP4_3	0.477	USP18_3	1.112
OTUB1_2	0.533	JOSD2_2	1.125	PRPF8_1	0.484	USP44_1	1.115
OTUD6B_2	0.545	USP17L4_3	1.128	USP14_3	0.485	USP43_2	1.116
JOSD2_1	0.546	OTUD3_1	1.129	POLR2I_1	0.490	BRCC3_2	1.120
USP21_3	0.554	USP10_1	1.133	ZRANB1_1	0.499	USP16_3	1.127
UCHL5_3	0.598	USP19_3	1.138	USP6_2	0.503	USP32_1	1.130
USP19_2	0.605	USP44_2	1.139	POLR2I_3	0.508	USP17L27_3	1.132
BAP1_2	0.619	ATXN3L_2	1.139	USP47_3	0.531	USP3_3	1.134
USP9X_2	0.629	USP41_1	1.141	USP19_1	0.534	ATXN3_1	1.136
NT_3	0.631	PSMD14_3	1.141	USP17L3_3	0.545	USP20_2	1.150
USP12_1	0.647	JOSD1_3	1.144	OTUD3_3	0.550	COPS5_1	1.153
OTUD3_2	0.654	USP45_2	1.147	USP3_1	0.558	USP18_2	1.155
USP17L7_3	0.654	OTUD6B_1	1.156	PAN2_3	0.564	USP17L10_3	1.157
OTUD6B_3	0.657	USP17L12_3	1.163	USP49_3	0.564	TNFAIP3_2	1.168
USP36_2	0.666	USP17L27_3	1.164	USP22_2	0.578	USP15_3	1.174
STAMBP_2	0.675	USP51_1	1.168	USP36_2	0.582	OTUD7A_1	1.176
USP2_2	0.676	USP9Y_2	1.170	USP12_3	0.586	USP7_1	1.182
OTUB1_1	0.680	OTUD5_3	1.172	PAN2_2	0.631	OTUD4_1	1.184
MYSM1_2	0.688	USP6NL_1	1.181	USP4_1	0.636	USP26_2	1.187
UCHL1_1	0.698	NT_12	1.187	USP6_1	0.642	USP28_3	1.191
USP4_1	0.720	USP7_1	1.189	USP43_1	0.643	TNFAIP3_1	1.195
ZRANB1_1	0.726	OTUD6A_3	1.189	USP21_3	0.649	USP54_3	1.197
BRCC3_1	0.727	USP46_3	1.191	MYSM1_2	0.657	USP25_2	1.198
MYSM1_3	0.729	UCHL1_3	1.191	USP12_1	0.658	USP27X_3	1.206
USP2_3	0.733	TNFAIP3_3	1.192	YOD1_2	0.672	USP48_3	1.210
USP33_1	0.738	USP8_2	1.195	USP37_3	0.674	OTUD1_1	1.215
USP37_3	0.745	OTUD7B_2	1.198	USP12_2	0.679	ATXN3L_1	1.216

USP35_1	0.747	USP36_3	1.206	ATXN3_2	0.684	USP31_1	1.217
USP28_1	0.747	USP16_1	1.209	USP10_1	0.694	USP27X_1	1.221
USP49_2	0.754	USP43_1	1.213	JOSD2_2	0.694	OTUD7A_3	1.221
USP39_1	0.755	OTUB2_3	1.218	STAMBP_2	0.701	USP9X_2	1.223
USP17L2_3	0.757	STAMBPL1_3	1.221	USP15_2	0.704	USP30_2	1.225
MPND_2	0.759	ATXN3_1	1.229	USP40_3	0.706	USP18_1	1.231
USP22_3	0.761	USP31_3	1.230	USP17L8_3	0.706	STAMBPL1_3	1.232
USP25_2	0.762	USP9X_1	1.250	USP41_3	0.718	OTUD4_2	1.235
OTUD1_3	0.762	USP35_3	1.256	NT_6	0.727	OTUD6A_1	1.236
USP20_3	0.763	USP45_3	1.257	JOSD1_2	0.729	OTUB2_3	1.239
VCPIP1_3	0.765	USP48_1	1.259	USP51_3	0.729	USP8_3	1.246
USP34_1	0.767	TNFAIP3_1	1.260	NT_3	0.738	USP17L10_2	1.247
OTUD7A_1	0.768	BRCC3_3	1.261	OTUD6B_1	0.746	ZRANB1_3	1.249
OTUD6A_2	0.773	USP47_2	1.261	USP33_1	0.753	USP14_2	1.250
USP48_3	0.774	USP42_3	1.268	USP49_1	0.754	USP17L15_1	1.253
USP1_1	0.783	USP50_2	1.273	USP41_1	0.755	USP44_3	1.256
USP18_3	0.785	USP47_3	1.275	USP39_3	0.762	USP9Y_2	1.263
USP17L5_3	0.788	USP21_2	1.288	VCPIP1_3	0.764	USP25_1	1.264
USP54_3	0.788	USP50_3	1.291	UCHL5_3	0.770	OTUD7B_3	1.264
YOD1_2	0.791	USP29_1	1.302	USP21_1	0.773	USP21_2	1.265
USP17L8_3	0.791	USP17L8_1	1.313	USP17L2_2	0.793	USP28_2	1.270
USP19_1	0.792	VCPIP1_1	1.319	USP17L8_2	0.795	USP20_1	1.272
USP18_2	0.796	USP17L8_2	1.320	USP30_3	0.796	USP51_1	1.273
USP8_3	0.797	USP32_3	1.322	USP37_2	0.797	USP9Y_1	1.275
USP17L2_2	0.813	USP53_1	1.327	UCHL1_1	0.797	USP42_2	1.282
USP18_1	0.838	USP22_2	1.336	UCHL1_2	0.798	USP1_3	1.288
USP27X_2	0.840	USP16_2	1.348	RPL32_2	0.798	USP31_3	1.296
USP7_3	0.843	USP7_2	1.349	ATXN3L_2	0.800	USP1_1	1.301
PAN2_2	0.843	NT_1	1.358	USP33_3	0.800	USP24_3	1.302
UCHL1_2	0.844	JOSD2_3	1.360	USP10_3	0.807	USP5_2	1.314
USP22_1	0.844	OTUD7A_3	1.361	USP34_1	0.810	OTUD7A_2	1.314
USP4_3	0.847	USP5_2	1.362	OTUD1_3	0.812	USP25_3	1.318
USP17L13_3	0.856	USP40_1	1.378	USP46_3	0.816	USP34_2	1.322
USP6_1	0.857	USP15_2	1.378	BRCC3_1	0.818	USP2_1	1.327
USP17L2_1	0.862	USP13_3	1.378	USP17L4_2	0.818	NT_9	1.328
UCHL3_2	0.866	USP14_2	1.381	USP45_2	0.821	OTUD6A_3	1.334
USP17L4_2	0.871	USP33_2	1.384	USP50_1	0.824	USP29_1	1.362
STAMBP_3	0.878	USP30_1	1.385	USP17L7_3	0.831	USP46_1	1.373
USP37_2	0.878	USP10_2	1.388	USP45_1	0.836	MYSM1_3	1.377
VCPIP1_2	0.879	USP17L15_1	1.392	USP32_3	0.837	USP31_2	1.378
USP17L3_2	0.882	USP46_2	1.394	NT_5	0.840	USP35_3	1.379
MYSM1_1	0.892	USP53_3	1.394	OTUB2_1	0.841	USP17L3_1	1.383

USP42_2	0.892	USP24_2	1.401	USP29_2	0.847	USP51_2	1.384
USP48_2	0.892	USP11_2	1.407	USP2_2	0.854	USP38_3	1.389
TNFAIP3_2	0.896	USP46_1	1.410	UCHL1_3	0.854	USP38_1	1.394
USP40_3	0.905	USP47_1	1.416	USP17L10_1	0.858	USP24_2	1.398
USP40_2	0.907	CYLD_1	1.427	USP17L3_2	0.863	USP1_2	1.401
MPND_3	0.913	NT_4	1.430	USP42_1	0.864	RPS19_1	1.418
NT_6	0.914	CYLD_2	1.430	USP17L13_3	0.872	USP53_3	1.421
OTUD4_2	0.916	ZRANB1_3	1.445	USP40_2	0.875	USP47_1	1.424
OTUD4_1	0.920	NT_8	1.445	USP20_3	0.878	OTUD6A_2	1.432
USP29_3	0.922	UCHL3_1	1.454	USP7_3	0.885	USP17L13_1	1.433
USP31_2	0.924	USP51_2	1.456	USP17L7_1	0.888	USP43_3	1.445
USP50_1	0.925	USP41_2	1.460	USP30_1	0.890	USP17L12_2	1.445
ATXN3L_3	0.927	OTUD7B_3	1.462	USP17L5_3	0.892	JOSD1_3	1.447
USP44_3	0.930	UCHL3_3	1.463	USP34_3	0.896	USP17L4_1	1.451
USP3_2	0.933	RPL32_2	1.477	USP26_3	0.898	USP11_3	1.451
USP26_3	0.936	USP6NL_3	1.479	OTUB2_2	0.901	NT_1	1.453
OTUD1_2	0.940	BRCC3_2	1.494	USP17L15_2	0.906	USP37_1	1.459
USP49_1	0.940	USP13_2	1.507	USP36_3	0.911	NT_8	1.463
USP28_3	0.940	USP27X_3	1.515	USP17L2_1	0.915	USP17L27_2	1.475
USP38_3	0.942	USP17L4_1	1.519	MYSM1_1	0.915	USP9Y_3	1.479
USP4_2	0.947	USP14_1	1.520	ATXN3L_3	0.917	MPND_3	1.487
USP36_1	0.952	USP8_1	1.531	OTUD1_2	0.919	NT_11	1.488
USP14_3	0.953	USP45_1	1.531	USP49_2	0.926	USP9X_1	1.494
USP49_3	0.957	ATXN3L_1	1.531	OTUD7B_2	0.927	TNFAIP3_3	1.498
NT_5	0.958	USP54_1	1.535	OTUB1_2	0.927	NT_4	1.500
STAMBPL1_1	0.961	USP20_2	1.550	USP33_2	0.929	USP11_2	1.506
USP34_2	0.961	USP17L13_1	1.550	YOD1_1	0.935	OTUD5_1	1.513
USP24_1	0.972	USP13_1	1.551	USP13_2	0.938	USP13_3	1.515
USP28_2	0.975	USP44_1	1.555	NT_2	0.943	MPND_2	1.520
USP34_3	0.977	USP17L10_3	1.556	USP4_2	0.947	USP6NL_3	1.526
USP2_1	0.983	USP37_1	1.556	ATXN3_3	0.952	USP45_3	1.538
MPND_1	0.983	USP17L3_1	1.558	YOD1_3	0.953	USP6NL_2	1.542
USP33_3	0.987	USP9Y_1	1.562	USP7_2	0.956	CYLD_3	1.546
OTUD6A_1	0.990	USP20_1	1.565	USP3_2	0.957	USP16_2	1.586
ATXN3_3	0.991	ATXN3_2	1.566	USP40_1	0.958	STAMBPL1_1	1.589
USP17L12_1	0.992	USP29_2	1.591	USP53_1	0.961	MPND_1	1.593
NT_2	0.998	USP17L7_1	1.600	USP48_2	0.962	CYLD_1	1.598
		USP17L27_2	1.609	UCHL3_1	0.972	UCHL5_2	1.624
		USP17L10_2	1.616	OTUD5_3	0.973	PRPF8_3	1.636
		USP11_1	1.629	USP48_1	0.974	USP35_2	1.650
		NT_11	1.638	PAN2_1	0.983	USP6_3	1.668
		USP11_3	1.640	USP17L7_2	0.987	USP15_1	1.681

USP43_2	1.642	STAMBP_1	0.996	OTUD4_3	1.749
USP9X_3	1.646	USP24_1	0.999	VCPIP1_1	1.798
CYLD_3	1.661			USP38_2	1.798
NT_9	1.668			JOSD1_1	1.820
USP17L12_2	1.671			OTUD3_1	1.832
PRPF8_3	1.700			JOSD2_3	1.888
NT_7	1.711			OTUD5_2	1.889
USP15_1	1.755			USP54_2	1.910
USP38_2	1.772			OTUD7B_1	1.933
JOSD1_1	1.799			USP16_1	1.977
USP9Y_3	1.802			USP39_2	1.982
USP25_1	1.825			STAMBPL1_2	2.003
USP24_3	1.826			USP35_1	2.016
UCHL5_2	1.830			USP41_2	2.166
USP31_1	1.858			USP22_1	2.252
USP1_2	1.878			CYLD_2	2.276
USP26_2	1.900			USP50_2	2.497
USP6_2	1.928			USP22_3	2.992
USP25_3	2.139			NT_7	3.342
OTUD7B_1	2.142				
USP39_2	2.154				
USP54_2	2.248				

12 Publication

Ella Fung*, **Carmen Richter***, Hong-Bin Yang, Isabell Schäffer, Roman Fischer, Benedikt M Kessler, Florian Bassermann and Vincenzo D'Angiolella. “FBXL13 directs the proteolysis of CEP192 to regulate centrosome homeostasis and cell migration”. EMBO Reports (2018) 19(3): e44799.

*Equal contribution

Carmen Richter, Oleksandra Karpiuk, Jana Zecha, Isabell Schäffer, Susan Kläger, Michaela Walzik, Rupert Öllinger, Thomas Engleitner, Jan Krönke, Roland Rad, Bernhard Küster, Florian Bassermann. “OTUD6B is a novel oncogene in multiple myeloma that activates the LIN28B-MYC axis”. Manuscript in preparation

13 Danksagung

Diese Dissertation wäre ohne die Hilfe und Unterstützung vieler Menschen nicht möglich gewesen und daher möchte ich an dieser Stelle ein großes Dankeschön aussprechen. Zu allererst bedanke ich mich bei Prof. Dr. Florian Bassermann für die Möglichkeit und das Vertrauen meine Dissertation in seiner exzellenten Forschungsgruppe durchführen zu können. Es war großartig in einem so ambitionierten Umfeld forschen zu dürfen, in dem seine begeisternde und motivierende Art immer neuen Antrieb und Ideen gab. In diesem Zusammenhang, danke ich insbesondere auch den tollen Menschen der AG Bassermann, mit denen ich unglaublich viel Spaß hatte, die immer hilfsbereit waren und ohne die die langen und teilweise kräftezehrenden Arbeitstage, die Forschung mit sich bringt, nicht möglich gewesen wären. Ich hatte eine tolle Zeit mit euch, vielen Dank! Des Weiteren möchte ich mich bei Prof. Dr. Christian Peschel dafür danken, dass ich meine Dissertation in der III. Medizinischen Klinik des Klinikums rechts der Isar der Technischen Universität München anfangen durfte.

Besonderer Dank geht an meine beiden Mentorinnen Dr. Bianca Targosz und Dr. Oleksandra Karpiuk. Danke Bianca, dass du dir die Zeit genommen hast, mich in die Techniken des Labors, insbesondere der langen Zellzyklusversuche, einzuarbeiten (… und für die anregenden Diskussionen über Fußball; wir sind Weltmeister zusammen geworden). And thank you Oleksandra for being a great mentor, for answering all my questions and for introducing me to the world of CRISPR.

Mein herzlichster Dank geht an Isabell Schäffer für die tolle Arbeit und die tatkräftige Hilfe bei den zahlreichen Experimenten. Danke, dass du mir in schwierigen Zeiten den Rücken freigehalten hast und immer ein Ohr für mich offen hattest. Es hat großen Spaß gemacht mit dir zusammenzuarbeiten. Ebenfalls bedanke ich mich bei meiner ambitionierten und hochmotivierten Masterstudentin Michaela Walzik für die harte Arbeit, die die Grundsteine dieses Projekts gelegt hat.

Großen Danke geht auch an alle Kollaborationspartner, ohne die diese umfangreiche und technisch vielseitige Arbeit nicht möglich gewesen wäre. Speziell bedanke ich mich bei Prof. Dr. Bernhard Küster, Dr. Susan Kläger und Jana Zecha für die massenspektrometrischen Analysen, die zu dem Vorangehen des Projektes maßgeblich beigetragen haben. Thank you Dr. Vincenzo d'Angiolella and Dr. Ella Fung for the great and fruitful collaboration on the FBXL13 project. Danke an Prof. Dr. Roland Rad, Dr. Rupert Öllinger und Thomas Engleitner für die NGS-Analyse und zuletzt an PD Dr. med. Jan Krönke und Denise Miller für die Analyse der Patientenproben.

Abschließend gilt mein besonderer Dank meiner Familie und meinen Freunden, die mich immer unterstützt haben und großes Interesse an meinem mentalen Wohlbefinden und dem Gelingen dieser Arbeit hatten. Großer persönlicher Dank an meinen Freund Christopher, der die vielen Stunden auch außerhalb normaler Arbeitszeiten im Labor akzeptiert hat, alle Launen ertragen und geduldig auf den Abschluss dieser Arbeit gewartet hat. Ihr habt mir immer wieder gezeigt, was wichtig ist im Leben und dafür danke ich euch!